# FUNCTIONAL ANNOTATION AND MECHANISTIC CHARACTERIZATION OF ENZYMES WITH UNKNOWN FUNCTIONS: STUDIES ON ADENINE DEAMINASE, N-6-METHYLADENINE DEAMINASE AND THE C-P LYASE PATHWAY

A Dissertation

by

SIDDHESH SHASHIKANT KAMAT

Submitted to the Office of Graduate Studies of
Texas A&M University
in partial fulfillment of the requirements for the degree

DOCTOR OF PHILOSOPHY

August 2012

Major Subject: Chemistry

Functional Annotation and Mechanistic Characterization of Enzymes with Unknown Functions: Studies on Adenine Deaminase, N-6-methyladenine Deaminase and the C-P Lyase Pathway

# FUNCTIONAL ANNOTATION AND MECHANISTIC CHARACTERIZATION OF ENZYMES WITH UNKNOWN FUNCTIONS: STUDIES ON ADENINE DEAMINASE, N-6-METHYLADENINE DEAMINASE AND THE C-P LYASE PATHWAY

A Dissertation

by

SIDDHESH SHASHIKANT KAMAT

Submitted to the Office of Graduate Studies of
Texas A&M University
in partial fulfillment of the requirements for the degree of

DOCTOR OF PHILOSOPHY

Approved by:

| | |
|---|---|
| Chair of Committee, | Frank M. Raushel |
| Committee Members, | Paul A. Lindahl |
| | David P. Barondeau |
| | Jean-Philippe Pellois |
| Head of Department, | David H. Russell |

August 2012

Major Subject: Chemistry

# ABSTRACT

Functional Annotation and Mechanistic Characterization of Enzymes with Unknown Functions: Studies on Adenine Deaminase, N-6-Methyladenine Deaminase and the C-P Lyase Pathway. (August 2012)

Siddhesh Shashikant Kamat, B. Tech., University of Mumbai

Chair of Advisory Committee: Dr. Frank M. Raushel

Adenine deaminase (ADE) catalyzes the conversion of adenine to hypoxanthine. Mechanistic characterization of ADE from *Escherichia coli* was performed along with biophysical studies. The structure of ADE was solved from *A. tumefaciens*. The structure, along with the biochemical and biophysical characterization, enabled the elucidation of the mechanism of the deaminase reaction of ADE. Elucidation of the origin of the oxygenation reactions within ADE led to the discovery of a promiscuous catalase reaction. The diiron ADE from all tested bacterial species exhibited this unusual reaction, along with the generation of superoxide and hydroxyl radicals, the latter being responsible for the oxygenation of the protein. The residues that were identified to be oxygenated were primarily the metal binding residues implying the origin of this reaction was the binuclear iron center.

A group of bacterial enzymes that are co-localized in the same genomic operon as ADE but of unknown function were identified. The enzyme Bh0637 from *Bacillus halodurans,* a representative member of this group of enzymes was characterized. This

enzyme was shown to preferentially catalyze the deamination of epigenetic base, N-6-methyadenine.

Lastly, gram-negative bacteria have a highly conserved *phn* operon composed of 14 genes to break the C-P bond of inert alkylphosphonates. The genes *phnGHIJKLM* are absolutely critical for this activity. We discovered that methylphosphonate reacts first with MgATP to form α-D-ribose-1-methylphosphonate-5-triphosphate (RPnTP) and adenine by the action of PhnI, PhnG, PhnH and PhnL. PhnI by itself was shown to perform a novel nucleosidase reaction converting MgATP to ribose-5-triphosphate and adenine. The triphosphate moiety of RPnTP is then hydrolyzed to pyrophosphate and α-D-ribose-1-methylphosphonate-5-phosphate (PRPn) by PhnM. The carbon-phosphorus bond of PRPn is subsequently cleaved via a radical-based reaction to α-D-ribose-1,2-cyclic-phosphate-5-phosphate (PRcP) and methane in the presence of *S*-adenosyl-L-methionine by PhnJ.

# DEDICATION

I dedicate this work to my parents,

Dr. Vinita Shashikant Kamat & Dr. Shashikant Vijayanand Kamat

# ACKNOWLEDGEMENTS

I am greatly indebted to my committee chair, Dr. Frank M. Raushel, for his guidance, support and constant encouragement over the last 5 years at Texas A&M University. I am thankful to Dr. Paul A. Lindahl, Greg Holmes-Hampton and Mrinmoy Chakrabarti for all their efforts and help with EPR and Mössbauer spectroscopy, Dr. David P. Barondeau and his lab-members for the use of the glovebox in his laboratory and for valuable advice throughout my graduate studies, Dr. Howard J. Williams for help with NMR spectroscopy, GC and GC-MS analysis and Dr. Jean-Philippe Pellois for serving as a member on my thesis committee. I also thank Dr. Dao Feng Xiang and Dr. Tinh T. Nguyen for serving as my mentors in the Raushel lab, and, Dr. Shane E. Tichy and Dr. Ryan Blasé for help with mass spectrometric analysis.

I am grateful to my family and friends for showing confidence and faith in me. I also express my deepest gratitude to all members of the Raushel lab, past and present for all the help and friendship.

# TABLE OF CONTENTS

Page

# LIST OF FIGURES

FIGURE Page

FIGURE Page

FIGURE Page

# LIST OF TABLES

# CHAPTER I

## INTRODUCTION

The advent of genome sequencing technologies has led to the explosion of the number of available gene sequences from various organisms. The databases bearing protein sequences translated from the available genes seem to be increasing exponentially. In September 2011, there were in excess of 16 million protein sequences available in the UniProtKB/ TrEMBL databases (*1*). This explosion in the publicly available protein sequences is of great benefit to biology and biochemical science community. It allows better understanding of cellular metabolism, identifies newer cellular metabolic pathways and enables simple comprehension of complex cellular physiology. A thorough knowledge of these physiological pathways might allow design of antibiotics that target harmful organisms and would advance fields of medicinal chemistry, pharmacokinetics, and synthetic biology. However, with the explosion in the number of protein sequences, there remains only a small fraction of these that have been experimentally validated.

The enormous number of protein sequences in various databases can be only partially annotated even with current high throughput methodologies. As a consequence, computational methods are required to predict protein functions for the millions of proteins that have yet to be experimentally characterized. Since the 1990s, the vast majority of the protein sequences found in public databases have been annotated using computational methods alone. This raises a major issue concerning the annotation

---

This dissertation follows the style of *Biochemistry*.

accuracy. Concomitant with the exponential increase in the protein sequences in the public databases, there has been an increased sophistication in the computational methodologies. However, with the over reliance on such computational methods, there has been significant annotation errors of molecular functions of protein throughout all these databases. Since computational methods assume that an annotation is the "true" annotation, errors made by the computational annotation seem to propagate through the databases almost proportional to the rate at which sequences are deposited to these databases. In a recent study by Babbitt and co-workers (*2*), a survey of 37 enzyme superfamilies were studied as a gold standard for comparing the accuracy of functional annotations in four public databases: Two large databases Genbank NR and TrEMBL, a secondary database KEGG and a manually curated database Swiss-Prot. Their research established that there is serious problem of misannotation of molecular function within all the databases except Swiss-Prot, which is the only manually curated database of the study. **Figures 1.1 and 1.2** (adapted from PLoS Comp. Biol. 5, e1000605) emphasize the problems from this study with regards to the amidohydrolase superfamily (discussed later in this chapter).

With the degree of the misannotations as high as 40% in various public databases, there arises a need for establishing more reliable methods to establish correct molecular function annotations to proteins that are experimentally uncharacterized. In a recent review outlining the goals of the Enzyme Function Initiative in *Biochemistry* (*1*), a few strategies currently employed for protein function annotation have been enlisted:

| Superfamily | Family | E.C. No. | Family Color | Number of Sequences Analyzed | | | |
|---|---|---|---|---|---|---|---|
| | | | | Database | | | |
| | | | | NR | TrEMBL | KEGG | Swiss-Prot |
| Amidohydrolase (AH) | Cytosine deaminase | 3.5.4.1 | | 82 | 62 | 75 | 1 |
| | Adenosine deaminase | 3.5.4.4 | | 238 | 142 | 136 | 50 |
| | N-acyl-D-amino-acid deacyclase | 3.5.1.81 | | 80 | 58 | 28 | 3 |
| | L-hydantoinase | 3.5.2.2 | | 4 | 2 | 0 | 1 |
| | D-hydantoinase | 3.5.2.2 | | 46 | 34 | 10 | 0 |
| | Urease | 3.5.1.5 | | 267 | 168 | 112 | 39 |
| | Isoaspartyl dipeptidase | — | | 26 | 25 | 19 | 1 |

**Figure 1.1:** *The constituent families within the amidohydrolase superfamily*.

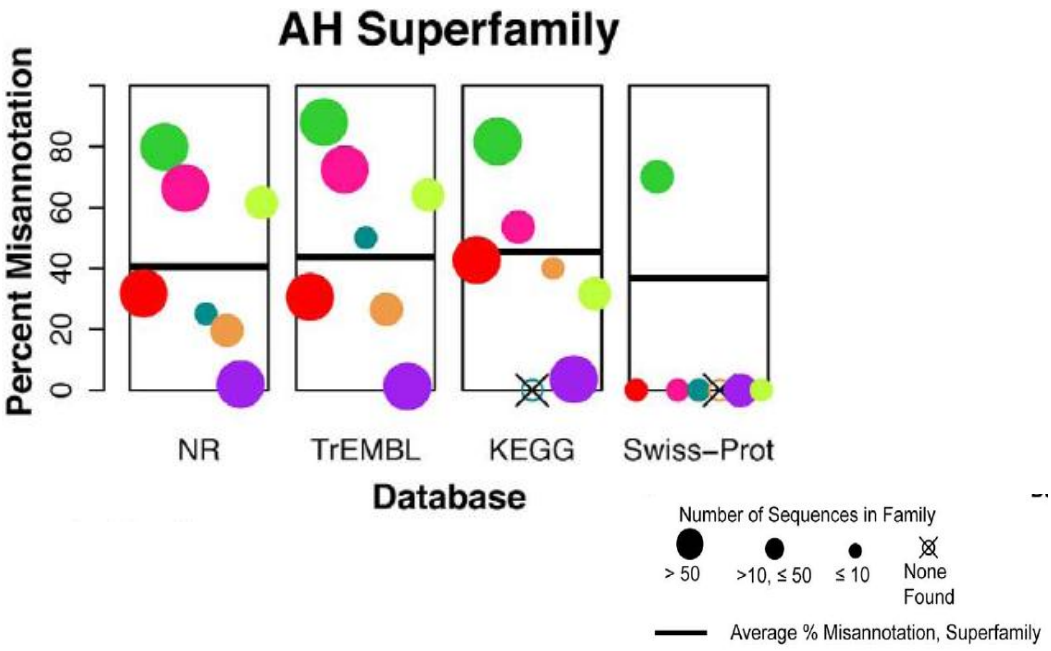


**Figure 1.2:** *Percent misannotations for the families within the amidohydrolase superfamily in the various public databases*. (from the studies of Babbitt and co-workers)

1. Sequence similarity approach: Comparing the protein sequences of orthologs and paralogs and determining the sequence specific elements, that form the basis set for establishing the constraints that determine a particular activity. This approach allows for computational approaches such as homology modeling and computational docking approaches.
2. Co-localization of genes: In prokaryotes, a particular metabolic activity is governed by the number of proteins that act simultaneously. These proteins are encoded by genes that are localized one after another at a particular location in the genome of the organism, thereby suggesting a particular molecular function in the metabolic reaction cascade.
3. Transcriptional analysis: This analysis is largely automated and is performed using chip-based technologies or RNA-sequencing technologies. These transcriptional levels indirectly infer the protein expression levels within cells thereby suggesting a metabolic molecular function under an array of conditions.
4. Gene knockout studies: Deleting genes from the genome of organisms and analyzing the phenotypes obtained from studies, suggest physiological effects of the genes in the genome. This deletion study can also be used to build up of certain cellular metabolites, which remain unused in the absence of the gene product, hinting at putative protein functions.
5. Protein-Protein interactions: Physiologically some reactions may require more than a single protein to occur. Hence *in vitro* reconstitution of such reactions may not be

possible without the partner protein. The knowledge of protein-protein interactions might help overcome such problems in annotating functions.

6. Multi-domain proteins: Some large proteins/ enzymes physiologically expressed within the organisms may contain more than one catalytic center. The two or more catalytic center performs various reactions; where in the product of one center would serve as substrate for the subsequent center. The knowledge of such systems might help in functional annotation studies.
7. The identification of upstream DNA binding motifs that might co-regulate transcription might help establish the basis of regulation of certain proteins, thereby limiting the available molecular functions for that protein.

With these strategies in mind, this study tries to annotate functions within the amidohydrolase superfamily and assess functions to the C-P lyase pathway.

The amidohydrolase superfamily (AHS) (*3*) was first identified in 1997, by Holm and Sander based on the striking structural similarities of the then available structures of phosphotriesterase (PTE) (1pta) (*4*), adenosine deaminase (ADA) (1ada replaced now with 2ada) (*5*) and urease (URE) (1krc) (*6*). This superfamily consists of a remarkable set of enzymes that catalyze hydrolytic reactions across a wide set of substrates at carbon and phosphorus centers. Members of this superfamily are involved in reactions involving metabolism of sugars, nucleic acids, amino acids, and organophosphorus esters. The most striking feature of the members of the AHS is a $(\beta/\alpha)_8$-barrel structural fold embedded within it a mononuclear or binuclear metal center, which serves as the active site for the hydrolytic reactions. The metal center of the AHS has dual function: (1) to

activate the scissile bond of the substrate for bond cleavage (2) to deprotonate the hydrolytic water molecule for the nucleophilic attack (*7*). In all cases studied to date, the nucleophilic water is activated through complexation with the metal center. Members of the AHS, have highly conserved metal binding ligands, depending on the nature of the metal center [binuclear – e.g. PTE (*4*), URE (*6*); α-mononuclear – e.g. ADA (*5*), cytosine deaminase (CDA) (*8*); β-mononuclear – e.g. N-acetyl-D-glucosamine-6-phosphate deacetylase (NagA) (*9*)]. Most metal binding residues are positioned to the C-terminal ends of the β-strands and are fine tuned to produce and deliver the nucleophilic hydroxide to the acceptor substrate in the appropriate orientation. The diversity in the reactions catalyzed and substrate specificities arise from the loops connecting the α-helices and β-strands. The eight loops are found immediately after the residues that serve as ligands that bind the metal center. These loops vary immensely in size, length, and conformation. The substrate diversity is dictated by the conformational restrictions imposed by the eight loops. As of 2011, the AHS consists of more than 12,000 non-redundant protein sequences from the approximately 1200 fully sequenced bacterial genomes as per the NCBI database. The AHS has been subclassified into 24 clusters of orthologous groups (COGs) (*10*).

The COGs database (http://www.ncbi.nlm.nih.gov/COG) has been designed as an attempt to classify proteins from completely sequenced genomes on the basis of orthology (*11*). Orthologs are direct evolutionary counterparts related by vertical descent as opposed to paralogs which are genes within the same genome related by gene duplication events. Orthologs typically have the same overall protein fold, similar

domain architectures and same or similar functions. The exception to orthologs having the same or similar functions arises in multicellular eukaryotic system. The COG database has been established so that one might transfer functional information from experimentally verified and/or characterized proteins to their homologs from organisms that are poorly studied based primarily on the similarity of the protein sequences. The organization within COGs implies one-to-many, many-to-many as well as one-to-one type relationships between protein sequences.

The COGs were constructed based on the protein sequences available from the fully sequenced genomes. This database was first established and publicly available in 2000. The rationale behind assembly of the COG database was that if a group of at least three proteins from the distant genomes are more similar to one another than they are to any other protein from the same genome they comprise an orthologous family. COGs were generated using the NCBI freeware BLAST, where in an all-by-all BLAST was performed using all the protein sequences from the completely sequenced genomes. The COGs account for a low-overall sequence similarity between sequences and thus can account for slow and fast evolving genomes. With the increasing number of fully sequenced genomes, the NCBI has developed an automated software, COGNITOR. This program gathers proteins sequences from the newly sequenced organisms and categorizes them into appropriate COGs that have been previously classified. This program also generates new COGs for protein sequences that lack homology to existing sequences beyond a certain pre-established threshold. Thus the COGs database serves as a very convenient platform in studying protein superfamilies like the AHS.

**Table 1.1**: *The COGs within the AHS*. This table also has the predicted and/or experimentally validated metal centers, and their respective annotations in the NCBI database.

| **COG number** | **Metal center** | **Annotations available in NCBI database** |
|---|---|---|
| 0044 | Binuclear | Dihydroorotase, Dihydroorotate like cyclic ring opening amidohydrolase, hydantoinase, dihydropyrimidinase, allantoinase |
| 0084 | Binuclear | TatD Mg-dependent deoxyribonuclease |
| 0402 | Mononuclear (alpha site) | Cytosine deaminase, guanine deaminase, N-formimino-L-glutamate deiminase, S-adenosylhomocysteine deaminase, N-isopropylammelide isopropylaminohydrolase, Chlorohydrolase, Selenium utilizing proteinSsnA, 8-oxoguanine deaminase, isoxanthopterin deaminase |
| 0418 | Binuclear | Dihydroorotase |
| 0613 | Trinuclear | Putative metal-dependent phosphoesterases, PHP family |

**Table 1.1** Continued

| COG number | Metal center | Annotations available in NCBI database |
|---|---|---|
| 0804 | Binuclear | Urease |
| **1001** | Binuclear | Adenine deaminase, isoaspartyl dipeptidase, enamidase |
| 1099 | Unknown | Putative metal-dependent hydrolase, TatD-related deoxyribonuclease |
| 1228 | Binuclear | Imidazolonepropionase, isoaspartyl dipeptidase, enamidase, peptidase M38, prolidase, carboxypeptidase |
| 1229 | Unknown | Formylmethanofuran dehydrogenase |
| 1387 | Trinuclear | Histidinol phosphate phosphatase, polymerase-histidinol phosphatase (PHP) domain-containing protein |
| 1574 | Unknown | Putative metal-dependent hydrolase with TIM barrel fold |
| 1735 | Binuclear | Phosphotriesterase, phosphotriesterase homology protein, phospho-sugar lactone hydrolase, aryldialkylphosphatase |
| 1816 | Mononuclear | Adenosine deaminase |

**Table 1.1** Continued

| COG number | Metal center | Annotations available in NCBI database |
|---|---|---|
| 1820 | Binuclear, Mononuclear (alpha or beta site) | N-acetyl-D-glucosamine deacetylase |
| 1831 | Unknown | TatD-related deoxyribonuclease |
| 1904 | Mononuclear (alpha site) | D-glucuronate isomerase, uronate isomerase |
| 2159 | Mononuclear (alpha site) | γ-resorcylic acid decarboxylase, α-amino-β-carboxymuconate-ε-semialdehyde decarboxylase, isoorotate decarboxylase, 5-carboxyvanillic acid |
| 2355 | Binuclear | Zn-dependent dipeptidase |
| **3454** | Mononuclear (alpha site) | Putative metal-dependent hydrolase involved in phosphonate metabolism (PhnM) |
| 3618 | Metal independent | Sugar lactonase, 2-pyrone-4,6-dicarboxylic acid hydrolase |
| 3653 | Binuclear | N-acyl-D-amino acid deacelyase |

**Table 1.1** Continued

| **COG number** | **Metal center** | **Annotations available in NCBI database** |
|---|---|---|
| 3964 | Binuclear | Putative metal-dependent hydrolase, dihydroorotase like |
| 4464 | Unknown | Capsular polysaccharide biosynthesis protein with a polymerase-histidinol phosphate (PHP) like C-terminal domain |

This study focuses on the functional annotations within COG 1001 (putative adenine deaminase) and COG 3454 (putative enzymes involved in phosphonate metabolism, PhnM), as well as annotations to functions on the carbon-phosphorus lyase pathway (C-P lyase) (both the COGs mentioned in bold red in **table 1.1**).

The COGs are better visualized using the Cytoscape software (*12*). Cytoscape is an open source bioinformatics software platform for visualizing molecular interaction networks and biological pathways. Cytoscape integrates these networks with gene annotations, gene expression profiles as well as other data. Although Cytoscape was initially designed for visualizing complex biological networks, it uses now stretch beyond biology. Additionally there are several plugins available with this software that allow for generating a myriad of networks based on different constraints. The most useful for the COG visualization is the BLAST plugin. This BLAST plugin is analogous to the NCBI blast program but it performs the same function for the sequences

incorporated into the cytoscape file being assessed, which in this case are the sequences within a COG. Several cytoscape networks can be generated by varying a single parameter called the E-value or the expectation value. The expectation value is simply a parameter that describes the number of hits within a sequence one might "expect" to see by chance when one is searching a database of defined size. The E-value takes into account both the number of matches as well as the length of the queries. The E-value decreases exponentially as the number of matches within a sequence increase. The lower the E-value, or closer the E-value to zero, the more significant the match. For a generic translation, an E-value of $10^{-70}$, implies a sequence identity between proteins of approximately 35%. Using the Cytoscape software, sequence similarity networks were made for COGs 1001 and 3454 (represented in **figures 1.3 and 1.4** respectively).

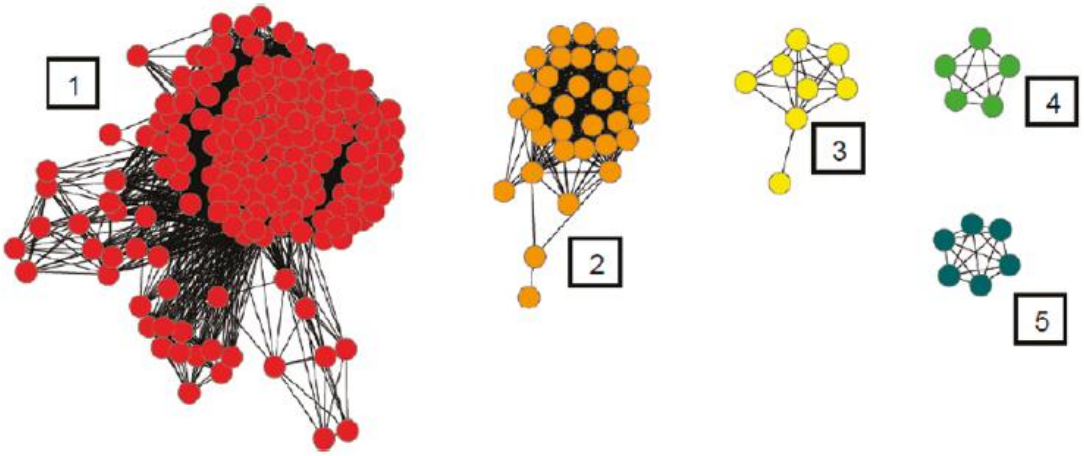


**Figure 1.3:** *Sequence similarity network of COG 1001 at an E-value of* $10^{-80}$ (sequence similarity ~ 40 %).

Groups 1 and 4 are annotated as adenine deaminases, group 2 is annotated as adenine deaminase, adenine deaminase-like, or unknown amidohydrolase, group 3 is

annotated as isoaspartyl dipeptidase and group 5 is annotated as enamidase. (This figure is adapted from J. Am. Chem. Soc. 133, 2080-2083 (2011)). More details on the functional annotations of the members within COG 1001 are presented in chapters 2, 3 and 5.

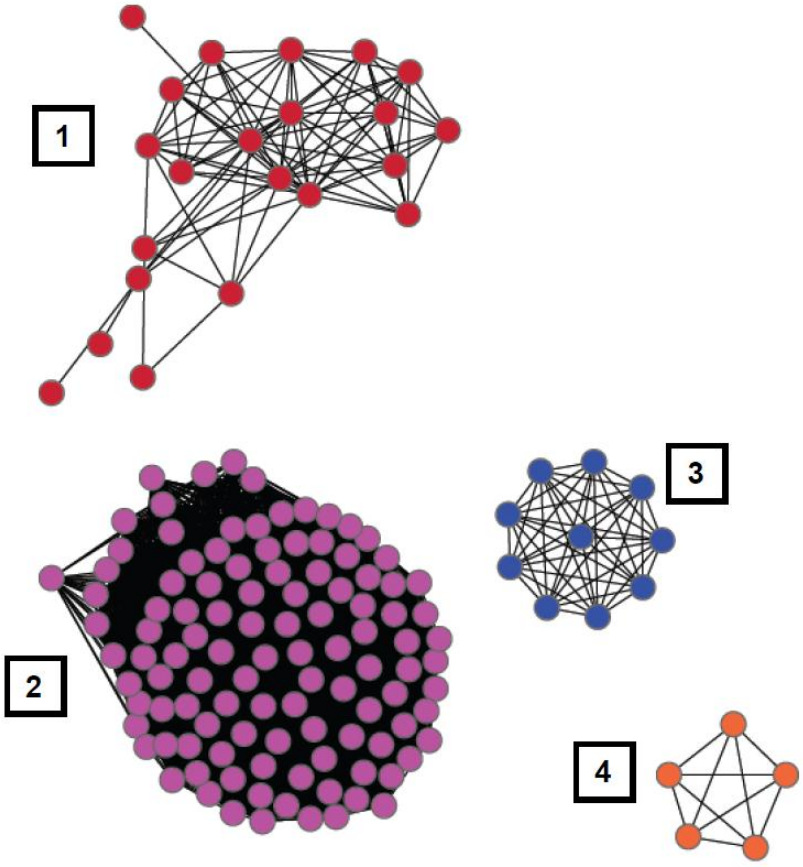


**Figure 1.4:** *Sequence similarity network of COG 3454 at an E-value of* $10^{-70}$ (sequence similarity ~ 35 %).

Groups 1-4 are annotated as metal-dependent hydrolase of the amidohydrolase superfamily involved in phosphonate metabolism (PhnM). The reason this COG splits into different groups even though all of the members are expected to perform the same

function, is due to the high constraint on the E-value. Since groups 1, 3 and 4 contain non-redundant sequences from closely related organisms, they split into smaller groups from group 2 at an E-value of $10^{-70}$. More details on the functional annotations of the members within COG 3454 are presented in chapter 6.

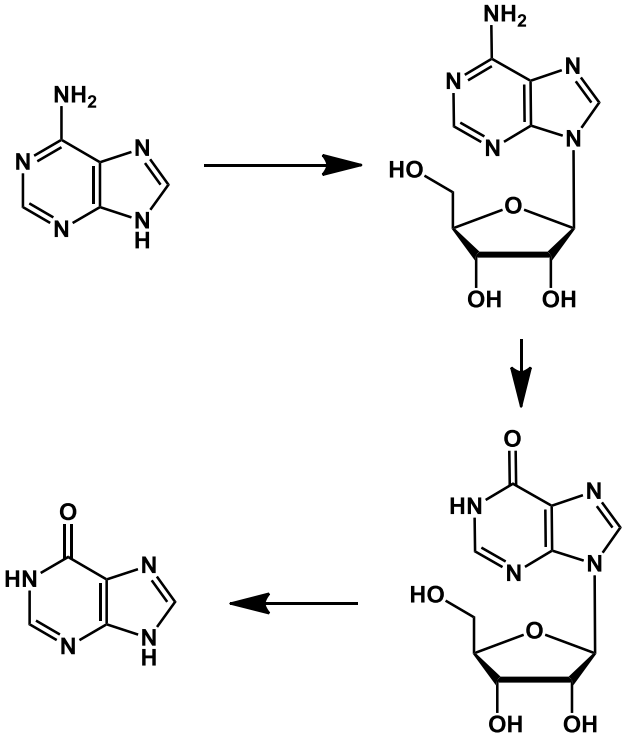


**Scheme 1.1:** Proposal by Koch and Vallee in 1959, for the 3-step deamination of adenine to hypoxanthine.

COG 1001 consists of approximately 250 non-redundant protein sequences. The majority of sequences within this COG are annotated as adenine deaminase. Adenine deaminase catalyzes the hydrolytic deamination of adenine to form hypoxanthine. Prior to genome sequencing, adenine deaminase was presumed to be non-existent. Studies from Koch and Vallee in the 1950s suggested the lack of any adenine deaminase activity in *E. coli* cell free extracts (*13*). They proposed from their studies that there were no

enzymes within the *E. coli* proteome that could attack adenine. They proposed adenine deamination to be a 3-step process, where adenine was firstly converted to adenosine, then adenosine was deaminated to inosine and finally inosine was cleaved to ribose and hypoxanthine (shown in **Scheme 1.1**). In another study by Schramm and co-workers (*14*) studying the degradation of adenylate in *E. coli*, they arrived at a similar conclusion that *E. coli* lacks adenine deaminase activity. **Scheme 1.2** shows the proposed mechanism for the degradation of adenosine 5'-monophosphate based on the enzymes identified in their study. However, with the availability of newer bacterial genomes, newer purine degradation and purine salvage pathways were discovered. In 1996, a study by Nygaard and co-workers found that certain mutants in *Bacillus subtilis* were deficient in metabolizing adenine (*15*). This study led to the discovery of the first adenine deaminase activity within bacteria. Their research suggested that adenine deaminase was the only enzyme in *B. subtilis* that could deaminate adenine, a reaction which was important for the utilization of adenine as a purine source. Their research also suggested that in some bacteria like *B. subtilis*, adenine was the only source for synthesizing guanine nucleotides via the purine salvage pathway. Their research culminated into the identification of the cryptic *ade* gene, responsible for the adenine deaminase in bacteria. Sequence analysis of the protein classified adenine deaminase as a member of the AHS and categorized it within COG 1001. The preliminary characterization of the *ade* gene product found that the adenine deaminase activity was a metal dependent activity, like the other members of the AHS. Finally in 2001-2002, two research groups found a gene in *E. coli* analogous to the *ade* gene in *B. subtilis*, the *yicP*

gene. Matsui and co-workers were the first to clone and express the *yicP* gene recombinantly and establish that it had adenine deaminase activity (*16*). Petersen and co-workers also arrived at the same conclusion, but their study was more complete (*17*). They found that adenine deaminase was part of a more silent purine salvage pathway, which is upregulated upon external abundance of purines. *Escherichia coli* auxotrophic mutants can utilize adenine as sole source of purines, and can biosynthesize guanine nucleotides from the adenine. This pathway was termed the purine salvage pathway (**scheme 1.3)**. The first step of this pathway is the deamination of adenine to hypoxanthine by adenine deaminase. Either adenine or hypoxanthine is then ribosylated by the gene product of *deoD*, purine nucleoside phosphorylase to form adenosine or inosine respectively. Adenosine is later acted upon by adenosine deaminase to form inosine. Deletion and gene knockout studies from their research have suggested that the flux of this pathway is towards adenine deaminase and that was found to be the major pathway, but there was still contribution from the adenosine deaminase pathway.

More recently the *nadA* gene from *Aspergillus nidulans,* was found to encode the adenine deaminase for that organism and was found to lie at the cross-roads to purine salvage and purine degradation pathways (*18*). In this purine catabolism pathway or the purine degradation pathway (**scheme 1.4)**, adenine is first converted to hypoxanthine by the action of adenine deaminase. Hypoxanthine is further used by xanthine dehydrogenase (also xanthine oxidase) to eventually form uric acid via a xanthine intermediate. Uric acid is then converted to allatoin by the enzyme urate oxidase.

Allatoin is then converted by allantoinase to allantoic acid, which is further transformed into urea and glyoxalic acid by allantoicase.

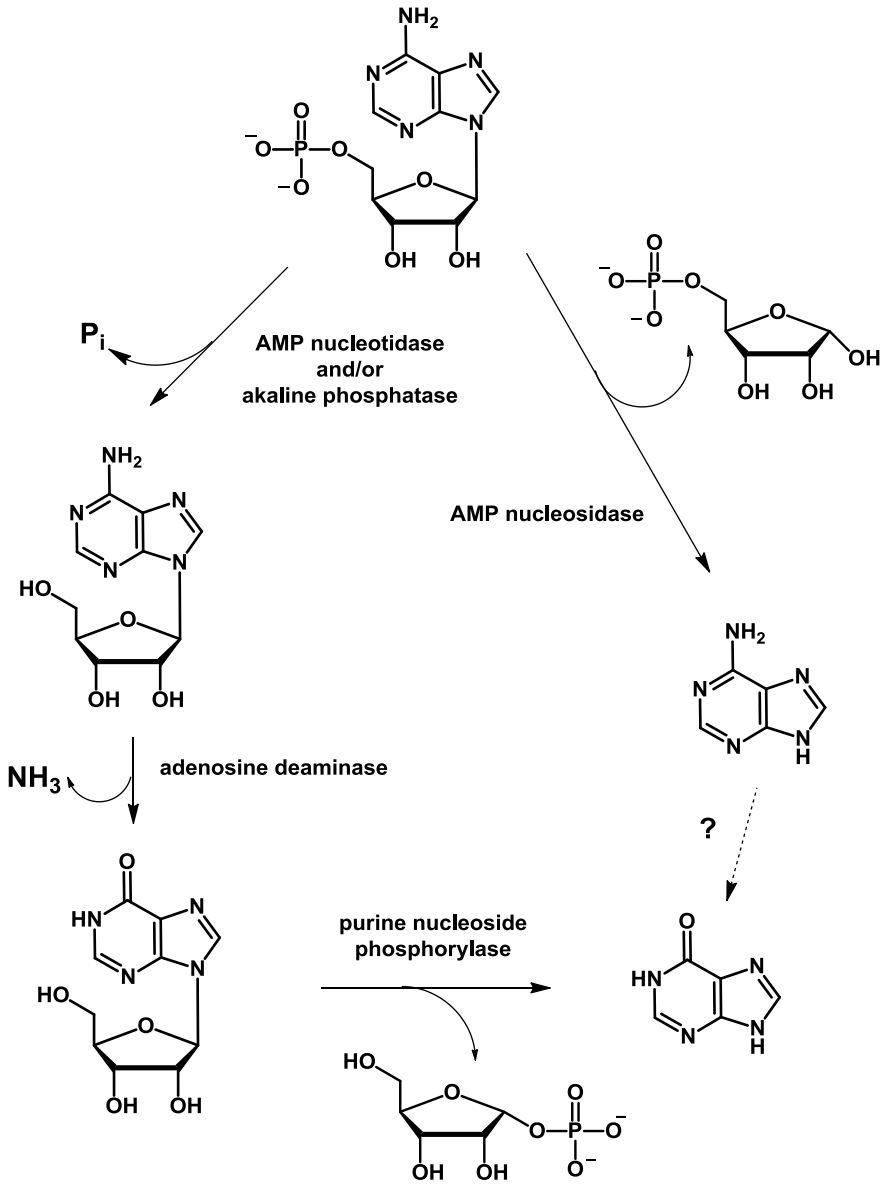


**Scheme 1.2:** The proposed adenylate degradation pathway proposed by Schramm and co-workers based on the identification of the various enzymes on the degradative pathway. Adenine deaminase activity was hypothesized but not found from the cell free extracts of *E. coli*.

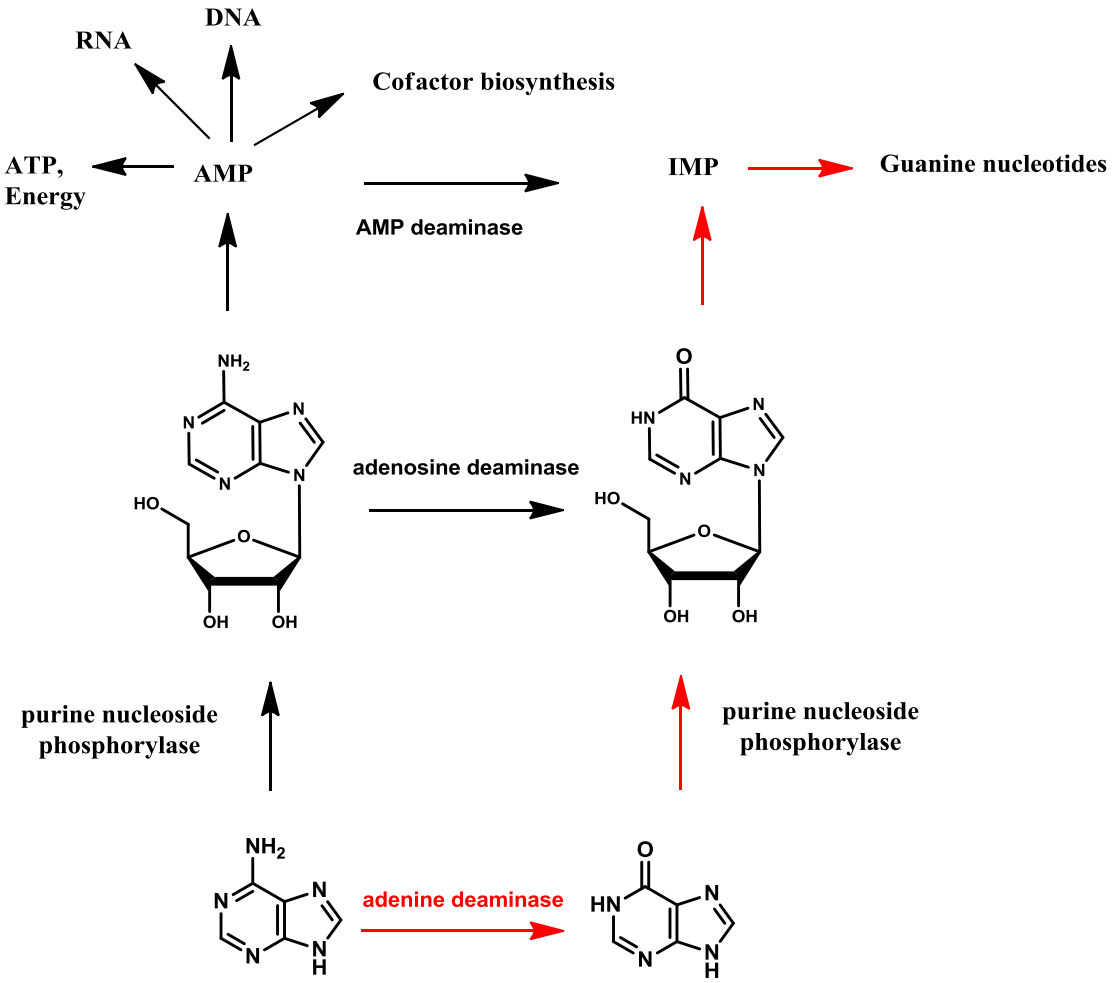


**Scheme 1.3:** The purine salvage pathway. The red arrows represent the major flux within this pathway of which the first committed step is the deamination of adenine to hypoxanthine by adenine deaminase.

**Figure 1.3** illustrates that COG 1001 consists of 5 groups within it. Groups 1 and 4 are annotated as adenine deaminase within the NCBI database. Functional and mechanistic studies have proved that groups 1 and 4 are adenine deaminases (*20*, *21*) (Details of the study available in chapters 2 and 3). The adenine deaminases clustered

within COG 1001 have been shown to be the only members with the AHS that perform a deamination reaction with a binuclear metal center.

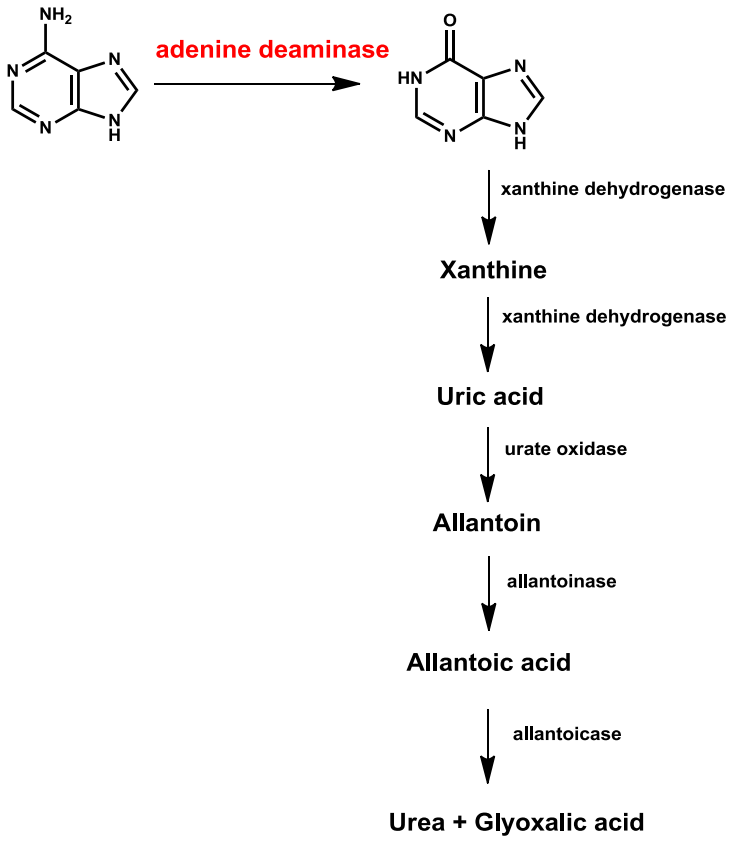


**Scheme 1.4:** The purine catabolism pathway (*19*).

All other deaminases have a mononuclear metal center. Also unique to adenine deaminases from COG 1001 is that they were shown to perform an aberrant catalase type reaction also catalyzing the disproportionation of hydrogen peroxide to oxygen and water, with the production of reactive oxygen species, superoxide and hydroxyl radical, during the catalase reaction (*21*). Based on the crystal structures, the identification of the critical residues in catalysis and the conservation of these residues, groups 3 and 5 were annotated as isoaspartyl dipeptidase (*22*) and enamidase (*23*) respectively. Within COG

1001 is a group of 32 bacterial protein sequences that are annotated as adenine deaminase, adenine deaminase like, or amidohydrolase of unknown function. Functional annotation studies have found that these protein sequences preferentially catalyze the deamination of the epigenetic base N-6-methyladenine (*24*) (Details of this study available in chapter 5). Thus COG 1001 has now been fully annotated for molecular functions to the corresponding protein sequences within the COG.

**Figure 1.4** represents all the non-redundant protein sequences within COG 3454. This COG contains close to 180 non-redundant protein sequences. All the members of this COG contain enzymes classified as PhnM, a member of the carbon-phosphorus lyase (C-P lyase) pathway, a pathway that metabolism phosphonates. PhnM is annotated within the NCBI as a metal-dependent hydrolase involved in phosphonate metabolism. At an expectatation value of $10^{-70}$ (~ 35 % sequence identity), COG 3454 is divided into 4 distinct groups. Group 1 consists of 22 non-redundant protein sequences arising from phylogenetically related α-proteobacterium species, living in marine environment or involved in nitrogen fixation. Group 3 consists of 10 non-redundant protein sequences coming solely from closely related *Rhizobium* species, a set bacterial species that are nitrogen fixing and found largely within the root nodules of leguminous plants. Group 4 consists of 5 protein sequences that are non-redundant from *Roseobacter* species, another α-proteobacterial species first isolated from marine algae. Their name arises from their ability to biosynthesize pink-pigment bacteriochlorophyll-A. Group 2 consists of an array of closely related non-redundant protein sequences coming from proteobacteria. All the 180 or so sequences from this COG fall within the highly

conserved C-P lyase pathway amongst proteobacteria and there appears to be a single function arising from the members within this COG, the putative hydrolytic function of PhnM. Hence the knowledge of the C-P lyase pathway as a whole would help elucidate the function of the COG 3454.

Carbon, nitrogen, oxygen, and phosphorus are essential elements required by all living organisms for survival. Of these elements, phosphorus is incorporated as a derivative of phosphate where it is an integral component of nucleic acids, carbohydrates, and phospholipids. Phosphorus has many roles in metabolic pathways and cell signaling. Most organisms have evolved to obtain phosphorus, as phosphate, directly from the environment. In the biosphere, phosphorus is bioavailable in its highest oxidation state (+5) as inorganic phosphate (Pi). However, under cases of Pi starvation most proteobacteria including *Escherichia coli*, have developed pathways to scavenge other forms of phosphorus from the external environment. In *E. coli* there exists a two component regulator system called the *Pho* system that regulates and mobilizes phosphorus sources across membranes and within cells. The genes associated with this regulatory system are PhoR and PhoB (*25*). The *Pho* system also broadly called the *Pho regulon* consisted of 31 validated genes organized in nine transcriptional units as of 2011. More genes and transcriptional units as expected to be governed by the *Pho regulon* (*26*). One such phosphorus source regulated by the *Pho regulon* is phosphonates. Phosphonates are organophosphorus compounds that contain a one C-P bond. This bond is chemically inert and hydrolytically stable. Phosphonates are ubiquitous and include antibiotics (fosfomycin and phosphonothrixin), herbicides

(glyphosate) and industrial detergent additives (amino-trimethylene phosphonate) (**Scheme 1.5)**. It is estimated that more than 20,000 tons of phosphonates are released annually in the US alone from herbicide and detergent wastes (*27, 28*). The large quantities of phosphonates that are being deposited into the environment suggest that there needs to be a greater understanding of how these compounds are metabolized and degraded. Biogenic phosphonates are found mainly in primitive life forms. They usually exist as 2-aminoethylphosphonic acid and 2-amino-3-phosphonoproionic acid, which are integral components of the membrane phosphonolipids. The presence of phosphonates within the lipid membranes confers rigidity to the membranes as well as protects them from enzymatic degradation from enzymes like phosphatases. The C-P bond of phosphonate is also resistant to photolysis and thereby confers protection against light as well for these primitive organisms (*29*).

All known biological sources of phosphonates arise from a single reaction converting phosphate to phosphonate. The reaction is catalyzed by the enzyme phosphoenolpyruvate (PEP) mutase, where there is an intramolecular transfer of the phosphoryl group from PEP to form phosphonopyruvate. PEP is a product readily available from the glycolysis reaction cascade. The phosphoryl transfer reaction catalyzed by PEP mutase, is an equilibrium reaction, with the equilibrium highly favoring the C-O-P bond of PEP and not the C-P bond of phosphonopyruvate (**Scheme 1.6**). However, most proteobacteria requiring phosphonates couple the reaction of PEP mutase to an enzyme phosphonopyruvate decarboxylase and drive the equilibrium towards the synthesis of phosphonates. The enzyme phosphonopyruvate decarboxylase

irreversibly converts phosphonopyruvate to phosphonoacetate and carbon dioxide (**Scheme 1.6**). Phosphoacetate is the first useful phosphonate metabolite available to cells from PEP (*30*).

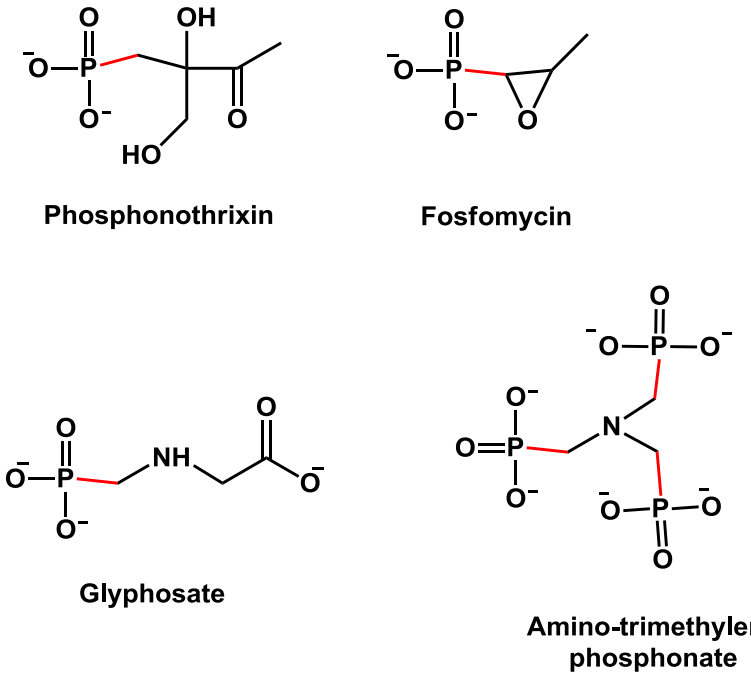


**Scheme 1.5:** Some of the more common phosphonates. The bonds highlighted in red in the characteristic C-P bond of phosphonates.

Phosphonate biosynthesis has just a single reaction, however depending on the nature of the phosphonates, microorganisms have developed several ways to break the C-P bond of phosphonates. Given the chemically inert, hydrolytically stable nature of phosphonate, there are two primary classes of enzymes that break C-P bonds: 1. Phosphonate hydrolases. 2. C-P lyases

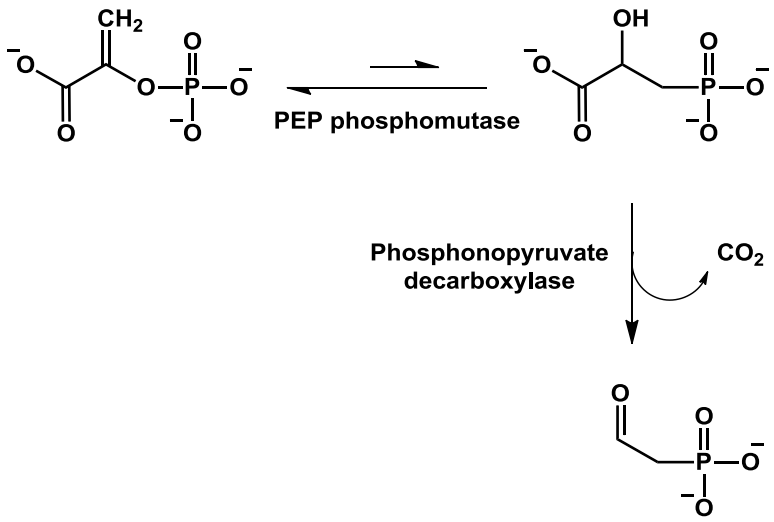


**Scheme 1.6:** Biogenic synthesis of phosphonoacetate from phosphoenol pyruvate (PEP), the central reaction for all phosphonate biosynthesis.

Phosphonate hydrolases are the more extensively studied class of enzymes of the two generic classes of enzymes breaking a C-P bond. These hydrolases are highly specific for their substrates phosphonoacetate, phosphonopyruvate or phosphonoacetaldehyde. All the hydrolytic reactions proceed through a similar mechanism. All the substrates listed above: phosphonoacetate, phosphonopyruvate and phosphonoacetaldehyde have a β-carbonyl group next to the C-P bond. This group is electron withdrawing in nature and allows for the heterolytic cleavage of the C-P bond (*31*) (**Scheme 1.7**). Phosphonate hydrolases are expressed by organisms under normal growth and are part of the transcriptional units of the global *Pho regulon*.

The second class of enzymes involved in breaking a C-P bond is called C-P lyase. C-P lyases enzymes conserved across all the proteobacteria and are quite promiscuous and enigmatic in their activity. These enzymes can cleave of unactivated alkyl and phenyl phosphonates to their corresponding alkanes and benzene products

(**Scheme 1.8**). In *E. coli*, one of the nine transcriptional units regulated by the *Pho regulon* encodes a 14-cistronic operon called the *Phn* operon. This operon encodes all of the components of the C-P lyase pathway. The C-P lyase pathway is involved in the cellular uptake and metabolism of phosphonates, and is expressed strictly under limiting environmental phosphorus conditions.

The C-P lyase is the most widespread amongst bacterial genomes of all the enzymes capable of catabolizing phosphonates. The *Phn* operon consists of 14 genes responsible for this activity in *E. coli*.

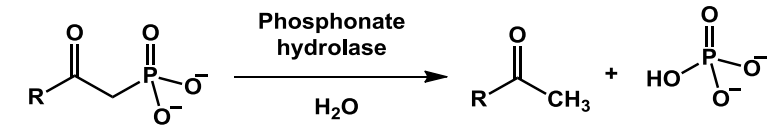


**Scheme 1.7:** The reaction catalyzed by the phosphonate hydrolase enzymes for their specific substrates. When R = H, susbtrate: phosphonoacetaldehyde, when R = OH, susbtrate: phosphonoacetate, and when R = COOH, susbtrate: phosphonopyruvate.

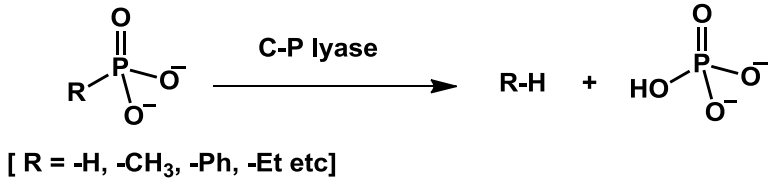


**Scheme 1.8:** The reaction catalyzed by the C-P lyase pathway.

This pathway uses unactivated phosphonates like methylphosphonate, ethylphosphonate, phenylphosphonate etc. and forms the corresponding alkane like methane, ethane and benzene (phenyl product) and phosphate.

Of the 14 genes, *phnC, phnD and phnE* constitute putative protein binding phosphonate transporters, based on sequence analysis and phenotype studies of transposon mutants (*32, 33*). The gene *phnF* was found to be a global regulator of the C-P lyase pathway. The genes *phnG, phnH, phnI, phnJ, phnK, phnL* and *phnM* were found to constitute the minimal catalytic set for the C-P activity, whereas the genes *phnN, phnO* and *phnP* were found to encode proteins that were responsible for metabolizing the products and intermediates of this pathway (*32, 33*). Of the genes absolutely essential for the C-P lyase activity, PhnM is a member of the AHS and classified within COG 3454 as described earlier. Chapter 6 of this study describes studies that functionally annotate of the essential genes of the C-P lyase pathway and identify in turn a function for COG 3454.

# CHAPTER II

# CATALYTIC MECHANISM AND THREE DIMENSIONAL STRUCTURE OF ADENINE DEAMINASE*

Adenine deaminase (ADE) catalyzes the conversion of adenine to hypoxanthine and ammonia. The enzyme isolated from *Escherichia coli* using standard expression conditions was largely inactive towards the deamination of adenine ($k_{cat}$ ~2 $s^{-1}$). When iron was sequestered with a metal chelator (2,2'-dipyridyl) and the growth medium was supplemented with $Mn^{2+}$ prior to induction, the purified enzyme was substantially more active for the deamination of adenine with values of $k_{cat}$ and $k_{cat}/K_m$ of 200 $s^{-1}$ and 5 x $10^5$ $M^{-1}s^{-1}$, respectively. The apo-enzyme was prepared and reconstituted with $Fe^{2+}$, $Zn^{2+}$, or $Mn^{2+}$. In each case, two enzyme-equivalents of metal were necessary for reconstitution of the deaminase activity. This work provides the first example of any member within the deaminase sub-family of the amidohydrolase superfamily (AHS) to utilize a binuclear metal center for the catalysis of a deamination reaction. [$Fe^{II}/Fe^{II}$]-ADE was oxidized to [$Fe^{III}/Fe^{III}$]-ADE with ferricyanide with inactivation of the deaminase activity.

---

*Reprinted with permission from "Catalytic mechanism and three-dimnsional structure of adenine deaminase" by S. S. Kamat, A. Bagaria, D. Kumaran, G. P. Holmes-Hampton, H. Fan, A. Sali, J. M. Sauder, S. K. Burley, P. A. Lindahl, S. Swaminathan and F. M. Raushel, *Biochemistry* 50, 1917-1927, 2011. 

Reducing [$Fe^{III}/Fe^{III}$]-ADE with dithionite restored the deaminase activity and thus the di-ferrous form of the enzyme is essential for catalytic activity. No evidence for spin-coupling between metal ions was evident by EPR or Mössbauer spectroscopies. The three-dimensional structure of adenine deaminase from *Agrobacterium tumefaciens* (Atu4426) was determined by X-ray crystallography at 2.2 Å resolution and adenine was modeled into the active site based on homology to other members of the amidohydrolase superfamily. Based on the model of the adenine-ADE complex and subsequent mutagenesis experiments, the roles for each of the highly conserved residues were proposed. Solvent isotope effects, pH rate profiles and solvent viscosity were utilized to propose a chemical reaction mechanism and the identity of the rate limiting steps.

INTRODUCTION

Adenine deaminase (ADE) catalyzes the conversion of adenine to hypoxanthine and ammonia as shown in **Scheme 2.1** (*16, 17, 20*). ADE is part of the purine degradation pathway where hypoxanthine is subsequently oxidized to uric acid by xanthine oxidase via a xanthine intermediate (*18, 19*). This enzyme also participates in the purine salvage pathway for the synthesis of guanine nucleotides (*17*). ADE from *Escherichia coli* is a member of the amidohydrolase superfamily (AHS) and is clustered within cog1001 in the NCBI database (*3, 7*). Enzymes capable of deaminating adenosine, guanine, cytosine, and *S*-adenosyl homocysteine (SAH) are also found within the AHS. All structurally characterized deaminases in the AHS have a distorted $(\beta/\alpha)_8$-barrel structural fold and have a single divalent cation in the active site that is utilized for the activation of the nucleophilic water molecule (*7*). For these enzymes, the lone

divalent metal ion is coordinated to two histidines at the end of β-strand 1, another histidine at the end of β-strand 5, an aspartate at the end of β-strand 8 and a water molecule. A triad of conserved active site residues catalyzes proton transfers from the metal ligated water molecule to the reaction products, ammonia and hypoxanthine (*7, 34, 35*). These three residues include a glutamate in the loop that follows β-strand 5 (HxxE motif), a histidine at the C-terminal end of β-strand 6 and the aspartate at the C-terminus of β-strand 8.

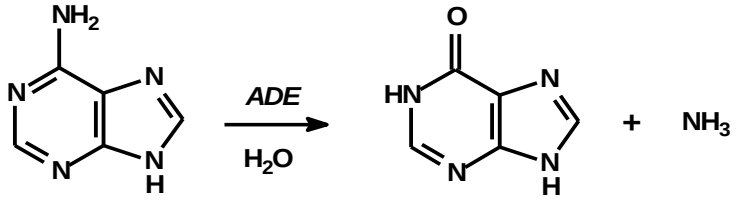


**Scheme 2.1:** Reaction catalyzed by adenine deaminase

Based on amino acid sequence alignments, the putative adenine deaminases found within cog1001 are predicted to bind two divalent cations in the active site to form a binuclear metal center structurally similar to those found in phosphotriesterase (*4, 36, 37*), urease (*6*) and iso-aspartyl dipeptidase (*22, 38*). In the known adenine deaminases from cog1001, there are four invariant histidine residues at the C-terminal ends of β-strands 1, 5 and 6, and an aspartate at the C-terminus of β-strand 8. A conserved glutamate residue that resides at the end of β-strand 4 is positioned to bridge the two divalent cations. For *E. coli* ADE, these residues are predicted to be His-90, His-92, Glu-185, His-214, His-235, and Asp-284. Adenine deaminase does not have the signature HxxE motif at the end of β-strand 5 that is conserved in all of the other known deaminases in the amidohydrolase superfamily (*7*). Therefore, the mechanism for the

deamination of adenine by ADE is expected to be somewhat different than the reactions catalyzed by adenosine, cytosine, and guanine deaminases.

Previous attempts to isolate and characterize ADE from *E. coli* using standard expression and purification protocols have shown that slightly more active enzyme could be obtained when the growth medium was supplemented with $Mn^{2+}$ (*16, 17, 20*). However, the specific activity of the purified enzyme was substantially lower when compared with the turnover numbers exhibited by other deaminases from the amidohydrolase superfamily (*16, 17, 20*). The turnover number for the deamination of adenine by ADE from *E. coli* was approximately 2 $s^{-1}$ and the enzyme isolated with a mixture of zinc, manganese and iron in the active site. Presented in this chapter is a novel iron-free expression and purification protocol resulting in the isolation of adenine deaminase with a turnover number of approximately 200 $s^{-1}$. The three dimensional structure of ADE from *Agrobacterium tumefaciens* (Atu4426) and proposed a novel catalytic reaction mechanism for the deamination of adenine is also proposed.

MATERIALS AND METHODS

*Materials.* All chemicals were purchased from Sigma-Aldrich unless otherwise stated. The genomic DNA for *E. coli str.* K12 substr. MG1655 was purchased from ATCC. *E. coli* BL21(DE3) and XL1-blue competent cells were obtained from Stratagene (Agilent). The expression vector pET30(+) and *Pfx* DNA polymerase were purchased from Invitrogen. All oligonucleotides were obtained from the Integrated DNA Technologies (IDT) from the Gene Technology Lab at Texas A&M University (GTL-TAMU).

*Cloning of Adenine Deaminase from E. coli.* The DNA sequence for adenine deaminase from *E. coli* K12 was cloned (gi|16131535). The PCR product was amplified utilizing the primer pair 5'-AGGCTATTAATGAATAATTCTATTAACCATAAATTTCATCACAT-3' and 5'-CCGGAATTCTTATTCCGTGACTTCCAGCGTAGTGAAG-3'. *Ase*I and *EcoR*I restriction sites were introduced into the forward and the reverse primers, respectively. The PCR product was purified with a PCR cleanup system (Promega), digested with *Ase*I and *EcoR*I, and ligated into a pET30a(+) vector that was previously digested with *Ase*I and *EcoR*I. The cloned gene fragment was sequenced at the GTL-TAMU to verify the fidelity of the PCR amplification.

*Standard Protein Expression and Purification of E. coli ADE*. The recombinant plasmid bearing the gene for adenine deaminase was transformed into *E. coli* BL21 (DE3) competent cells by electroporation. A single colony was grown overnight at 37 $^{o}$C in 5 mL of LB medium containing 50 μg/mL kanamycin. Five mL aliquots were used to inoculate 6 L of the same medium. The cell cultures were grown at 37 $^{o}$C and induced with 0.5 mM isopropyl-β-thiogalactoside (IPTG) when the $A_{600}$ reached ~ 0.6 in the presence of 1.0 mM $MnCl_2$. Protein expression was confirmed by SDS-PAGE. The cells were centrifuged and then resuspended in 50 mM HEPES, pH 7.5, containing 0.1 mg/mL phenylmethylsulfonyl fluoride (PMSF) and lysed by sonication. The soluble proteins were separated from the cell debris by centrifugation at 12,000 x g for 15 minutes at 4 $^{o}$C. The nucleic acids were removed by dropwise addition of 2% w/v protamine sulfate. After centrifugation, solid ammonium sulfate was added to 60%

saturation to the supernatant solution. The precipitated protein was dissolved in buffer and then applied to a High Load 26/60 Superdex 200 prep grade gel filtration column (GE HealthCare). The active fractions were pooled and loaded onto a ResourceQ (anion exchange) column (6 mL) and eluted with a gradient of NaCl in 20 mM HEPES, pH 7.5. The identity of the purified protein was verified by N-terminal amino acid sequencing at the Protein Chemistry Lab, Texas A&M University (PCL-TAMU).

*Iron-Free Protein Expression of E. coli ADE.* The iron content of our LB medium (Research Products International Corp.) was determined to be approximately 36 μM by inductively coupled plasma mass spectrometry (ICP-MS). The iron-specific chelator 2,2'-dipyridyl was used to remove this metal during protein expression. A single colony was grown overnight at 37 $^{o}$C in 5 mL of LB medium containing 50 μg/mL kanamycin and then added to 6 L of the same medium. When the $A_{600}$ reached 0.15 – 0.20, 50 μM 2,2'-dipyridyl was added to sequester the iron, followed by the addition of 0.5 mM IPTG and 1.0 mM $MnCl_2$ when the $A_{600}$ was ~ 0.6.

*Cloning, Expression and Purification of Atu4426.* The gene (*Atu4426*) for adenine deaminase (gi|15890557) was obtained from *A. tumefaciens* genomic DNA (ATCC 33970D) (ADE from *A. tumefaciens* is abbreviated as Atu4426) and cloned, expressed and purified by the protein production team at New York Structural GenomiX Research Consortium (NYSGXRC) (*20*). The expression plasmid is available through the PSI Material Repository (dnasu.asu.org) as NYSGXRC clone ID 9206a1BCt6p1, and other experimental information is available in the Protein Expression Purification Crystallization Database (PepcDB.pdb.org) as TargetID "NYSGXRC-9206a" (*20*).

*Protein and Metal Analysis.* The concentration of ADE from *E. coli* was estimated by measuring the absorbance at 280 nm using an extinction coefficient of 42,000 $M^{-1}$ $cm^{-1}$ (*39*). The metal content of the protein was determined by ICP-MS (*40*). The protein samples for ICP-MS were digested with $HNO_3$ by refluxing for ~45 minutes to prevent protein precipitation during the measurement. The protein concentration was adjusted to ~1.0 μM with 1% v/v $HNO_3$.

*Preparation and Reconstitution of Apo-Enzyme.* Apo-ADE was prepared by dialyzing the enzyme purified from the iron-free expression protocol against 10 mM 1,10-phenanthroline in 20 mM HEPES, pH 7.0, for 36 hours with two changes of buffer. The apo-enzyme was separated from 1,10-phenanthroline using a PD-10 column (GE HealthCare) and then reconstituted with various amounts of $Mn^{2+}$, $Zn^{2+}$ or $Fe^{2+}$ at 4 $^{o}$C for 48 hours. In these experiments, 1.0 μM apo-ADE was titrated with 0-5 μM of the above mentioned metals. Iron was added anaerobically to prevent air oxidation. All samples were passed through a PD-10 column to remove any unbound metal and then assayed for adenine deaminase activity. The same experiment was performed with Atu4426 to verify the metal requirement for this enzyme.

*Adenine Deaminase Activity.* The deamination of adenine was determined using a coupled assay with glutamate dehydrogenase (GDH). Formation of ammonia was followed at 340 nm using a SpectraMax-340 UV-vis spectrophotometer in the presence of 20 mM HEPES, pH 7.5, 0.15 mM NADH, 25 mM α-ketoglutarate, 4 μg/mL glutamate dehydrogenase (GDH) and various concentrations of adenine in a final volume of 0.25 or 1.0 mL (*41*). All the assays were carried out at 30 $^{o}$C.

*Crystallization and Structure Determination of Atu4426*. The crystal structure of Atu4426 was solved by the Swaminathan laboratory from the Biology department, Brookhaven National Laboratory, NY. The details for the crystallization, refienement and structure elucidation are reported (*20*). The atomic coordinates and structure factor amplitudes were deposited in the Protein Data Bank (PDB ID: 3nqb).

*Model for Binding of Adenine to Atu4426.* Since all the attempts to crystallize Atu4426 with adenine, hypoxanthine and 6-chloropurine failed, docking was employed as the means to develop a model for binding of adenine in the active site of Atu4426. The ligand-free structure of Atu4426 (chain A) was used for structural modeling (*20*). The modeling studies were performed by the Sali laboratory at the Department of Pharmaceutical Sciences, University of California, San Francisco.

*Oxidation and Reduction of Iron Center*. The binuclear metal center of $[Fe^{II}/Fe^{II}]$-ADE (100 μM) was oxidized with varying amounts of potassium ferricyanide ranging from 25 to 500 μM at room temperature in 20 mM HEPES, pH 7.5. Aliquots of the enzyme were assayed for catalytic activity after 3 hours. $[Fe^{III}/Fe^{III}]$-ADE was reduced to $[Fe^{II}/Fe^{II}]$-ADE through the anaerobic addition of solid sodium dithionite and the deaminase activity was determined after 20, 40, and 60 minutes of incubation. As a control, 2.0 equivalents of ferricyanide (40 μM) were added to $[Mn^{II}/Mn^{II}]$-ADE (20 μM).

*Mössbauer and EPR Spectroscopy.* $[Fe^{II}/Fe^{II}]$-ADE was prepared for Mössbauer spectroscopy by reconstituting apo-ADE (300 μM) with 2 equivalents of $^{57}FeCl_3$ (IsoFlex USA) and 2.0 equivalents of ascorbic acid at 4 $^{o}$C for 48 hours at pH 7.0 in a

volume of 1.2 mL. Samples were passed through a PD-10 column to remove excess metal and then concentrated by ultrafiltration with a YM30 (Millipore) membrane. The spectra were collected with a MS4 WRC spectrometer (SEE Co, Edina, MN) at either 5 K or 100 K and then analyzed using the WMOSS software package provided by the manufacturer. Chemical shifts were calibrated relative to Fe metal at 298 K. EPR spectra were collected on an EMX X-band spectrometer in perpendicular mode equipped with an Oxford ER910A cryostat (Bruker Biospin, Billerica, MA). Spin concentrations were determined using a 1.0 mM CuEDTA standard. For the g = 4.3 signal, double integral values were multiplied by 3 to account for the total spin population of all three doublet levels of the S = 5/2 manifold. The Mössbauer and EPR studies were performed in the Lindahl laboratory at Texas A&M University.

*Mutation of ADE from E. coli.* All single site mutations were constructed using the standard QuikChange PCR protocol according to the manufacturer's instructions. All of the mutants were expressed and purified using the iron-free expression protocol. The apo-proteins (20 μM) were purified as described earlier and reconstituted with 2.0 enzyme equivalents of $Fe^{2+}$ (40 μM) under anaerobic conditions. Excess metal was removed using a PD-10 column and the metal content was measured using ICP-MS. In an attempt to rescue the loss of activity of the E185G mutant, various concentrations of propionic acid (0.5 – 10 mM) and $Mn^{2+}$ (0.1-1.0 mM) were added to the apo-E185G mutant and allowed to incubate for 6 hours in 200 mM HEPES, pH 7.5, at 4 $^{o}$C.

*pH-Rate Profiles.* The dependence of $k_{cat}$ and $k_{cat}/K_m$ as a function of pH was determined for the $Mn^{2+}$, $Zn^{2+}$ and $Fe^{2+}$ reconstituted ADE over the pH range of 6.0-9.0.

The buffers used for this study were 20 mM MES (pH 6.0-6.6), 20 mM HEPES (6.8-8.2) and 20 mM CHES (pH 8.4-9.0). The pH values of the final solutions were measured before and after the completion of the assays. Above pH 9, the coupling system was inefficient and below pH 6, ADE was unstable. Equivalent profiles were also obtained in 100% $D_2O$.

*Solvent Viscosity Effects.* The effects of solvent viscosity on $k_{cat}$ and $k_{cat}/K_m$ of Mn/Mn-ADE were determined at pH 7.5 with 50 mM HEPES at 30 $^oC$. The viscosity was varied by increasing the concentration of sucrose (*42*).

*Inhibition of ADE by 6-Chloropurine.* The inhibition of ADE by 6-chloropurine was evaluated by incubating Mn/Mn-ADE (4 nM) with varying concentrations of 6-chloropurine at 30 $^oC$ for 1 hour. Aliquots were removed and assayed for the deamination of 5.0 mM adenine at pH 7.5 at 30 $^oC$.

*Data Analysis.* Initial velocity data were fit to **equation 2.1** using the non-linear least squares fitting program SigmaPlot 9.0 where $v$ is the initial velocity, [A] is the substrate concentration, $E_t$ is the total enzyme concentration, $k_{cat}$ is the turnover number and $K_m$ is the Michaelis constant. For pH rate profiles, **equation 2.2** was used to fit the bell-shaped pH profiles to determine values of $K_a$ and $K_b$, for the ionization of groups at low and high pH values respectively. In **equation 2.2**, c is the maximum value for either $k_{cat}$ or $k_{cat}/K_m$, depending on the fit, and H is the proton concentration. The tight binding inhibition constant of 6-chloropurine to ADE was obtained using **equation 2.3** (*43*). In this equation, $E_t$ is the total enzyme concentration, $I$ is the inhibitor concentration, $v_o$ is

the activity of the enzyme in the absence of inhibitor, and $v_i$ is the activity of the enzyme in the presence of varying inhibitor concentrations.

$$v / E_t = k_{cat} [A] / (K_m + [A]) \quad \textbf{(Equation 2.1)}$$

$$\log y = \log(c/(1 + [H]/K_a + K_b/[H])) \quad \textbf{(Equation 2.2)}$$

$$v_i/v_o = ([E_t] - K_i - [I] + (([I] + K_i - [E_t])^2 + (4K_i[E_t]))^{1/2})/(2[E_t]) \quad \textbf{(Equation 2.3)}$$

RESULTS

*Purification and Properties of ADE.* ADE from *E. coli* was purified to apparent homogeneity. The enzyme purified in the presence and absence of added $Mn^{2+}$ displayed similar kinetic properties and heterogeneous metal content. The kinetic constants for the enzyme purified without $Mn^{2+}$ supplementation were 1.6 ± 0.2 $s^{-1}$, 0.81 ± 0.08 mM and (2.0 ± 0.2) x $10^3$ $M^{-1}$ $s^{-1}$ for the values of $k_{cat}$, $K_m$, and $k_{cat}/K_m$, respectively. The metal content of this enzyme contained 0.25 ± 0.05 equivalents of Fe and 0.20 ± 0.03 equivalents of Zn per subunit. The kinetic constants for the enzyme purified with $Mn^{2+}$ supplementation in the growth medium were 2.0 ± 0.3 $s^{-1}$, 0.76 ± 0.1 mM and (2.5 ± 0.2) x $10^3$ $M^{-1}$ $s^{-1}$ for the values of $k_{cat}$, $K_m$, and $k_{cat}/K_m$, respectively. The metal content of this sample was 0.31 ± 0.04 equivalents Fe and 0.24 ± 0.03 equivalents Mn per subunit. The kinetic constants for Atu4426 purified using the standard expression protocol were 1.8 ± 0.2 $s^{-1}$, 0.40 ± 0.08 mM and (4.5 ± 0.4) x $10^3$ $M^{-1}$ $s^{-1}$ for $k_{cat}$, $K_m$, and $k_{cat}/K_m$, respectively. The metal content for Atu4426 purified using

standard protocols was 0.80 ± 0.05 equivalents of Fe and 0.41 ± 0.05 equivalents of Mn per subunit.

*Sequestration of Iron.* The addition of 50 μM 2, 2'-dipyridyl to the growth medium was utilized to sequester the iron at the time of induction. The cells were supplemented with Mn and the purified enzyme contained 2.0 ± 0.1 equivalents of Mn per protein subunit. The kinetic constants for the deamination of adenine by *E. coli* ADE were determined to be 200 ± 5 $s^{-1}$, 0.40 ± 0.04 mM, and (5 ± 0.4) x $10^5$ $M^{-1}$ $s^{-1}$ for $k_{cat}$, $K_m$, and $k_{cat}/K_m$, respectively. The kinetic constants for the deamination of adenine by Atu4426 were determined to be 155 ± 5 $s^{-1}$, 0.32 ± 0.04 mM, and (4.8 ± 0.4) x $10^5$ $M^{-1}$ $s^{-1}$ for $k_{cat}$, $K_m$, and $k_{cat}/K_m$, respectively. The iron free expression protocol yielded a protein with 2.4 ± 0.1 equivalents of Mn per protein subunit for Atu4426. All of the remaining experiments were conducted with protein expressed in *E. coli* from cells grown in the presence of the iron chelator.

*Reconstitution of Apo-Enzyme.* Apo-ADE from *E. coli* was prepared by dialysis of [Mn/Mn]-ADE with 10 mM 1,10-phenanthroline at pH 7.0. The apo-enzyme had less than 0.2% of the original adenine deaminase activity and removal of manganese was confirmed by ICP-MS. Apo-ADE was reconstituted with variable amounts of $Mn^{2+}$, $Zn^{2+}$ or $Fe^{2+}$ for 48 hours at pH 7.5 and 4 $^oC$ to determine the stoichiometry of metal ion and protein required for optimal catalytic activity. There was a linear increase in catalytic activity as the concentration of the divalent cation was increased from zero to two equivalents relative to the subunit concentration. The titrations are shown in **Figure 2.1**. These titrations confirm that two metal ions are required for optimal catalytic

activity of ADE and the linearity of the titration curve is consistent with a cooperative assembly of the binuclear metal center (*44*). The kinetic constants and metal content of the reconstituted forms of ADE from *E. coli* are presented in **Table 2.1**. The $Mn^{2+}$-reconstituted ADE has essentially the same turnover number (196 $s^{-1}$) as the enzyme isolated from *E. coli* (200 $s^{-1}$). The elution of adenine deaminase from the gel filtration column supports an oligomeric structure as a homodimer (data not shown). The apo-Atu4426 could also be prepared by dialysis and the lack of metal for apo-Atu4426 was confirmed by ICP-MS. The reconstitution of Atu4426 with $Mn^{2+}$ and $Fe^{2+}$ (anaerobically) resulted in profiles identical to those obtained for the *E. coli* ADE shown in **figure 2.2**.

**Table 2.1**: *Kinetic parameters and metal content of metal-reconstituted forms of E. coli ADE*[a]

| enzyme | $k_{cat}$ ($s^{-1}$) | $k_{cat}/K_m$ ($M^{-1}$ $s^{-1}$) | metal/subunit |
|---|---|---|---|
| [Mn/Mn]-ADE | 185 ± 5 | (6.1 ± 0.5) x $10^5$ | 2.0 ± 0.1 |
| [Zn/Zn]-ADE | 123 ± 8 | (5.4 ± 0.5) x $10^5$ | 1.9 ± 0.1 |
| [Fe/Fe]-ADE | 196 ± 3 | (5.9 ± 0.5) x $10^5$ | 1.9 ± 0.1 |

[a]pH 7.5 and 30 $^oC$

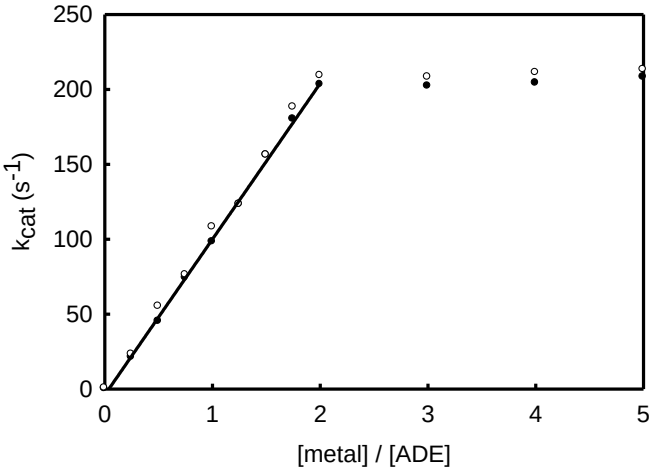


**Figure 2.1:** *Metal titration with apo-ADE*. Titration of varying enzyme equivalents of $Mn^{2+}$ (open circles) and $Fe^{2+}$ (closed circles) to apo-ADE (1.0 μM) at 4 $^{o}$C. The enzyme assays were performed after allowing the mixture of apo-ADE and metal to equilibrate for 48 hours at pH 7.5. The reconstitution with iron was done anaerobically.

*Three-Dimensional Structure of Atu4426.* The asymmetric unit contains two protomers that are very similar to one another (rmsd of 0.26 Å). Each protomer contains three domains: an N-terminal β sandwich, a TIM barrel and a C-terminal α/β domain shown in **Figure 2.3** (*20*). The active site of Atu4426 contains three $Mn^{2+}$ ions (**Figure 2.4**). A stereoview of the active site is presented in **Figure 2.4**. The first two metal ions form a binuclear metal center that is similar, but not identical, to other members of the amidohydrolase superfamily (*3, 7*). The HxH motif (His-92 and His-94) from β-strand 1 and the aspartate (Asp-289) from β-strand 8 coordinate the α-metal ion. The β-metal ion is ligated by His-218 from β-strand 5, His-239, and Glu-240 (both from β-strand 6). The two metal ions are bridged to one another by Glu-187 (from β-strand 4) and a hydroxide/water from solvent. The third metal ion is coordinated to His-122, Glu-123,

His-477 and Asp-478 and is 6.6 Å from the α-metal and 8.2 Å from the β-metal of the binuclear metal center.

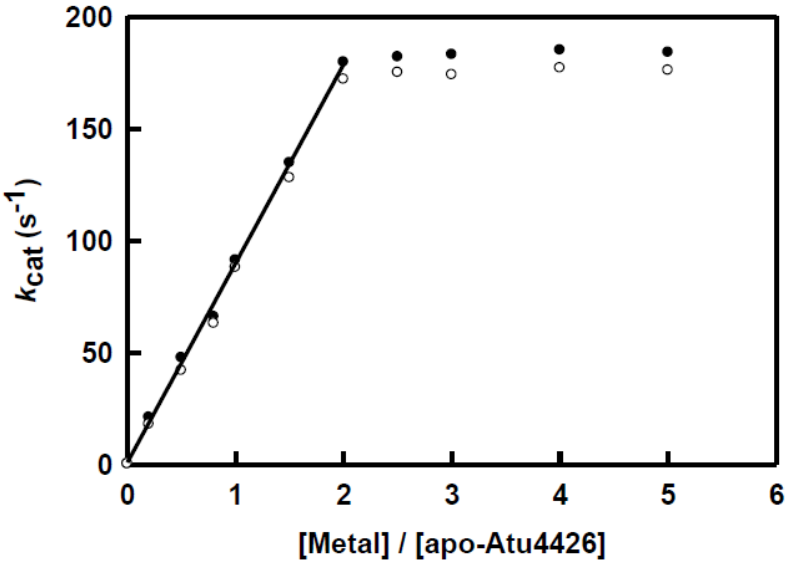


**Figure 2.2**: *Metal titration with apo-Atu4426*. Titration of varying enzyme equivalents of $Mn^{2+}$ (open circles) and $Fe^{2+}$ (closed circles) to apo-Atu4426 (1.0 μM) at 4 $^{o}$C. The enzyme assays were performed after allowing the mixture of apo-Atu4426 and metal to equilibrate for 48 hours at pH 7.5. The reconstitution with iron was done anaerobically.

The polypeptide segments consisting of residues 9-87 and 338-375 of the N-terminal domain are shown in purple and cyan color, respectively. TIM barrel and C-terminal domains are shown in green and marine blue, respectively. The loop residues 376 to 386, connecting the N- and C-terminal domains are shown in brown. The manganese ions are shown as magenta spheres. In the stereoview, metal ions and coordinating water molecules are shown in grey and red, respectively.

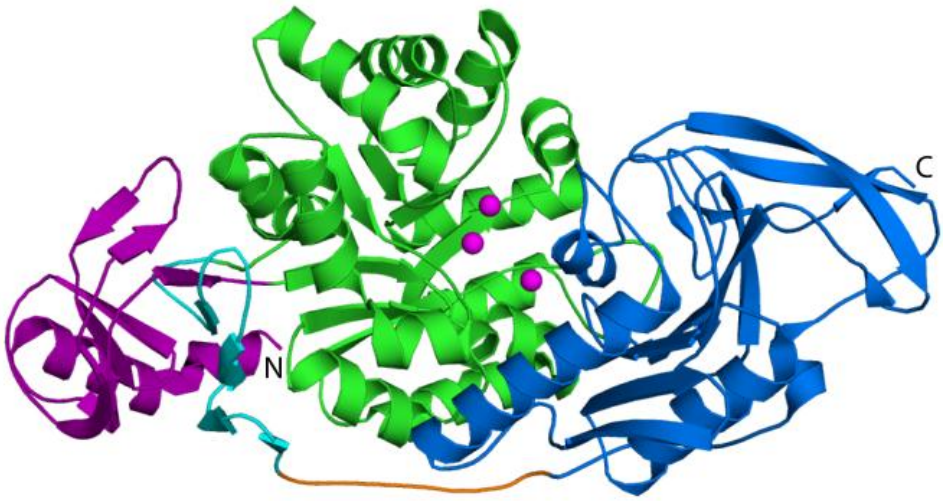


**Figure 2.3:** *Ribbon representation of the structure of Atu4426*.

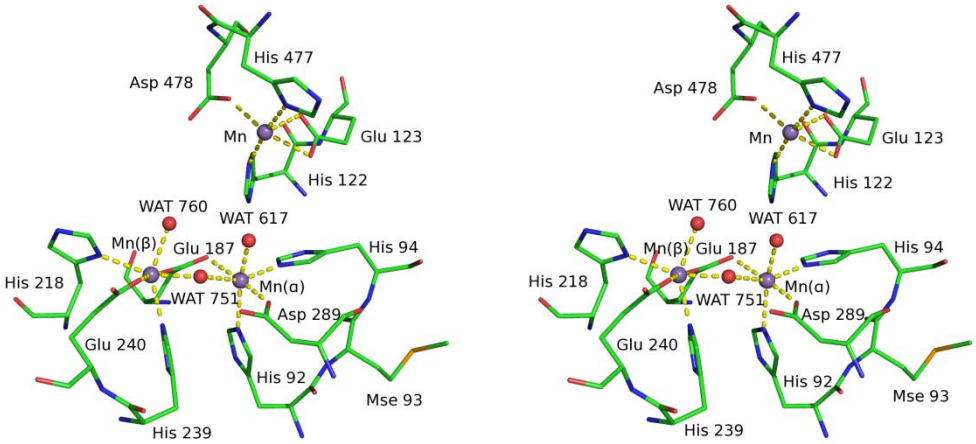


**Figure 2.4:** *Stereoview of the Atu4426 active site residues*.

*Model of Adenine Bound in Active Site.* A comparison between the binding site in the ligand-free crystal structure and the binding site in the proposed model is presented in **Figure 2.5A**. The model of the binuclear metal center (His-92, His-94, Glu-187, His-218, His-239 and Asp-289) is nearly identical to that in the crystal

structure. The differences include the side chain of Arg-220 that is rotated by ~90° so that the guanidino group is not in proximity of the binuclear metal center. Model side chains of Glu-240 and Asp-290 were adjusted to result in more favorable electrostatic interactions between the carboxylate groups and the two metals. Furthermore, His-122, Glu-123 and His-477 form a more closed ligand-binding site in comparison to the open conformation in the crystal structure. The best-scored binding pose of adenine in the modeled binding site is shown in **Figure 2.5B**. The tetrahedral intermediate was formed by the bridging hydroxide attacking C-6 on the *re*-face of adenine. In this complex, the ammonia leaving group hydrogen bonds with the side chains of Asp-289 and Asp-290. The protonated N-1 nitrogen of adenine hydrogen bonds with the side chain of Glu-240. In addition, the N-7 nitrogen of adenine coordinates the α-metal and the N-9 (NH) nitrogen hydrogen bonds with the side chain of Glu-123. The Nε nitrogen in His-122, which was assigned to be protonated during modeling, is adjacent to the adenine N-3 nitrogen (3.7 Å) and Glu-123 OE2 oxygen (3.1 Å).

*Substrate Specificity.* A number of compounds having adenine like moieties were tested as substrates or competitive inhibitors for ADE from *E. coli.* Among these compounds were 2-hydroxyadenine, N-6-methyladenine, 6-chloropurine, 7-methyladenine, 2,6-diaminopurine, adenosine, 6-methoxypurine, 6-methylpurine, 6-mercaptopurine and 6-methylmercaptopurine. 6-Chloropurine was a very effective tight binding inhibitor for ADE from *E. coli.* However none of the other compounds was either a substrate or competitive inhibitor for ADE.

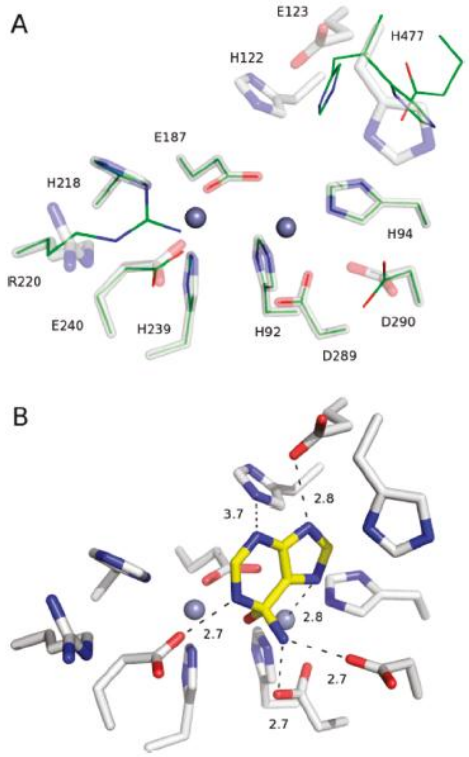


**Figure 2.5:** *Model of adenine in the active site of Atu-4426* **(A)** Binding site conformation in the model of Atu4426 (transparent sticks) compared to the binding site in the ligand-free crystal structure of Atu4426 (solid line). The two metal ions in the model are depicted in dark blue, occupying identical places as the two metal ions in the crystal structure. (**B)** The binding mode of the tetrahedral intermediate formed during the deamination of adenine in the modeled binding site of Atu4426. Polar contacts between adenine and binding site residues are indicated by dashed lines with distances given in Ångstroms.

*EPR and Mössbauer Spectroscopy of [Fe/Fe]-ADE.* The 5 K low-field Mössbauer spectrum of the reconstituted and fully active [Fe/Fe]-ADE (**Figure 2.6**) exhibited a quadrupole doublet typical of high-spin $Fe^{II}$ ions (*45*). Lineshapes and

linewidths revealed no evidence of multiple species. Given the presence of two irons per protein, this suggests a very similar ligand environment for both ferrous ions.

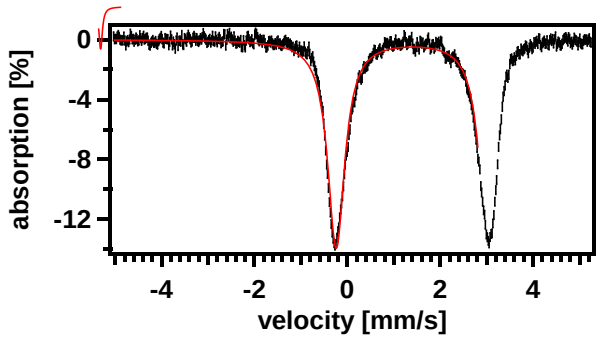


**Figure 2.6:** *Mössbauer spectrum of [$Fe^{II}/Fe^{II}$]-ADE* (265 μM). The spectrum was collected at 5 K, 400 G magnetic field applied parallel to the radiation. The red line represents a simulation with δ= 1.39 mm/s, $\Delta E_q$= 3.27 mm/s with line width of 0.47 mm/s.

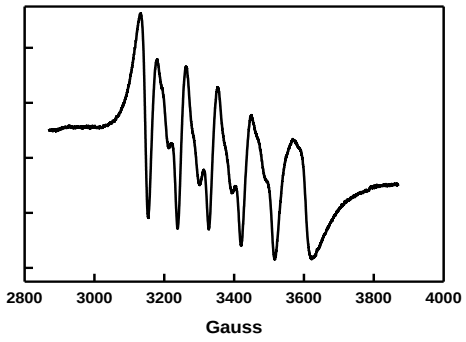


**Figure 2.7:** *EPR spectrum of Mn/Mn-ADE* (220 μM). EPR parameters: temperature, 10 K; microwave 9.46 GHz, 0.02 mW.

The enzyme in the [$Fe^{II}/Fe^{II}$] state was EPR-silent. To determine whether [$Fe^{II}/Fe^{II}$]-ADE is air-sensitive, this protein was incubated aerobically at room

temperature and then assayed for catalytic activity. There was no loss of activity after 24 hours and the Mössbauer spectrum (not shown) demonstrated that the iron remained high-spin ferrous. The EPR spectrum of [Mn/Mn]-ADE showed a prototypical six-line pattern for $Mn^{2+}$ (F**igure 2.7**) with no evidence of antiferromagnetic coupling (*46*).

*Oxidation and Reduction of [Fe/Fe]-ADE.* Potassium ferricyanide was used to oxidize the binuclear metal center to determine if the di-ferric state of the binuclear metal center is active for the deaminase reaction. Increasing concentrations of ferricyanide to [$Fe^{II}/Fe^{II}$]-ADE (100 μM) linearly inactivated the catalytic activity (**Figure 2.8**) with two equivalents of the reagent being sufficient to fully inactivate the enzyme. The Mössbauer spectrum of iron bound ADE treated with two equivalents of ferricyanide exhibited a six-line pattern typical of a high-spin ferric oxidation state (**Figure 2.9A**). The EPR spectrum of [$Fe^{III}/Fe^{III}$]-ADE exhibited a signal at g = 4.3, typical of $Fe^{III}$ ions with rhombic symmetry (**Figure 2.9B**). The spin concentration of the signal corresponded to 1.9 spins/mol protein, suggesting that the ferric ions are not magnetically interacting and that each ion affords the EPR signal. [$Fe^{III}/Fe^{III}$]-ADE was reduced back to the di-ferrous state with the anaerobic addition of sodium dithionite and the deaminase activity was fully reconstituted within 1 hour. The Mössbauer spectrum of this sample (data not shown) resembled the spectrum of [$Fe^{II}/Fe^{II}$]-ADE shown in **Figure 2.6**. Addition of 0.25 mM $H_2O_2$ to 1.5 μM [$Fe^{II}/Fe^{II}$]-ADE resulted in the irreversible oxidation of the iron center and oxygenation of the protein.

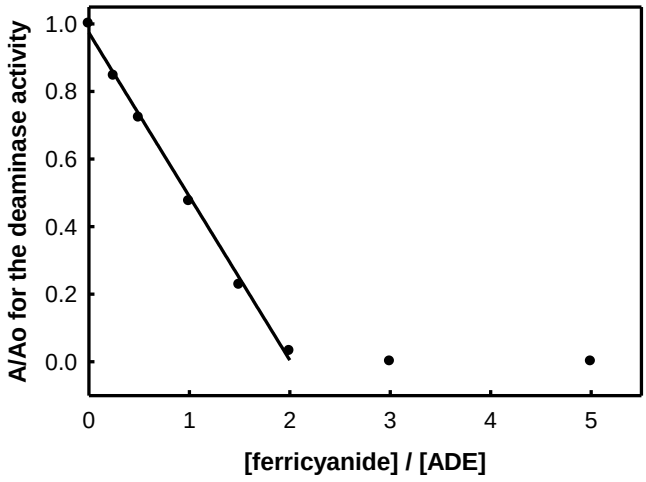


**Figure 2.8:** *The loss of adenine deaminase activity after the addition of various amounts of potassium ferricyanide to [Fe$^{II}$/Fe$^{II}$]-ADE* (100 µM).

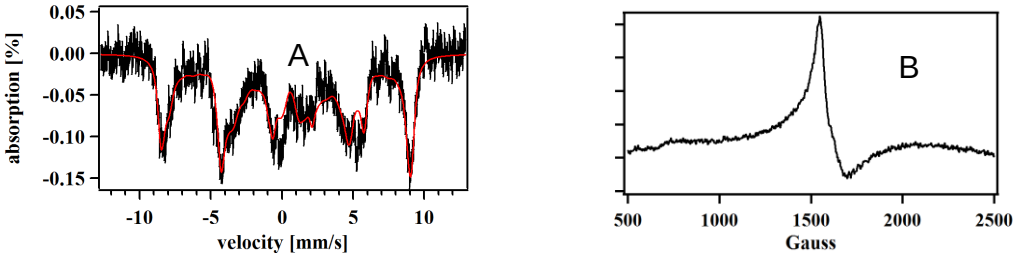


**Figure 2.9:** *Mössbauer and EPR spectrum of [Fe/Fe]-ADE after treatment with ferricyanide* (A) Mössbauer spectrum of [Fe/Fe]-ADE (200 µM) after the addition of two equivalents of ferricyanide (400 µM). Collection parameters: temperature, 5 K; field, 700 G; counts of radiation, 2.2 x $10^7$. The red line is a simulation assuming a single species (B) EPR spectrum of 200 µM [Fe$^{III}$/Fe$^{III}$]-ADE after treatment with ferricyanide.

The figure **2.9** has a Mössbauer spectrum (A) that was fit to standard single species simulation explained previously and the EPR parameters (B) were same as described in figure **2.7**.

*Mutagenesis of ADE.* Amino acid sequence alignments and the X-ray structure of Atu4426 indicate that His-90, His-92, Glu-185, His-214, His-235, Glu-236 and Asp-284 are the direct metal ligands to the binuclear metal center of ADE from *E. coli*. Mutation of His-92, His-214, His-235 and Glu-185 resulted in the total loss of catalytic activity as well as the ability to bind divalent metals in the active site. The D284A and E236Q mutants were able to bind two equivalents of $Mn^{2+}$ or $Fe^{2+}$ in the active site but these mutants were unable to catalyze the deaminase reaction. The H90N mutant was able to bind ~2 equivalents of $Mn^{2+}$ or $Fe^{2+}$ per monomer and had a $k_{cat}$ of about 5% of the wild-type enzyme. The H90C and H90D mutants were unable to bind either iron or manganese. The S95A, D118N, H120N, E121Q, E236Q, D285A, H473N and D474N mutants were constructed based upon the conservation of residues in the active site and the working model of adenine bound in the active site of Atu4426 (**Figure 2.5**). All of these mutants are able to bind ~2 metals per active site. The kinetic constants and metal content for the mutants are presented in **Table 2.2.** The reconstitution of apo-E185G with propionic acid and $Mn^{2+}$ was conducted to establish the role of the carboxylate side chain of Glu-185 as a bridge for the binuclear metal center. The addition of 10 mM propionic acid and 1.0 mM $Mn^{2+}$ to 5.0 nM apo-E185G, resulted in the reconstitution of ~85 % of the activity of the wild type enzyme ($k_{cat}$ ~168 $s^{-1}$).

**Table 2.2**: *Catalytic constants and metal binding properties of E. coli ADE mutants.*

| mutant | $k_{cat}$ ($s^{-1}$) | $k_{cat}/K_m$ ($M^{-1}$ $s^{-1}$) | Metal content (Mn) |
|---|---|---|---|
| H90D | 0.036 ± 0.004 | 82 ± 8 | 0.022 ± 0.004 |
| H90C | 0.053 ± 0.008 | 103 ± 9 | 0.032 ± 0.003 |
| H90Q | 0.8 ± 0.1 | (2.0 ± 0.2) x $10^3$ | 0.043 ± 0.002 |
| H90N | 8.0 ± 1.2 | (2.2 ± 0.3) x $10^4$ | 1.8 ± 0.2 |
| H92D | 0.8 ± 0.1 | (2.1 ± 0.3) x $10^3$ | 0.12 ± 0.05 |
| H92C | 0.69 ± 0.08 | (1.4 ± 0.2) x $10^3$ | 0.23 ± 0.05 |
| H92Q | 0.08 ± 0.03 | 166 ± 12 | 0.08 ± 0.01 |
| H92N | 0.05 ± 0.01 | 119 ± 10 | 0.13 ± 0.03 |
| S95A | 78 ± 2 | (1.6 ± 0.2) x $10^5$ | 2.1 ± 0.1 |
| D118N | 173 ± 2 | (5.6 ± 0.3) x $10^5$ | 2.1 ± 0.1 |
| H120N | 0.13 ± 0.01 | 361 ± 17 | 2.1 ± 0.1 |
| E121Q | 57 ± 1 | (1.3 ± 0.2) x $10^5$ | 2.0 ± 0.1 |
| E185Q | 0.06 ± 0.005 | 38 ± 4 | 0.030 ± 0.001 |
| H214Q | 1.3 ± 0.2 | (4.0 ± 0.5) x $10^3$ | 0.33 ± 0.05 |
| H214N | 0.5 ± 0.2 | (1.3 ± 0.3) x $10^3$ | 0.12 ± 0.06 |
| H235D | 1.2 ± 0.08 | (2.5 ± 0.3) x $10^3$ | 0.42 ± 0.05 |
| H235C | 1.5 ± 0.1 | (1.3 ± 0.2) x $10^3$ | 0.34 ± 0.05 |
| H235Q | 1.3 ± 0.1 | (1.6 ± 0.3) x $10^3$ | 0.23 ± 0.05 |
| H235N | 0.5 ± 0.1 | 609 ± 35 | 0.33 ± 0.05 |
| E236Q | 0.072 ± 0.002 | 170 ± 16 | 1.8 ± 0.1 |
| D284A | 0.022 ± 0.005 | 26 ± 5 | 1.9 ± 0.2 |
| D285A | 37 ± 2 | (1.3 ± 0.2) x $10^5$ | 2.1 ± 0.1 |
| H473N | 178 ± 2 | (5.6 ± 0.3) x $10^5$ | 2.0 ± 0.1 |
| D474N | 171 ± 2 | (5.5 ± 0.2) x $10^5$ | 1.9 ± 0.2 |

*pH-Rate Profiles.* The kinetic constants for the deamination of adenine by ADE were obtained as a function of pH and the profiles are shown in **Figure 2.10**. The pH profiles for $k_{cat}$ (A) and $k_{cat}/K_m$ (B) are bell-shaped. Similar results were obtained for the profiles in $D_2O$, with the exception that the values of $k_{cat}$ and $k_{cat}/K_m$ are doubled in $D_2O$ with an inverse solvent isotope effect of 0.49 ± 0.02 at pH 7.5. The p$K_a$ values are listed in **Table 2.3**.

**Table 2.3**: *Kinetic p$K_a$ values obtained for ADE in $H_2O$ and $D_2O$.*

$H_2O$

| Metal reconstitution | $k_{cat}$ | | $k_{cat}/K_m$ | |
|---|---|---|---|---|
| | p$K_a$ | p$K_b$ | p$K_a$ | p$K_b$ |
| Fe/Fe | 6.6 ± 0.1 | 8.5 ± 0.1 | 6.3 ± 0.1 | 8.2 ± 0.1 |
| Zn/Zn | 6.4 ± 0.1 | 8.6 ± 0.1 | 6.6 ± 0.1 | 8.5 ± 0.1 |
| Mn/Mn | 6.2 ± 0.2 | 8.3 ± 0.1 | 6.9 ± 0.1 | 8.2 ± 0.1 |

$D_2O$

| Metal reconstitution | $k_{cat}$ | | $k_{cat}/K_m$ | |
|---|---|---|---|---|
| | p$K_a$ | p$K_b$ | p$K_a$ | p$K_b$ |
| Fe/Fe | 6.1 ± 0.1 | 8.7 ± 0.1 | 6.5 ± 0.1 | 8.3 ± 0.1 |
| Zn/Zn | 6.7 ± 0.1 | 8.4 ± 0.1 | 6.9 ± 0.1 | 8.1 ± 0.1 |
| Mn/Mn | 6.5 ± 0.1 | 8.6 ± 0.1 | 6.5 ± 0.1 | 8.3 ± 0.1 |

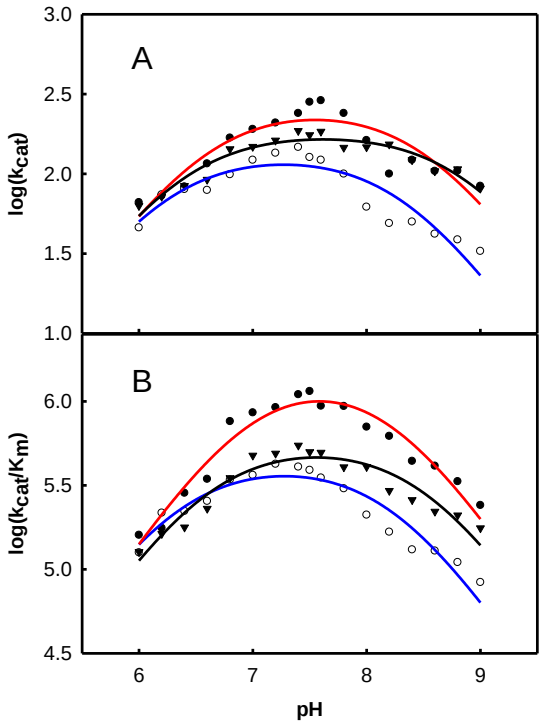


**Figure 2.10**: *pH-rate profiles for the different metal reconstituted forms of ADE.* [Fe/Fe]-ADE (●) is indicated in red, [Zn/Zn]-ADE (○) is indicated in blue and [Mn/Mn]-ADE (▼) is indicated in black. The lines represent fits of the data to equation 2.

*Solvent Viscosity Effects.* Increasing solvent viscosity had a small effect on the relative values of $k_{cat}$ and $k_{cat}/K_m$ for the deamination of adenine. At pH 7.5, the slope for the $k_{cat}$ profile was 0.020 ± 0.002 and the slope for $k_{cat}/K_m$ the profile was 0.18 ± 0.02 (data not shown).

*Inhibition by 6-Chloropurine.* ADE was incubated with various concentrations of 6-chloropurine for 1 hour at, pH 7.5, 30 $^{o}$C and then assayed for catalytic deaminase activity. The deaminase activity decreased with an increase in the concentration of 6-chloropurine when the adenine concentration was fixed at 5.0 mM. The apparent $K_i$ for

6-chloropurine was determined to be 130 ± 15 nM from a fit of the data to equation 3 (*43*).

DISCUSSION

*Metal Requirement.* Fully active ADE was successfully purified from *E. coli* only when the iron in the growth medium was sequestered with a suitable chelator (2,2'-dipyridyl). The isolated enzyme under these conditions contained two manganese ions in the active site. The turnover number for the deamination of adenine (~200 $s^{-1}$) is approximately two orders of magnitude greater than that for any ADE previously reported in the literature (*16, 17, 20*). [Mn/Mn]-ADE is stable and apo-ADE can be prepared from this enzyme form by chelation of the metal ions with *o*-phenanthroline. Apo-ADE can be reconstituted with two equivalents of $Zn^{2+}$, $Fe^{2+}$ or $Mn^{2+}$. The linear increase in the catalytic activity when zero to two equivalents of these cations are added to apo-ADE is consistent with the cooperative formation of a binuclear metal center (*44*). [$Fe^{II}/Fe^{II}$]-ADE prepared in this manner is as active for the deamination of adenine as [Mn/Mn]-ADE and [Zn/Zn]-ADE, and this enzyme also remains catalytically active in the presence of oxygen overnight at room temperature. Similar results were seen for the metal reconstitution of apo-Atu4426, indicating that the binuclear metal center is critical for the deaminase activity of Atu4426.

Seven amino acid residues in the active site and that bind to either of the two divalent cations were changed and the mutant proteins characterized. Metal binding and catalytic activity were lost upon the single-site mutation of His-92, Glu-185, His-214, or His-235. Metal binding was also disrupted when His-90 was mutated to aspartate,

cysteine, or glutamine, but not asparagine. Mutation of Asp-284 and Glu-236 to alanine and glutamine, respectively, did not disrupt the binding of metal to the active site. However, the D284A and E236Q mutants were inactive as an adenine deaminase. These results are consistent with the formation of a binuclear metal center where one metal ion is coordinated to His-90 and His-92 while the second metal ion is coordinated to His-214 and His-235. This model is confirmed by the three-dimensional structure determination of Atu4426. The two metal ions are bridged by Glu-185 and a bridging water/hydroxide. The conserved aspartate residue from β-strand 8 and the glutamate from β-strand 6 are not essential for metal binding, but they are critical for the activation of water and protonation of the transition state to form the reaction products.

*Oxidative State of Iron.* Mössbauer spectroscopy (in conjunction with the absence of an EPR signal) demonstrates that both Fe ions in reconstituted and catalytically active [Fe/Fe]-ADE are high spin ferrous. A single quadrupole doublet was observed and the inability of Mössbauer spectroscopy to distinguish between the two irons suggests that the environment of both irons is similar. The presence of a g = 4.3 EPR signal in the ferricyanide-oxidized state, along with the metal analysis showing two irons per ADE and low-field Mössbauer spectra showing a 6-line pattern, indicate that the ferric ions are high-spin S = 5/2 and magnetically isolated rather than being magnetically coupled. Our data provide no evidence as to whether the two ferrous ions are spin-coupled. However, given the general lack of coupling in the diferric state, we suspect that the two ferrous ions are not spin-coupled. [$Fe^{II}/Fe^{II}$]-ADE can be oxidized to [$Fe^{III}/Fe^{III}$]-ADE by the addition of ferricyanide but this enzyme is unable to catalyze

the deamination of adenine. The [$Fe^{III}/Fe^{III}$]-ADE can, however, be reduced back to [$Fe^{II}/Fe^{II}$]-ADE by the addition of dithionite with full recovery of catalytic activity. Therefore, oxidation of the metal center with ferricyanide does not irreversibly damage the active site. These experiments demonstrate that the active deaminase is in the di-ferrous state and that the two metals are not easily oxidized by air to the di-ferric state. Addition of $H_2O_2$ results in the irreversible oxidation of di-ferrous-ADE to form di-ferric-ADE and protein damage. However, the addition of hydrogen peroxide to Mn/Mn-ADE has no effect. Enzyme treated with $H_2O_2$ can be reduced to the di-ferrous form but no deaminase activity could be reconstituted. These results suggest that irreversible oxygenation reactions are occurring after the addition of $H_2O_2$ to [$Fe^{II}/Fe^{II}$]-ADE, possibly because of the generation of hydroxyl radicals (*47*).

*pH-Rate profiles*. The pH-rate profiles display a bell-shaped profile. This result is consistent with two groups being involved in catalysis, one of which is protonated and the other unprotonated for optimal activity. The pH-rate profiles also indicate a fairly broad pH range over which the deaminase activity occurs. The optimum pH is ~7.5. The various metal reconstituted forms of ADE do not significantly change the kinetic p$K_a$ values of the groups involved in catalysis. The structure of adenine deaminase from *A. tumefaciens* can be used to assist in the identification of residues involved in catalysis. Based on previous studies for other members of the AHS, it is likely that the p$K_a$ of ~6.4 reflects the ionization of Asp-284, the highly conserved residue at the end of β-strand 8, or the protonation of the bridging hydroxide. Asp-284 must be unprotonated and is critical for the activation of the hydrolytic water molecule. Mutation of this residue

(D284A) confirms that this residue is essential for the deamination of adenine. The second ionization with a kinetic p$K_a$ of ~8.5 is assigned for the highly conserved glutamate residue from β-strand 6 that coordinates one of the metal ions. The E236Q mutant retains the metal binding properties of ADE, but this mutant is inactive to the deaminase activity. This result is consistent with this residue protonating N1 of the purine ring during the formation of hypoxanthine.

*Solvent Isotope Effects.* The reaction catalyzed by ADE in $D_2O$ is twice as fast as in $H_2O$ giving an inverse isotope effect of ~ 0.5 for both $k_{cat}$ and $k_{cat}/K_m$. Large inverse isotope effects have been seen for other members of the AHS catalyzing different deaminase reactions. For example, adenosine deaminase (*48, 49*) and adenosine monophosphate deaminase (*50*) have inverse solvent isotope effects of 0.45 ± 0.04 and 0.71 ± 0.07, respectively (*48, 50*). In all cases, the large inverse isotope effect has been attributed to a compressed hydrogen bond in the transition state, where the p$K_a$ of the acceptor and donor groups are fairly close or similar (*48, 49*). For ADE from *E. coli*, this means that the protonated form of Glu-236 and the N-1 nitrogen of the purine moiety of adenine have a fairly close p$K_a$, which enables the protonation of N-1, concomitant with hydrolytic attack at C-6. Analogous to the model described by Cleland (*49*) for adenosine deaminase, once the OH adds to C-6 of the adenine moiety, the p$K_a$ of N-1 increases relative to that of the protonated form of Glu-236. This increase would enable proton transfer from Glu-236 to the N-1 nitrogen of adenine.

*Proposed Mechanism of Action.* ADE requires two divalent cations for catalytic activity. The X-ray structure of Atu4426 also shows a third metal in the active site, coordinated to His-120, Glu-121, His-473, and Asp-474 These residues were mutated to assess the effects on metal binding capacity and catalytic activity. The metal binding capacity of these mutants was found to be ~2.0 per monomer of ADE. These results suggest that the binding of the third metal ion in the active site is not required for catalytic activity. Apparently, the third metal appears in the structure as a result of metal supplementation during bacterial growth and/or protein crystallography and plays no role in the deaminase reaction.

A sequence alignment of *E. coli* ADE and Atu4426 is presented in **Scheme 2.2**. The residues highlighted in yellow are direct ligands to the binuclear metal center. All of the other structurally characterized aromatic deaminases found within the amidohydolase superfamily bind a single divalent cation in the active site (*3*). These deaminases bind a single divalent cation at the α-site and use a conserved HxxE motif from the end of β-strand 5 to deliver a proton to a ring nitrogen of the reaction product. The conserved aspartate at the end of β-strand 8 protonates the leaving group ammonia. The HxxE motif is absent from all of the adenine deaminases from cog1001 and thus the details of the catalytic mechanism for ADE must be different from those for the other deaminases in the AHS. The residues highlighted in green represent the residues that are highly conserved in all the adenine deaminases in cog1001 and are close to the active site. These residues were mutated to determine their significance in catalytic activity.

Based upon our model for the binding of adenine in the active site of ADE, we conclude that the invariant glutamate from the end of β-strand 6 functions to protonate N-1 of adenine during catalysis. In *E. coli,* this residue is Glu-236. This residue is part of the highly conserved HE motif found in all adenine deaminases in cog1001. We also conclude that Asp-284 in the *E. coli* protein is unprotonated and functions in catalysis by abstraction of the proton from the tetrahedral intermediate and subsequent delivery of this proton to the ammonia leaving group. Shown in **Scheme 2.3** is our working model for the chemical mechanism for adenine deaminase from *E. coli*. In this scheme a proton is transferred from the bridging water molecule to Glu-236. The bridging hydroxide attacks C-6 on the *re*-face of adenine to form a tetrahedral intermediate with *R*-stereochemistry and the proton from Glu-236 is transferred to N-1 of the intermediate. Subsequently, the proton from the attacking hydroxide is transferred to Asp-284. The tetrahedral intermediate collapses, leading to the transfer of the proton from Asp-284 to ammonia.

```
E. coli     GDAVADYIIDNVSILDLINGGEISGPIVIKGRYIAGVGAEYTDAPALQRIDARGATAVPG  85
Atu4426     GDQRFDVLITGGTLVDVVTGELRPADIGIVGALIASVHEPASRRDAAQVIDAGGAYVSPG  87

E. coli     FIDAHLHIESSMMTPVTFETATLPRGLTTVICDPHEIVNVMGEAGFAWFARCAEQARQNQ  145
Atu4426     LIDTHMHIESSMITPAAYAAAVVARGVTTIVWDPHEFGNVHGVDGVRWAAKAIENLPLRA  147

E. coli     YLQVSSCVPALEGCDVNGASF---TLEQMLAWRDHPQVTGLAEMMDYPGVISGQNALLDK  202
Atu4426     ILLAPSCVPSAPGLERGGADFDAAILADLLSW---PEIGGIAEIMNMRGVIERDPRMSGI  204

E. coli     LDA--FRHLTLDGHCPGLGGKELNAYITAGIENCHESYQLEEGRRKLQLGMSLMIREGSA  260
Atu4426     VQAGLAAEKLVCGHARGLKNADLNAFMAAGVSSDHELVSGEDLMAKLRAGLTIELR-GSH  263

E .coli     ARNLNALAPLINEFNS-PQCM-LCTDDRNPWEIAHEGHIDALIRRLIEQHNVPLHVAYRV  318
Atu4426     DHLLPEFVAALNTLGHLPQTVTLCTDDVFPDDLLQGGGLDDVVRRLV-RYGLKPEWALRA  322

E. coli     ASWSTARHFGLNHLGLLAPGKQADIVLLSDARKVTVQQVLVKGEPIDAQTLQAEESARLA  378
Atu4426     ATLNAAQRLGRSDLGLIAAGRRADIVVFEDLNGFSARHVLASGRAV-------AEGGRML  375

E. coli     QSAPPYGNTIARQPVS-----ASDFALQFTPGKRYRVIDVIHNELITHSHSSVYSENGF-  432
Atu4426     VDIPTCDTTVLKGSMKLPLRMANDFLVK-SQGAKVRLATIDRPRFTQWGETEADVKDGFV  434

E. coli     -DRDDVSFIAVLERYGQ-RLAPACGLLGGFGLNEGALAATVSHDSHNIVVIGRSAEEMAL  490
Atu4426     VPPEGATMISVTHRHGMAEPTTKTGFLTGWGRWNGAFATTVSHDSHNLTVFGGNAGDMAL  494

E. coli     AVNQVIQDGGGLCVVRNGQVQSHLPLPIAGLMSTDTAQSLAEQIDALKAA  540
Atu4426     AANAVIGTGGGMAVASEGKVTAILPLPLSGLVSDAPLEEVARAFEDLREA  544
```

**Scheme 2.2:** Sequence alignments of ADE from *E. coli* and *A. tumefaciens*

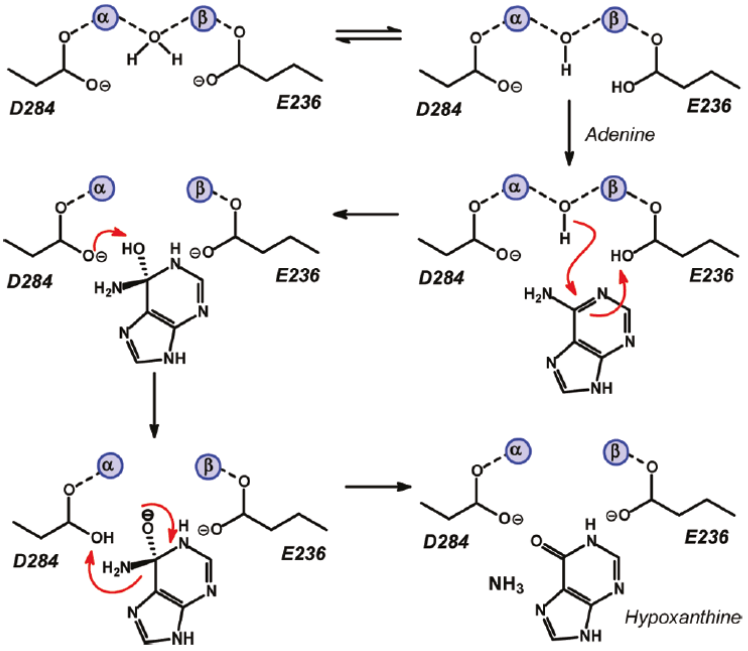


**Scheme 2.3**: Mechanism of the reaction catalyzed by ADE.

# CHAPTER III

## THE CATALASE ACTIVITY OF DIIRON ADENINE DEAMINASE*

Adenine deaminase (ADE) from the amidohydrolase superfamily of enzymes catalyzes the conversion of adenine to hypoxanthine and ammonia. The enzyme isolated from *Escherichia coli* using standard expression conditions was largely inactive towards the deamination of adenine ($k_{cat}$ ~2 $s^{-1}$). Molecular weight determinations by mass spectrometry provided evidence that multiple histidine and methionine residues were oxygenated. When iron was sequestered with a metal chelator and the growth medium supplemented with $Mn^{2+}$ prior to induction, the post-translational modifications disappeared. The enzyme expressed and purified under these conditions was substantially more active for the deamination of adenine, with values of $k_{cat}$ and $k_{cat}/K_m$ of 200 $s^{-1}$ and 5 x $10^5$ $M^{-1}s^{-1}$, respectively. Apo-enzyme was prepared and reconstituted with two equivalents of $FeSO_4$; ICP-MS and Mössbauer spectroscopy demonstrated that this protein contained two high-spin ferrous ions per monomer of ADE. In addition to the adenine deaminase activity, [$Fe^{II}/Fe^{II}$]-ADE catalyzed the conversion of $H_2O_2$ to $O_2$ and $H_2O$. The values of $k_{cat}$ and $k_{cat}/K_m$ for the catalase activity are 200 $s^{-1}$ and 2.4 x $10^4$ $M^{-1}s^{-1}$ respectively.

---

*Reprinted with permission from "The catalase activity of diiron adenine deaminase" by S. S. Kamat, G. P. Holmes-Hampton, A. Bagaria, D. Kumaran, S. E. Tichy, T. Gheyi, X. Zheng, K. Bain, C. Groshong, S. Emtage, J. M. Sauder, S. K. Burley, S. Swaminathan, P. A. Lindahl and F. M. Raushel, *Protein Science* 20, 2080-2094, 2011. Copyright 2011 Wiley-Blackwell, The Protein Society

[$Fe^{II}/Fe^{II}$]-ADE underwent more than 100 turnovers with $H_2O_2$ before the enzyme was inactivated due to oxygenation of histidine residues critical for metal binding. A model is proposed for the disproportionation of hydrogen peroxide by [$Fe^{II}/Fe^{II}$]-ADE that involves the cycling of the binuclear metal center between the di-ferric and di-ferrous oxidation states. Oxygenation of active site residues occurs from the release of hydroxyl radicals. The three-dimensional structure of [$Fe^{II}/Fe^{II}$]-ADE was determined by X-ray diffraction methods. This is the first report of a redox reaction for any member of the amidohydrolase superfamily.

INTRODUCTION

Adenine deaminase (ADE), a member of the amidohydrolase superfamily (AHS), catalyzes the hydrolytic deamination of adenine to hypoxanthine and ammonia as shown in **Scheme 3.1**.

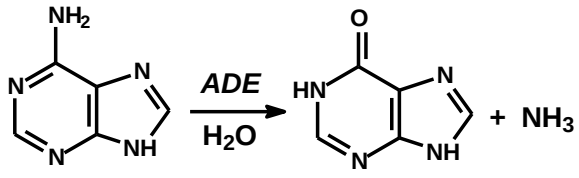


**Scheme 3.1:** Reaction catalyzed by ADE

One of the apparent roles of this enzyme within bacteria is to recycle purine nucleotides and scavenge ammonia. Other enzymes within the AHS catalyze the deamination of *S*-adenosyl homocysteine, adenosine, guanine, cytosine, 8-oxoguanine and additional aromatic substrates (*7*). The three-dimensional structure of adenine deaminase from *Agrobacterium tumefaciens* ($ADE_{at}$; locus tag: Atu4426) has been determined (PDB id: 3nqb) and the mechanism of action for the enzyme from

*Escherichia coli* K12 ($ADE_{ec}$; locus tag: b3665) has been elucidated (*20*). The adenine deaminases from cog1001are unique members of the AHS since they require two divalent cations for maximal catalytic activity while the other deaminases from this superfamily require a single divalent cation in the active site (*7*, *20*). The active site structure of ADE from *A. tumefaciens* is presented in **Figure 3.1**.

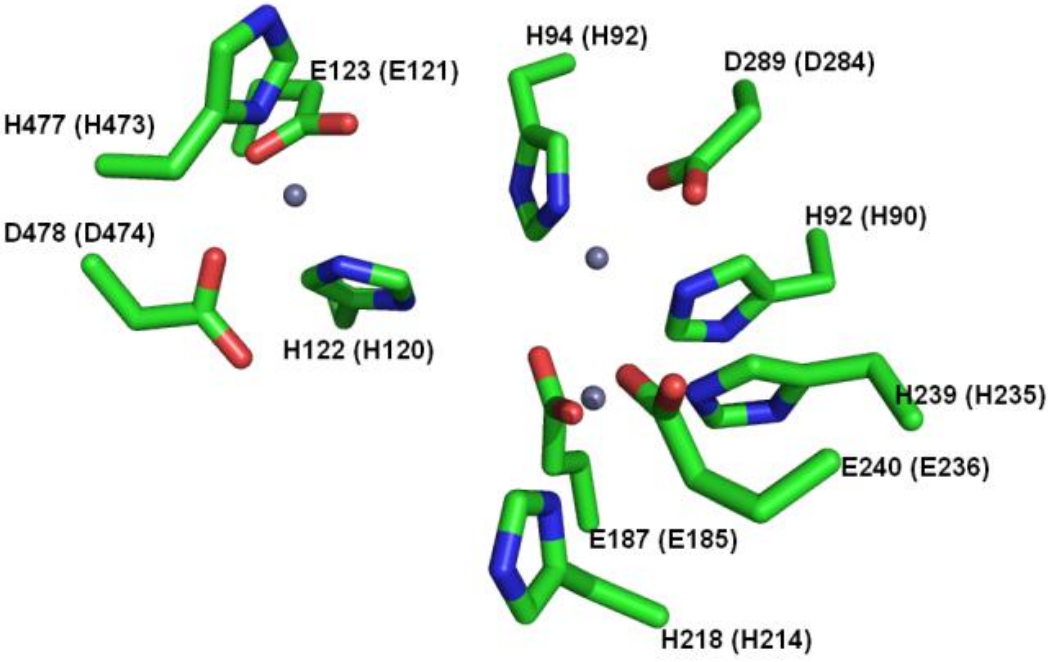


**Figure 3.1:** *Active site structure of [$Mn^{II}/Mn^{II}$]-$ADE_{at}$ taken from PDB id: 3nqb*. The residue numbers shown in parentheses are for the equivalent residues from adenine deaminase from *E. coli*. In this structure there is a third manganese ion bound in the active site that is currently thought to be unimportant for the catalytic activity of adenine deaminase.

ADEs from a variety of bacterial sources are highly sensitive to the presence of iron in the cell (*20, 21*). Unless precautions are made to exclude the incorporation of iron into the enzyme during protein expression, the isolated enzyme is damaged and the catalytic activity is severely compromised. However, the diferrous form of $ADE_{ec}$, made via the reconstitution of apo-protein, is remarkably stable, even in the presence of $O_2$ (*20, 21*). In this chapter, we demonstrate the extreme lability of ADE in the cell is due to the reaction of $H_2O_2$ with the diferrous form of the enzyme and suggest that this reaction may serve as a marker for oxidative stress in certain bacteria. $[Fe^{II}/Fe^{II}]$-ADE catalyzes the disproportionation of $H_2O_2$ peroxide to water and $O_2$, and the formation of hydroxyl radical and superoxide from the same substrate. The hydroxyl radicals oxygenate multiple amino acid side chains within the active site and the catalytic activity is completely abolished. This is the first report of an enzyme in AHS that is able to catalyze an oxidation/reduction reaction. A chemical mechanism for the reaction of hydrogen peroxide with the iron-bound form of ADE is proposed.

## MATERIALS AND METHODS

*Materials.* All chemicals were purchased from Sigma-Aldrich unless otherwise stated. *Escherichia coli* BL21(DE3) and XL1-blue competent cells were obtained from Stratagene. The expression vector pET30a(+), *Pfx Platinum* DNA polymerase and *Pfu Turbo* DNA polymerase were purchased from Invitrogen.

*Adenine Deaminase from E. coli and A. tumefaciens.* The cloning of adenine deaminase from *E. coli* ($ADE_{ec}$) and *A. tumefaciens* (Atu4426; gi|15890557) was performed as described (*20*). Mutations to these proteins were constructed using the

QuikChange PCR protocol according the manufacturer's instructions. These enzymes were expressed and purified using an iron-free expression protocol (*20*). The deamination of adenine was followed spectrophotometrically at 340 nm (*20*).

*Adenine Deaminase from Other Sources.* The clones for adenine deaminase from *Bacillus halodurans* (Bh0640; gi|15613203), *Bacillus subtilis* (Bsu14520; gi|16078516) and *Clostridium acetobutylium* (Cac0887; gi|15894174) were cloned, expressed and purified by the New York Structural GenomiX Research Consortium (NYSGXRC) (*21*).

*Preparation of [$Fe^{II}/Fe^{II}$]-ADE.* Apo-ADE was reconstituted by the anaerobic addition of two equivalents of $Fe^{2+}$ (*20*). The samples were subsequently passed through a PD-10 column to remove unbound metal (*20*). The stoichiometry of the reconstituted metal center was determined by titration of apo-ADE (10 μM) with $Fe^{2+}$.

*Measurement of Catalase Activity.* The formation of $O_2$ was determined with a YSI 5300A biological oxygen monitor at 30 $^{o}$C. The standard assay conditions were 20 mM HEPES, pH 7.5, variable amounts of $H_2O_2$ and enzyme in a final volume of 3.0 mL. The $H_2O_2$ concentration was calibrated with an oxygen electrode and bovine liver catalase. The $H_2O_2$ concentration was also measured spectrophotometrically at 240 nm using a molar extinction coefficient of 43.6 $M^{-1}$ $cm^{-1}$ (*51*). For control experiments, 250 μM $H_2O_2$ was added to a buffered solution containing 3.0 μM $Fe^{2+}$ and 1.0 mM EDTA, or 3.0 μM $Fe^{2+}$, 1.0 mM EDTA, and 1.0 mM ascorbate.

*Redox Titrations.* The reduction potential of [$Fe^{II}/Fe^{II}$]-$ADE_{ec}$ was determined with the redox dye, thymol indophenol (TCI America). [$Fe^{II}/Fe^{II}$]-$ADE_{ec}$ (20 μM) was

incubated with 2-14 equivalents of thymol indophenol in 20 mM HEPES, pH 7.5, at room temperature for 4 hours. Similar experiments were conducted with $[Fe^{II}/Fe^{II}]$-$ADE_{ec}$ treated previously with 5 equivalents of $H_2O_2$. Determination of the reduction potential of fully oxygenated $[Fe^{II}/Fe^{II}]$-$ADE_{ec}$ was conducted with protein that had been treated previously with 3.0 mM $H_2O_2$. The excess $H_2O_2$ was removed by passage through a PD-10 column. The reduced form of Crystal Violet was used to reduce the oxidized binuclear metal center back to the di-ferrous state in 20 mM HEPES, pH 7.5. The concentrations of the oxidized and reduced forms of the dye were determined at 590 nm after 6 hours of incubation.

*Mass Spectrometry.* $ADE_{ec}$ (5 µg) was loaded onto a 10% SDS-PAGE gel. The Coomasie Blue-stained protein band was excised from the gel, cut into pieces and digested with trypsin (Promega). The excised gel bands were washed with 25 mM ammonium bicarbonate, pH 8.0, dehydrated with 50 µL of a 2:1 mixture of acetonitrile/50 mM ammonium bicarbonate for 5 minutes and then dried in a vacuum centrifuge. Gel pieces were further rehydrated for 40 minutes in an ice bath with 20 µM trypsin (Promega) in 25 mM ammonium bicarbonate buffer to a final volume of 12 µL. Following rehydration, samples were digested for 4 hours at 37 °C. The digested gel slices (1-2 µL) were analyzed by tandem mass spectrometry (Agilent 6520 quadrupole time-of-flight instrument with chip cube electrospray ionization). Samples were injected using a protein chip (160-nL trap, 75 µm x 150 mm, 5 µm, C-18 SB-Zorbax, 300Å) at a flow rate 300 nL/min. Data acquisition was performed using MassHunter (version B.02.00) in a 2-GHz extended dynamic range at a rate of three scans per second

followed by data-dependent tandem mass spectrometric fragment scans of the four most intense ions. Precursor ion exclusion was set to 6 seconds after two consecutive tandem mass spectrometric scans. Acquired tandem mass spectrometric spectra were analyzed against a trypsin-specific enzyme search within Spectrum Mill (Agilent Technologies) with the defined protein sequence. The mass spectrometry data acquisition was performed by Shane E. Tichy at Agilent Technologies, Santa Clara, CA. For intact mass analysis of ADE from *B. halodurans*, *A. tumefaciens*, *B. subtilis*, and *C. actobutylium*, matrix-assisted laser desorption/ionization (MALDI, Voyager-DE) and Liquid Chromatography Electrospray Ionization Mass Spectrometry (LC-ESI-MS, Agilent 1100, API150EX) were used to assess the purity and measure accurate masses of proteins by the NYSGXRC (*21*).

*EPR and Mössbauer Spectroscopy.* The samples for EPR and Mössbauer spectroscopy were made as described previously and the data was collected by the Lindahl laboratory, Texas A&M University (*20*).

*Titration with Hypochlorous Acid.* $[Fe^{II}/Fe^{II}]$-$ADE_{ec}$ (1.0 μM) was treated with hypochlorous acid (HOCl) ranging from 0-20 μM for 5 minutes at 30 $^{o}$C, pH 7.5. At the end of the reaction, the adenine deaminase activity was determined as described (*20*). In addition, HOCl (200 μM) was added to 16 μM $[Fe^{II}/Fe^{II}]$-$ADE_{ec}$ and the absorbance spectrum was measured. The same experiments were performed with $[Mn^{II}/Mn^{II}]$-$ADE_{ec}$ as a control. The concentration of HOCl was determined at 292 nm ($\varepsilon$ = 3241 $M^{-1}cm^{-1}$) (*52*).

*Detection of Superoxide.* The formation of superoxide was measured using the dye hydroethidine (Invitrogen). The concentration of hydroethidine was determined at 345 nm ($\varepsilon = 9.75 \times 10^3\ M^{-1}\ cm^{-1}$) (*53*). Hydroethidine reacts with superoxide to form 2-hydroxyethidium which was monitored at 470 nm ($\varepsilon = 1.2 \times 10^4\ M^{-1}\ cm^{-1}$) (*53*). $[Fe^{II}/Fe^{II}]$-$ADE_{ec}$ (1.50 μM) was mixed with 1.0 mM hydroethidine in a final volume of 3.0 mL in a YSI 5300A biological oxygen monitor system at 30 $^oC$. Hydrogen peroxide (250 μM) was added and the evolution of $O_2$ was measured as a function of time. After $O_2$ production ceased, 1.0 mL from this reaction mixture was removed and the absorbance was measured at 470 nm.

*pH-Rate Profiles.* The pH dependence of $k_{cat}$ and $k_{cat}/K_m$ for the catalase activity was determined for $[Fe^{II}/Fe^{II}]$-$ADE_{ec}$ over the pH range of 5.5-10.0. The buffers used for this study were 20 mM MES (pH 5.5-6.5), 20 mM HEPES (7.0-8.0) and 20 mM CHES (pH 8.5-10.0). The pH values of the solutions were measured before and after the completion of the assays.

*6-Chloropurine Inhibition of Catalase Activity.* A solution of $[Fe^{II}/Fe^{II}]$-$ADE_{ec}$ (1.5 μM) was incubated with 3.0 mM 6-chloropurine for 1 hour in 50 mM HEPES buffer, pH 7.5 and then assayed for adenine deaminase and catalase activity as described previously (*20*).

*Data Analysis.* Initial velocity kinetic data were fit to **equation 2.1** using SigmaPlot 9.0 where *v* is the initial velocity, [A] is the substrate concentration, $E_t$ is the total enzyme concentration, $k_{cat}$ is the turnover number and $K_m$ is the Michaelis constant. For pH-rate profiles, **equation 3.1** was used to fit the half-bell shaped pH profiles to

determine values of p$K_a$ for the ionization of residues at low pH. In **equation 3.1**, the value of *c* is the maximum value for either $k_{cat}$ or $k_{cat}/K_m$, depending on the fit, and H is the proton concentration. In **equation 3.2**, E is the reduction potential of the metal center, $E^o$ is the reduction potential of the dye, R is the universal gas constant, T is the temperature, *n* is the number of electrons transferred during the redox reaction and F is the Faraday constant. $A_{ox}$ is the concentration of the species involved in the oxidation reaction of the enzyme and $A_{red}$ is the concentration of the species involved in the reduction reaction of the enzyme.

$$v / E_t = k_{cat} [A] / (K_m + [A]) \qquad \textbf{(Equation 2.1)}$$

$$\log y = \log[c/(1 + H/K_a)] \qquad \textbf{(Equation 3.1)}$$

$$E = E^o - (RT \ln [A_{red}]/[A_{ox}])/nF \qquad \textbf{(Equation 3.2)}$$

*Structure Determination of Atu4426.* The iron/manganese hybrid ($[Fe^{II}/Mn^{II}]$-$ADE_{at}$) and the diferrous form ($[Fe^{II}/Fe^{II}]$-$ADE_{at}$) of adenine deaminase from *A. tumefaciens* were crystallized by the sitting drop vapor diffusion method at room temperature using conditions similar to [Mn/Mn]-$ADE_{at}$ (*20, 21*). The atomic coordinates and structure factors were deposited in the Protein Data Bank (PDB Id: 3T81 ($[Fe^{II}/Fe^{II}]$-$ADE_{at}$) and 3T8L ($[Fe^{II}/Mn^{II}]$-$ADE_{at}$)). The structures were determined by the Swaminathan laboratory at the Brookhaven National Laboratories, NY. The PDB co-ordinates have now been deposited in the Protein Data Bank and are released to be viewed and downloaded.

RESULTS

*Isolation of Adenine Deaminase.* The gene for $ADE_{ec}$ was expressed in *E. coli* using standard methods (*20, 21*). However, the identity of the isolated protein could not be verified by mass spectrometry because multiple levels of post-translational modification made the spectrum impossible to interpret. Mass spectrometric analysis of the trypsin-generated fragments (70% coverage) identified the following residues as oxygenated: His-90, His-92, Met-97, Met-98, Met-186, Met-187, His-235, Met-251, Met-254, His-513 and Met-522. Of these residues, His-90, His-92 and His-235 are metal binding residues, based on amino acid sequence identity and the three-dimensional structure of $ADE_{at}$ (PDB: 3nqb). The kinetic constants for the deamination of adenine by the oxygenated $ADE_{ec}$ are $2 \pm 0.3$ $s^{-1}$, $0.8 \pm 0.1$ mM and $(2.5 \pm 0.2) \times 10^3$ $M^{-1}$ $s^{-1}$ for $k_{cat}$, $K_m$, and $k_{cat}/K_m$, respectively. The mass spectrum of $ADE_{ca}$ from *C. acetobutylicum* (locus tag: Cac0887) also exhibited multiple species from oxygenation when expressed in *E. coli*. The mass spectrum pinpointed oxygenation sites at His-73, His-75, His-105, His-198, and His-219. Of these residues His-73, His-75, His-198 and His-219 are metal binding residues based on the structure of $ADE_{at}$ (*21*).

*Sequestration of Iron.* It was initially postulated that oxygenation of amino acid residues throughout the protein was initiated by reactions catalyzed by iron bound in the active site of adenine deaminase (*20, 21*). The addition of 50 μM 2,2'-dipyridyl and 1.0 mM $Mn^{2+}$ to the growth medium was utilized to sequester the iron at the time of induction. $ADE_{ec}$ purified from iron-depleted medium yielded a single species via analysis by mass spectrometry with a molecular weight of 63741 Da. Trypsin digestion

of this protein gave a 91% sequence coverage and no residues were found to be oxygenated. The total metal content was 2.0 ± 0.1 eq of Mn per protein subunit. The kinetic constants for the deamination of adenine by $[Mn^{II}/Mn^{II}]$-$ADE_{ec}$, expressed and isolated by this protocol, are 200 ± 5 $s^{-1}$, 0.40 ± 0.04 mM, and (5 ± 0.4) x $10^5$ $M^{-1}$ $s^{-1}$ for $k_{cat}$, $K_m$, and $k_{cat}/K_m$, respectively. The mass spectrum of $ADE_{ca}$, isolated using the iron-free expression protocol, is presented in (*21*). The kinetic constants and average metal content for ADE cloned from various bacterial sources and expressed in *E. coli* in the presence and absence of the iron chelator are presented in **Table 3.1**.

$[Mn^{II}/Mn^{II}]$-$ADE_{ec}$ was used to prepare apo-$ADE_{ec}$ and this protein was reconstituted with variable amounts of $Fe^{2+}$, $Mn^{2+}$, or $Zn^{2+}$. There was a linear increase in the adenine deaminase activity until two equivalents of metal were added (*20, 44*). Beyond two equivalents of metal per subunit, the deaminase activity remained constant and ICP-MS confirmed the binding of two equivalents of metal per enzyme subunit. Previous Mössbauer spectra of the diiron-reconstituted enzyme indicates that both irons are high-spin ferrous, which is denoted as $[Fe^{II}/Fe^{II}]$-$ADE_{ec}$ (*20*).

*Inactivation of $ADE_{ec}$ by $H_2O_2$.* A large molar excess of $H_2O_2$ (250 μM) was added to the metal-reconstituted forms of $ADE_{ec}$ (1.50 μM). Evolution of $O_2$ was observed when $H_2O_2$ was added to $[Fe^{II}/Fe^{II}]$-$ADE_{ec}$ but not when it was added to either $[Mn^{II}/Mn^{II}]$-$ADE_{ec}$ or $[Zn^{II}/Zn^{II}]$-$ADE_{ec}$. After the addition of a large excess of $H_2O_2$ to $[Fe^{II}/Fe^{II}]$-$ADE_{ec}$, the enzyme was unable to catalyze the deamination of adenine, whereas $[Mn^{II}/Mn^{II}]$-$ADE_{ec}$ and $[Zn^{II}/Zn^{II}]$-$ADE_{ec}$ had catalytic activities that were unchanged (*21*).

**Table 3.1**: *Kinetic parameters of ADE using a standard and iron-free expression protocol*

Standard Expression Protocol

| Locus tag | gi | $k_{cat}$ ($s^{-1}$) | $k_{cat}/K_m$ ($M^{-1}s^{-1}$) | Metal content |
|---|---|---|---|---|
| b3665 | 16131535 | 2.0 ± 0.3 | (2.5 ± 0.2) x $10^3$ | 0.3 eq. Fe<br>0.2 eq. Zn |
| Bh0640 | 15613203 | 2.4 ± 0.4 | (1.2 ± 0.2) x $10^4$ | 0.3 eq. Fe<br>0.2 eq. Zn |
| Atu4426 | 15890557 | 1.4 ± 0.1 | (5.0 ± 0.4) x $10^3$ | 0.6 eq. Mn<br>0.4 eq. Fe |
| Bsu14520 | 16078516 | 1.1 ± 0.4 | (3.6 ± 0.3) x $10^3$ | 0.2 eq. Fe<br>0.2 eq. Zn |
| Cac0887 | 15894174 | 0.52 ± 0.02 | (5.2± 0.3) x $10^3$ | 0.5 eq. Fe<br>0.1 eq. Zn |

Iron-Free Expression Protocol

| Locus tag | gi | $k_{cat}$ ($s^{-1}$) | $k_{cat}/K_m$ ($M^{-1}s^{-1}$) | Metal content |
|---|---|---|---|---|
| b3665 | 16131535 | 200 ± 5 | (5.0 ± 0.4) x $10^5$ | 2.0 eq. Mn |
| Bh0640 | 15613203 | 120 ± 4 | (4.0 ± 0.3) x $10^5$ | 1.9 eq. Mn<br>0.1 eq. Fe |
| Atu4426 | 15890557 | 155 ± 5 | (4.8 ± 0.3) x $10^5$ | 2.3 eq. Mn |
| Bsu14520 | 16078516 | 140 ± 6 | (3.5 ± 0.5) x $10^5$ | 1.6 eq. Mn<br>0.1 eq. Fe |
| Cac0887 | 15894174 | 180 ± 7 | (4.5 ± 0.4) x $10^5$ | 1.5 eq. Mn<br>0.1 eq. Fe |

*Disproportionation of $H_2O_2$.* The initial rate of $O_2$ evolution catalyzed by $[Fe^{II}/Fe^{II}]$-$ADE_{ec}$ increased with the concentration of $H_2O_2$. The kinetic constants for the catalase activity of $[Fe^{II}/Fe^{II}]$-$ADE_{ec}$ were 200 ± 24 $s^{-1}$, 8.8 ± 2.2 mM, and (2.4 ± 0.5) x $10^4$ $M^{-1}s^{-1}$ for $k_{cat}$, $K_m$, and $k_{cat}/K_m$, respectively (based on $H_2O_2$ consumption). The net increase in the concentration of $O_2$ produced after the addition of an excess of $H_2O_2$ to $[Fe^{II}/Fe^{II}]$-$ADE_{ec}$ was proportional to the concentration of added enzyme (**Figure 3.2).** The ratio of $O_2$ produced, relative to the initial concentration of $[Fe^{II}/Fe^{II}]$-$ADE_{ec}$, was 64 ± 3. No $O_2$ evolution (<1%) was observed for any of the control reactions when 3.0 μM $Fe^{2+}$ was incubated with either EDTA or ascorbate, or by $Fe^{2+}$ itself, when 250 μM $H_2O_2$ was added. Therefore, the formation of $O_2$ was due entirely to the catalytic activity of the iron bound to the active site of adenine deaminase. The time course for the formation of $O_2$ after adding 250 μM $H_2O_2$ to 1.50 μM $[Fe^{II}/Fe^{II}]$-$ADE_{ec}$ was followed with an oxygen electrode (**Figure 3.4**, open circles) and the net change in $O_2$ concentration was 97 μM (342-245 μM). After $O_2$ formation ceased, bovine liver catalase was added to determine the concentration of $H_2O_2$ that remained. The $O_2$ concentration increased from 342 to 356.5 μM and thus an additional 14.5 μM $O_2$ was produced. Since bovine liver catalase consumes two molecules of $H_2O_2$ for every $O_2$ produced, the concentration of $H_2O_2$ remaining at the time of addition of bovine catalase was 29 μM. Therefore, addition of 1.50 μM $[Fe^{II}/Fe^{II}]$-$ADE_{ec}$ to 250 μM $H_2O_2$ consumed 221 μM (250-29 μM) hydrogen peroxide and produced 97 μM $O_2$. The formation of 97 μM $O_2$ accounts for 194 μM of the hydrogen peroxide consumed.

Addition of 3.0 mM 6-chloropurine to a solution containing 1.5 μM $[Fe^{II}/Fe^{II}]$-$ADE_{ec}$ completely inhibited the disproportionation of $H_2O_2$.

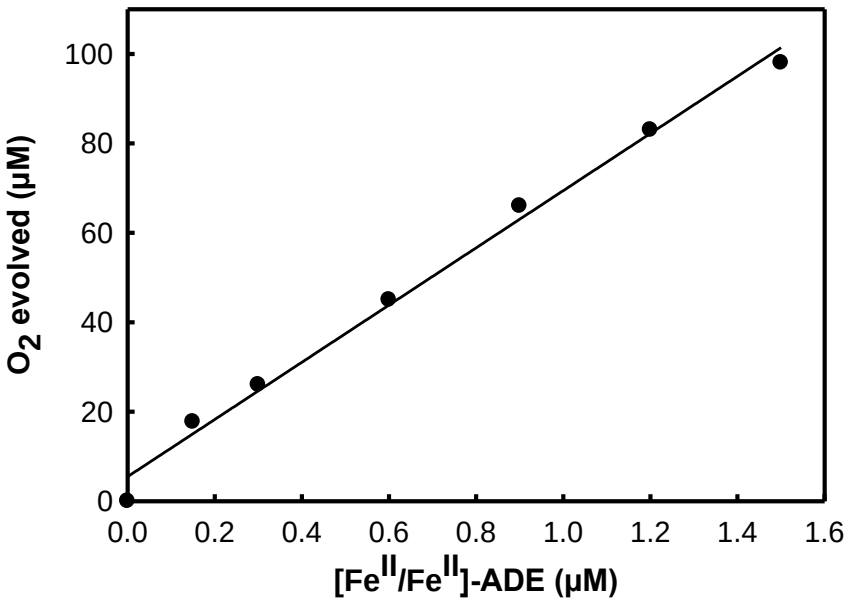


**Figure 3.2**: *Total concentration of $O_2$ evolved from $[Fe^{II}/Fe^{II}]$-$ADE_{ec}$.* The addition of 250 μM $H_2O_2$ to variable amounts of $[Fe^{II}/Fe^{II}]$-$ADE_{ec}$ at pH 8.0, 30 $^oC$.

Titration of $Fe^{2+}$ to apo-$ADE_{ec}$ (**figure 3.3**) shows a linear increase in the catalase activity with increasing $Fe^{2+}$ concentration. Maximum catalase activity is observed at two equivalents of $Fe^{II}$ per monomer of apo-$ADE_{ec}$.

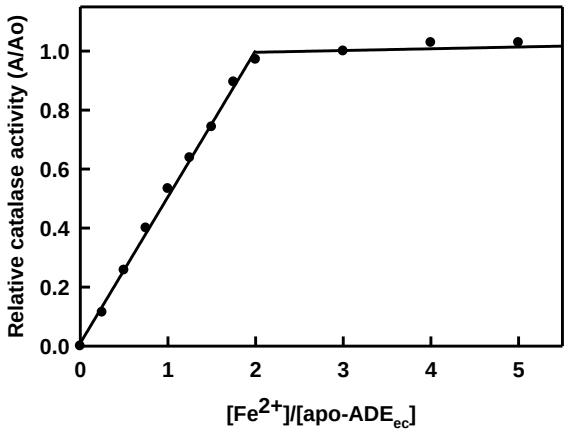


**Figure 3.3:** *The catalase activity after anaerobic addition of $Fe^{II}$ to apo-$ADE_{ec}$.* The maximal activity is obtained at two enzyme equivalents of iron per monomer of $ADE_{ec}$.

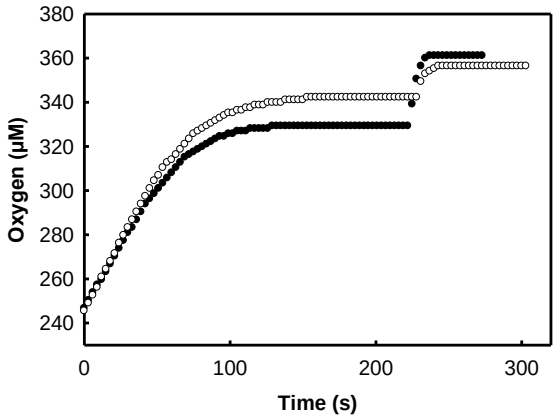


**Figure 3.4**: *Time course for $O_2$ formation as a function of time after the addition of $[Fe^{II}/Fe^{II}]$-$ADE_{ec}$ to an excess of hydrogen peroxide at pH 8.0*. The open circles are in the absence of hydroethidine and the closed circles are in the presence of 1.0 mM hydroethidine. After cessation of $O_2$ evolution, catalase from bovine liver was added to determine the concentration of the unreacted $H_2O_2$.

Aliquots were removed after the addition of $H_2O_2$ to [$Fe^{II}/Fe^{II}$]-$ADE_{ec}$ and then assayed for adenine deaminase activity. The activity decreased as a function of time, with a first-order rate constant of 0.011 ± 0.001 $s^{-1}$ (data not shown). EPR and Mössbauer spectra of $ADE_{ec}$ after cessation of $O_2$ formation indicated a high spin ferric oxidation state (**Figures 3.5a** and **3.5b**) (*45, 54*). Mass spectrometry of the tryptic peptides from $ADE_{ec}$ treated with an excess of $H_2O_2$ demonstrated that the following amino acids were oxygenated: His-90, His-92, Met-97, Met-98, His-176, Met-186, Met-187, Met-251, Met-254, His-513 and Met-522. These are the same amino acid residues that were identified as oxygenated in the protein expressed in *E. coli* without the addition of 2,2'-dipyridyl to sequester the iron prior to induction (*21*).

*Titration of [$Fe^{II}/Fe^{II}$]-ADE with Hydrogen Peroxide*. The amount of $O_2$ produced when 1-5 molar equivalents of $H_2O_2$ were added to 20 μM [$Fe^{II}/Fe^{II}$]-$ADE_{ec}$ was determined. After the first equivalent of $H_2O_2$ was added, 2.2 μM $O_2$ was formed. The second equivalent of $H_2O_2$ resulted in the formation of 5.9 μM $O_2$. The sequential addition of three more equivalents of $H_2O_2$ resulted in the formation of 9.0 μM $O_2$ with each added equivalent. No $O_2$ was produced when wild-type [$Fe^{II}/Fe^{II}$]-$ADE_{ec}$ was oxidized by ferricyanide to [$Fe^{III}/Fe^{III}$]-$ADE_{ec}$ prior to the addition of $H_2O_2$. Mass spectrometry of $ADE_{ec}$ revealed that the first molar equivalent of $H_2O_2$ added to untreated [$Fe^{II}/Fe^{II}$]-$ADE_{ec}$ oxygenated either Met-99 or Met-98 while the second molar equivalent oxygenated either His-90 or His-92 (data not shown). The Mössbauer spectra after the addition of one to four equivalents of $H_2O_2$ to [$Fe^{II}/Fe^{II}$]-$ADE_{ec}$ are presented in **Figure 3.6**. In each case the metal center is found in the diferrous oxidation state.

*Detection of Superoxide*. The formation of superoxide was probed with the reagent hydroethidine (*53*). Addition of hydroethidine (1.0 mM) to a solution of hydrogen peroxide (256 μM) and [$Fe^{II}/Fe^{II}$]-ADE (1.50 μM) reduced the net production of $O_2$ from 97 μM (in the absence of hydroethidine) to 81 μM (329-248 μM) as shown in **Figure 3.4 (**closed circles). After cessation of $O_2$ formation, bovine liver catalase was added to the reaction mixture to determine the concentration of the remaining $H_2O_2$. The $O_2$ concentration in the solution increased from 329 to 361 μM and thus 64 μM $H_2O_2$ remained from the initial concentration of 256 μM. The change in absorbance at 470 nm was 0.20, which corresponds to the formation of 17 μM 2-hydroxyethidium using an extinction coefficient of 1.2 x $10^4$ $M^{-1}$ $cm^{-1}$ (*53*), and thus 17 μM superoxide was formed. Overall, the concentration of $O_2$ and superoxide increased by 81 and 17 μM, respectively, and the concentration of $H_2O_2$ decreased by 192 μM.

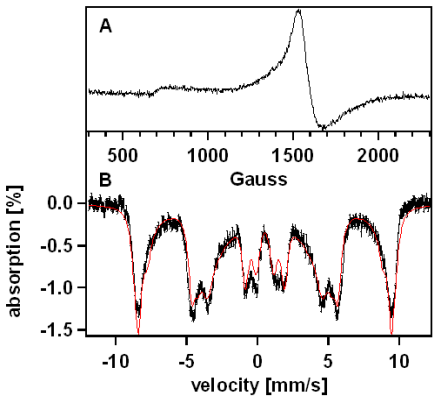


**Figure 3.5**: *EPR and Mössbauer spectrum of [$Fe^{III}/Fe^{III}$]-ADE after the addition of 15 mM $H_2O_2$*

From the figure 3.5; (A) EPR parameters: temperature, 10 K; microwave power, 9.46 GHz, 0.2 mW. (B) The spectrum was collected at 4.5 K, 400 G magnetic field

applied parallel to the radiation. Red line represents a simulation of the data with a single species with the following parameters: D = 0.129, E/D = 0.194, $g_x = g_y = g_z = 2.0$, $\Delta E_q = 0$ mm/sec, Eta = -1.00, $A_x = -222.271$ kG, $A_y = -247.824$ kG, $A_z = -224.863$ kG, $\delta = 0.504$, $\Gamma = 0.500$ mm/sec. (Data collected by the Lindahl Lab).

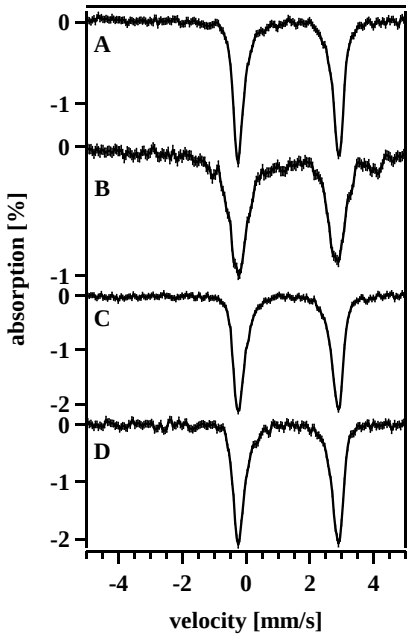


**Figure 3.6:** *Mössbauer spectra of [$Fe^{II}/Fe^{II}$] –ADE with different $H_2O_2$* (A) 1 equivalent of $H_2O_2$ added, (B) 2 equivalents of $H_2O_2$ added, (C) 3 equivalents of $H_2O_2$ added, and (D) 4 equivalents of $H_2O_2$ added. All spectra were recorded at 5K with a 700G magnetic field applied parallel to the radiation. All spectra can be fit with a single quadrupole doublet with $\delta = 1.39$ mm/s and $\Delta E_q = 3.27$mm/s. (Data collected by the Lindahl Lab).

*Hydroxyl Radical Formation.* Lidocaine is a potent hydroxyl radical scavenger (*55*). The addition of a large excess of lidocaine (0.5 M) did not affect the rate of $O_2$ evolution after 250 μM $H_2O_2$ was added to 1.5 μM [$Fe^{II}/Fe^{II}$]-$ADE_{ec}$. When other hydroxyl radical scavengers (thiourea, ethanol, methanol, ethylene glycol and DMSO)

were added at a concentration of 0.50 M, no change was observed in the rates of $O_2$ evolution and ADE inactivation. HOCl has been shown to produce hydroxyl radicals in reactions with specific iron complexes (*56*). $[Fe^{II}/Fe^{II}]$-$ADE_{ec}$ was titrated with HOCl and ~12 enzyme equivalents of this reagent were needed to inactivate the deaminase activity as shown in **Figure 3.7**. The formation of chloride was verified by the formation of a precipitate after the addition of silver nitrate. At the end of the reaction of $[Fe^{II}/Fe^{II}]$-$ADE_{ec}$ with HOCl, the iron was found in a high-spin ferric oxidation state (**figure 3.8).**

*Preparation of Mn/Fe Hybrids.* $[Mn^{II}/Mn^{II}]$-$ADE_{ec}$ is active as a deaminase but not as a catalase. In contrast, $[Fe^{II}/Fe^{II}]$-$ADE_{ec}$ catalyzes both reactions. To determine whether the binuclear metal center of this enzyme must be occupied with two equivalents of iron, or if a manganese/iron hybrid would be sufficient for catalase activity, apo-$ADE_{ec}$ (1.5 μM) was reconstituted with two equivalents of metal using a mixture of manganese and iron of different ratios (3.0 μM total metal concentration). ICP-MS verified that the metal content of $ADE_{ec}$ after reconstitution was in accordance with the ratio of metal ions added to apo-$ADE_{ec}$. The adenine deaminase activity was independent of the ratio of $Mn^{2+}$ and $Fe^{2+}$ added to the enzyme (**Figure 3.9**). However, no catalase activity was observed until the ratio of iron to manganese was greater than 1.0. When more than one equivalent of iron was added to apo-$ADE_{ec}$ there was a linear increase in the catalase activity with an increase in the iron content (**Figure 3.9**). These results are consistent with the preferential binding of manganese and/or iron at one of the two metal sites within the binuclear metal center and a requirement for both sites to be

occupied by iron for the catalase activity but not the deaminase activity. EPR and Mössbauer spectra of $[Mn^{II}/Fe^{II}]$-$ADE_{ec}$ are shown in **Figures 3.10** and **3.11**.

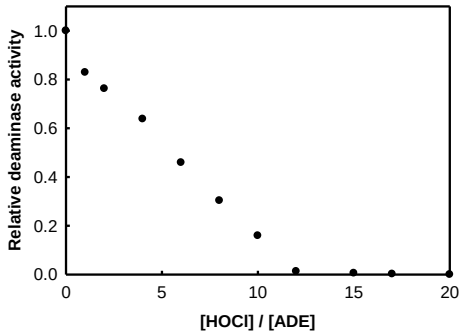


**Figure 3.7**: *The loss of adenine deaminase activity after addition of HOCl to* $[Fe^{II}/Fe^{II}]$-$ADE_{ec}$ (1.0 μMat 30 °C). The deaminase activity was assayed 5 minutes after addition of HOCl to $[Fe^{II}/Fe^{II}]$-$ADE_{ec}$.

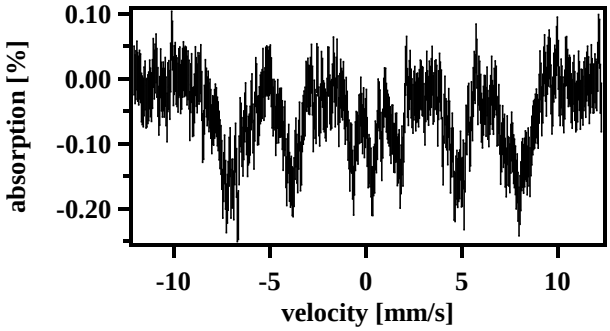


**Figure 3.8:** *Mössbauer spectrum of Fe/Fe ADE with 15 equivalents of HOCl* (~ 3 mM). Spectrum was collected at 5K with a 700G field applied parallel to the radiation. (Data collected by the Lindahl Lab). Fe/Fe-ADE = 205 μM

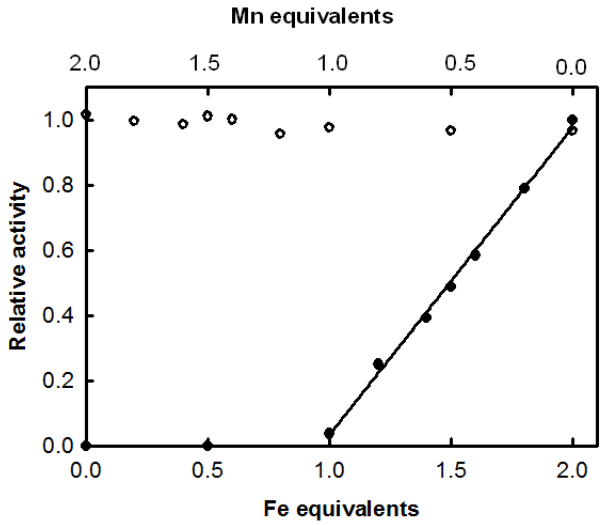


**Figure 3.9**: *ADE and catalase activity and metal dependence*. Adenine deaminase (open circles) and catalase activities (closed circles) after apo-$ADE_{ec}$ (1.5 μM) was reconstituted with two enzyme equivalents of total metal (3.0 μM) using various ratios of $Mn^{2+}$ and $Fe^{2+}$.

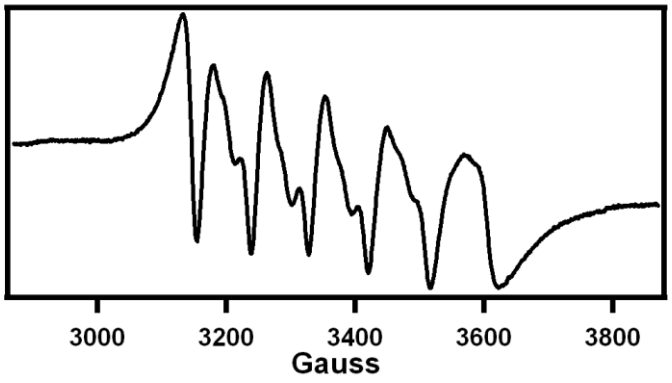


**Figure 3.10:** *EPR spectrum of Mn/Fe ADE* (200 μM). EPR parameters: temperature, 10 K; microwave 9.46 GHz, 0.02 mW. (Data collected by the Lindahl Lab).

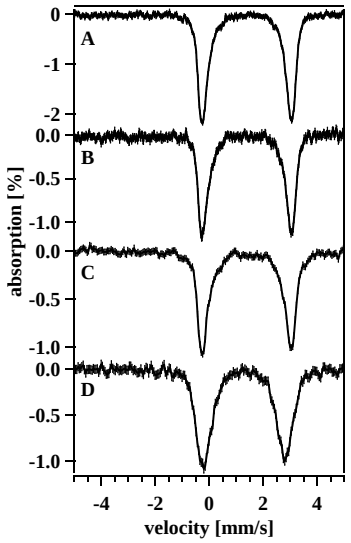


**Figure 3.11:** *Mössbauer spectra of Fe/Fe-ADE and Fe/Mn-ADE* (A) 200 μM Fe/Fe-ADE. (B) 200 μM Mn/Fe-ADE. (C) 200 μM Mn/Fe-ADE with 1equivalent of $H_2O_2$. (D) 200 μM Mn/Fe-ADE with 10 equivalents of $H_2O_2$. The spectra were collected at 5 K, 400 G (A-C) or 700G (D) magnetic field applied parallel to the radiation. The data can be fit with a single quadrupole doublet with $\delta$= 1.39 mm/sec, $\Delta E_q$= 3.27 mm/sec. (Data collected by the Lindahl Lab).

*Mutagenesis of ADE.* Based on the three-dimensional structure of [$Mn^{II}/Mn^{II}$]-$ADE_{at}$ (PDB: 3nqb), the metal coordinating residues His-90, Glu-236 and Asp-284 of $ADE_{ec}$ were mutated to asparagine, glutamine and alanine, respectively, and the mutant proteins were shown to bind two equivalents of metal per protein monomer. Other conserved active site residues, Ser-95, Asp-118, His-120, Glu-121, Asp-285, His-473 and Asp-474 were subsequently chosen as targets for mutagenesis based on their proximity to the binuclear metal center from the structure of $ADE_{at}$. Of these seven residues, His-120, Glu-121, His-473 and Asp-474 coordinate an adventitiously-bound

third metal ion that is ~6-8 Å from the binuclear metal center (see **Figure 3.1**). The metal-free forms of these mutants were prepared and reconstituted with $Fe^{2+}$. The adenine deaminase activity and the metal content of the iron-reconstituted mutants were measured and the results are presented in **Table 3.2**.

The catalase activity of these ten mutants, except for H473N and D474N, was the same as the wild-type enzyme reconstituted with iron. These two mutants (H473N and D474N) were unable to catalyze the disproportionation of $H_2O_2$ and were not inactivated by $H_2O_2$. The diferrous form of the H90N mutant (20 μM) was titrated with 1-5 equivalents of $H_2O_2$. Unlike the wild-type enzyme (see above), this mutant produced ~9 μM $O_2$ for each equivalent of $H_2O_2$ added. Mössbauer spectroscopy confirmed that ferricyanide treatment of $[Fe^{II}/Fe^{II}]$-H90N produced the oxidized $[Fe^{III}/Fe^{III}]$-state. The oxidized H90N mutant catalyzed the disproportionation of $H_2O_2$.

*Measurement of Reduction Potentials*. The reduction potentials for the inter-conversion of the diferrous and diferric states of $ADE_{ec}$ were measured with redox-active dyes. In these titrations it was assumed that both irons in the binuclear metal center are oxidized or reduced in pairs and that the deaminase activity could be used as a direct measure of the relative concentration of $[Fe^{II}/Fe^{II}]$-$ADE_{ec}$. The titration of freshly prepared $[Fe^{II}/Fe^{II}]$-$ADE_{ec}$ (20 μM) with thymol indophenol is presented in **Figure 3.12**. A total of 7.9 ± 0.2 equivalents of the dye was required to reduce the deaminase activity by 50%. Given the reduction potential of thymol indophenol of +174 mV *vs* NHE (*57*), substitution into equation **3** provides an apparent reduction potential of +209 ± 4 mV for the interconversion of the diferric and diferrous forms of wild-type ADE. After

$[Fe^{II}/Fe^{II}]$-$ADE_{ec}$ was treated with five equivalents of $H_2O_2$ it became easier to oxidize the binuclear metal center.

**Table 3.2**: *Catalytic constants for deaminase activity and metal content of $ADE_{ec}$ mutants.*

| $ADE_{ec}$ mutant | $K_m$ (mM) | $k_{cat}$ ($s^{-1}$) | $k_{cat}/K_m$ ($M^{-1}$ $s^{-1}$) | Metal content (Mn) |
|---|---|---|---|---|
| Wild type | 0.40 ± 0.04 | 200 ± 5 | (5.0 ± 0.4) x $10^5$ | 2.0 ± 0.1 |
| H90N | 0.33 ± 0.03 | 10 ± 0.8 | (3.0 ± 0.3) x $10^4$ | 1.8 ± 0.3 |
| S95A | 0.47 ± 0.04 | 98 ± 3 | (2.0 ± 0.2) x $10^5$ | 1.8 ± 0.1 |
| D118N | 0.36 ± 0.03 | 170 ± 2 | (4.7 ± 0.3) x $10^5$ | 2.1 ± 0.2 |
| H120N | 0.49 ± 0.05 | 0.17 ± 0.02 | (3.5 ± 14) x $10^2$ | 2.1 ± 0.1 |
| E121Q | 0.42 ± 0.04 | 50 ± 1 | (1.2 ± 0.2) x $10^5$ | 1.9 ± 0.2 |
| E236Q | 0.40 ± 0.04 | 0.012 ± 0.002 | 30 ± 4 | 1.8 ± 0.1 |
| D284A | 0.85 ± 0.07 | 0.042 ± 0.006 | 49 ± 5 | 2.0 ± 0.3 |
| D285A | 0.39 ± 0.04 | 40 ± 2 | (1.0 ± 0.2) x $10^5$ | 1.9 ± 0.1 |
| H473N | 0.34 ± 0.03 | 170 ± 2 | (5.0 ± 0.3) x $10^5$ | 1.8 ± 0.1 |
| D474N | 0.31 ± 0.03 | 173 ± 4 | (5.6 ± 0.2) x $10^5$ | 1.8 ± 0.1 |

The titration of *partially oxygenated* ADE with the redox active dye thymol indophenol is shown in **Figure 3.12**. This titration required 2.8 ± 0.1 equivalents of thymol indophenol to reduce the deaminase activity by 50%. This is consistent with a reduction potential of +194 ± 2 mV for the binuclear metal center of partially

oxygenated ADE. The addition of thymol indophenol to [$Mn^{II}/Mn^{II}$]-$ADE_{ec}$ showed no change in catalytic activity indicating that the dye cannot oxidize manganese.

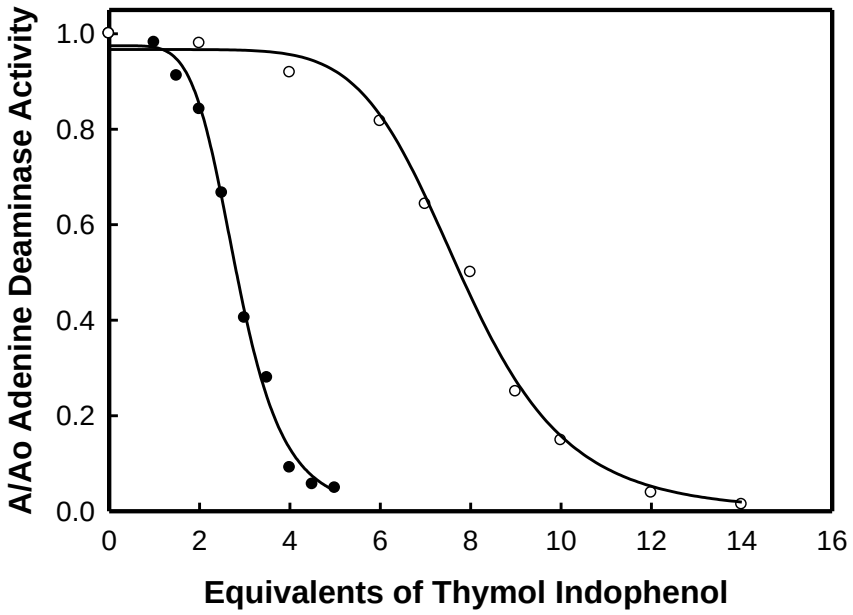


**Figure 3.12**: *Titration of [$Fe^{II}/Fe^{II}$]-ADE with various amounts of thymol indophenol*. The open circles are for enzyme (20 μM) prior to the addition of hydrogen peroxide. The closed circles are for enzyme after the addition of five equivalents (100 μM) of hydrogen peroxide. Additional details are provided in the text.

When [$Fe^{II}/Fe^{II}$]-$ADE_{ec}$ was treated with a large excess of $H_2O_2$, the binuclear metal center was left in the diferric state, the deaminase activity was lost and not recoverable, even after reduction to the ferrous state using the dithionite. Since the ratio of the diferrous and diferric states of the binuclear metal center could not be determined from a direct measurement of the deaminase activity, the distribution of the oxidized and

reduced species during the redox titration was determined spectrophotometrically with a dye that is colored in the oxidized state and colorless in the reduced state. The dye Crystal Violet has a reduction potential of 167 mV (*57*). The oxidized form of the dye absorbs at 590 nm with an extinction coefficient of 54,000 $M^{-1}$ $cm^{-1}$ (*58*). The reduced form of Crystal Violet was utilized to reduce the binuclear metal center in *fully oxygenated* ADE. In this titration 1.4 ± 0.3 equivalents of the reduced dye were required to reduce 50% of the binuclear metal centers in ADE. Therefore, the reduction potential for the binuclear metal center of $[Fe^{III}/Fe^{III}]$-$ADE^{ox}$ is +175 ± 4 mV.

The reduction potentials of two mutants, $[Fe^{II}/Fe^{II}]$-H90N and $[Fe^{II}/Fe^{II}]$-H473N were measured using the thymol indophenol dye. The manganese-reconstituted enzymes for both of these mutants were used as controls. $[Fe^{II}/Fe^{II}]$-H90N required 2.6 ± 0.2 enzyme equivalents of thymol indophenol to reduce the adenine deaminase activity by 50%. This translates to a redox potential of +192 ± 4 mV. $[Fe^{II}/Fe^{II}]$-H473N required 8.0 ± 0.3 equivalents of thymol indophenol to reduce the adenine deaminase activity by 50%. The redox potential of $[Fe^{II}/Fe^{II}]$-H473N from this titration is + 210 ± 6 mV.

*pH Profiles.* The kinetic constants for the catalase activity of $[Fe^{II}/Fe^{II}]$-$ADE_{ec}$ were obtained as a function of pH (**Figure 3.13**). The profiles for $k_{cat}$ and $k_{cat}/K_m$ exhibited a single ionization for a group that is unprotonated for optimal catalytic activity. The p$K_a$ of this group from the $k_{cat}$ profile is 7.6 ± 0.3, and 7.9 ± 0.2 from the $k_{cat}/K_m$ profile.

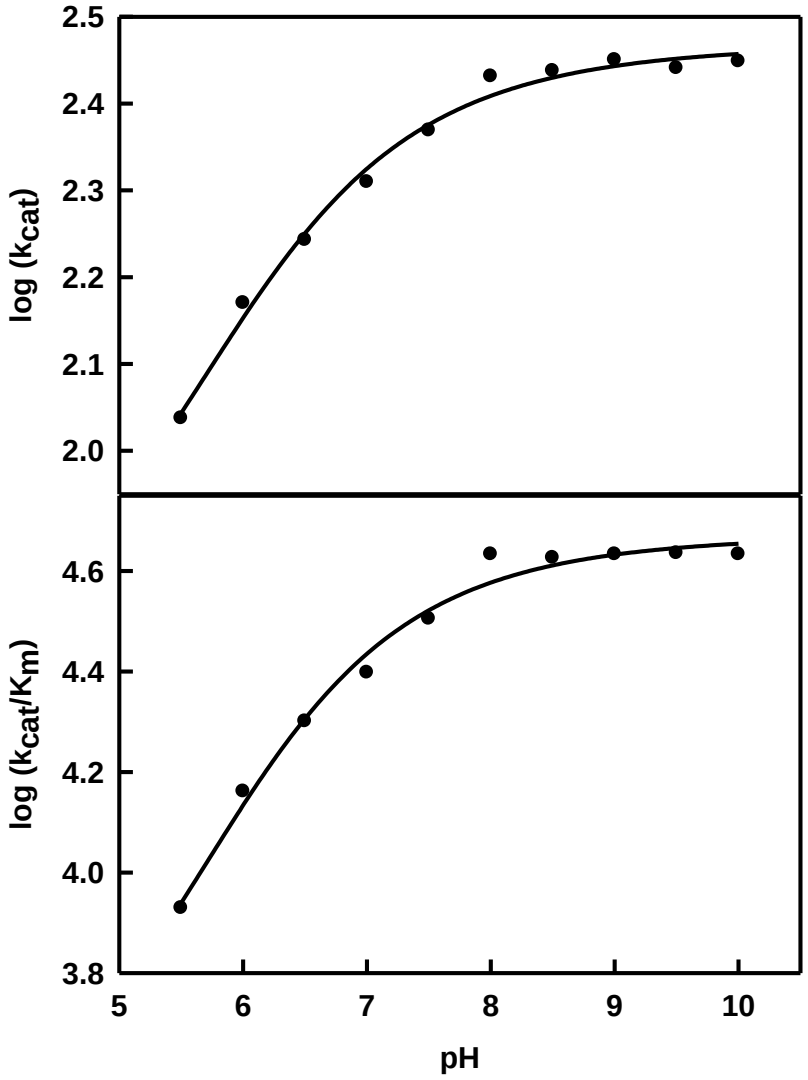


**Figure 3.13**: *pH rate profiles for the catalase activity of [Fe/Fe]-ADE$_{ec}$.* The data were fitted to equation 2.

*Structures of [Fe$^{II}$/Fe$^{II}$]-ADE$_{at}$ and [Fe$^{II}$/Mn$^{II}$]-ADE$_{at}$.* The three-dimensional structures of the iron/manganese hybrid ([Fe$^{II}$/Mn$^{II}$]-ADE$_{at}$) and the diferrous form ([Fe$^{II}$/Fe$^{II}$]-ADE$_{at}$) of adenine deaminase from *A. tumefaciens* were determined to 2.63 Å and 2.8 Å resolution, respectively. Overall, the structures and active sites of [Fe$^{II}$/Fe$^{II}$]-

$ADE_{at}$ and $[Fe^{II}/Mn^{II}]$-$ADE_{at}$ are essentially identical to the [Mn/Mn]-$ADE_{at}$ structure determined previously (RMSD is < 1 Å for all Cα atom pairs). In the [Mn/Mn]-$ADE_{at}$ structure, the active site contains a binuclear manganese center ($Mn_{\alpha}$ and $Mn_{\beta}$) and a third manganese center located 6.6 Å from $Mn_{\alpha}$ (*20*). $[Fe^{II}/Fe^{II}]$-$ADE_{at}$ and $[Fe^{II}/Mn^{II}]$-$ADE_{at}$ were prepared from apo-$ADE_{at}$ and the metal content for both proteins prior to crystallization was determined to be 0.95 ± 0.10 Mn, 1.1 ± 0.1 Fe per subunit for the iron/manganese hybrid and 2.1 ± 0.1 Fe per subunit for the di-iron ADE by ICP-MS. However, in the crystal structure the active sites of both protein preparations contained three metal ions, similar to the previous structure determined with the di-manganese activated enzyme.

In the diferrous form of adenine deaminase, $Fe_{\beta}$ in the binuclear center and the third iron are five-coordinate whereas $Fe_{\alpha}$ is four-coordinate (**Figure 3.14A**). $Fe_{\alpha}$ coordinates with His-92, His-94 (HxH motif), Asp-289 and Glu-187 (**Figure 3.14A**). Glu-187, His-218, His-239, Glu-240 and water (W1) coordinate with $Fe_{\beta}$. Glu-187 bridges $Fe_{\alpha}$ and $Fe_{\beta}$. Waters that are bridging $Mn_{\alpha}$ and $Mn_{\beta}$ in the [Mn/Mn]-$ADE_{at}$ are missing in the current structure. The third iron coordinates His-122, Glu-123 (bidendate), His-477 and Asp-478 (**Figure 3.14A**). In the manganese/iron hybrid enzyme it was not possible to determine the preferential binding locations of the two different metal ions (**Figure 3.14B**). The two metal ions in the binuclear metal center are four-coordinate and the third metal ion is five-coordinate. The coordinating ligands are the same as for $[Fe^{II}/Fe^{II}]$-$ADE_{at}$ except that there is no water coordination with $M_{\beta}$.

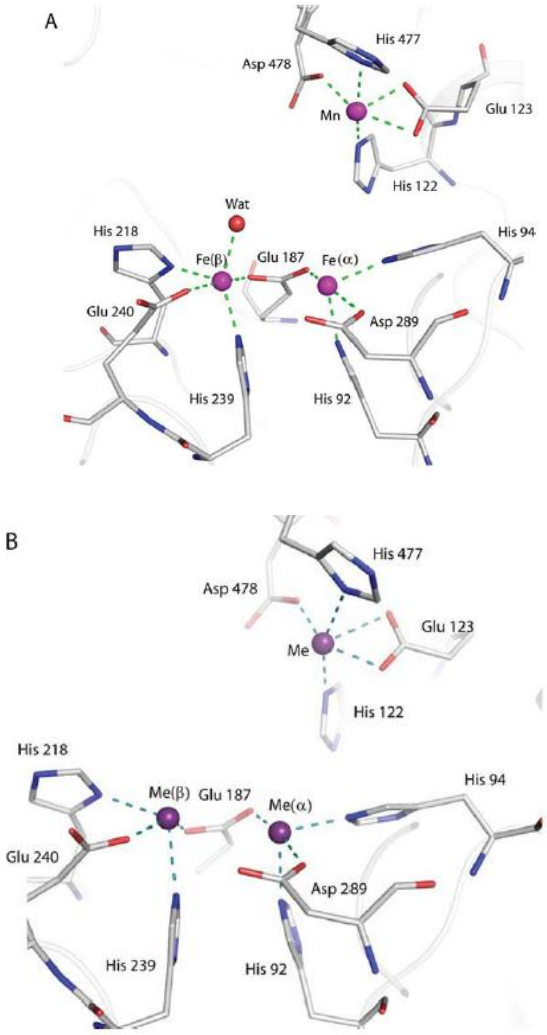


**Figure 3.14**: *Close up view of the active site of [$Fe^{II}/Fe^{II}$]-$ADE_{at}$ (A) and [$Fe^{II}/Mn^{II}$]-$ADE_{at}$ (B).* Grey color ribbon represents the secondary elements at the vicinity of the active site. Active site residues that are coordinating to metals are shown as stick models. Metals and water are shown as spheres.

DISCUSSION

*Oxidative Damage to Adenine Deaminase.* When adenine deaminases from cog1001 of the AHS are aerobically expressed in *E. coli*, the isolated enzymes are largely inactive and multiple histidine and methionine residues are damaged by oxygenation. The oxidative damage can be completely eliminated if the iron in the medium is sequestered by an iron-specific chelator prior to induction. Enzymes isolated under these conditions contain two manganese ions in the active site and the turnover numbers for the deamination of adenine are approximately two orders of magnitude greater than any ADE previously reported in the literature (*20, 21*). The oxygenation reactions are consistent with the generation of a reactive oxygen species (ROS) from the iron-bound form of adenine deaminase from a physiological oxidant such as $H_2O_2$ (*47*). Apo-ADE can be readily prepared from the undamaged manganese-activated enzyme and reconstituted with two equivalents of manganese, zinc, or iron. The diferrous form of adenine deaminase, $[Fe^{II}/Fe^{II}]$-$ADE_{ec}$, has been utilized here to unravel the mechanism for oxidative damage to this enzyme.

*Inactivation with Hydrogen Peroxide*. In the presence of excess $H_2O_2$, $[Fe^{II}/Fe^{II}]$-$ADE_{ec}$ rapidly loses its ability to deaminate adenine. EPR and Mössbauer spectroscopy of the inactivated enzyme demonstrate that the iron in the active site is in an uncoupled high spin ferric oxidation state. The metal ions can be reduced back to the di-ferrous state with dithionite but the deaminase activity is not recovered. Therefore, the addition of an excess of $H_2O_2$ to $[Fe^{II}/Fe^{II}]$-$ADE_{ec}$ damages the protein in an irreversible manner and stabilizes the $[Fe^{III}/Fe^{III}]$ state. Mass spectrometric analysis of the trypsin-treated

enzyme confirms that multiple histidine and methionine residues within the protein are oxygenated and that the labeling pattern is identical to enzyme expressed in *E. coli* in the absence of an iron chelator. These results are consistent with the generation of a reactive oxygen species such as hydroxyl radical or superoxide by the reaction of $H_2O_2$ with the binuclear iron center of adenine deaminase.

*Discovery of Catalase Activity*. The addition of $H_2O_2$ to $[Fe^{II}/Fe^{II}]$-$ADE_{ec}$ results in the formation of $O_2$. The catalase-like activity diminishes over the course of a few minutes and is lost in approximately the same time-frame as the deaminase activity. More than 100 turnovers occur before the enzyme is completely inactivated. The promiscuous catalase activity of $[Fe^{II}/Fe^{II}]$-ADE is as fast as the deamination reaction, but significantly slower than other catalases (*59*, *60*). There is no effect by $H_2O_2$ with either $[Mn^{II}/Mn^{II}]$-ADE or $[Zn^{II}/Zn^{II}]$-ADE and thus the oxidation reactions are specific for the iron-reconstituted enzyme.

The apparent reaction stoichiometry for the catalase-like activity of $[Fe^{II}/Fe^{II}]$-$ADE_{ec}$ changes as a function of time. When one equivalent of $H_2O_2$ is added to $[Fe^{II}/Fe^{II}]$-$ADE_{ec}$ that had not been previously exposed to $H_2O_2$, ~0.11 equivalents of $O_2$ are produced. After the second equivalent of $H_2O_2$ is added, ~0.29 equivalents of $O_2$ are produced. Additional $H_2O_2$ results in the formation of ~0.45 equivalents of $O_2$ for every $H_2O_2$ added. However, the stoichiometry for a physiological catalase is 0.50 equivalents of $O_2$ for every $H_2O_2$ utilized (*59*, *60*). These results are therefore consistent with the leakage of single electron products from the active site, including hydroxyl radical and superoxide.

The formation of superoxide was probed with the reagent hydroethidine. When this reagent is added to a reaction mixture containing $[Fe^{II}/Fe^{II}]$-$ADE_{ec}$ and an excess of hydrogen peroxide, the formation of 2-hydroxyethidium is detected. The amount of 2-hydroxyethidium produced is consistent with ~11 equivalents (17 μM/1.50 μM) of superoxide produced for every enzyme inactivated. During this process ~54 (81 μM/1.50 μM) equivalents of $O_2$ are produced and ~128 (192 μM/1.50 μM) equivalents of $H_2O_2$ are consumed, leaving ~9 equivalents (128-108-11) of $H_2O_2$ unaccounted. This latter number approximates the number of oxidized histidine and methionine residues sites detected by mass spectrometry that most likely occur from the reaction of hydroxyl radicals with the protein.

It is likely that the oxygenation of methionine residues is of minor importance for changes in catalytic activity. However, the oxygenation of four histidine residues that coordinate the two irons in the active site can modulate oxidation/reduction reactions via changes in the reduction potential and/or coordination geometry of the binuclear metal center. From the structure of ADE from *A. tumefaciens* (PDB: 3nqb), the oxygenation sites are mapped and shown in **Figure 3.15.** These oxygenation sites are predominantly in and around the binuclear metal center and seem to migrate from there to other parts of the protein. This result is consistent with the conclusion that the catalase activity originates at the binuclear metal center and is further supported by the fact that 6-chloropurine, a potent inhibitor of the deaminase reaction, inhibits the catalase activity.

The reduction potential of the binuclear metal center changes with the extent of protein oxygenation. For enzyme not previously exposed to $H_2O_2$, the reduction

potential for the inter-conversion of the ferric and ferrous forms of [Fe/Fe-ADE] is +209 mV. When the protein is partially oxygenated the reduction potential decreases to +194 mV and decreases further to +175 mV when the protein is fully oxygenated and the enzyme is unable to catalyze either the deaminase or catalase reactions. These results are consistent with the continuous modulation of the catalytic properties of the binuclear iron center with time as hydroxyl radicals escape and react directly with the metal ligands.

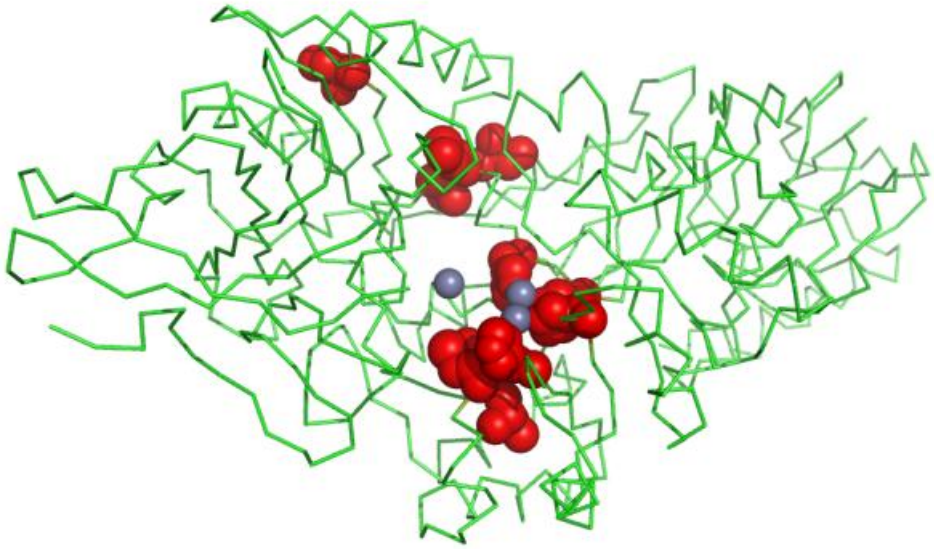

**Figure 3.15**: *Map of the oxygenation sites after adding $H_2O_2$ to [$Fe^{II}/Fe^{II}$]-ADE*. The protein backbone is represented in green and the red spheres represent the amino acid side chains that were oxygenated.

*Proposed Mechanism of Action.* How does the binuclear iron center in ADE catalyze the oxidation and reduction of hydrogen peroxide? EPR and Mössbauer spectroscopy demonstrated that the enzyme can cycle between the diferrous and diferric states of oxidation. We have not observed any spectra that are consistent with a ferryl-oxo species (Fe(IV)=O), although this latter species is likely to be too unstable to be detected by the methods employed in this investigation (*59-61*). Both metal ions within the binuclear metal center must be iron. A unique Mn/Fe hybrid can be prepared, but it is not known which of the two sites within the binuclear metal center is occupied by iron and which by manganese. This hybrid is completely inactive for reaction with hydrogen peroxide (**Figure 3.9)**.

**Scheme 3.2** is a working model to explain the development and decay of the catalase-like activity of iron-substituted ADE. We propose that the observed changes in the reactivity of the enzyme are due to changes in the redox properties and structural changes to the diiron center as the protein becomes oxygenated. When $H_2O_2$ is first added to [$Fe^{II}/Fe^{II}$]-ADE, the predominant reaction is the formation of water and a hydroxyl radical that is coupled with the transient formation of [$Fe^{II}/Fe^{III}$]-ADE. The hydroxyl radical subsequently reacts with histidine and methionine residues that are near the active site. The initial odd-electron oxygenated product loses an electron that subsequently reduces the mixed-valent binuclear center to [$Fe^{II}/Fe^{II}$]-ADE. This form of the protein is represented as [$Fe^{II}/Fe^{II}$]-$ADE^{ox}$ in **Scheme 3.2**. This *induction phase* is similar to the reaction of [$Fe^{II}/Fe^{II}$]-ADE with HOCl. With this substrate the reaction products are chloride anion and hydroxyl radical, and the protein is initially left as a

mixed valent [$Fe^{II}/Fe^{III}$]-ADE complex. Since the enzyme can react with approximately 12 molecules of HOCl before the enzyme is inactivated, the active site must therefore cycle between the [$Fe^{II}/Fe^{II}$]-ADE and [$Fe^{II}/Fe^{III}$]-ADE oxidation states. The initial odd-electron products from the reaction of methionine and histidine residues must lose an electron that reduces [$Fe^{II}/Fe^{III}$] back to [$Fe^{II}/Fe^{II}$]. However, HOCl is different from $H_2O_2$ since it cannot be oxidized.

During the induction phase of the reaction of ADE with $H_2O_2$, the direct metal ligands to the binuclear metal center become oxygenated (**Scheme 3.2**). This lowers the reduction potential of the binuclear metal center from +209 V to +194 V that apparently enables the enzyme to cycle between the [$Fe^{II}/Fe^{II}$] and [$Fe^{III}/Fe^{III}$] states in a *sustaining phase*. Mutation of the four histidine residues that coordinate the two irons in the active site suggests that the oxidation of His-90 is the key modification for the transition from the induction phase to the sustaining phase. During this stage the stoichiometry of the catalase reaction is not perfect and there is continual leakage of the reactive oxygen species, hydroxyl radical and superoxide, which continue to oxygenate the protein. Eventually, the enzyme enters the final *death phase* after multiple residues within the active site become oxygenated. This form of the enzyme is represented as [$Fe^{III}/Fe^{III}$]-ADE $^{\mathbf{ox\text{-}ox}}$ in **Scheme 3.2**. At this point the reduction potential of the metal center is lowered to +174 V and the diferric form of ADE can no longer be reduced to the diferrous state by hydrogen peroxide. The modulation of the catalytic properties of the binuclear iron center may occur with changes in the reduction potential but the changes

in catalytic activity may also be the result of conformational changes to the metal center itself.

***induction phase***

$$[Fe^{II}/Fe^{II}]\text{-ADE} + H_2O_2 + H^+ \rightarrow [Fe^{II}/Fe^{III}]\text{-ADE} + H_2O + {}^{\bullet}OH$$

$$[Fe^{II}/Fe^{III}]\text{-ADE} + {}^{\bullet}OH \rightarrow [Fe^{II}/Fe^{II}]\text{-ADE}^{ox} + H^+$$

***sustaining phase***

$$[Fe^{II}/Fe^{II}]\text{-ADE}^{ox} + H_2O_2 + 2\,H^+ \rightarrow [Fe^{III}/Fe^{III}]\text{-ADE}^{ox} + 2\,H_2O$$

$$[Fe^{III}/Fe^{III}]\text{-ADE}^{ox} + H_2O_2 \rightarrow [Fe^{II}/Fe^{II}]\text{-ADE}^{ox} + O_2 + 2\,H^+$$

$$[Fe^{III}/Fe^{III}]\text{-ADE}^{ox} + H_2O_2 \rightarrow [Fe^{II/}Fe^{III}]\text{-ADE}^{ox} + HO_2 + H^+$$

$$[Fe^{II}/Fe^{III}]\text{-ADE}^{ox} + H_2O_2 \rightarrow [Fe^{II/}Fe^{II}]\text{-ADE}^{ox} + HO_2 + H^+$$

***death phase***

$$[Fe^{II}/Fe^{II}]\text{-ADE}^{ox} + H_2O_2 + H^+ \rightarrow [Fe^{II}/Fe^{III}]\text{-ADE}^{ox} + H_2O + {}^{\bullet}OH$$

$$[Fe^{II}/Fe^{III}]\text{-ADE}^{ox} + {}^{\bullet}OH \rightarrow [Fe^{II}/Fe^{II}]\text{-ADE}^{\mathbf{ox\text{-}ox}} + H^+$$

$$[Fe^{II}/Fe^{II}]\text{-ADE}^{\mathbf{ox\text{-}ox}} + H_2O_2 \rightarrow [Fe^{III}/Fe^{III}]\text{-ADE}^{\mathbf{ox\text{-}ox}} + 2\,H_2O$$

**Scheme 3.2:** Working model for the catalase activity of diiron ADE.

When an excess of $H_2O_2$ is added to ADE in the presence of a superoxide scavenger, ~128 enzyme equivalents of hydrogen peroxide are consumed and ~54 equivalents of $O_2$ are produced. The other products are hydroxyl radicals and ~11 equivalents of superoxide. Since the inclusion of hydroxyl radical scavengers had no effect on the kinetics of $O_2$ formation, it appears that the hydroxyl radicals are fully trapped by the protein and do not escape to the bulk solvent. Based on the number of residues found to be oxidized after ADE is no longer active, approximately 10-12

enzyme equivalents of hydroxyl radicals are produced for every enzyme inactivated. This value is very similar to the number of HOCl molecules that are required to fully inactivate ADE. During the sustaining phase, the predominant reaction is the conversion of hydrogen peroxide to $O_2$ and water. However, there is significant formation of hydroxyl radical and superoxide that must occur via single electron transfers. The oxidation and reduction of $H_2O_2$ during the sustaining phase may occur by two single electron transfers to form superoxide and hydroxyl radical intermediates or by a coupled two-electron transfer to form $O_2$ and water directly. The mechanism proposed for the disproportionation of hydrogen peroxide by [Fe/Fe]-ADE is similar to that of dimanganese catalase found in some organisms, where the enzyme uses $Mn^{II}/Mn^{II}$ and $Mn^{III}/Mn^{III}$ as the metal center to catalyze the conversion of hydrogen peroxide to oxygen and water via a coupled two electron transfer process (*62, 63*). We further propose that hydrogen peroxide binds to the binuclear metal center and that single and/or coupled two electron transfers occur to and from these two metal ions. However, in all of the crystal structures of ADE obtained thus far there are three metal ions in the active site even though the crystallizations were initiated with protein with two metals per subunit. At this point it is not clear how the third metal ion was incorporated into the protein. There are four protein residues that coordinate the third metal ion in $ADE_{ec}$: His-120, Glu-121, His-473, and Asp-474. His-473 and Asp-474 form an invariant and fully conserved HD dyad in all adenine deaminases in cog1001 and are absolutely critical for the catalase activity but have no role in the deaminase activity. The pH rate profiles for the catalase activity indicate that a single group must be unprotonated for

catalytic activity with a p$K_a$ of 7.6 - 7.9. This p$K_a$ value is consistent with His-473 serving in proton transfer reactions in the oxidation and reduction of hydrogen peroxide. Computational docking to the three-dimensional structure of $ADE_{tu}$ suggests that His-120 is required to hydrogen bond to N3 of adenine (*20*).

*Comparison with Other Catalases*. Catalase activity is supported by various types of metal sites, including hemes (*59, 60*), binuclear manganese centers (*62, 63*) and binuclear iron centers (*45, 54*). The latter are found in monooxygenase enzymes and model compounds (*45, 54, 64*). Perhaps the best studied of these is toluene/*o*-xylene monooxygenase from *Pseudomonas* sp. OX1 (*54*). For this enzyme the two irons are antiferromagnetically coupled and the diferric form is stable in air. The mechanism for the disproportionation of $H_2O_2$ proposed for [Fe/Fe]-ADE is similar to that of the binuclear manganese catalases found in some organisms, where the enzyme cycles between the [$Mn^{II}/Mn^{II}$] and [$Mn^{III}/Mn^{III}$] oxidation states. Interestingly, [$Mn^{II}/Mn^{II}$]-ADE exhibits no catalase activity, presumably because this state may lack sufficient reducing power to reduce $H_2O_2$ to water.

*Potential Physiological Significance.* The physiological significance of the inherent catalase activity of adenine deaminase substituted with iron is unclear. However, it is known that in certain bacteria the deamination of adenine can function as a key step in the purine salvage pathway for formation of guanine nucleotides (*15, 17*). Therefore, under conditions of oxidative stress the inactivation of ADE would block formation of guanine nucleotides via the purine salvage pathway, which in turn might slow cell growth under conditions of oxidative stress. There are known bacterial

transcription factors that use metal-catalyzed oxidation of histidine (via $H_2O_2$) as a redox sensor for controlling oxidative stress levels in cells. An example of such a protein is PerR, which uses iron in the ferrous oxidation state to oxidize a histidine residue critical for DNA binding, thereby regulating the oxidative stress levels within cells (*65, 66*). Another example is the iron enzyme ribulose-5-phosphate 3-epimerase, which is irreversibly inactivated with $H_2O_2$, presumably from Fenton chemistry catalyzed by the $Fe^{2+}$ in the active site. This enzyme can be protected by incorporation of manganese in the active site (*67*). It is apparent that there is insufficient catalase in the cell when *E. coli* is grown aerobically to reduce the hydrogen peroxide concentration to a level that does not inactivate adenine deaminase. The catalytic domain of ADE comprises the N-terminal half of the protein and there is a rather large C-terminal domain of approximately 300 amino acids that has no obvious function. The N-terminal half of the protein is required for the coordination of the binuclear metal center and has all of the residues necessary for the deaminase activity. The C-terminal domain has the highly conserved HD dyad. The mutation of either these two residues results in total loss of the catalase activity but has absolutely no effect on the deaminase activity. These two residues are postulated to function in proton transfers during the conversion of $H_2O_2$ to $H_2O$ and $O_2$. The promiscuous catalase activity is not limited to adenine deaminase from *E. coli*. We have also interrogated the adenine deaminases from *B. subtilis* (Bsu14520), *A. tumefaciens* (Atu4426), *B. halodurans* (Bh0640), and *C. acetobutylicum* (Cac0887). All of these enzymes catalyze the deamination of adenine and all catalyze the disproportionation of hydrogen peroxide when iron is bound to the active site. Members

of the amidohydrolase superfamily have been show to catalyze hydrolytic, hydration, decarboxylation (*68*), and isomerization reactions (*69, 70*). This is the first instance from this superfamily of enzymes for a redox-type reaction. It is thus interesting to consider that other enzymes of unknown function within this superfamily will catalyze similar reactions.

# CHAPTER IV

# DISCOVERY OF A LOW-BARRIER HYDROGEN BOND IN ADENINE DEAMINASE FROM *ESCHERICHIA COLI*

Adenine deaminase (ADE) is a member of the amidohydrolase superfamily (AHS). ADE has shown to catalyze two distinct reactions, the hydrolytic deamination of adenine and the redox disproportionation of hydrogen peroxide for diiron ADE. Kinetic studies for ADE yield similar inverse solvent isotope effects as adenosine deaminase and cytosine deaminase, which are the other kinetically characterized members of the AHS. Proton inventory studies on ADE show two distinct patterns, for $k_{cat}$ and $k_{cat}/K_m$, suggesting involvement of two distinct protons in the kinetic mechanism. A single downfield proton with a chemical shift ($\delta \sim 17.0$ to 18.0 ppm) consistent with those identified for low-barrier hydrogen bonds (LBHBs) was identified using $^1$H-NMR analysis for the Zn/Zn-ADE. LBHBs have been found to be critical in other enzymes and have been extensively studied for serine proteases. Here we use mutagenesis and inhibitor studies coupled to $^1$H-NMR analysis to reveal the nature of the downfield proton and found it was associated with the deaminase activity. The exact assignment of the downfield proton still remains unknown; however this study reports the first instance of any metalloenzyme possessing a LBHB in catalysis. Previous experiments performed on serine proteases in the identification of the LBHB might prove useful in finding the LBHB of ADE.

INTRODUCTION

Physical organic chemists have known of the existence of low-barrier hydrogen bonds (LBHB) in organic reactions for years. However, the existence of LBHB in proteins and enzymes is only recent as compared to organic reactions (*71*). Researchers have proposed that a weak hydrogen bond in the initial enzyme or enzyme-substrate complex in converted into a LBHB in the transition state intermediate. In a proposal by Cleland, an enzyme converts a weak hydrogen bond into a LBHB by changing the p*K*a of the substrate close to that of the hydrogen bond donor, thereby increasing the strength of the hydrogen bond. The strength of the hydrogen bond involved in enzyme catalysis via formation of the LBHB depends on the length and linearity of the bond, the micro-environment of the bond, and the degree to which the p*K*a values of the heavy atom conjugate acids sharing the proton are matched (*49, 72*). Cleland and Kreevoy have also proposed the idea of a special type of hydrogen-bond (H-bond) they termed a low-barrier hydrogen bond (LBHB). They suggested that the missing link in most transition states of enzyme catalyzed reactions involving a proton transfer, would involve a transition state stabilization that is provided by this "special" proton (*73*). Various physicochemical parameters are now used to define and identify the LBHBs associated with enzymes. LBHBs are characterized most unambiguously by the characteristic $^{1}$H- nuclear resonance magnetic (NMR) chemical shift with the proton showing up at extreme low-field values ($\delta > 16$ ppm). LBHBs are also identified by deuterium isotope effects, low isotopic fractionation factors and deuterium isotope effects on the infrared and Raman frequencies on the LBHBs (*74*).

The first class of enzymes that were identified to involve a LBHB in catalysis was the serine proteases. Studies from Robillard and Shulman in 1972 identified a single proton at low fields in the $^1$H-NMR spectra of chymotrypsin and chymotryosinogen (*75*). The resonance peak appeared between 15 and 18 ppm relative to dimethyl-silapentane sulfonate in the $^1$H-NMR and, was sharp at extreme pH values and broadens at intermediate pH (p$K$ ~ 7). They also found that upon dissolving the protein in $D_2O$ there was a loss of the resonance signal. A similar study using $^1$H-NMR performed by Markley in 1981 revealed that other serine proteases also had this characteristic downfield proton around 18 ppm (*76*). In this $^1$H-NMR study by Markley, bovine trypsinogen, bovine trypsin, bovine chymotrypsinogen, bovine chymotrypsin $A_\delta$ and bovine chymotrypsin $A_\alpha$ were tested. The studies revealed that the downfield proton was more pronounced at lower pH values (< 4.0) and lower temperatures (< 3$^o$C). In a series of subsequent studies from Cleland, Frey and Markley, using various serine protease mechanism-based inhibitors, model synthetic compounds, mutagenesis, isotope effects and fractionation factors, it was established that the downfield proton was the hydrogen atom termed now as the LBHB between the aspartate and histidine (N-δ1) of the catalytic triad amongst the various serine proteases (*77-80*). **Scheme 4.1** represents the LBHB of chymotrypsin from the studies performed by Frey and co-workers (*81*).

$^1$H-NMR spectroscopy was able to identify the existence and nature of the LBHB in serine proteases. However, there was much speculation throughout literature about the assignment of the LBHB throughout this enzyme superfamily. Finally a study by Bachovchin (*82*) in 1985 on α-lytic protease, a bacterial serine protease answered the

issue with regards to the assignment of this LBHB. α-lytic protease was made recombinantly using synthetic L-histidine labeled specifically with $^{15}N$ at $N^{\delta 1}$as the sole source of histidine. The resulting α-lytic protease was enriched in $^{15}N$ at $N^{\delta 1}$ of the histidine of the catalytic triad. The resulting downfield proton around 17 ppm at pH 4.0 split into a doublet resulting from the additional coupling to the $^{15}N$ of histidine $N^{\delta 1}$. This study unambiguously assigned the position of the LBHB to serine proteases.

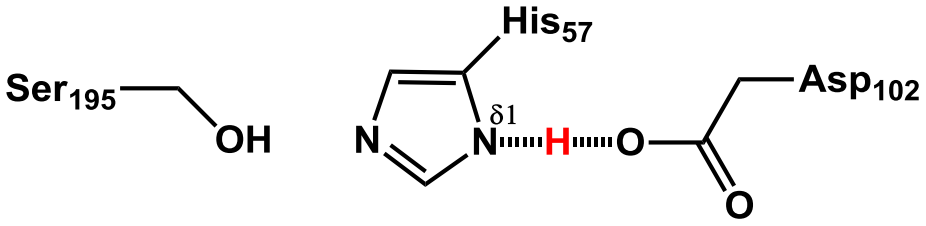


**Scheme 4.1:** The catalytic triad of chymotrypsin. The hydrogen atom in red represents the downfield proton seen in the $^{1}H$-NMR studies and is termed the LBHB of the serine proteases.

Since the discovery and assignment of the LBHB in serine proteases, several other enzymes have been studied for involvement of protons as LBHB in catalysis. Phospholipase A2 is a small calcium dependent lipolytic enzyme that catalyzes the hydrolysis of phospholipids. Its active site contains an invariant catalytic dyad of an aspartate and histidine residue. These residues hydrogen bond with water to form a catalytic triad analogous to the serine proteases. Studies from Tsai and co-workers have shown, using a variety of $^{1}H$-NMR and inhibitor studies, that this enzyme utilizes a LBHB in enzyme catalysis (*83*). Dunn and co-workers have indirect evidence through a variety of isotope effects and fractionation factors for the involvement of a LBHB in the catalytic mechanism of tryptophan synthase (*84*). More recently, a newer technique

called high-resolution neutron crystallography has been employed in the discovery of LBHBs. Kataoka and co-workers have used this technique in detecting a LBHB in photoactive yellow protein (PYP) from *Halorhodospira halophila*. PYP is a putative photoreceptor for negative phototaxis in purple phototropic bacteria (*85*). A review by Cleland, Frey and Gerlt (*72*), has postulated more enzymes to involve LBHB in enzyme catalysis from kinetic isotopic studies performed on these enzymes. They have listed ketosteroid isomerase, triose phosphate isomerase, citrate synthase and mandelate racemase to employ a transition state proton i.e. a LBHB in their respective enzymatic mechanisms.

In this chapter, we discuss the discovery of a LBHB in adenine deaminase from *Escherichia coli* (ADE) (*20*). We have described the kinetic studies involving solvent isotope effects as well as proton inventory studies for ADE. We have used $^{1}$H-NMR spectroscopy complemented with mutagenesis to identify the putative residues that might be involving the LBHB associated with ADE. Our studies indicate that this LBHB is involved in a proton transfer event at the transition state for the deamination reaction and we have proposed the residues that might be involved with this LBHB.

MATERIALS AND METHODS

*Materials.* All chemicals were purchased from Sigma-Aldrich unless otherwise stated. The genomic DNA for *E. coli str.* K12 substr. MG1655 was purchased from ATCC. *E. coli* BL21(DE3) and XL1-blue competent cells were obtained from Stratagene (Agilent). The expression vector pET30(+) and *Pfx* DNA polymerase were purchased from Invitrogen. All oligonucleotides were obtained from the Integrated

DNA Technologies (IDT) from the Gene Technology Lab at Texas A&M University (GTL-TAMU).

*Cloning, Mutagenesis and Purification.* Adenine deaminase (ADE) from *Escherichia coli* was cloned as described previously (*20*). Mutagenesis was performed using the Quik-Change PCR protocol as per manufacturer's instructions. All the plasmids were verified for the appropriate gene sequence at the Gene Technology laboratory, Department of Biology, Texas A&M University. The wild-type ADE and all mutants were expressed using the iron-free expression protocol and purified as described before (*20*). The pure fraction was pooled for every protein and tested for activity, and tested for $Mn^{2+}$ content by ICP-MS.

*Preparation of Zn/Zn-ADE.* The ADE was dialyzed with 10 mM 1,10-phenanthroline in 50 mM phosphate buffer, pH 7.0 over 36 hours with 2 buffer exchanges. The resulting apo-protein was further purified using a PD-10 size exclusion column, and the proteins were analyzed by inductively coupled plasma mass spectrometry (ICP-MS) for the absence of any metal associated with the protein. Apo-ADE was then reconstituted by adding the 20 fold-enzyme excess of zinc chloride ($ZnCl_2$) as a zinc source ($Zn^{2+}$) previously dissolved in 50 mM phosphate buffer pH 7.0 for 48 hours at $4^oC$. The excess metal was separated from the reconstituted protein by passing through a PD-10 size exclusion column. The reconstituted protein was tested for activity as well as tested by ICP-MS for metal incorporation. The reconstituted protein was concentrated using the 10 kDa vivaspin 6 concentrators (GE Healthcare) and

analyzed by NMR. For this study the mutants were H90N, D284A, E236Q, D285A, H473N and E474Q.

*NMR Analysis*. The wild-type ADE and mutants expressed, purified and reconstituted were analyzed by $^{1}$H-NMR spectroscopy by Dr. Howard J. Williams, Department of Chemistry, Texas A&M University. After the reconstitution with zinc and kinetic analysis, the proteins were exchanged in 50 mM phosphate buffer, pH 5.5 for NMR analysis. The proteins were analyzed initially as reconstituted and later after addition of the ADE inhibitor 6-chloropurine (*20*). The typical ADE concentrations in these experiments ranged from 220-300 μM depending on the yield from the protein expressions and purifications. All NMR spectra were collected on a Bruker Avance III 500 MHz NMR instrument equipped with an HCN cryoprobe. Samples were analyzed by $^{1}$H NMR (10% $D_2O$) using the WATERGATE solvent ($H_2O$) suppression program at 1$^{o}$C for 14-24 hours.

*Proton Inventory Kinetics.* To determine the effect of varying proton concentration on the deaminase reaction, various proportions of $H_2O$ and $D_2O$ were made in the final reaction mixture. Mn/Mn-ADE was used for this study, since prior kinetic studies showed that the di-manganese, di-iron and di-zinc enzyme behave the same kinetically. The $D_2O$ concentrations in the assays were 0, 25, 50, 75 and 100 %. All assays were performed using the ammonia release coupling assay with glutamate dehydrogenase as described previously at the optimum pH 7.5 for ADE reaction in 50 mM HEPES buffer at 30 $^{o}$C using a SpectraMax 384 Plate Reader, from Molecular Devices (*20*). The assays were performed in duplicates.

*Data Analysis.* All kinetic assays were analyzed using the non-linear least squares fitting program SigmaPlot 9.0. Initial velocity kinetic data were fit to **equation 2.1** where $v$ is the initial velocity, [A] is the substrate concentration, $E_t$ is the total enzyme concentration, $k_{cat}$ is the turnover number and $K_m$ is the Michaelis constant. The inverse-concave proton inventories were fit to **equation 4.1** for the $k_{cat}$ values obtained with increasing $D_2O$ concentrations. In this equation, $v_n$ is the activity at different $D_2O/H_2O$ ratios, $v_o$ is the activity in the absence of $D_2O$, $n$ is the ratio of $D_2O/H_2O$, and $\Phi^R$ is the fractionation factor for the reactant-state site. For the linear proton inventories for $k_{cat}/K_m$, **equation 4.2** was used to fit the data. In this equation, $v_n$ is the activity at different $D_2O/H_2O$ ratios, $v_o$ is the activity in the absence of $D_2O$, $n$ is the ratio of $D_2O/H_2O$, and $\Phi^T$ is the fractionation factor for the transition-state (*86*).

$$v / E_t = k_{cat} [A] / (K_m + [A]) \quad \textbf{(Equation 2.1)}$$

$$v_n = v_0/(1 - n + n\Phi^R) \quad \textbf{(Equation 4.1)}$$

$$v_n = v_0(1 - n + n\Phi^T) \quad \textbf{(Equation 4.2)}$$

RESULTS

*ADE Properties.* All the proteins were assayed for their adenine deaminase activity, since the buffer was exchanged from 50 mM HEPES, pH 7.5 to 50 mM phosphate buffer, pH 7.0 during the preparation of the apo-enzyme and the subsequent reconstitution was performed in phosphate buffer, 50 mM pH 7.0. **Table 4.1** represents the kinetic constants and the metal-content of the wild-type and mutants ADE proteins reconstituted with $Zn^{2+}$. The kinetic constants for the Zn/Zn-ADE wild type and the

mutant forms of ADE are in accordance with the Mn/Mn-reconstituted forms of ADE (*20*).

**Table 4.1:** *Kinetic constants of the various zinc reconstituted forms of ADE.*

| ADE | $k_{cat}$ ($s^{-1}$) | $k_{cat}/K_m$ ($M^{-1}s^{-1}$) | Zinc content per monomer of ADE measured by ICP-MS |
|---|---|---|---|
| Wild type | 115 ± 5 | (4.7 ± 0.3) x$10^5$ | 1.8 ± 0.2 |
| D284A | 0.05 ± 0.01 | 130 ± 12 | 1.9 ± 0.2 |
| E236Q | 0.06 ± 0.02 | 25 ± 7 | 1.6 ± 0.2 |
| H90N | 4.1 ± 0.3 | (1.8 ± 0.2) x$10^3$ | 1.7 ± 0.1 |
| D285A | 30 ± 6 | (0.9 ± 0.1) x$10^5$ | 1.8 ± 0.2 |
| H473N | 110 ± 8 | (4.5 ± 0.2) x$10^5$ | 2.1 ± 0.2 |
| D474N | 121 ± 10 | (4.9 ± 0.6) x$10^5$ | 2.0 ± 0.2 |

All kinetic analysis were performed in phosphate buffer, pH 7.0 at 30°C

*Proton Inventories.* Varying amounts of $D_2O$ were added to adenine deaminase assay with the Mn/Mn-ADE (wild type) enzyme. **Table 4.2** represents the kinetic constants obtained from the increasing $D_2O$ concentrations. **Figures 4.1** and 4.**2** represent the data obtained from the proton inventory studies. In **Figures 4.1 and 4.2**, the blue line represents a straight line connecting the points at 0 and 100 % $D_2O$ and the red line represents the fit to the data. The data obtained for $k_{cat}$ was fit to equation 2, and the data for $k_{cat}/K_m$ was fit to equation 3. The data for $k_{cat}$ appears to have an inverse-concave shape, whereas the $k_{cat}/K_m$ appears to be linear. Based on the fit to equation 2,

$\Phi^R$ which is the fractionation factor for the reactant-state site equals (0.46 ± 0.01). Based on the fit to equation 3, $\Phi^T$ which is the fractionation factor for the transition-state equals (2.34 ± 0.02). pH-rate profiles performed on Mn/Mn-ADE in $H_2O$ and $D_2O$ have shown two p*K*a values at 6.5 and 8.2. These p*K*a values are not affected by the solvent. Also pH-rate profiles suggest that pH 7.5 is the optimal pH for the deaminase activity for the various metal-reconstituted forms of ADE. Hence the proton inventory studies were performed at pH 7.5 (*20*).

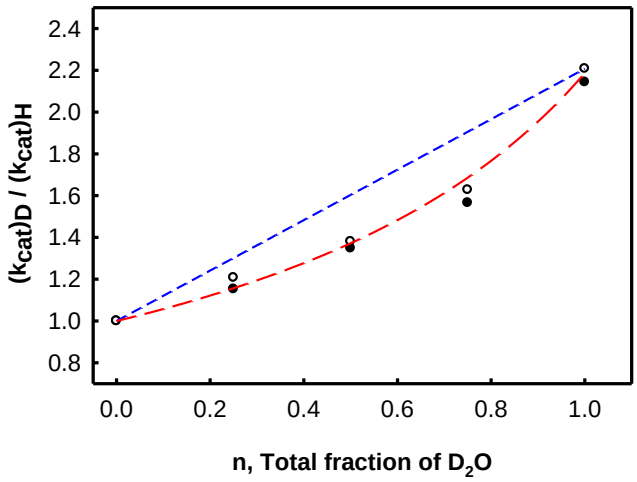


**Figure 4.1**: *Data for $k_{cat}$ for increasing $D_2O$ fractions for the adenine deaminase activity of Mn/Mn-ADE.*

The x-axis represents the fraction of the $D_2O$ in the final reaction mixture, and the y-axis represents the ratio of the $k_{cat}$ at the fraction of $D_2O$ to the $k_{cat}$ at zero $D_2O$ in the reaction mixture. The black circles represent experiment 1 where as open circles represent experiment 2. The blue dashed line is a straight line connecting the ratios at 0

and 100 % $D_2O$ concentrations. The red dashed line represents the data fit for $k_{cat}$ fit to equation 2.

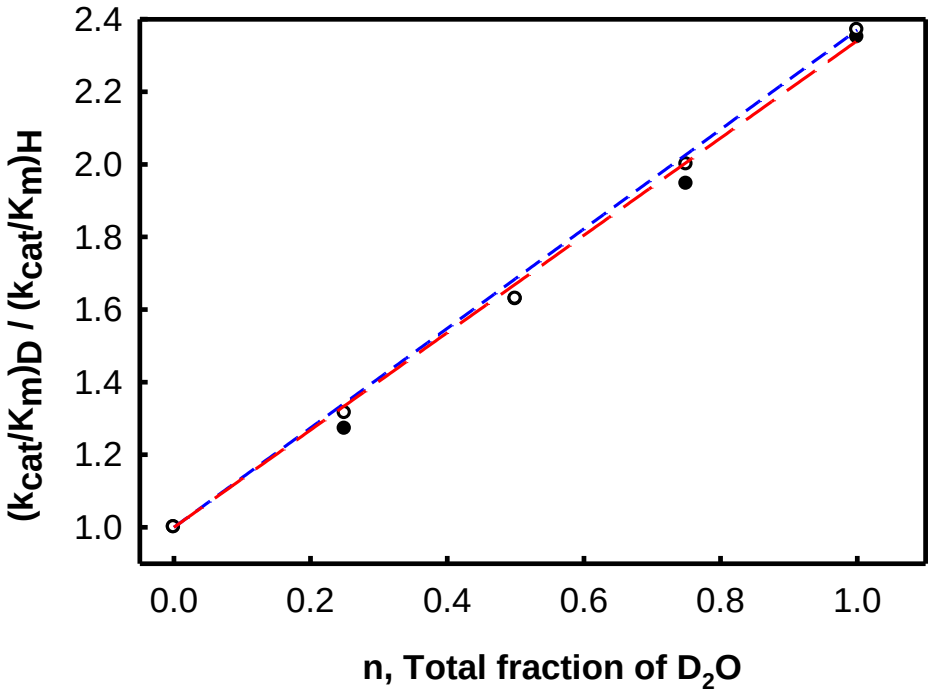


**Figure 4.2**: *Data for $k_{cat}/K_m$ for increasing $D_2O$ fractions for the adenine deaminase activity of Mn/Mn-ADE.*

The x-axis represents the fraction of the $D_2O$ in the final reaction mixture, and the y-axis represents the ratio of the $k_{cat}/K_m$ at the fraction of $D_2O$ to the $k_{cat}/K_m$ at zero $D_2O$ in the reaction mixture. The black circles represent experiment 1 where as open circles represent experiment 2. The blue dashed line is a straight line connecting the ratios at 0 and 100 % $D_2O$ concentrations. The red dashed line represents the data fit for $k_{cat}$ fit to equation 3.

**Table 4.2:** *Kinetic constants upon increasing the solvent $D_2O$ concentration for Mn/Mn-ADE*

| n Fraction of $D_2O$ | **Experiment 1** | | **Experiment 2** | |
|---|---|---|---|---|
| | $k_{cat}$ ($s^{-1}$) | $k_{cat}/K_m$ ($M^{-1}s^{-1}$) ($x10^5$) | $k_{cat}$ ($s^{-1}$) | $k_{cat}/K_m$ ($M^{-1}s^{-1}$) ($x10^5$) |
| 0 | 230 ± 12 | 5.6 ± 0.5 | 212 ± 18 | 5.4 ± 0.4 |
| 0.25 | 265 ± 24 | 7.2 ± 0.8 | 256 ± 18 | 7.1 ± 0.5 |
| 0.50 | 310 ± 19 | 9.1 ± 0.9 | 305 ± 24 | 8.8 ± 1.0 |
| 0.75 | 360 ± 29 | 10.9 ± 1.0 | 345 ± 18 | 10.8 ± 1.2 |
| 1.0 | 470 ± 35 | 12.6 ± 1.1 | 468 ± 23 | 12.8 ± 1.4 |

Experiment 1 and 2 are duplicates of the same experiment. Assay performed in 50 mM HEPES, pH 7.5 at 30°C.

*NMR Analysis.* The $^1$H-NMR spectra were collected for the various proteins that were purified and kinetically characterized. All the NMR spectra were collected by Dr. Howard J. Williams. For wild-type ADE, the $^1$H-NMR spectra were collected at 1 °C and 25 °C initially. After observing a proton resonance around 17 ppm for the measurement at 1 °C and not for those at 25 °C, all subsequent experiments were performed at 1 °C. For wild type ADE, $^1$H-NMR spectra were obtained with the addition

of substrate and the inhibitor, 6-chloropurine (**Figure 4.3**). Spectra were collected for 16 hours each.

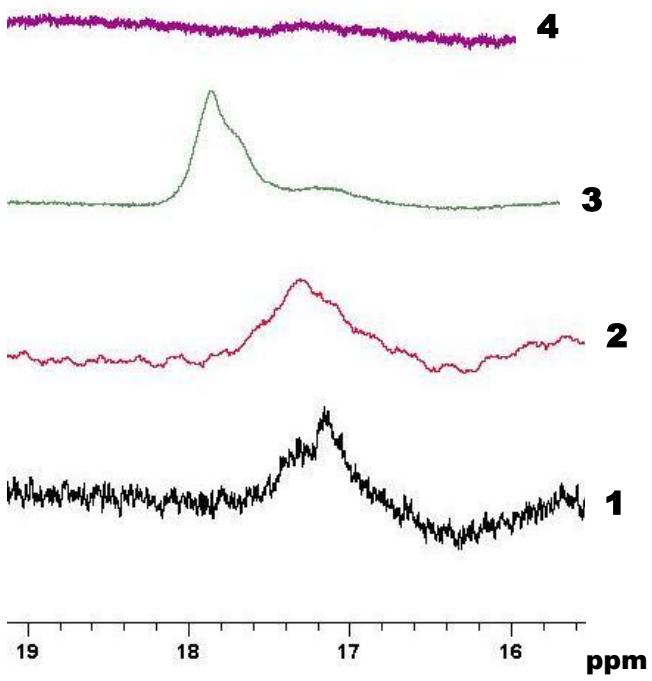


**Figure 4.3**: *$^{1}$H-NMR spectra of zinc reconstituted ADE*: [1] wild type-ADE (230 μM) at pH 5.5 in 50 mM phosphate buffer collected at 1$^{o}$C showing the downfield proton at 17.2 ppm. [2] wild type-ADE (225 μM) + 3 mM adenine, at pH 5.6 in 50 mM phosphate buffer. Spectrum collected at 1$^{o}$C showing the downfield proton at 17.4 ppm. [3] wild type-ADE (260 μM) + 3 mM 6-chloropurine, at pH 5.5 in 50 mM phosphate buffer. Spectrum collected at 1 $^{o}$C, showing the downfield proton at 18.0 ppm. [4] wild type-ADE wild type-ADE (250 μM) at pH 5.5 in 50 mM phosphate buffer. Spectrum collected at 25 $^{o}$C showing loss of signal for the downfield proton.

To quantify the downfield proton observed in the $^{1}$H-NMR spectra of ADE, the –methyl group of methionine was used as a comparative standard. Since ADE has 13 methionine residues, the integration was adjusted for a single –methyl group for a methionine residue by dividing the total integration by 13 for the methyl group resonance arising from the methionine residues of ADE. For **Figure 4.3.1** when the proton at 17.2 ppm was assigned 1.00, the protons of the –methyl group of methionine were 121.31. Thus is the absence of substrate or inhibitor, the downfield proton amounts to 0.8% of a single proton. This indicates a rapid exchange of the downfield proton with solvent even at 1 $^{o}$C. For **Figure 4.3.2** when the proton at 17.4 ppm was assigned 1.00, the protons of the –methyl group of methionine were 66.54. Thus is the absence of substrate or inhibitor, the downfield proton amounts to 1.5% of a single proton. For **Figure 4.3.3** when the proton at 18.0 ppm was assigned 1.00, the protons of the –methyl group of methionine were 9.42. Thus is the absence of substrate or inhibitor, the downfield proton amounts to 10.6% of a single proton.

To assign the proton associated with the LBHB various mutants were analyzed by $^{1}$H-NMR spectroscopy. Two sets of mutants were selected for this study, where residues critical for the deaminase activity were mutated (His-90, Glu-236 and Asp-284) and in the second set, residues critical for the catalase activity were mutated (His-473 and Asp-474) as well as the highly conserved (Asp-285) of the DD-motif amongst various deaminases was also mutated. **Figures 4.4 and 4.5** represent the $^{1}$H NMR spectra of the mutants.

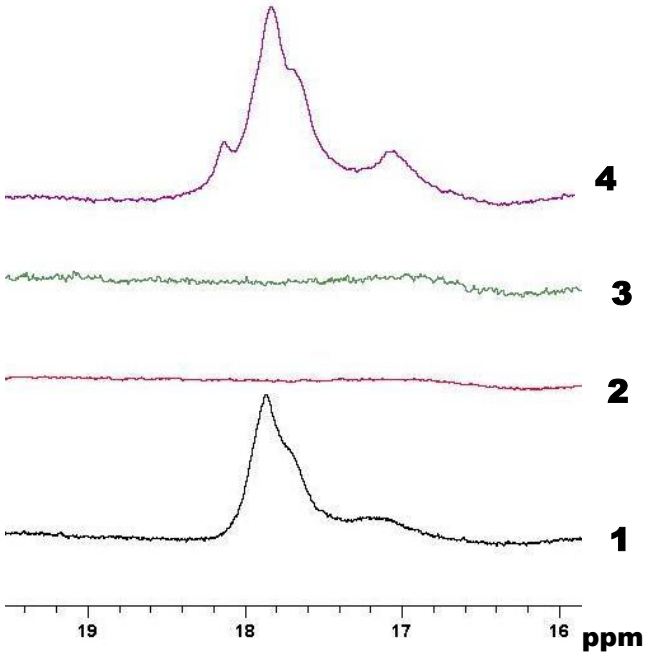


**Figure 4.4**: *$^{1}$H-NMR spectra of the zinc reconstituted metal ligand mutants of ADE*. All spectra were collected at 1 $^{o}$C, in 50 mM phosphate buffer. All spectra were collected for 16 hours. [1] wild type-ADE (260 μM) + 3 mM 6-chloropurine, at pH 5.5, showing the downfield proton at 18.0 ppm. [2] ADE D284A mutant (280 μM) + 3.2 mM 6-chloropurine, at pH 5.4, showing the absence of the downfield proton. [3] ADE E236Q (300 μM) + 3 mM 6-chloropurine, at pH 5.5, showing the absence of the downfield proton. [4] ADE H90N (265 μM) + 3 mM 6-chloropurine, at pH 5.6, showing the downfield proton at 18 ppm.

Similar strategy was used in quantification of the downfield protons for the various ADE mutants shown in **Figures 4.4 and 4.5**. No downfield proton was observed for the D284A and E236Q mutants. The H90N and D285A mutants, showed more than a single proton in the downfield region for the LBHB. This may result from the

perturbation of the active site resulting from these mutants, which are in close proximity to the binuclear metal center. For the H90N mutants, the net protons in the downfield resonance region amount to 9.8% of a single proton (**Figure 4.4**), whereas for the D285A mutant, the net protons in the downfield resonance region amount to 10.1% of a single proton (**Figure 4.5**). The H473N and D474N mutants display broad proton peaks, due to pH effects, and amount to 7.5% and 7.0% of a single proton respectively when quantified.

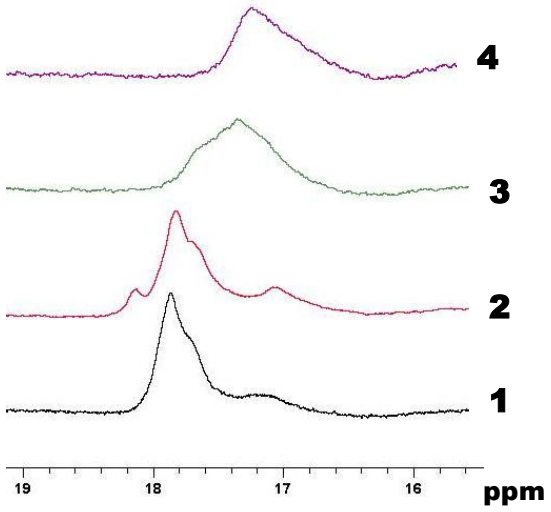


**Figure 4.5**: *$^{1}$H-NMR spectra of the zinc reconstituted mutants of ADE*. All spectra were collected at 1 $^{o}$C, in 50 mM phosphate buffer with the addition of 3 mM 6-chloropurine. All spectra were collected for 16 hours. [1] wild type-ADE (260 μM) at pH 5.5, showing the downfield proton at 18.0 ppm. [2] ADE D285A mutant (270 μM) at pH 5.8, showing the downfield proton at 17.8 ppm. [3] ADE H473N (300 μM), at pH 5.8, showing the downfield proton at 17.5 ppm. [4] ADE D474N (285 μM) at pH 5.7, showing the downfield proton at 17.3 ppm.

DISCUSSION

*Kinetic and Proton Inventory Analysis.* The wild type-ADE and the various ADE mutants reconstituted with zinc display similar kinetic properties as those for the manganese and iron reconstituted ADE mutants (*20*). Previous studies done on Mn/Mn-ADE have shown that at pH 7.5, there is an inverse solvent deuterium isotope effect of 0.49 ± 0.02 (*20*). The inverse solvent isotope effect for ADE is consistent with the findings of other members of the amidohydrolase superfamily, involved in deamination reactions. Cook, Cleland and co-workers found that adenosine deaminase (*48*) exhibits an inverse solvent deuterium isotope effect of 0.45 on $k_{cat}/K_m$ and 0.74 on $k_{cat}$. Raushel and co-workers have found that cytosine deaminase exhibited an inverse solvent deuterium effect of 0.62 and 0.40 on $k_{cat}$ and $k_{cat}/K_m$ respectively (*8*). Proton inventory studies were employed to study the nature of the inverse isotope effects in ADE. Since the Zn-reconstituted and Mn-reconstituted forms of ADE exhibit similar kinetic characteristics, Mn-reconstituted ADE was used for the proton inventory studies. For inverse solvent deuterium effects, there are three conventional curves that can fit the inverse proton inventory profiles (*86*). The first being a convex curve that comprises of mechanistic models that have a single "tight" transition-site, second being a concave curve that represents systems having a single "loose" reactant-state site and lastly the linear profile that encompasses all the proton transfer steps from multiple sites on the enzyme (*86*). Equation 2 represents the measurement of the isotopic fractionation factor for the reactant site ($\Phi^R$). Fractionation factors are parameters that are used to define the contribution of a particular site in a particular molecular state in catalysis. $\Phi^R$ is the

measure of the deuterium preference of the reactant state relative to the deuterium preference of the average-deuterium from the bulk water solvent. Since $k_{cat}$ does not take into account the binding of the substrate, only the $\Phi^R$ can be calculated from the $k_{cat}$ profile. $\Phi^T$ is the fractionation factor for the transition-state can be calculated from the $k_{cat}/K_m$ profile as this kinetic parameter accounts for the binding of the substrate to the enzyme and can account for the transition state of the reaction. Equation 3 represents that measure of the $\Phi^T$ obtained for smaller concave curves in $k_{cat}/K_m$ profiles.

For the profile obtained for the $k_{cat}$ for the proton inventory study on ADE (**Figure 4.1**), the blue dashed line represents a straight line connecting the $k_{cat}$ of ADE at 100 % $H_2O$ and 100% $D_2O$. As the fraction of $D_2O$ increases, the experimentally obtained values of $k_{cat}$ in duplicates lie close to each other for every other fraction of $D_2O$ lie below this straight line. Thus the nature of the profile for the proton inventory for $k_{cat}$ is concave. The fractionation factor of the reactant state ($\Phi^R$) obtained from this fit to equation 2 was 0.46 ± 0.01, indicates that the reactant state of the enzyme has single proton site responsible for catalysis and this proton transfer is the rate limiting step of the reaction. In ADA, it was concluded by Cleland that this proton was likely to be the proton that is transferred from Glu-217 to N1 of adenosine (*49*). In CDA, it was hypothesized by Raushel and co-workers that this proton was likely to be the proton that is transferred from Glu-217 to N1 of cytosine (*8*). For the proton inventory profile obtained for $k_{cat}/K_m$ (**figure 4.2**), the blue line represents a straight line connecting points for 100% $H_2O$ and 100% $D_2O$. The red line represents the data fit to equation 3, which represents a line of intermediate curvature for proton inventory profiles. The

fractionation factor of the transition-state site ($\Phi^T$) obtained from the fit from equation 3, was 2.34 ± 0.02, indicative that there is more than proton transfer event occurring during the transition state. The first is presumably the transfer of the proton from the protonated Glu-236 to the N-1 of adenine, and the second being the proton shuttling by Asp-284 eventually protonating the leaving ammonia group. Similar protonation events are seen for ADA (*34*) and CDA (*8*). If there were multiple sites experiencing a tightened potential as the transition state was formed, a line of intermediate curvature would provide a better fit, hence the profile of $k_{cat}/K_m$ was fit to equation 3. Thus the proton inventory profiles identify a single proton transfer as the rate limiting step of the adenine deaminase reaction, and also identify the two proton transfer events during the catalytic cycle.

*Discovery of the Low-Barrier Hydrogen Bond of ADE.* Extensive studies on the serine protease, chymotrypsin led researcher to identify the elusive low-barrier hydrogen bond (LBHB) implicated in enzyme catalysis. The LBHB is chymotrypsin exists between Asp-102 and His-57 of chymotrypsin, which is part of the proton relay system associated with the catalytic triad of the serine proteases. The proton associated with the LBHB has a characteristic downfield $^1$H-NMR signal between 17.0 – 18.0 ppm. In a proposal by Cleland, enzymes with lower fractionation factors, generally involve low barrier hydrogen bonds in their catalytic cycles. Since it has been previously shown that ADE, ADA and CDA three mechanistically characterized representative examples of deaminase enzymes from the AHS have low fractionation factors from their proton inventory studies, an attempt was made to identify a LBHB in this class of enzymes.

Prior studies on the LBHB from the research group of Frey and, Markley, have shown that the downfield protons are generally seen at lower pH and lower temperatures as it prevents exchange of the desired proton with solvent protons (*76-81*). Hence ADE samples were prepared with pH around 5.5 since it was the lowest pH that allowed ADE to remain soluble and all spectra were collected at 1 $^{o}$C.

Since manganese and iron are both paramagnetic in nature, the use of Mn/Mn-ADE or Fe/Fe-ADE for NMR analysis would prove futile. Since Zn in permissible for NMR, Zn/Zn-ADE was used in the NMR study. Also since Zn/Zn-ADE has similar kinetic properties to Mn/Mn-ADE and Fe/Fe-ADE for the deaminase reaction, the zinc-reconstituted ADE would prove ideal for the NMR study. **Figure 4.3** shows the $^{1}$H-NMR spectra for the region 16.0 to 19.0 ppm for various wild type Zn/Zn-ADE conditions. For the wild type Zn/Zn-ADE at pH 5.5 and 1$^{o}$C, a resonance peak is observed at 17.2 ppm consistent with the existence of a LBHB in ADE (**Figure 4.3[1]**). As the temperature increases from 1 $^{o}$C to 25 $^{o}$C the peak disappears, consistent with the findings of other enzymes possessing LBHB (*76-81*). In a review by Cleland, Frey and Gerlt (*72*) there is proposal that in a mechanism involving some unstable intermediate, the transition state for it will closely resemble the intermediate. A LBHB would be found in such systems in the intermediate or in an enzyme-inhibitor complex mimicking this state. To test this proposal, adenine (the substrate of ADE) and 6-chloropurine (an inhibitor of ADE), were added to ADE at pH ~ 5.5. In both cases the downfield proton corresponding to the LBHB, was observed between 17.0 and 18.0 as shown in figure 3. The signal to noise for the proton was marginally better with adenine as compared to the

sample of the enzyme by itself. The signal to noise was significantly better for the sample of the enzyme and inhibitor as compared to the enzyme alone. This finding was consistent to the proposal from the review by Cleland, Frey and Gerlt (*72*).

Adenine deaminase is a unique deaminase from the AHS. It catalyzes a promiscuous catalase type reaction along with its native adenine deaminase reaction. ADE is relatively large protein as compared to the other deaminases of the AHS. It contains approximately 600 amino acids. The catalytic components for the deaminase reaction, i.e. the binuclear metal center as well as the residues implicated in the hydrolytic deamination reaction are all located within the first 300 amino acids of the protein, which comprise the $(\beta/\alpha)_8$-barrel, a common structural fold for all the members of the AHS. Aspartate-284 and glutamate-236 for the *Escherichia coli* are critical residues for this reaction and mutation of these residues results in dramatic loss of the deaminase activity (*20*). Asp-284 and Glu-236 are metal binding residues as well but play a more important role in activating water for the hydrolytic attack as well as protonate the leaving groups and act as a proton relay system (*20*). Towards the C-terminal end of the protein, lies an invariant HD-dyad for all the binuclear adenine deaminase enzymes from the AHS. Mutation of Histidine-473 or aspartate-474 from the *E. coli* ADE results in complete loss of the catalase activity of the enzyme (*21*). Since ADE has two different set of residues identified in two different reactions, it was imperative to study the effect of these mutations on the downfield proton implicated as being the LBHB for ADE. To probe the effect on the deamination reaction, D284A, E236Q and H90N were chosen as the mutants to analyze. His-90 is a ligand to the

binuclear metal center but upon mutation to only Asn binds two metals in the active site. These mutants were previously shown to bind two equivalents of manganese or iron per monomer of enzyme (*20*) and the zinc reconstitutions showed that all these mutants bound two equivalents of zinc per monomer of enzyme. Another mutant D285A was considered for the NMR study, as it is part of a highly conserved DD-motif at the end of β-strand 8, for all the deaminase enzymes in the AHS. Based on studies on ADA (*87*) and ADE (*20*) as well as 6-MAD (*24*), the second aspartate residue is responsible for recognition of the leaving ammonia group as well as orienting the ammonia group in the proper position for protonation and leaving of the active site.

The $^{1}$H-NMR spectra in **figure 4.4** represent the spectra for the mutants involved in the deaminase reaction. Upon mutation of the residues involved in activating the water for the hydrolytic attack, i.e. Asp-284 and Glu-236, there is a loss of the downfield proton implicated in the LBHB. Upon mutation of the His-90 the downfield proton is observed. The residues involved for proton shuttling in the catalase reation, His-473 and Asp-474 show the presence of the downfield upon mutation of the residues (**figure 4.5**). Asp-285 the residue implicated in the proton shuttling to the leaving ammonia group also shows the presence of the downfield proton (**figure 4.5**). Thus based on the $^{1}$H-NMR spectra shown in **figures 4.4 and 4.5** it is suggestive that the downfield proton coincides with the residues implicated in the activating water for the hydrolytic attack. The net quantification of the downfield proton amounts to 10% of a single proton when quantified with respect to the methyl group of the methionine residues of ADE in presence of the inhibitor 6-chloropurine. This value gets smaller in the absence of

inhibitor. This suggests that the downfield proton is readily exchangeable with solvent even at such low temperatures and pH. The broad shapes of the protons are attributed largely to the pH. In order to get sharper peaks, the pH needs to be reduced to 3 or lower based on studies on serine proteases, however due to limit in solubility of ADE at low pH values; such studies could not be performed. The observation of multiple peaks in the D285A and H90N mutants arises primarily from perturbation of the active site of ADE due to the close proximity of these residues to the binuclear metal center. H90 is ligand to one of the metals of the binuclear metal center and only the H90N mutants binds two metals in the active site. The D285 residue is implicated in orienting the leaving ammonia group and well as hydrogen bonding to the leaving ammonia group in the mechanism of ADE.

Thus based on the previously proposed chemical mechanism of deamination of adenine (shown in **scheme 4.2**), the activated hydroxide attacks the *re*-face of C-6 forming a tetrahedral intermediate with R stereochemistry. This intermediate has a negative charge on the N-1 and shown in red of scheme 2 is the hydrogen bond shared between Glu-236 and the N-1 of the tetrahedral intermediate. In a review by Cleland, he suggests that for ADA, the putative LBHB would come from the proton being transferred to the N-1 of the tetrahedral intermediate (*48, 49*). In his proposal he suggests that upon attack by the hydroxide at C-6, the p*K*a of the N-1 increases relative to that of the protonated glutamate responsible for the proton transfer. This increase in the p*K*a accounts for the inverse isotope effects and the proton inventory profiles (*49*). Thus based on the proton inventory studies for ADE, $^{1}$H-NMR studies for wild type-ADE and

ADE mutants, the downfield proton seems to coincide with the deaminase reaction and seems to be associated with the residues that are involved in activating the water for the hydrolytic attack. The exact position of the LBHB remains uncertain but based on the preliminary studies, it seems consistent with the LBHB being associated with the proton being transferred from Glu-235 to the N-1 of the tetrahedral intermediate. This increase in signal associated with the inhibitor 6-chloropurine further reinforces this proposal. Currently there is an attempt to synthesize $^{15}$N-1 6-chloropurine to determine whether there is a splitting observed in the downfield proton arising from the $^{15}$N of the inhibitor. Positive results from this study would confirm the exact nature and position of the LBHB in ADE analogous to the study performed in chymotrypsin. LBHB has been now conclusively identified in 4 enzymes (serine proteases (*75-82*), phospholipases (*83*), tryptophan synthase (*84*) and photoactive yellow protein (*85*)) and proposed for at least 4 other systems (*72*). The identification of the LBHB in ADE, as well as unpublished results from the Raushel lab on ADA (Ms. Alissa Goble) and CDA (Ms. Samantha Burrows) further extend the range of enzymes that utilize LBHB in catalysis. The findings amongst the deaminase enzymes from the AHS represent that first example of metal-dependent enzymes using LBHB in catalysis.

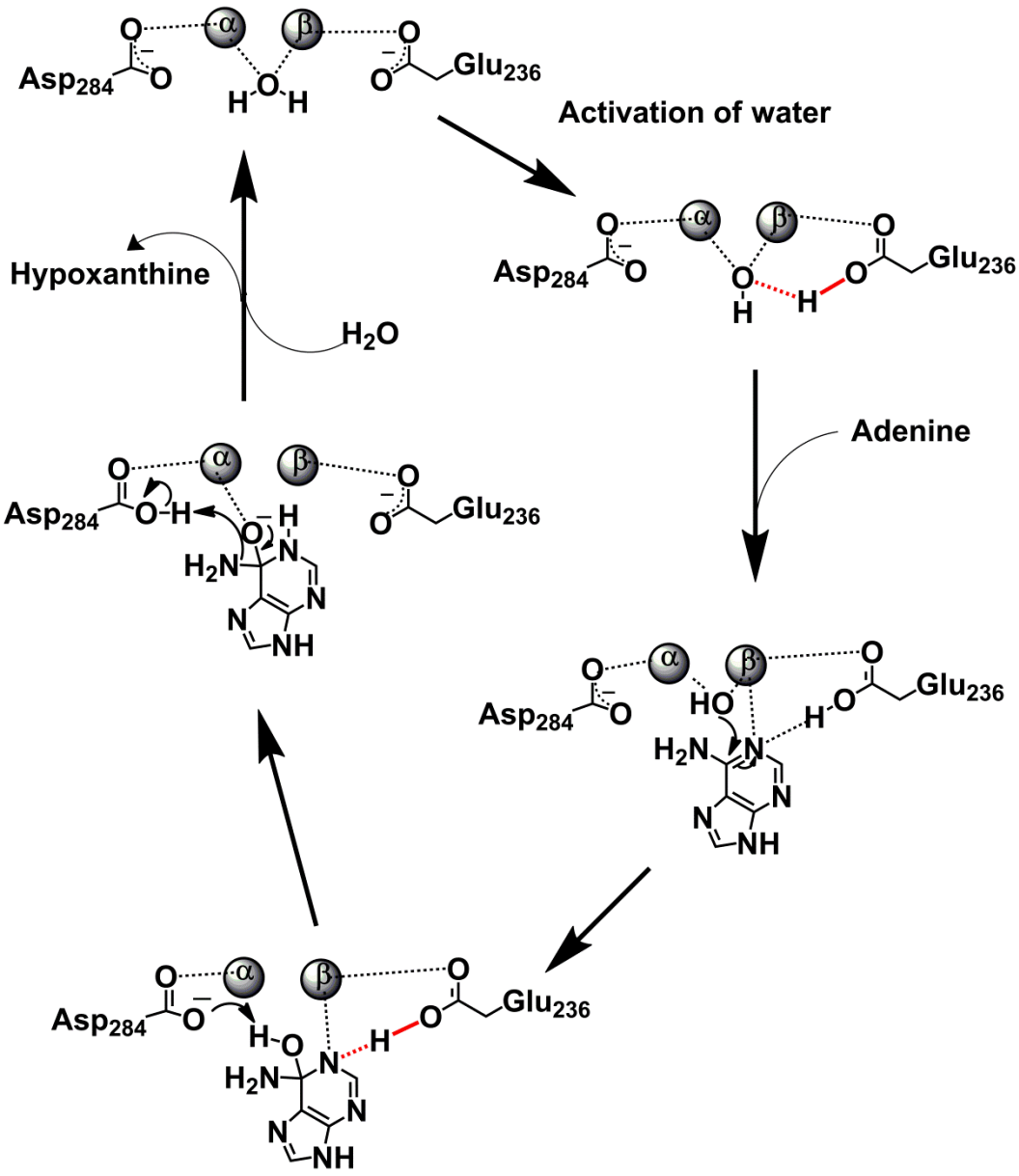


**Scheme 4.2:** Mechanism of the deamination of adenine. The bonds shown in red are the predicted downfield proton implicated in the low-barrier hydrogen bond in the adenine deaminase reaction.

# CHAPTER V

# ENZYMATIC DEAMINATION OF THE EPIGENETIC BASE N-6-METHYLADENINE*

Two enzymes from the amidohydrolase superfamily (AHS) were discovered to catalyze the deamination of N-6-methyladenine to hypoxanthine and methylamine. The methylation of adenine in bacterial DNA is a common modification for protection of the host DNA against restriction endonucleases. The enzyme from *Bacillus halodurans*, Bh0637, catalyzes the deamination of N-6-methyladenine with a $k_{cat}$ of 185 $s^{-1}$ and a $k_{cat}/K_m$ of 2.5 x $10^6$ $M^{-1}s^{-1}$. Bh0637 catalyzes the deamination of N-6-methyladenine 2 orders of magnitude faster than adenine. A comparative model of Bh0637 was computed using the three dimensional structure of Atu4426 (PDB code: 3nqb) as a structural template and computational docking was used to rationalize the preferential utilization of N-6-methyladenine over adenine. This is the first identification of an N-6-methyladenine deaminase (6-MAD).

---

INTRODUCTION

N-6-methyladenine is found in the genomes of all bacteria. Its prevalence in almost life forms resulted in it being considered as the 6$^{th}$ DNA base pair with 5-methylcytosine being the 5$^{th}$. The occurrence of N-6-methyladenine in most bacterial genomes varies from 1.4 – 2.0 % of the total adenine content. It functions as a signal for genome defense against restriction enzymes and is responsible of viability of most bacteria (*88, 89*). More recently, N-6-methyladenine has been implicated in DNA repair and replication, nucleotoid segregation, regulation of gene expression, control of transposition, and host-pathogen interactions (*88, 89*). In bacteria, DNA methylases like DNA adenine methylases (Dam) and cell-cycle regulated methyltransferases (CcrM) are responsible for the N-6 methylation of adenine (*88*). Previous studies with cell free extracts from various sources have suggested a cryptic activity where N-6-methyladenine was converted to hypoxanthine (*90-92*). However there has been no enzyme known to recycle N-6-methyladenine in this manner to date.

The NCBI database has classified in cog 1001 predominantly enzymes belonging to the amidohydrolase superfamily (AHS). Members within this superfamily, hydrolyze a variety of bonds at carbon and phosphorus centers (*7*). Members of the AHS utilize one or two divalent metal ions in the active site of the characteristic $(\beta/\alpha)_8$ barrel fold to catalyze these hydrolytic reactions. All the members of cog1001 have conserved HxH motif at end of β-strand 1, conserved histidines at end of β-strands 5 and 6, a bridging glutamate at end of β-strand 4 and an aspartate at end of β-strand 8 (*24*). This represents

a prototypical binuclear metal center with a bridging glutamate like phosphotriesterase homology protein (PHP) (*93*) and adenine deaminase (ADE) (*20*).

Cluster of Orthologus Group (COG) 1001 predominantly consists of enzymes annotated as adenine deaminase (ADE) (*20*). ADE is a very promiscuous enzyme that catalyzes the deamination of adenine to hypoxanthine and ammonia as well as the redox disproportionation of hydrogen peroxide to oxygen and water (*21*). COG 1001 also consists of members that are annotated as isoaspartyl dipeptidase (IAD) (*22*) and enamidase (*23*). There is however another cluster of sequentially related bacterial protein annotated as adenine deaminase but has less than 40 % sequence identity to experimentally validated ADE. There are also the some organisms that have more than one ADE lying in similar genomic contexts in the genome which is rather unusual. Most of these organisms are closely related *bacillus* species.

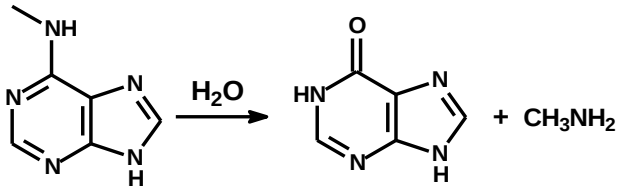


**Scheme 5.1:** Reaction catalyzed by Bh0637 and other N-6-methyladenine deaminase (6-MAD).

In this chapter, we demonstrate a set of bacterial enzymes from COG 1001 that recycle N-6-methyladenine through the demethylaminase reaction (**scheme 5.1**), where they hydrolyze N-6-methyladenine to form hypoxanthine and methyl amine. These

enzymes come from closely related bacterial species and expand the bacterial purine salvage pathway for the utilization of N-6-methyladenine.

MATERIALS AND METHODS

*Materials.* All chemicals were purchased from Sigma-Aldrich unless otherwise stated. The genomic DNA for *B. halodurans C-125* was purchased from ATCC. *E. coli* BL21 (DE3) and XL1-blue competent cells were obtained from Stratagene (Agilent). The expression vector pET30(+) and *Pfx* DNA polymerase were purchased from Invitrogen. All oligonucleotides were obtained from the Gene Technology Lab at Texas A&M University.

*Cloning of Bh0637 from B. halodurans (C-125).* The DNA sequence for Bh0637 from *B. halodurans C-125* was cloned (gi|15613200). The gene for Bh0637 was amplified utilizing the primer pair 5'-AAAGAGAATCATATGTGTGAACAAAAGTATCGCTGGACGAAAAAGC-3' and 5'-AGAAGAAAGCTTTTAACGCATAATTGAAGGAAAGAGAACTGTTTTCTTATGAAC-3'. *NdeI* and *HindIII* restriction sites were introduced into the forward and the reverse primers, respectively. The PCR product was purified with a PCR cleanup system (Qiagen), digested with *Nde*I and *HindIII*, and ligated into a pET30a(+) vector which was previously digested with *Nde*I and *HindIII*. Colony PCR was used to verify whether the colony had the gene-insert prior to sequencing. The cloned gene fragment was sequenced to verify the fidelity of the PCR amplification.

*Protein Expression and Purification*. The recombinant plasmid bearing the gene for Bh0637 was transformed into *E. coli* BL21 (DE3) competent cells by electroporation. A single colony was grown overnight at 37 $^{o}$C in 5 mL of LB medium containing 50 μg/mL kanamycin. Five mL aliquots were used to inoculate 6 L of the same medium. The cell cultures were grown at 37 $^{o}$C and induced with 0.5 mM isopropyl-β-thiogalactoside (IPTG) when the $A_{600}$ reached ~ 0.6 in the presence of 1.0 mM $MnCl_2$. The cells were centrifuged and then resuspended in 50 mM Hepes, pH 7.5, containing 0.1 mg/mL phenylmethylsulfonyl fluoride and lysed by sonication. The soluble proteins were separated from the cell debris by centrifugation at 12000 x g for 15 minutes at 4 $^{o}$C. The nucleic acids were removed by dropwise addition of 2% w/v protamine sulfate. After centrifugation, solid ammonium sulfate was added to 60% saturation to the supernatant solution. The precipitated protein was dissolved in buffer and then applied to a High Load 26/60 Superdex 200 prep grade gel filtration column (GE HealthCare). The active fractions were pooled and loaded onto a ResourceQ column (6 mL) and eluted with a gradient of NaCl in 20 mM Hepes, pH 7.5. The protein purity was confirmed by SDS-PAGE.

*Protein and Metal Analysis.* The protein concentration was estimated by measuring the absorbance at 280 nm using an extinction coefficient of 100,000 $M^{-1}$ $cm^{-1}$ (*39*). The metal content of the protein was determined by induced coupled plasma mass spectrometry (ICP-MS) (*40*). The protein samples for ICP-MS were digested with $HNO_3$ by refluxing for ~45 minutes to prevent protein precipitation during the ICP-MS run. The protein concentration was adjusted to ~1.0 μM in 1% v/v $HNO_3$.

*Substrate Screening.* Various adenine derivatives were tested for changes in UV absorbance spectra after incubating 100 μM compounds dissolved in 20 mM Hepes buffer pH 7.5 with 1 μM purified Bh0637 for 2 hours. As a control the substrates without the enzyme was used to check for any degradation of substrate over time. The following substrates were tried: adenine, N-6-methyladenine, 2-hydroxyadenine (isoguanine), guanine, 2,6-diaminopurine, 6-chloropurine, 7-methyladenine, cytosine, 6-methoxypurine, 6-methylmercaptopurine, 6-mercaptopurine, toxopyrimidine, 6-methylpurine, adenosine, adenosine-5'-monophosphate, 2'deoxyadenosine, 5-amino-4-imidazole-carboxyamide, deisopropyl-hydroxyatrazine, 5-acetylamino-6-amino-3-methyluracil, 2-hydroxy-4-amino-6-(cyclopropylamino)-1,3,5-triazine (**Scheme 5.2**). The UV spectra were collected from 240 nm to 350 nm using a SpectraMax-340 UV-vis spectrometer.

*Kinetic constants.* The deamination of adenine was determined using a coupled assay with glutamate dehydrogenase (GDH). The formation of ammonia was followed at 340 nm using a SpectraMax-340 UV-vis spectrometer in the presence of 20 mM Hepes, pH 7.5, 0.15 mM NADH, 25 mM α-ketoglutarate (Calbiochem), 4 μg/mL GDH and various concentrations of adenine in a final volume of 0.25 ml (*41*). The demethylamination of N-6-methyladenine was followed at 270 nm ($\varepsilon$ = 15,000 $M^{-1}cm^{-1}$) (*90*) for the loss of N-6-methyladenine. Various concentrations of N-6-methyladenine were added to final volume of 0.25 mL. The removal of methanethiol from 6-methylmercaptopurine was monitored at 290 nm ($\varepsilon$ = 20200 $M^{-1}cm^{-1}$) (*94*) and removal of methanol from 6-methoxypurine was monitored at 270 nm ($\varepsilon$ = 3760 $M^{-1}cm^{-1}$) (*95*)

when various concentrations of the substrate were added to a final volume of 0.25 ml. All the assays were carried out at 30 $^{o}$C.

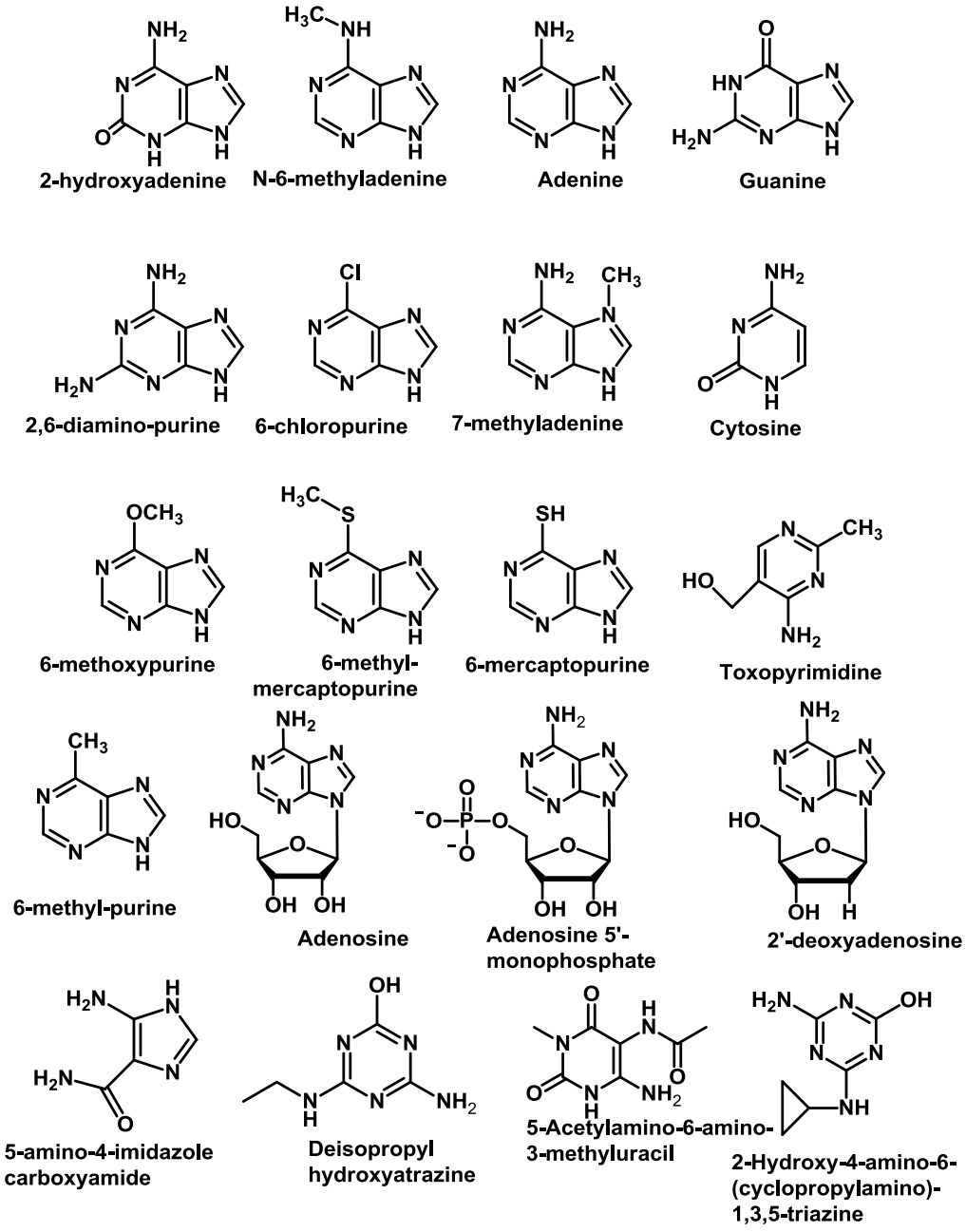


**Scheme 5.2:** Library of compounds tested against Bh0637

*Mass spectrometry.* The methylamine released from the demethylamination of N-6-methyladenine by Bh0637 was identified using mass spectrometry using electrospray ionization (ESI) in the (+)-mode with acetonitrile as the solvent matrix. The mass spectroscopy was done at the Laboratory of Biological Mass Spectrometry, Texas A&M University.

*Preparation and Reconstitution of Apo-Enzyme.* Apo-Bh0637 was prepared by dialyzing the enzyme purified against 10 mM 1,10-phenanthroline in 20 mM Hepes, pH 7.0, for 36 hours with two changes of buffer. The apo-enzyme was separated from 1,10-phenanthroline using a PD-10 column (GE HealthCare) and then reconstituted with 2 enzyme equivalents of $Mn^{2+}$, $Zn^{2+}$ or $Fe^{2+}$ at 4 $^{o}$C for 48 hours. Iron was added anaerobically to the apo-enzyme to prevent air oxidation. All samples were passed through a PD-10 column to remove any unbound metal.

*Redox testing of Fe/Fe-Bh0637.* To measure the susceptibility of Fe/Fe-Bh0637 to oxygen the enzyme reconstituted with iron was exposed to air and the kinetic constants for the demethylamination reaction with N-6-methyladenine were used to determine loss of any activity. [$Fe^{II}/Fe^{II}$]-Bh0637 was oxidized with the redox dye, thionine (Finn Scientific Inc.). [$Fe^{II}/Fe^{II}$]-Bh0637 (1 μM) was incubated anaerobically with 1 to 20 μM (1-20 enzyme equivalents) of thionine in 20 mM Hepes, pH 7.5, at room temperature for 16 hours. As a control 20 enzyme equivalents of thionine was added Mn/Mn-Bh0637 and assayed for the demethylamination activity. 250 μM hydrogen peroxide was added to 1.5 μM Fe/Fe-Bh0637 to check for any catalase activity

(*20, 21*). As a control the same amount of hydrogen peroxide was added to Mn/Mn-Bh0637 and both samples were assayed for demethylamination activity.

*Sequence similarity networking and genomic analysis of COG 1001.* Sequence similarity networking was used to classify and separate Cluster of Orthologous Group (COG) 1001 (*11*) using the software Cytoscape version 2.7.0 (*12, 96*). The COG 1001 based on NCBI classification was split in groups based on primary sequence identity at an E-value $10^{-80}$ and further analyzed for substrate specificity and catalytic activity. Genomic context analysis of group 2 in COG 1001 was done using the Microbes Online program.

*Data Analysis.* Initial velocity kinetic data were fit to **equation 2.1** using SigmaPlot 9.0 where $v$ is the initial velocity, [A] is the substrate concentration, $E_t$ is the total enzyme concentration, $k_{cat}$ is the turnover number and $K_m$ is the Michaelis constant.

$$v / E_t = k_{cat} [A] / (K_m + [A]) \qquad \textbf{(Equation 2.1)}$$

RESULTS

*Sequence similarity networking and genomic analysis of COG 1001.* COG 1001 at E-value $10^{-80}$ forms 5 groups (**Figure 5.1**). Groups 1 and 4 previously studied by us are adenine deaminase (ADE) with a promiscuous catalase activity (*20, 21*). The split is due to the high constraint put on the E-value. Group 3 members are isoaspartyl dipeptidase (IAD) based on classification in NCBI and comparison of the primary sequence and conservation of residues to the crystal structure of IAD from *E. coli* (PDB: 1ybq) (*22*). Group 5 members are enamidase based on classification in NCBI and comparison to primary sequence and conservation of residues to the crystal structure of

enamidase from *Eubacterium bakeri* (PDB: 2vun) (*23*). Members from group 2 are annotated as adenine deaminase or members of the amidohydrolase superfamily with unknown function in the NCBI database. They have less than 40 % sequence identity to the ADE from group 1. There are 32 sequences in group 2 from closely related *bacillus* species and there are at least 12 these organisms that have more than 1 ADE (**Table 5.1)**. Genomic analysis of the protein sequences in group 2 reveals that these genes are co-localized in the same operon as ADE that have been previously validated for function (*20, 21*). This suggested that the substrate used by these enzymes was similar to adenine and the product of the reaction would be hypoxanthine or something very similar.

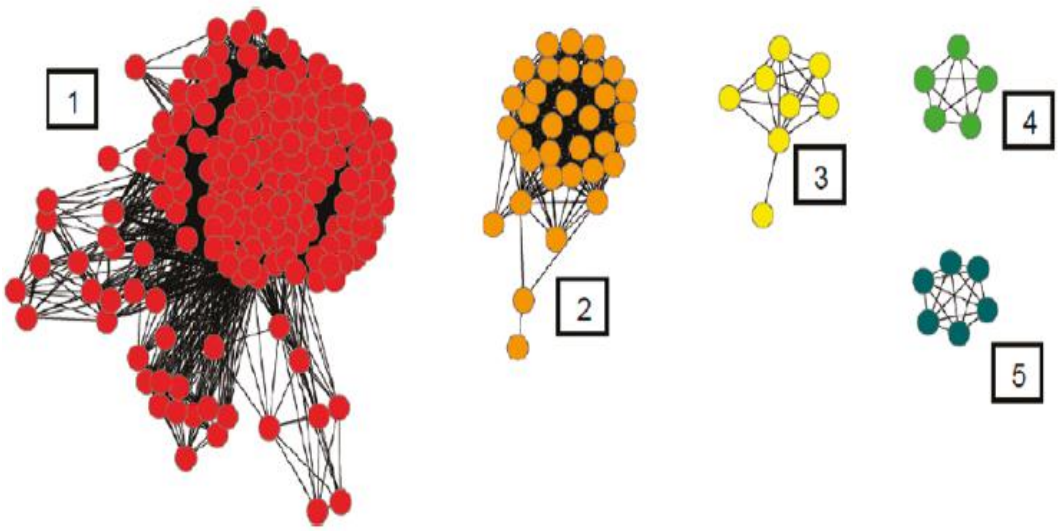


**Figure 5.1:** *Sequence similarity network representation of COG1001 obtained at E-value* $10^{-80}$. Groups 1, 4 are ADE, group 3 is IADs and group 5 is enamidases.

**Table 5.1:** *Members of group 2 of COG1001*

| Organism | Locus tag | Gi number |
|---|---|---|
| *Bacillus halodurans C-125* | Bh0637 | 15613200 |
| *Bacillus clausii KSM-K16* | ABC1075 | 56962849 |
| *Geobacillus kaustophilus HTA426* | GK0271 | 56418806 |
| *Anoxybacillus flavithermus WK1* | Aflv_0242 | 212638091 |
| *Geobacillus thermodenitrificans NG80* | GTNG_0250 | 138893926 |
| *Bacillus cereus Q1* | BCQ_2842 | 222096502 |
| *Lysinibacillus sphaericus C3-41* | Bsph_0221 | 169825824 |
| *Bacillus licheniformis ATCC 14580* | BL01492 | 52079144 |
| *Bacillus amyliquefaciens FZB42* | RBAM_006960 | 154685151 |
| *Bacillus subtilis str. 168* | BSU06560 | 16077724 |
| *Bacillus pumilus SAFR-032* | BPUM_0617 | 157691407 |
| *Bacillus cereus ATCC 14579* | BC3012 | 30021127 |
| *Bacillus cereus B4264* | BCB_4264_A3029 | 218233799 |
| *Exiguobacterium sibiricum 255-15* | Exig_0459 | 172056498 |
| *Bacillus cereus G9842* | BCG9842_B2218 | 218898088 |
| *Bacillus thuringiensis str. Al Hakam* | BALH_2712 | 118478348 |
| *Bacillus cereus 03BB102* | BCA_3097 | 225864990 |
| *Bacillus cereus E33L* | BCZK2753 | 52142489 |
| *Bacillus thuringiensis serovar konkukian str. 97-27* | BT9727_2766 | 49480044 |

**Table 5.1** Continued

| Organism | Locus tag | Gi number |
|---|---|---|
| *Bacillus anthracis str. 'Ames Ancestor'* | GBAA3032 | 47528323 |
| *Bacillus anthracis str. Ames* | BA_3032 | 30262986 |
| *Bacillus anthracis str. Sterne* | BAS2818 | 49185824 |
| *Bacillus cereus AH820* | BCAH820_3026 | 218904142 |
| *Bacillus weihenstephanensis KBAB4* | BcerKBAB4_2823 | 163940762 |
| *Oceanobacillus iheyensis HTE831* | OB0751 | 23098206 |
| *Picrophilus torridus DSM 9790* | PTO1085 | 48478157 |
| *Brevibacillus brevis NBRC 100599* | BBR47_06120 | 226310199 |
| *Rubrobacter xylanophilus DSM 9941* | Rxyl_1744 | 108804579 |
| *Geobacillus thermodenitrificans NG80-2* | GTNG_1889 | 138895539 |
| *Geobacillus kaustophilus HTA426* | GK1989 | 56420524 |
| *Bacillus cereus AH187* | BACH_A3083 | 217960451 |

*Purification and Properties of Bh0637.* Wild type Bh0637 over-expressed in *E. coli* and could be purified to homogeneity. The protein identity was confirmed by N-terminal amino acid sequencing at the Protein Chemistry Laboratory, Department of Biochemistry and Biophysics, Texas A&M University. ICP-MS analysis of Bh0637 showed the protein had 2 equivalents of $Mn^{2+}$ per monomer of Bh0637. There was no change in the metal content when the iron free expression protocol was used (*20*). Of the

various substrates incubated with Bh0637, a change in absorbance spectrum was observed in case of the adenine, N-6-methyladenine, 6-methylmercatopurine and 6-methyoxypurine .The kinetic constants obtained for the all of these substrates are presented in **Table 5.2**. No change in kinetic constants was seen for the enzyme purified using the iron free expression.

**Table 5.2**: *The kinetic constants for the various substrates for Bh0637.*

| Substrate | $k_{cat}$ ($s^{-1}$) | $K_m$ (μM) | $k_{cat}/K_m$ ($M^{-1}s^{-1}$) |
|---|---|---|---|
| Adenine | 4.7 ± 0.2 | 430 ± 40 | (1.1± 0.2) x $10^4$ |
| N-6-methyladenine | 135 ± 5 | 46 ± 4 | (2.9 ± 0.2) x $10^6$ |
| 6-methylmercaptopurine | 5.8 ± 0.3 | 96 ± 9 | (6.1 ± 0.4) x $10^4$ |
| 6-methoxypurine | 1.7 ± 0.1 | 113 ± 17 | (1.5 ± 0.1) x $10^4$ |

*Demethylamination of N-6-methyladenine by Bh0637.* Bh0637 catalyzed the demethylamination of N-6-methyladenine a 100 fold better than the next substrate (**Scheme 5.1**). The resulting products hypoxanthine and methylamine were identified when N-6-methyladenine was incubated with Bh0637. Hypoxanthine was identified from the change in absorbance spectrum (**Figure 5.2**) and the spectrum matched that of authentic hypoxanthine. Methylamine was identified using mass spectrometry. A peak at 32.1 Da in the ESI mass spectrometry (+)-mode matched the ($M+H^+$) peak expected for methylamine (31 Da neutral mass). No products were obtained when N-6-

methylamine was incubated without Bh0637. Bh0637 has specificity for a methyl group at N-6 position of adenine and also used 6-mercaptomethylpurine and 6-methoxypurine. The presence of hypoxanthine was detected spectroscopically in both cases. The other product methanethiol for 6-mercaptomethylpurine was detected using 5,5'-Dithiobis(2-nitro-benzoic acid) (DTNB). Methanol from 6-methoxypurine was detected by checking for formation of NADH from $NAD^+$ at 340 nm using alcohol dehydrogenase from *Saccharomyces cerevisiae*.

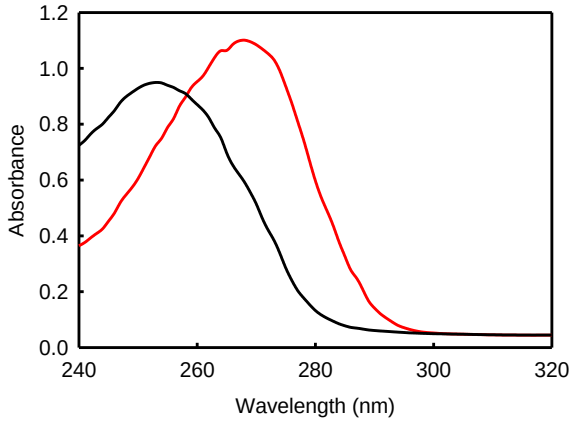


**Figure 5.2:** *Absorption spectrum of 100 µM N-6-methyladenine (in red) and 100 µM N-6-methyladenine + 1 µM Bh0637 (in black)* (incubated for 5 minutes at 30°C).

*Demethylaminase activity of NYSGXRC 9208a.* NYSGXRC 9208a was identified as a protein from *Bacillus subtilis* (gi: 16077724). It was cloned, expressed and purified by the protein production team at NYSGXRC. Like Bh0637, it lies in group 2 in COG 1001 and has 71 % sequence identity to Bh0637. It also catalyzed the demethylamination of N-6-methyladenine with $k_{cat} = 151 \pm 5\ s^{-1}$, $K_m = 60 \pm 6$ µM,

$k_{cat}/K_m$ = (2.5 ± 0.2) x $10^6$ $M^{-1}s^{-1}$. The metal content of this protein was 1.7 ± 0.2 equivalents of $Mn^{2+}$ per monomer of protein.

*Preparation and Reconstitution of Apo-Bh0637. D*ialysis with 1,10-phenantholine resulted in enzyme without any metal and a loss of more than 99 % of the demethylaminase activity. The resulting apo-enzyme could be reconstituted with $Zn^{2+}$ and $Fe^{2+}$. After 48 hours the demethylaminase activity was measured. The kinetic constants and the measured metal content by ICP-MS for these enzymes are represented in **Table 5.3**.

**Table 5.3**: *The kinetic constants for the demethylaminase activity for the various metal reconstituted forms of Bh0637.*

| Metal | $k_{cat}$ ($s^{-1}$) | $K_m$ (μM) | $k_{cat}$ / $K_m$ ($M^{-1}s^{-1}$) (x $10^6$) | Metal content by ICP-MS |
|---|---|---|---|---|
| Mn/Mn | 135 ± 5 | 46 ±4 | 2.9 ± 0.2 | 2.1 ± 0.2 |
| Zn/Zn | 185 ± 3 | 73 ± 2 | 2.5 ± 0.2 | 1.7 ± 0.2 |
| Fe/Fe | 151 ± 3 | 40 ± 3 | 3.8 ± 0.3 | 2.1 ± 0.1 |

*Redox Sensitivity of Fe/Fe-Bh0637.* The Fe/Fe-Bh0637 was exposed to air to determine the sensitivity of Fe/Fe-Bh0637 to oxygen. Oxygen oxidized the iron center resulting in loss of activity. The loss of demethylaminase activity followed a first order exponential decay with rate constants of (0.228 ± 0.007) $hour^{-1}$ for the loss of $k_{cat}$ and

(0.275 ± 0.008) hour$^{-1}$ for $k_{cat}/K_m$. The loss of activities is shown in **figure 5.3.** Addition of a 100 fold molar excess of hydrogen peroxide to Fe/Fe-Bh0637 resulted in the complete loss of the demethylaminase activity. No oxygen evolution was observed as was observed in the case of ADE. The resulting metal content of Fe/Fe-Bh0637 treated with an excess of hydrogen peroxide was 0.4 enzyme equivalents of iron. No loss of activity was observed when the same amount of hydrogen peroxide was added to the Mn/Mn-Bh0637. The incubation on the Fe/Fe-Bh0637 treated with excess hydrogen peroxide with 2 equivalents of $Zn^{2+}$, $Mn^{2+}$ and $Fe^{2+}$ (anaerobically) resulted in the reconstitution of the demethylaminase activity.

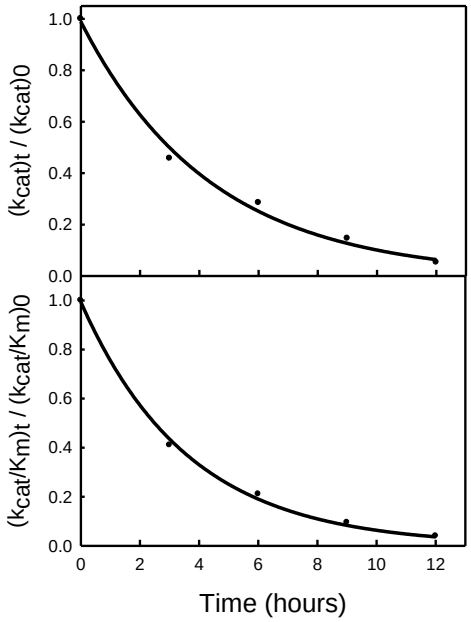


**Figure 5.3**: *Loss of activity for Fe/Fe-Bh0637 when exposed to air*. Aliquots from a stock were assayed with varying N-6-methyladenine concentrations with a fixed Bh0637 concentration (1.5 nM)

*Redox Potential of Fe/Fe-Bh0637.* The measurement of the redox potential for Fe/Fe-Bh0637 was determined using redox active dye, thionine (2 electron acceptor). In these titrations, both irons were assumed to be oxidized or reduced in pairs and that the ferrous state was the active form of the enzyme for the demethylaminase activity. All the titrations were done anaerobically to prevent any air oxidation of Fe/Fe-Bh0637. A figure of the titration is represented in **figure 5.4**. 4.0 ± 0.08 enzyme equivalents of dye were required to reduce the demethylaminase activity by 50 % to give the mid-point of the redox reaction. Assuming a 50:50 distribution of the di-ferrous and di-ferric forms of Bh0637 at this point, the equilibrium values were fit into the modified Nerst equation. Given that the value of thionine is +62 ± 2 mV (*57*), the redox potential for the interconversion of the ferrous and ferric forms of Bh0637 was +76 ± 3 mV. The addition of 20 fold excess thionine to Mn/Mn-Bh0637 did not inhibit or affect the activity and hence the dye must be oxidizing the iron center and not affecting the enzyme otherwise.

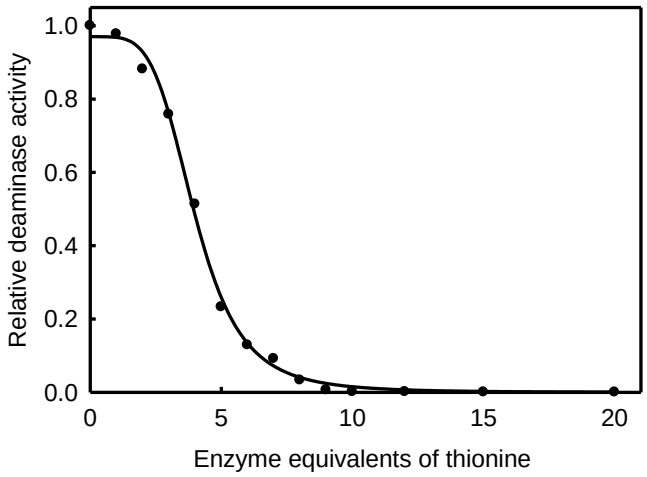


**Figure 5.4**: *Redox titration for [$Fe^{II}/Fe^{II}$-Bh0637] (1 µM) with various enzyme equivalents of thionine.*

DISCUSSION

*Genomic Context and Sequence analysis for Group 2 of cog 1001.* All the bacterial species containing the gene that lies in group 2 of cog 1001 are localized with the *PUR* gene cluster. This gene cluster codes for enzymes that form the ribose-purine bond, leading to the formation of coumpounds like guanosine, adenosine and inosine and are primarily involved in the purine salvage pathway. Authentic ADEs are localized within this gene cluster as well. The product of the ADE reaction, hypoxanthine results in the formation of inosine by the *PUR* gene cluster. In case of *B. halodurans*, the genes for ADE (Bh0640) (*21*) and Bh0637 are co-localized within this gene cluster. This indicates that these two enzymes use the same or similar substrate and that the product of the reaction catalyzed by both these enzymes must be very similar if not the same. Thus we assumed that Bh0637 would have an adenine like substrate and that the product would resemble hypoxanthine. A limited number of moieties resemble adenine in nature. Hence, a small highly focused library of about 20 compounds resembling adenine was generated.

Purine and pyrimidine deaminases ADE, adenosine deaminase (ADA), cytosine deaminase (CDA) and guanine deaminase (GDA) have two invariant aspartate residues at end of strand 8 forming a signature DD motif. The first aspartate is responsible for activation of the water for the hydrolytic reaction and also for the protonation of the leaving group as well as serving a metal binding residue for the α-metal (*7*). The function of the other aspartate remains unclear. In most of the X-ray structures of ADA, the second aspartate residue is in hydrogen bonding distance to the leaving ammonia

group. We speculated that this conservation of this DD is responsible for recognition of the $-NH_2$ group on the purine or pyrimidine that is deaminated as well as for the orientation of the leaving ammonia. The members in group 2 of COG 1001 lack this DD motif at the end of strand 8. They have a single conserved aspartate at that position followed by a glycine, forming a DG motif. This led us to believe that the substrate for Bh0637 might be modified adenine with some modification at position 6.

*Library for Screening Bh0637.* Based on all the genomic context and sequencing it seemed that Bh0637 would have adenine like substrate. Hence a library of compounds shown in **scheme 5.2** was selected with modifications on adenine at various positions. Of these adenine is the most common physiological molecule. N-6-methyladenine is physiologically prevalent. It accounts for 2.0 % of bacterial adenine. It has a variety of functions ranging from protection against restriction enzymes to cell replication and viability (*88, 89*). Adenosine is the ribosylated form of adenine needed for incorporation into DNA. 7-methyladenine is another methylated form of adenine found in bacterial genomes (*97*) and functions to protect bacterial genomes against restriction enzymes. 2-hydroxyadenine (isoguanine) is the most common oxidative product of adenine resulting from oxidation from hydroxyl radicals (*98*). All other compounds are not physiologically prevalent but were used as probes to determine whether any of them have any activity and those scaffolds could be used to search for relevant physiological counterparts.

*Substrate screening for Bh0637.* Bh0637 showed spectral changes for adenine, N-6-methyladenine, 6-methylmercaptopurine and 6-methoxyadenine. Based on the kinetic constants obtained, N-6-methyladenine was a 100 fold better than the next best

substrate. N-6-methyladenine is a known physiological compound and is considered to be prevalent in all bacterial species. We predict this enzyme recycles N-6-methyladenine to form hypoxanthine which is taken up in the purine salvage pathway to form guanine nucleotides from inosine (*15*). Bh0637 also uses adenine to form hypoxanthine but not at the same rate as N-6-methyladenine. The $K_m$ for adenine is 10 fold higher than N-6-methyladenine. Similar results were obtained for the *NYSGXRC 9208a, B, subtilis* (gi: 16077724) which lies in the same group 2 in cog 1001. Thus we have 2 examples of proteins in that cog with similar substrate profiles and we conclude that N-6-methyadenine is the natural substrate for the members of this group in cog 1001.

*Metal Center Analysis.* The different metal reconstituted forms of Bh0637 have similar activities towards the demethylaminase reaction. ICP-MS confirmed the presence of 2 equivalents of respective metal per monomer of Bh0637. All the different metal reconstituted forms have similar demethylaminase activity. Mn/Mn-Bh0637 and Zn/Zn-Bh0637 are stable under aerobic conditions. However, Fe/Fe-Bh0637 is unstable under aerobic conditions. More than 98 % of activity is lost over 12 hours when Fe/Fe-Bh0637 is exposed to air. Air oxidation of the ferrous form results in an inactive ferric form of Bh0637. ICP-MS confirmed no metal lost over this time period, hence the loss of activity is only due to oxidation of the iron center. Mn/Mn-Bh0637 and Zn/Zn-Bh0637 did not any activity over the same time. The use of strong oxidizing agent hydrogen peroxide resulted in the complete loss of activity of the Fe/Fe-Bh0637. The rapid oxidation of the ferrous form of Bh0637 resulted in the iron being oxidized and falling out of the active site. When a milder oxidizing agent like thionine was used, the iron is

only oxidized but does not fall out of the active site. This phenomenon was confirmed by ICP-MS. Addition of 2 equivalents of Mn, Zn or Fe (ferrous form) to the Fe/Fe-Bh0637 resulted in complete reconstitution of the demethylaminase activity. This suggests that the metal either displaces the remaining ferric iron in the active or occupies the vacant active site and results in restoration of activity. Hydrogen peroxide does not damage this protein like ADE (*20, 21*). Lastly, the 2+ oxidation state of the metal is essential for catalytic activity. The redox potential of Fe/Fe-Bh0637 of +76 ± 3 mV is significantly lesser than that of ADE (+ 209 mV). This also explains why Fe/Fe-ADE is air stable where as Fe/Fe-Bh0637 is easily air oxidized (*21*).

*Homology Modeling and Docking of Bh0637.* In collaboration with the Sali and Shoichet laboratories at the Department of Pharmaceutical Sciences, University of California, San Francisco, a homology model of Bh0637 was generated in order to ascertain the substrate specificity of Bh0637. The amino acid sequence of Bh0637 was first submitted to the PSI-BLAST server in NCBI to identify suitable template structures. A comparative model of the three-dimensional structure for Bh0637 was constructed based on the crystal structure of adenine deaminase (Atu4426, PDB code: 3NQB) which was the only template that produced a significant alignment with an E-value ($6 \cdot 10^{-20}$) better than the default threshold of $6 \cdot 10^{-3}$.

The high-energy intermediate (HEI) library of KEGG molecules was docked to all eight comparative models of Bh0637 by DOCK 3.5.54. The model yielding the highest enrichment for *N*-6-methyladenine was selected to represent the binding mode of this substrate in Bh0637. A comparison of the binding site in the ligand-free template

structure of Atu4426 (PDB: 3NQB) and the binding site in the comparative model of Bh0637 is presented in **Figure 5.5**. In the Bh0637 model, Glu-233 and the six residues that coordinate the binuclear metal center (His-88, His-90, Glu-180, His-211, His-232 and Asp-284) overlap with the aligned residues from the structural template. Several residues that likely interact with *N*-6-methyladenine are not conserved between the target and the template enzymes. Ser-97, His-122, Glu-123, Asp-290 and Gly-563 in Atu4426 are replaced by Phe-92, Leu-117, Met-118, Gly-285 and Phe-550 in Bh0637, respectively. The substrate binding site of Bh0637 is thus more hydrophobic than that of Atu4426. A binding model for *N*-6-methyladenine in the active site of Bh0637 is presented in **Figure 5.5**. The tetrahedral intermediate was formed by attack of the bridging hydroxide on the C-6 carbon from the *re*-face of *N*-6-methyladenine. In this model, the N6 amino group hydrogen bonds with the side chain of Asp-284. The protonated N1 nitrogen hydrogen bonds with the side chain of Glu-233. In addition, the N7 nitrogen coordinates the α-metal ion and the N9 nitrogen hydrogen bonds with the side chain of Thr-467. The N3 nitrogen is adjacent to the Nε nitrogen from His-555 (3.9 Å), which was protonated during virtual screening. The methyl group of the substrate is not in close contact with any of the neighboring residues. However, if Gly-285 is replaced by a larger residue, such as the aspartate found at the equivalent position in Atu4426, the methyl group of the substrate will be within 4 Å of the side chain of the larger residue.

Besides N6-methyladenine, the top ranked compounds that were attacked by the hydroxide from the *re*-face were inspected visually. The docked pose of adenine is

nearly identical to that of *N*-6-methyladenine, but the relative rank of adenine (ranked 282) is worse than that of *N*-6-methyladenine (ranked 176). The better ranking of *N*-6-methyladenine over adenine is due to the more favorable van der Waals interactions between the methyl group in *N*-6-methyladenine and the hydrophobic residues in the substrate binding site, such as Phe-92 and Phe-550. As a consequence, the high-energy intermediate complex of *N*-6-methyladenine is more stable than that of adenine. 5 other compounds that scored well in computational docking were subsequently tested as substrates but found not to be deaminated at measureable rates. These compounds included 5-amino-4-imidazolecarboxyamide, toxopyrimidine, 5-acetylamino-6-amino-3-methyluracil, 2-hydroxy-4-amino-6-(cyclopropylamino)-1,3,5-triazine, and deisopropylhydroxyatrazine.

*Physiological Relevance*. For Bh0637 and Bsu06560, *N*-6-methyladenine is a 100-fold better substrate than the next best compound based on the relative values of $k_{cat}/K_m$. *N*-6-methyladenine is a known physiological compound and is considered to be prevalent in all bacterial species. Bh0637 and Bsu06560 thus recycle *N*-6-methyladenine to form hypoxanthine, which is presumably taken up by the purine salvage pathway to subsequently form guanine nucleotides from inosine (*15*). These two enzymes can also use adenine to form hypoxanthine, but not nearly at the same rate as *N*-6-methyladenine. The $K_m$ for adenine is 10-fold higher than for *N*-6-methyladenine. We conclude that *N*-6-methyadenine is the physiological substrate for members of subgroup **2** in cog1001 and thus these enzymes should now be annotated as 6-methyladenine deaminases (6-MAD). The prototypical adenine deaminases in *B.*

*halodurans* (Bh0640) and *B. subtilus* (Bsu14520) cannot use *N*-6-methyladenine as substrate (*20*, *21*). The kinetic constants for the deamination of adenine by Bh0640 are 120 ± 4 $s^{-1}$, 0.30 ± 0.04 mM and (4 ± 0.3) x $10^5$ $M^{-1}$ $s^{-1}$ for $k_{cat}$, $K_m$ and $k_{cat}/K_m$ respectively. The kinetic constants for the deamination of adenine by Bsu14520 are 140 ± 6 $s^{-1}$, 0.38 ± 0.04 mM and (3.8 ± 0.3) x $10^5$ $M^{-1}$ $s^{-1}$ for $k_{cat}$, $K_m$ and $k_{cat}/K_m$ respectively (*21*).

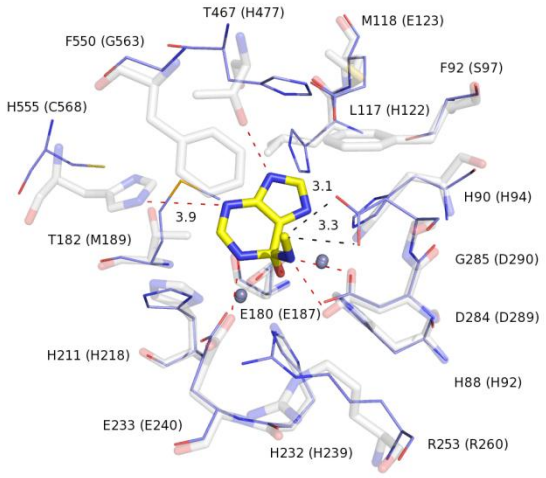


**Figure 5.5:** *Model of transition state into active site of Bh0637.*

The predicted binding pose of the high energy intermediate for the deamination of *N*-6-methyladenine in the modeled binding site of Bh0637 (transparent stick representation) superposed on the apo-crystal structure of Atu4426 (solid stick representation). Polar interactions between *N*-6-methyladenine and Bh0637 model are shown by red dashed lines. The residue numbering for Bh0637 is indicated, with the numbers for the corresponding residues in Atu4426 given in parentheses.

*Strategy for Functional Annotation*. It has been estimated that nearly one third of the currently sequenced genes have an unknown, uncertain, or incorrect functional annotation (*2*). We have demonstrated that Bh0637 and Bsu06560 catalyze the deamination of *N*-6-methyladenine. Based on the conservation of residues, we further conclude that the rest of the enzymes in group 2 of **Figure 5.1** will also catalyze the same enzymatic reaction; they are listed in the **table 5.1**. The key pieces of information that led to the successful experimental annotation of these proteins included the following: recognition of adenine deaminase as the closest functional homologue, localization of the gene for this enzyme near the operon for purine synthesis, and identification of specific residues within the substrate binding site that could accommodate larger substituents attached to the N6 nitrogen. These hints enabled a relatively modest compound library to be experimentally validated. The construction of a homology model and the successful docking of *N*-6-methyl adenine in the active site provided the rationale for the preferential deamination of this compound relative to the much poorer substrate, adenine.

# CHAPTER VI

# INTERMEDIATES IN THE TRANSFORMATION OF PHOSPHONATES TO PHOSPHATE BY BACTERIA*

The reaction mechanism for the enzymatic conversion of methyl phosphonate to phosphate and methane in *Escherichia coli* has eluded researchers over the last three decades despite significant genetic and *in-vivo* studies. The *phn* operon governs the C-P lyase activity in *E. coli.* The essential genes within the *phn* operon are *phnGHIJKLM*. The proteins encoded by *phnGHM* were over-expressed in *E. coli* and purified to homogeneity using standard protocols. The proteins encoded by *phnIJKL* were soluble only when expressed as N-terminal fusion proteins with glutathione S-transferase (GST). PhnI catalyzes the formation of α-D-ribose-1-methylphosphonate-5-triphosphate (RPnTP) from MgATP and methylphosphonate in the presence of PhnG, PhnH, and PhnL after *in situ* cleavage of the GST-tags. PhnI alone catalyzes the hydrolytic cleavage of MgATP to adenine and D-ribose-5-triphosphate. PhnM catalyzes the hydrolysis of α-D-ribose-1-methylphosphonate-5-triphosphate to α-D-ribose-1-methylphosphonate-5-phosphate (RPnP) and pyrophosphate with attack of water on the α-phosphoryl group of the triphosphate moiety of RPnTP.

---

PhnJ was reconstituted with an iron-sulfur cluster via the anaerobic addition of $FeSO_4$, $Na_2S$ and $Na_2S_2O_4$ under strictly anaerobic conditions. The $[Fe_4S_4]$-reconstituted PhnJ GST-fusion protein catalyzes the radical cleavage of the phosphorus-carbon bond of α-D-ribose-1-methylphosphonate-5-phosphate to α-D-ribose-1,2-cyclic-phosphate-5-phosphate and methane in the presence of *S*-adenosyl-L-methionine under strictly anaerobic conditions, upon *in situ* cleavage of the GST-tag.

INTRODUCTION

Carbon, nitrogen, oxygen, and phosphorus are essential elements required by all living organisms for survival. Of these elements, phosphorus is incorporated as a derivative of phosphate where it is an integral component of nucleic acids, carbohydrates, and phospholipids. Phosphorus has many roles in metabolic pathways and cell signaling. Most organisms have evolved to obtain phosphorus, as phosphate, directly from the environment. However, many gram-negative bacteria, such as *Escherichia coli*, have the capability of utilizing organophosphonates as a nutritional source of phosphorus under conditions of phosphate starvation via the cryptic C-P lyase activity (*32, 33*). Phosphonates are organophosphorus compounds that contain a one C-P bond. This bond is chemically inert and hydrolytically stable. Phosphonates are ubiquitous and include antibiotics (fosfomycin and phosphonothrixin), herbicides (glyphosate) and industrial detergent additives (amino-trimethylene phosphonate). It is estimated that more than 20,000 tons of phosphonates are released annually in the US alone from herbicide and detergent wastes (*27, 28*). The large quantities of

phosphonates that are being deposited into the environment suggest that there needs to be a greater understanding of how these compounds are metabolized and degraded.

In *E. coli* the catalytic machinery for the "C-P lyase" activity has been localized to the *phn* gene cluster, which is induced only under conditions of limiting phosphate by the global *pho* regulation system. This operon consists of 14 genes denoted as *phnCDEFGHIJKLMNOP*. Genetic and biochemical experiments have demonstrated that the *phnGHIJKLM* genes encode proteins that are essential for the enzymatic conversion of phosphonates to phosphate. The genes *phnCDEF* encode proteins responsible for the binding and/or transport of phosphonates across cell membranes as well as regulation and modulation of the C-P lyase activity. The genes *phnNOP* encode proteins that have auxiliary functions and these three proteins have been functionally characterized (*27-28, 32-33, 100*). Wanner, Hove-Jensen and co-workers have shown that PhnN catalyzes the ATP-dependent phosphorylation of α-D-ribose-1,5-bisphosphate (PRbP) to α-D-ribose-1-pyrophosphate-5-phosphate (PRPP) (*101*). Blanchard and co-workers have shown that PhnO catalyzes the metal-dependent acetylation of aminoalkylphosphonic acids with acetyl CoA as the co-substrate (*102*). Zechel, Hove-Jensen and co-workers have shown that PhnP catalyzes the metal-dependent hydrolysis of α-D-ribose-1,2-cyclic phosphate-5-phosphate (PRcP) to PRbP (*103*). These reactions are summarized in **Scheme 6.1**. At the start of our investigation there were no functional annotations for any of the seven proteins considered essential for C-P bond cleavage despite three decades of research on this pathway. The primary difficulty in elucidating the reactions catalyzed by these enzymes has been the extremely poor solubility of the

essential proteins when removed from the cellular environment. The protein encoded by *phnH* was the only protein to have been reported as soluble. This protein has been crystallized and the three-dimensional structure (PDB id: 3fsu) has been solved (*104*).

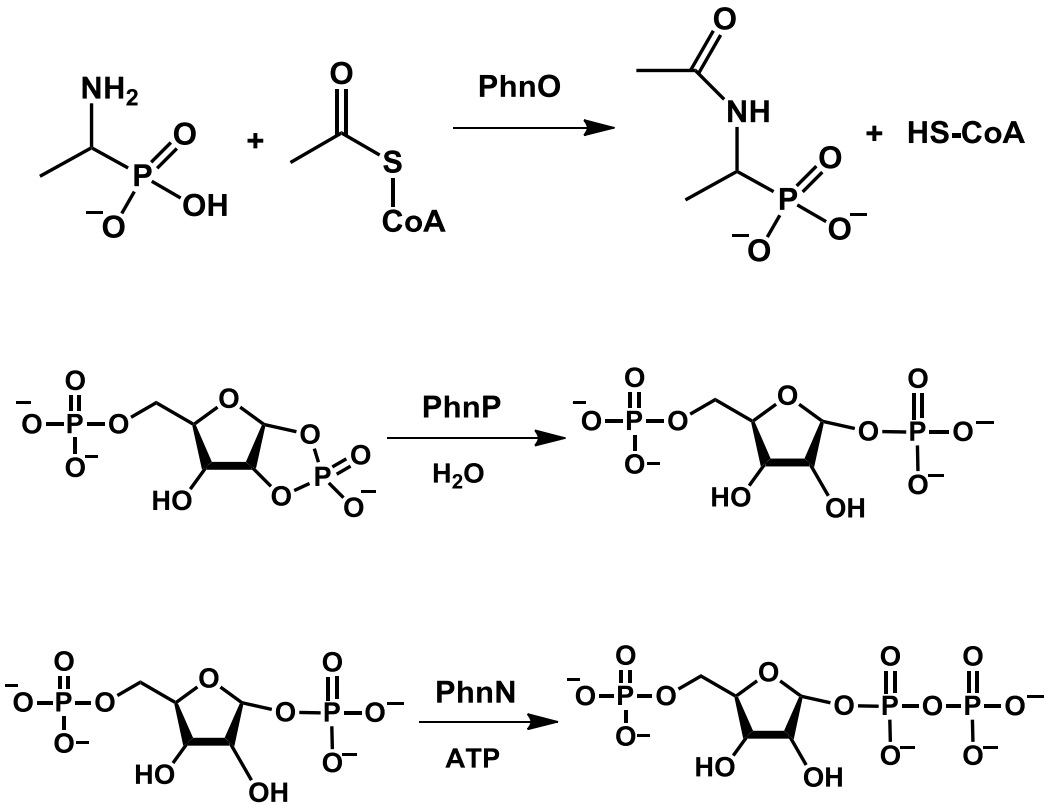


**Scheme 6.1:** Reactions catalyzed by PhnO, PhnP and PhnN.

In *E. coli* methyl phosphonate is converted to phosphate and methane as shown in **Scheme 6.2** via the C-P lyase pathway. This transformation is the equivalent to the addition of water during the cleavage of the carbon-phosphorus bond, but an enzymatic mechanism for the conversion of unactivated phosphonates to phosphate is unknown.

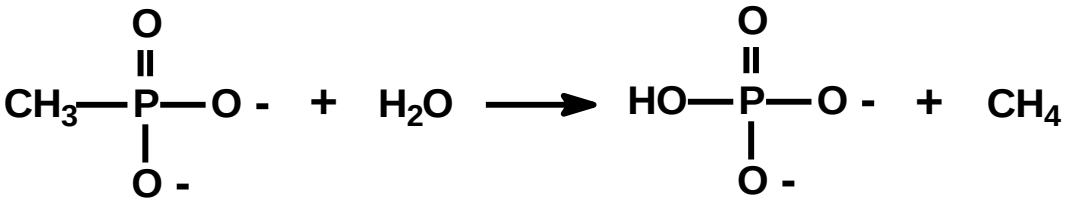

**Scheme 6.2:** Conversion of methyl phosphonate to phosphate and methane by the C-P lyase reaction.

Despite computational and ligand binding studies, no clues were available that would have provided hints of the catalytic role of PhnH in the C-P lyase pathway. PhnM was predicted to be a hydrophobic protein and this has led to the speculation that the *phnGHIJKLM* gene products form a membrane-associated enzyme complex that functions collectively to catalyze C-P bond cleavage. Zechel, Hove-Jensen and co-workers recently purified the gene products from the expression of the genes *phnGHIJK* as a soluble multi-protein complex (*32, 105*). Walsh, Floss and co-workers have shown that C-P bond cleavage occurs with racemization of stereochemistry at the carbon center. This result suggests that the bond cleavage reaction proceeds via a radical-based mechanism (*106*) (**Scheme 6.3**). Frost and co-workers isolated α-D-ribose-1-ethylphosphonate from the extracellular medium after providing ethylphosphonate to *E. coli* as the sole phosphorus source (*107, 108*). This transformation is illustrated in **Scheme 6.4**. Based on the functional annotations to the auxillary proteins (PhnNOP), and the previous literature available on the C-P lyase complex in *E. coli*, there were three conclusions that could be drawn at the start of this investigation: (a) there is a ribose donor/intermediate involved in the pathway for the metabolism of phosphonates (b) the

chemistry on this pathway is initiated at the C-1 position of the ribose moiety and (c) the C-P bond breaks via a radical mechanism. Sequence analysis of PhnI indicated a weak similarity to purine and pyrimidine nucleosidases at very relaxed expectation values when BLASTED using the NCBI protein database. PhnJ has four conserved cysteine residues at the C-terminal end of the protein with a highly conserved spacing between the four cysteine residues. The conserved cluster of cysteine residues is suggestive of a metal binding site and a high probability of an iron-sulfur cluster (*109*). PhnM is a member of the amidohydrolase superfamily (AHS) and is found within COG3454 of the Cluster of Orthologous Groups (COG) of proteins. Enzymes within this superfamily of proteins catalyze hydrolysis reactions at carbon and phosphorus centers using a mono- or binuclear metal center (*7*). PhnK and PhnL were predicted to be ATP-binding proteins of unknown function and perhaps function as permeases (*110*).

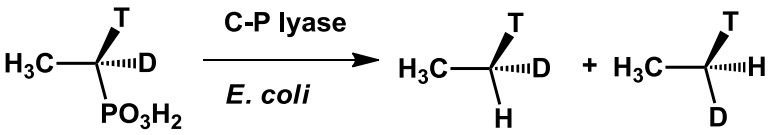


**Scheme 6.3:** Racemization of the stereochemistry at the carbon center by the CP lyase reaction.

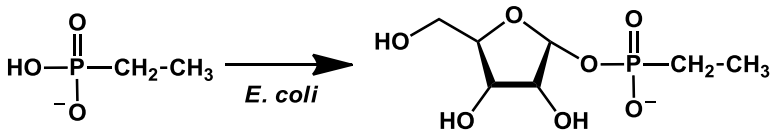


**Scheme 6.4:** Formation of α-D-ribose-1-ethylphosphonate in *E. coli* from ethylphosphonate.

Therefore, the preliminary bioinformatic and sequence analysis yielded hints for three probable reactions for the metabolism of organophosphonates: (a) a nucleosidase-type reaction catalyzed by PhnI – presumably involving the synthesis of aphosphonate-ribose adduct; (b) a hydrolytic reaction catalyzed by PhnM; and (c) a radical-based reaction for the cleavage of the C-P bond catalyzed by PhnJ that would require an iron-sulfur cluster (*99*).

MATERIALS AND METHODS

*Materials.* All chemicals were purchased from Sigma-Aldrich unless otherwise stated. The genomic DNA for *E. coli str.* K12 substr. MG1655 was purified from XL1-blue competent cells (Strategene, Agilent). *E. coli* BL21 (DE3), XL1-blue competent cells and *Pfu Turbo* polymerase were purchased from Stratagene (Agilent). The expression vectors, pET28b(+), pET30a(+) and pET42a(+) were purchased from Novagen (EMD chemicals). pET42a(+) vector contains a GST-tag for enhancing protein solubility and ease of purification. *Pfx Platinum* was purchased from Invitrogen. Green Go *Taq* was purchased from Promega. All oligonucleotides were purchased from the Integrated DNA Technologies (IDT) from the Gene Technology Lab at Texas A&M University (GTL-TAMU).

*Cloning of phnG from Escherichia coli K12 MG1655.* The DNA sequence for *phnG* from *E. coli K12 MG1655* was cloned (gi|16131927). The gene for *phnG* was amplified utilizing the primer pair 5'-AAAAAAGGATCCATGCACGCAGATACCGCGACCCGCCAGCA-3' and 5'-AGAAGAAAGCTTTCATGCGTTGTCTCCGCGAACCATCGTAAAGAAGTCCGA-

3' using *Pfu Turbo* as described by manufacturer. *BamHI* and *HindIII* restriction sites were introduced into the forward and the reverse primers, respectively. The PCR product was purified with a PCR cleanup system (Qiagen), digested with *BamHI* and *HindIII*, and ligated into a pET30a(+) vector which was previously digested with *BamHI* and *HindIII*. *phnG* was cloned into pET30a(+) and pET42a(+) vectors.

*Protein Expression and Purification of PhnG.* Preliminary solubility experiments indicated PhnG was soluble with an N-terminal poly-histidine tag (pET30a(+) vector) and hence this clone was used for the remaining studies with PhnG. The recombinant plasmid bearing the gene for *phnG* was transformed into *E. coli* BL21 (DE3) competent cells by electroporation. A single colony was grown overnight at 37 $^{o}$C in 5 mL of LB medium containing 50 μg/mL kanamycin. Five mL aliquots were used to inoculate 3 L of the same medium. The cell cultures were grown at 37 $^{o}$C until the $A_{600}$ reached ~ 0.3 - 0.4. The temperature was reduced to 18 $^{o}$C and the culture was induced with 0.5 mM isopropyl-β-thiogalactoside (IPTG) when the $A_{600}$ reached ~ 0.6. The cells were harvested by centrifugation 18 - 21 hours after induction. The cells were resuspended in 50 mM HEPES, 150 mM NaCl and 20 mM imidazole at pH 8.5 (binding buffer), containing 0.1 mg/mL PMSF and lysed by sonication. The soluble proteins were separated from the cell debris by centrifugation at 12000 x g for 15 minutes at 4 $^{o}$C. The nucleic acids were removed by dropwise addition of 2% w/v protamine sulfate dissolved in the binding buffer. After centrifugation, the supernatant solution was applied to a HisTrap column (GE Healthcare 5 mL) previously equilibrated with the binding buffer. The protein was eluted by applying a gradient of 50 mM HEPES, 150

mM NaCl and 1 M imidazole at pH 8.5 (Elution buffer). The fractions were analyzed for purity by SDS-PAGE. The appropriate fractions were pooled and dialyzed at 4 $^{o}$C with 50 mM HEPES, 150 mM NaCl at pH 8.5. The protein was concentrated using a 10 kDa ultra-filtration membrane (Amicon) by centrifugation. Typical yields for PhnG were 15 – 20 mg PhnG / L of LB media (~ 4 gm of cells/L of LB media).

*Cloning* of *phnH from Escherichia coli K12 MG1655.* The DNA sequence for *phnH* from *E. coli K12 MG1655* was cloned (gi|16131926). The gene for *phnH* was amplified utilizing the primer pair 5'-AAAGAGAATCATATGACCCTGGAAACCGCTTTTATGCTTCCCGTG-3' and 5'-AGAAGAAAGCTTTCAGCACACCTCCACATGAGTGGTTCGCGG-3' using *Pfx Platinum*. *NdeI* and *HindIII* restriction sites were introduced into the forward and the reverse primers, respectively. The PCR product was purified with a PCR cleanup system (Promega), digested with *Nde*I and *HindIII*, and ligated into a pET28b(+) vector which was previously digested with *NdeI* and *HindIII*.

*Expression and Purification of PhnH.* The recombinant plasmid bearing the gene for *phnH* was transformed into *E. coli* BL21 (DE3) competent cells by electroporation. A single colony was grown overnight at 37 $^{o}$C in 5 mL of LB medium containing 50 µg/mL kanamycin. Five mL aliquots were used to inoculate 2 L of the same medium. The cell cultures were grown at 37 $^{o}$C until the $A_{600}$ reached ~ 0.3 - 0.4. The temperature was reduced to 18 $^{o}$C and induced with 0.5 mM IPTG when the $A_{600}$ reached ~ 0.6. The cells were harvested by centrifugation 18 - 21 hours after induction. The cells were resuspended in 50 mM HEPES and 20 mM imidazole at pH 8.0 (binding

buffer), containing 0.1 mg/mL PMSF and lysed by sonication. The soluble proteins were separated from the cell debris by centrifugation at 12000 x g for 15 minutes at 4 $^{o}$C. Nucleic acids were removed by dropwise addition of 2% w/v protamine sulfate. After centrifugation, the supernatant solution was applied to a HisTrap column (GE Healthcare 5 mL) previously equilibrated with the binding buffer. The protein was eluted by applying a gradient of 50 mM HEPES and 1 M imidazole at pH 8.0 (elution buffer). The fractions were analyzed for purity by SDS-PAGE. The fractions were pooled and dialyzed at 4 $^{o}$C into 50 mM HEPES at pH 8.0. The protein was concentrated using a 30 kDa ultra-filtration membrane (Amicon) by centrifugation. Typical yields for PhnH obtained were 150 – 160 mg PhnH / L of LB media (~ 4 gm of cells/L of LB media).

*Cloning* of *phnI from Escherichia coli K12 MG1655.* The DNA sequence for *phnI* from *E. coli K12 MG1655* was cloned (gi|16131925). The gene for *phnI* was amplified utilizing the primer pair 5'-AAAAAAGGATCCATGTACGTTGCCGTGAAAGGGGGCGAGAAG-3' and 5'-AGAAGAAAGCTTTTAGCCATGGTTCTGCTCCTGTTGCAGACGTTTGAG-3' using *Pfu Turbo*. *BamHI* and *HindIII* restriction sites were introduced into the forward and the reverse primers, respectively. The PCR product was purified with a PCR cleanup system (Qiagen), digested with *BamHI* and *HindIII*, and ligated into a pET28b(+) and pET42a(+) vector which was previously digested with *BamHI* and *HindIII*.

*Protein Expression and Purification of PhnI.* Preliminary studies indicated PhnI was insoluble under all conditions expect when expressed as an N-terminal GST-fusion

protein. The recombinant plasmid (pET42a(+)) bearing the gene for *phnI* was transformed into *E. coli* BL21 (DE3) competent cells by electroporation. A single colony was grown overnight at 37 $^{o}$C in 5 mL of LB medium containing 50 µg/mL kanamycin. Five mL aliquots were used to inoculate 6 L of the same medium. The cell cultures were grown at 37 $^{o}$C the $A_{600}$ reached ~ 0.3 - 0.4. The temperature was reduced to 18 $^{o}$C and induced with 0.5 mM IPTG when the $A_{600}$ reached ~ 0.6. The cells were harvested by centrifugation 18 - 21 hours after induction. The cells were resuspended in 100 mM HEPES, 0.5 M NaCl, 10% glycerol (v/v), 1 mM dithiothreitol (DTT) and 1 mM EDTA at pH 8.8 (binding buffer), containing 0.1 mg/mL PMSF,1 µL of protease inhibitor cocktail (Sigma P8340)/mL and 0.4 mg deoxyribonuclease I (Sigma DN25)/mL. The cells were lysed by sonication. The soluble proteins were separated from the cell debris by centrifugation at 12000 x g for 10 minutes at 4 $^{o}$C. After centrifugation, the supernatant solution was applied to a GSTrap column (GE Healthcare 5 mL) previously equilibrated with the binding buffer. The protein was eluted by applying a gradient of 100 mM HEPES, 0.5 M NaCl, 10% glycerol (v/v), 1 mM DTT, 1 mM EDTA and 10 mM reduced glutathione at pH 8.8 (elution buffer). The fractions were analyzed for purity by SDS-PAGE, pooled and concentrated using a 30 kDa ultra-filtration membrane (Amicon) by centrifugation. Typical yields for PhnI obtained were 1 – 1.5 mg PhnI / L of LB media (~ 4 gm of cells/L of LB media).

*Cloning* of *phnJ from Escherichia coli K12 MG1655.* The DNA sequence for *phnJ* from *E. coli K12 MG1655* was cloned (gi|16131924). The gene for *phnJ* was amplified utilizing the primer pair 5'-

AAAAAAGGATCCATGGCTAATCTGAGCGGCTACAACTTTGCCTAC-3' and 5'-AGAAGAAAGCTTTCATTGGTTTTTTGCCTCGCTCTGTTGGCGG-3' using *Pfu Turbo*. *BamHI* and *HindIII* restriction sites were introduced into the forward and the reverse primers, respectively. The PCR product was purified with a PCR cleanup system (Qiagen), digested with *BamHI* and *HindIII*, and ligated into a pET28b(+) and pET42a(+) vector which was previously digested with *BamHI* and *HindIII*.

*Protein Expression and Purification of PhnJ.* Preliminary studies indicated PhnJ was insoluble under all conditions expect when expressed as an N-terminal GST-fusion protein. The recombinant plasmid (pET42a(+)) bearing the gene for *phnJ* was transformed into *E. coli* BL21 (DE3) competent cells by electroporation. A single colony was grown overnight at 37 $^{o}$C in 5 mL of LB medium containing 50 µg/mL kanamycin. Five mL aliquots were used to inoculate 6 L of the same medium. The cell cultures were grown at 37 $^{o}$C the $A_{600}$ reached ~ 0.3 - 0.4. The temperature was reduced to 18 $^{o}$C and induced with 0.5 mM IPTG when the $A_{600}$ reached ~ 0.6. The cells were harvested by centrifugation 18 - 20 hours after induction. The cells were resuspended in 100 mM HEPES, 0.5 M NaCl, 10% glycerol (v/v) and 1 mM EDTA at pH 8.8 (binding buffer), containing 0.1 mg/mL PMSF, 1 µL of protease inhibitor cocktail (Sigma P8340)/mL and 0.4 mg deoxyribonuclease I (Sigma DN25)/mL. The cells were lysed by sonication. The soluble proteins were separated from the cell debris by centrifugation at 12000 x g for 10 minutes at 4 $^{o}$C. After centrifugation, the supernatant solution was applied to a GSTrap column (GE Healthcare 5 mL) previously equilibrated with the binding buffer. The protein was eluted by applying a gradient of 100 mM HEPES, 0.5

M NaCl, 10% glycerol (v/v), 1 mM EDTA and 10 mM reduced glutathione at pH 8.8 (elution buffer). The fractions were analyzed for purity by SDS-PAGE. The fractions were pooled and concentrated using a 30 kDa ultra-filtration membrane (Amicon) by centrifugation. Typical yields for PhnJ obtained were 2 – 2.5 mg PhnJ / L of LB media (~ 4 gm of cells/L of LB media).

*Chemical Reconstitution of PhnJ.* EDTA was added to the purification buffers to remove all adventitious Fe bound to PhnJ. PhnJ eluted from the GSTrap column (6 – 8 mg from 12 gm cells from 3 L LB media) was introduced into an anaerobic chamber (MBraun Lab Master SP glovebox , Barondeau Laboratory, Texas A&M University). Argon was bubbled through the PhnJ solution for an hour to remove most of the oxygen from the solution. The PhnJ solution was concentrated using a 30 kDa ultra-filtration membrane (VWR chemicals) to 100 – 150 μM depending on the protein yield. To this concentrated PhnJ solution, 5 mM ferrous sulfate was added dropwise over an hour (50 fold excess). The mixture of PhnJ and $Fe^{2+}$ was allowed to react for 3 hours. 5 mM sodium sulfide was added to the mixture of PhnJ and $Fe^{2+}$ dropwise over an hour (50 fold excess). The mixture was allowed to react for another 3 hours. The insoluble ferrous sulfide was removed from the protein reconstituted with the [4Fe-4S]-cluster by centrifugation. The unreacted iron and sulfide was further separated from the protein by ultra-filtration using a 30 kDa membrane (VWR chemicals). 1 mM sodium dithionite was added to the resulting protein to reduce the [4Fe-4S]-cluster to the active $[4Fe\text{-}4S]^{+}$ form from the $[4Fe\text{-}4S]^{2+}$ form. PhnJ was further concentrated to 150 – 200 μM (600 – 800 μL) using a 30 kDa ultra-filtration, to separate any residual sodium dithionite. The

chemical reconstitution of the [4Fe-4S]-cluster of PhnJ was possible without interference from the N-terminal GST-fusion solubility tag.

*Cloning of phnK from Escherichia coli K12.* The DNA sequence for *phnK* from *E. coli K12* was cloned (gi|16131923). The gene for *phnK* was amplified utilizing the primer pair 5'-AAAAAAGGATCCATGAATCAACCGTTACTTTCGGTCAATAACCTGACCACCTTTACGCG-3' and 5'-AGAAGAAAGCTTTCAATTCTGCAAAACCGATGACACCAGCAGCTGTGTATACGGA-3' using *Pfu Turbo*. *BamHI* and *HindIII* restriction sites were introduced into the forward and the reverse primers, respectively. The PCR product was purified with a PCR cleanup system (Qiagen), digested with *BamHI* and *HindIII*, and ligated into a pET30a(+) and pET42a(+) vector which was previously digested with *BamHI* and *HindIII*.

*Protein Expression and Purification of PhnK.* Preliminary studies indicated PhnK was insoluble under all conditions expect when expressed as an N-terminal GST-fusion protein. The recombinant plasmid (pET42a(+)) bearing the gene for *phnK* was transformed into *E. coli* BL21 (DE3) competent cells by electroporation. A single colony was grown overnight at 37 $^{o}$C in 5 mL of LB medium containing 50 μg/mL kanamycin. Five mL aliquots were used to inoculate 6 L of the same medium. The cell cultures were grown at 37 $^{o}$C until the $A_{600}$ reached ~ 0.3 - 0.4. The temperature was reduced to 18 $^{o}$C and induced with 0.5 mM IPTG when the $A_{600}$ reached ~ 0.6. The cells were harvested by centrifugation 18 - 21 hours after induction. The cells were

resuspended in 100 mM HEPES, 0.5 M NaCl, 10% glycerol (v/v) and 1 mM DTT at pH 8.8 (binding buffer), containing 0.1 mg/mL PMSF and 0.4 mg deoxyribonuclease I (Sigma DN25)/mL. The cells were lysed by sonication. The soluble proteins were separated from the cell debris by centrifugation at 12000 x g for 10 minutes at 4 $^{o}$C. After centrifugation, the supernatant solution was applied to a GSTrap column (GE Healthcare 5 mL) previously equilibrated with the binding buffer. The protein was eluted by applying a gradient of 100 mM HEPES, 0.5 M NaCl, 10% glycerol (v/v), 1 mM DTT and 10 mM reduced glutathione at pH 8.8 (elution buffer). The fractions were analyzed for purity by SDS-PAGE gels. The pure fractions (< 2 % impurities) were pooled and concentrated using a 30 kDa ultra-filtration membrane (Amicon) by centrifugation. Typical yields for PhnK obtained were 1 – 1.5 mg PhnK / L of LB media (~ 4 gm of cells/L of LB media).

*Cloning of phnL from Escherichia coli K12.* The DNA sequence for *phnL* from *E. coli K12* was cloned (gi|16131922). The gene for *phnL* was amplified utilizing the primer pair 5'-AAAAAAGGATCCATGATTAACGTACAAAACGTCAGTAAAACCTTCATCCTGCACCAGCAA-3' and 5'-AGAAGAAAGCTTTCATGAAGAGGCTCCCATTGGGTGCAGGCGGT-3' using *Pfu Turbo*. *BamHI* and *HindIII* restriction sites were introduced into the forward and the reverse primers, respectively. The PCR product was purified with a PCR cleanup system (Qiagen), digested with *BamHI* and *HindIII*, and ligated into a pET30a(+) and pET42a(+) vector which was previously digested with *BamHI* and *HindIII*.

*Protein Expression and Purification of PhnL.* The recombinant plasmid (pET42a(+)) bearing the gene for *phnL* was transformed into *E. coli* BL21 (DE3) competent cells by electroporation. A single colony was grown overnight at 37 $^{o}$C in 5 mL of LB medium containing 50 μg/mL kanamycin. Five mL aliquots were used to inoculate 6 L of the same medium. The cell cultures were grown at 37 $^{o}$C the $A_{600}$ reached ~ 0.3 - 0.4. The temperature was reduced to 18 $^{o}$C and induced with 0.5 mM IPTG when the $A_{600}$ reached ~ 0.6. The cells were harvested by centrifugation 18 - 20 hours after induction. The cells were resuspended in 100 mM HEPES, 0.5 M NaCl, 10% glycerol (v/v) and 1 mM DTT at pH 8.5 (Binding buffer), containing 0.1 mg/mL phenylmethylsulfonyl fluoride and 0.4 mg deoxyribonuclease I (Sigma DN25)/mL. The cells were lysed by sonication. The soluble proteins were separated from the cell debris by centrifugation at 12000 x g for 10 minutes at 4 $^{o}$C. After centrifugation, the supernatant solution was applied to a GSTrap column (GE Healthcare 5 mL) previously equilibrated with the binding buffer. The protein was eluted by applying a gradient of 100 mM HEPES, 0.5 M NaCl, 10% glycerol (v/v), 1 mM DTT and 10 mM reduced glutathione at pH 8.5 (elution buffer). The fractions were analyzed for purity by SDS-PAGE gels. The fractions were pooled and concentrated using a 30 kDa ultra-filtration membrane (Amicon) by centrifugation. Typical yields for PhnL obtained were 8 – 10 mg PhnL / L of LB media (~ 4 gm of cells/L of LB media).

*Cloning of phnM from Escherichia coli K12.* The DNA sequence for *phnM* from *E. coli K12* was cloned (gi|16131921). The gene for *phnM* was amplified utilizing the primer pair 5'-GGGACTTCCATATGATTATCAATAACGTTAAGCTGGTGCTGG-3'

and 5'-CCGGAATTCTCAGAACACCCTTTTACCCTGACG-3' using *Pfx Platinum*. *NdeI* and *EcoRI* restriction sites were introduced into the forward and the reverse primers, respectively. The PCR product was purified with a PCR cleanup system (*Promega*), digested with *NdeI* and *EcoRI*, and ligated into a pET30a(+) vector which was previously digested with *NdeI* and *EcoRI*.

*Protein Expression and Purification of PhnM.* Preliminary studies indicated PhnM was insoluble under all conditions expect when the pH of the buffer exceeded 8.8. The recombinant plasmid bearing the gene for *phnM* was transformed into *E. coli* BL21 (DE3) competent cells by electroporation. A single colony was grown overnight at 37 $^{o}$C in 5 mL of LB medium containing 50 μg/mL kanamycin. Five mL aliquots were used to inoculate 6 L of the same medium. The cell cultures were grown at 37 $^{o}$C the $A_{600}$ reached ~ 0.3 - 0.4. The temperature was reduced to 18 $^{o}$C and induced with 0.5 mM IPTG when the $A_{600}$ reached ~ 0.6 in the presence of 1.0 mM $ZnCl_2$. The cells were harvested by centrifugation 18 - 20 hours after induction. Protein expression was confirmed by SDS-PAGE. The cells were centrifuged and then resuspended in 100 mM HEPES, 1 mM $ZnCl_2$ at pH 8.8 (purification buffer), containing 0.1 mg/mL PMSF and lysed by sonication. The soluble proteins were separated from the cell debris by centrifugation at 12,000 x g for 15 minutes at 4 $^{o}$C. The nucleic acids were removed by dropwise addition of 2% w/v protamine sulfate. After centrifugation, solid ammonium sulfate was added to 60% saturation to the supernatant solution. The precipitated protein was dissolved in purification buffer and then applied to a High Load 26/60 Superdex 200 prep grade gel filtration column (GE Healthcare), which was previously

equilibrated with the purification buffer. The fractions were pooled and loaded onto a ResourceQ column 6 mL (GE Healthcare) and eluted with a gradient of NaCl (0 – 1M) in 50 mM HEPES, pH 8.8. The fractions were pooled and exchanged into 100 mM HEPES, 1 mM $ZnCl_2$ at pH 8.8. Typical yields for PhnM were 4 - 5 mg / L of LB media (~ 4 gm of cells/L of LB media).

*Nucleosidase Reaction.* To establish the substrate profile for PhnI, a library of nucleosides and nucleotides was initially developed. The compounds were incubated with 10 μM PhnI in 100 mM HEPES buffer containing 250 mM NaCl and 10 % v/v glycerol at pH 8.5 for 6 hours. At the end of 6 hours, coupling enzymes capable of deaminating the free base released from the respective substrates were added and the UV-vis spectrum was observed from 240 – 350 nm using a SpectraMax-340 UV-vis spectrometer in a 1.0 mL quartz cuvette. For inosine containing compounds 50 units of xanthine oxidase (Sigma) was added and the spectrum was collected.

After initial spectroscopic screening, 10 μM PhnI was incubated with 2 mM adenine and guanine nucleoside di- and tri-phosphates overnight in the presence of 3 mM $Mg^{2+}$ in 100 mM HEPES buffer containing 250 mM NaCl and 10 % v/v glycerol at pH 8.5 at 30 $^{o}$C. The reactions with ATP and GTP were analyzed by HPLC. 0.25 mL of the reaction mixture was loaded onto a ResourceQ column 1 mL (GE Healthcare) pre-equilibrated with 25 mM HEPES pH 8.0. The reaction mixture was eluted with a 0-1 M NaCl gradient over 10 column volumes using an AKTA 10 Basic FPLC system. The ResourceQ column was caliberated with adenine and ATP or guanine and GTP standards prior to loading the reaction to determine the reaction products. In order to

establish the products of the enzyme mixture the same reaction was carried out using 10 μM PhnI, 20 μM PhnL, 40 μM PhnG and 40 μM PhnH for 5 mM ATP or GTP in the presence of 7 mM $Mg^{2+}$ under the same conditions.

*Nucleosidase Kinetics.* All kinetic assays were carried out in 50 mM HEPES buffer pH 8.5 at 30 $^{o}$C in the presence of 1.0 mM $Mg^{2+}$ using a SpectraMax-340 UV-vis spectrometer using a 96 well quartz plate. The nucleosidase activity of PhnI with ATP and ADP were measured by coupling the nucleosidase activity to the deamination of the released free base with adenine deaminase (ADE) from *E. coli* (*20*). In the assay, the ATP concentrations were varied from 0 – 300 μM and ADP concentrations were varied from 0 – 350 μM. In the assay, the final PhnI concentration was 0.5 μM for kinetic assays with ATP and 1.0 μM for kinetic assays with ADP. The final ADE concentration in the assay was 10.0 μM. To test the kinetics of PhnI in the presence of PhnG, PhnH and PhnL with Factor Xa the following concentrations were used: PhnI = 0.1 μM, PhnG = 0.4 μM, PhnH = 0.4 μM, PhnL = 0.2 μM and Factor Xa = 10 units. In this kinetic assay the methylphosphonate and $Mg^{2+}$ concentrations were constant at 1 and 2 mM respectively. All the kinetics of the ADE coupled assays were measured at 260 nm using a differential extinction coefficient of 4100 $M^{-1}cm^{-1}$ for the decrease in adenine concentration forming hypoxanthine.

The nucleosidase activity of PhnI with GTP and GDP was measured by coupling the nucleosidase activity to the deamination of the released free base guanine by guanine deaminase (guaD) from *E. coli* (*111*). In the assay, GTP concentrations were varied from 0 – 300 μM and GDP concentrations were varied from 0 – 300 μM. In the assay,

the final PhnI concentration was 0.1 μM for kinetic assays with GTP and 0.5 μM for kinetic assays with GDP. The final guaD concentration in the assay was 15.0 μM. To test the kinetics of PhnI in the presence of PhnG, PhnH and PhnL in the presence of Factor Xa the following concentrations were used: PhnI = 0.1 μM, PhnG = 0.4 μM, PhnH = 0.4 μM, PhnL = 0.2 μM and Factor Xa = 10 units. In this kinetic assay the methylphosphonate and $Mg^{2+}$ concentrations were constant at 1 and 2 mM respectively. All of the guaD coupled assays were measured at 253 nm using a differential extinction coefficient of 3920 $M^{-1}cm^{-1}$ for the decrease in guanine concentration forming xanthine (*112*).

The nucleosidase activity of PhnI with ITP and IDP was measured by coupling the nucleosidase activity to the oxidation of the released free base hypoxanthine to uric acid by xanthine oxidase from bovine milk (Sigma). In the assay, ITP concentrations were varied from 0 – 300 μM and IDP concentrations were varied from 0 – 300 μM. In the assay, the final PhnI concentration was 0.5 μM for kinetic assays with ITP and 1.2 μM for kinetic assays with IDP. The final xanthine oxidase was 50 units per assay as described in Sigma catalog. All the kinetics of the xanthine oxidase coupled assays were measured at 293 nm using an extinction coefficient of 12600 $M^{-1}cm^{-1}$ for the increase in uric acid concentration (*113*).

*Purification of D-ribose-5-triphosphate (RTP) and α-D-ribose-1-methylphosphonate-5-triphosphate (RPnTP).* The ResourceQ column (GE Healthcare) was pre-calibrated for the elution profiles of adenine, AMP, ADP and ATP to determine the volumes of elution of each. Baseline separations were obtained for adenine, AMP,

ADP and ATP. The binding buffer for these separations included ammonium bicarbonate (100 mM) pH 8.5 and the elution buffer was 1 M ammonium bicarbonate pH 8.5. The gradient was run over 10 column volumes. Since both D-ribose-5-triphosphate (RTP) and α-D-ribose-1-methylphosphonate-5-triphosphate (RPnTP) do not have any chromophore to check absorbance, these elution volumes were used as standards to collect fractions.

The enzymatic synthesis of D-ribose-5-triphosphate (RTP) was carried out by incubating 15 μM PhnI with 5 mM ATP and 7 mM $Mg^{2+}$ to a total volume of 1.0 mL for 5 hours in 50 mM HEPES buffer containing 250 mM NaCl and 10 % v/v glycerol at pH 8.5. 0.5 mL of the reaction mixture was loaded onto the ResourceQ column (two times) and the fractions corresponding to the elution volumes of ATP were collected. The solvent was evaporated using a SpeedVac Concentrator (Savant) for about 6 hours. The final yields varied from 1.5 – 2.0 mg. The resulting solid was white in color and was stored at – 20 $^{o}$C. D-ribose-5-diphosphate (RDP) was enzymatically synthesized by the reaction of PhnI with ADP. All concentrations were the same except that ADP was used in place of ATP. The purification was also the same except that the fractions eluting around ADP were collected instead of the fractions eluting around ATP from the ResourceQ column. The final yields were also the same.

The enzymatic synthesis of α-D-ribose-1-methylphosphonate-5-triphosphate (RPnTP) was carried out by incubating 10 μM PhnI, 20 μM PhnL, 40 μM PhnG, 40 μM PhnH, 50 units Factor Xa, 1X Factor Xa buffer, 5 mM methylphosphonate, 5 mM ATP and 7 mM $Mg^{2+}$ in 50 mM HEPES buffer containing 250 mM NaCl and 10 % v/v

glycerol at pH 8.5 in a total volume of 1.5 mL. 0.5 mL of the reaction mixture was loaded onto the ResourceQ column and all fractions eluting after the elution volumes of ATP were collected. The solvent was evaporated using a SpeedVac Concentrator (Savant). The final yields obtained varied from 1.8 – 2.2 mg. The resulting solid was white in color and was stored at – 20 $^{o}$C.

*PhnM Kinetics.* All PhnM assays were performed using a Pi Colorlock (Gold) phosphate detection colorimetric system from Innova Biosciences according to the manufacturer's instructions. Since all reactions were performed in 50 mM HEPES containing 5 mM $Mg^{2+}$, 1 mM $Zn^{2+}$ and 5 units of inorganic pyrophosphatase from Baker's yeast (Sigma) at pH 8.5, a calibration curve was made with this standard assay condition to account for any background phosphate in the assay. All kinetic data was fit to standard Michaelis-Menten kinetics.

PhnM was shown to cleave the phosphodiester bond of α and β- phosphoryl groups of the triphosphate moiety of the putative substrates releasing pyrophosphate for a triphosphate substrate and phosphate for a diphosphate substrate. For the kinetics with RTP, the RTP concentration in the assay was varied from 0 – 500 μM. The PhnM concentration in the assay was 10 nM . For the kinetics of RPnTP, the concentration of RPnTP was varied from 0 – 750 μM, with a fixed PhnM concentration of 10 nM. For both of these assays, end points for the kinetic assays were collected at 0, 3, 6, 9 and 12 minutes. Inorganic pyrophosphatase was added as a coupling enzyme to the assay to convert the pyrophosphate released from the substrate to phosphate to allow detection by

the Pi ColorLock (Gold) kit. For RDP, the concentration of RDP was varied from 0 – 1 mM, with the PhnM concentration being 1.0 μM in the assay.

*Purification of α-D-ribose-1-methylphosphonate-5-phosphate.* The enzymatic synthesis of α-D-ribose-1-methylphosphonate-5-phosphate was performed by incubating 5 mM RPnTP with 10 μM PhnM, 5 mM $Mg^{2+}$ and 1 mM $Zn^{2+}$ in 50 mM HEPES pH 8.5. The reaction was monitored by quantifying the phosphate produced after adding inorganic pyrophosphatase from Baker's yeast to the reaction over time in conjunction with $^{31}P$ NMR. The reaction of PhnM with RPnTP was allowed to incubate at 30 $^{o}C$ for about 5 hours for complete turnover. Zinc supplementation was essential for complete turnover of RPnTP. The reaction was filtered through a 10 kDa ultra-filtration membrane (VWR Chemicals) to remove the enzymes from the mixture. At the end of the filtration the flow through was a mixture of α-D-ribose-1-methylphosphonate-5-phosphate and pyrophosphate containing 5 mM $Mg^{2+}$ and 1 mM $Zn^{2+}$ in 50 mM HEPES pH 8.5. $^{31}P$ NMR was used to confirm the relative ratios of α-D-ribose-1-methylphosphonate-5-phosphate and pyrophosphate. The α-D-ribose-1-methylphosphonate-5-phosphate purified using this protocol was used as a substrate for all assays with PhnJ.

*Enzymatic assays with PhnJ.* All enzymatic assays with PhnJ were carried out in a glove box (MBraun Lab Master SP, Barondeau Laboratory, Texas A&M University) because of the air sensitivity of the iron-sulfur cluster of PhnJ. All buffers were degassed for oxygen and introduced into the glove box prior to any assay. All assays in the glove box were carried out at 10 – 12 $^{o}C$ with oxygen concentration less than 5 ppm. The buffer used for all assays with PhnJ was 150 mM HEPES, 500 mM NaCl, 10 % v/v

glycerol and 1X Factor Xa reaction buffer at pH 6.8. All assays contained fixed concentrations of 2 mM S-adenosyl-L-methionine (SAM) and 1 mM dithionite. The PhnJ concentrations in the assay varied from 100 – 160 μM (6.5 – 10 mg/mL). The substrate, α-D-ribose-1-methylphosphonate-5-phosphate, concentration in the assay varied from 0.5 – 3 mM depending on the nature of the assay. All the reactions were initiated by the addition of 50 units of Factor Xa. All reactions were allowed to proceed for 3 – 5 hours anaerobically. The reaction volumes were usually 1.0 mL. At the end of the reaction most of the enzyme would have precipitated due to the poor solubility after cleaving the GST-tag. The precipitated enzyme was removed by centrifugation. To the supernatant, 2 mg of activated charcoal (Sigma) was added to remove unreacted SAM and the products of SAM from the reaction for about 30 minutes. 2 mg of activated charcoal was found to be sufficient to remove any SAM and related compounds from control reactions performed earlier in the absence of PhnJ. The activated charcoal was removed by centrifugation and the supernatant was filtered through a 10 kDa ultra-filtration membrane to remove any enzyme that might have remained in solution. The reaction was transferred into a NMR tube anaerobically and the NMR tube was sealed anaerobically. All the reactions were analyzed by $^{31}$P NMR (Varian Inova 300 MHz and 500 MHz) spectroscopy to check for products with help from Dr. Howard J. Williams or Dr. Chengfu Xu.

*UV-visible spectrum of PhnJ.* The chemically reconstituted PhnJ (2 mg/mL ~ 31 μM) was transferred to a 1.0 mL anaerobic cuvette (Precision Cells Inc.) and sealed to prevent air from entering the cuvette. The UV-visible absorbance spectrum was

collected in a SpectraMax Plus 384 spectrophotometer from 260 – 700 nm. After the spectrum was collected, PhnJ was treated with 1 mM dithionite anaerobically in the glove box for 1 hour. The excess dithionite was separated from PhnJ using a PD-10 column (GE Healthcare). The PhnJ fractions were collected and concentrated using a 30 kDa ultra-filtration membrane. The reduced form of PhnJ (1.7 mg/mL ~ 27 μM) was again transferred to the 1.0 mL anaerobic cuvette and the spectrum was collected.

*Gas Chromatography and GC-MS experiments with PhnJ.* The samples for the GC and GC-MS experiments were prepared anaerobically in a glove box. For the GC experiment the concentration of the reconstituted PhnJ was 150 μM. The enzyme was premixed with 2 mM SAM, 1 mM dithionite, 1X Factor Xa buffer, 2 mM α-D-ribose-1-methylphosphonate-5-phosphate in 150 mM HEPES containing 250 mM NaCl, 10 % v/v glycerol at pH 8.5. The reaction volume was 2.3 mL. The reaction was transferred to a NMR tube in the glovebox and the NMR tube was sealed with a self-sealable rubber-cap and further sealed using parafilm to prevent any escape of the contents within the tube. The reaction was initiated by addition of 50 units of Factor Xa using a 1 ml 27G 3/8 allergy syringe (BD). The reactions were allowed to proceed for 6 hours at 12 $^{o}$C. 50 μL of the headspace (500 μL) was removed using a gas-tight Hamilton syringe and injected into the GC instrument (Hewlett Packard HP 6890 GC system with FID detector and manual injection) equipped with a 30 m X 0.32 mm I.D. SGE Solgel 1 column used in splitless injection mode, at constant 20 psig He carrier pressure, with a temperature program of 50 $^{o}$C/1 min, to 100 $^{o}$C @ 10 $^{o}$C / min. The same reaction was set up for the GC-MS experiment using a Thermo Electron Corporation DSQ quadrulpole GC-MS

instrument with Finnigan Trace GC Ultra chromatograph at 70 E.V. EI ionization. The temperature program and injection mode were the same. The column was a 30 m X 0.25 mm I.D. SGE BP1 column operated at 1 mL/min constant flow He; with the exception that the PhnJ concentration was 160 μM in a final volume of 2.5 mL. 100 μL of the headspace was injected into the GC-MS instrument. The GC and GC-MS experiments were preformed with Dr. Howard J. Williams, at the Deparment of Entomology (Texas A&M University) (GC experiments) and U.S Department of Agriculture (College Station) (GC-MS experiments).

*HPLC analysis of the products of SAM.* The HPLC analysis for determining the reaction products of SAM with PhnJ was performed on an AKTA Purifier FLPC/HPLC system with a C18 column (Cosmosil 5C18-AR-II 4.6x150 mm Nacalai, USA). All reactions were monitored at 260 nm using a linear gradient of 0 – 50 % buffer B over 10 column volumes over 35 minutes at a flow rate of 1.0 ml/min. Buffer A was 50 mM ammonium acetate pH 5.4 and buffer B was 50 % v/v methanol/water. The loading volume for all the reactions was 250 μL. The C18-column was pre-calibrated with 0.5 mM SAM, 0.5 mM 5'-deoxyadenosine (5DA) and 0.5 mM 5'-deoxy-5'-methylthioadenosine (MTA) for the elution profiles of the standards.

For the reactions involving PhnJ, the concentrations of the components were: PhnJ = 60 μM, SAM = 0.5 mM, dithionite = 1 mM, α-D-ribose-1-methylphosphonate-5-phosphate = 2 mM in 150 mM HEPES, containing 250 mM NaCl, 10 % v/v glycerol and 1X Factor-Xa reaction buffer at pH 8.5. The reaction was initiated by adding 50 units of Factor-Xa to the reaction. The total reaction volume was 1.0 mL. As controls, in one

reaction dithionite was eliminated and in another PhnJ was eliminated. All the reactions were kept anaerobic for 3 hours after which the precipitated enzyme was removed by centrifugation. The reaction was filtered through a 10 kDa ultra-filtration membrane and the flow-through was collected. 250 μL of this material was loaded onto the C18-column and the HPLC traces were collected.

*Amino acid analysis of the products of SAM.* Amino acid analysis of the reaction products from SAM in the reaction catalyzed by PhnJ was performed in the Protein Chemistry Laboratory, Texas A&M University by Dr. Jinny Johnson using the AminoQuant method. The AminoQuant analyzes the samples by pre-column derivatization of the amino acids with o-phthalaldehyde (OPA) and 9-fluoromethyl-chloroformate (FMOC). OPA reacts with primary amino acids and FMOC with secondary amino acids (proline). The derivatized amino acids are separated by reverse phase HPLC and detected by UV absorbance with a diode array detector or by fluorescence using an in-line fluorescence detector.

For the reactions involving PhnJ, the concentrations of the components were: PhnJ = 70 μM, SAM = 2.0 mM, dithionite = 1.0 mM, α-D-ribose-1-methylphosphonate-5-phosphate = 1.0 mM in 150 mM HEPES, containing 250 mM NaCl, 10 % v/v glycerol and 1X Factor Xa reaction buffer at pH 8.5. The reaction was initiated by adding 50 units of Factor Xa to the reaction. The total reaction volume was 1.0 mL. As a control PhnJ was eliminated from the reaction mixture. All the reactions were kept anaerobic for 3 hours after which the precipitated enzyme was removed by

centrifugation. The reaction was filtered through a 30 kDa ultra-filtration membrane and the flow through was collected.

*Detection of $CH_3OH$ in PhnJ Reconstitution Reaction.* Alcohol dehydrogenase (ADH) from *Saccharomyces cerevisiae* (Sigma) was used to detect and quantify the amount of methanol (if any produced) from the reaction of α-D-ribose-5-phosphate-1-methylphosphonate [PRPn] with $[4Fe\text{-}4S]^{1+}$ reconstituted PhnJ in the presence of SAM, dithionite and Factor-Xa. A standard calibration curve was generated for the change in absorbance at 340 nm using $[NAD^+]$ = 2 mM, [ADH] = 0.1 mg/mL and varying concentrations of methanol (10 – 100 μM) in 20 mM HEPES buffer pH 7.5 at 30 $^oC$. For the PhnJ reaction; [PhnJ] = 150 μM, [SAM] = 2 mM, [dithionite] = 1m M, [PRPn] = 1.5 mM, 50 units of Factor-Xa in 1X Factor-Xa buffer was used in and the enzyme was removed by ultrafiltration through 10 kDa membrane and the unreacted SAM and 5'-deoxyadenosine were removed by treatment with activated charcoal at the end of the reaction. The remaining reaction was incubated with $NAD^+$ and ADH at pH 7.5 and the changes in spectrum were measured at 340 nm for 5 hours for 30 $^oC$. The control used for this test was all the ingredients except PhnJ.

*Detection of HCHO in PhnJ Reconstitution Reaction.* The heterocyclic dye Purpald (Sigma) (*114, 115*) was used to detect and quantify the amount of formaldehyde (if any produced) from the reaction of α-D-ribose-5-phosphate-1-methylphosphonate [PRPn] with $[4Fe\text{-}4S]^{1+}$ reconstituted PhnJ in the presence of SAM, dithionite and Factor-Xa. A standard curve was generated by using 100 % formalin (37 % w/v formaldehyde) as the source of formaldehyde and purpald by measuring the change in

absorbance at 550 nm. In this experiment the purpald (10 mM) was initially allowed to react with varying formaldehyde concentrations (0 – 15 μM) for 10 minutes and the reaction was quenched with $NaIO_4$ (10 mM) after which the absorbance was measured. For the PhnJ reaction; [PhnJ] = 150 μM, [SAM] = 2 mM, [dithionite] = 1m M, [PRPn] = 1.5 mM, 50 units of Factor-Xa in 1X Factor-Xa buffer. No effort was made to separate any ingredient at the end of the reaction. A reference for this was all the ingredients except PhnJ.

*NMR Analysis.* All the NMR analysis in this study was performed by Dr. Howard J. Williams, Department of Chemistry, Texas A&M University. All products were analyzed by $^{1}H$, $^{13}C$ (natural abundance) and $^{31}P$ NMR. The samples for $^{31}P$ NMR ($D_2O$, 85% $H_3PO_4$ corresponds $\delta = 0.00$) were made in 50 mM HEPES, pH 8.5 – 8.8 in 10 % $D_2O$ and analyzed with a Varian Unity Inova 500 MHz NMR spectrometer or a Bruker Avance III 400 MHz NMR spectrometer. $^{1}H$ and $^{13}C$ NMR spectra were acquired on a Bruker Avance III 500 MHz NMR spectrometer equipped with an HCN cyroprobe.

*Data Fitting.* All kinetic data was fit to **equation 2.1** using non-linear least squares fitting program SigmaPlot 9.0.

$$\upsilon / E_t = k_{cat}[A] / (K_m + [A]) \qquad \textbf{(Equation 2.1)}$$

where $\upsilon$ is the initial velocity, [A] = substrate concentration, $E_t$ = total enzyme concentration, $k_{cat}$ = turnover number and $K_m$ = Michaelis constant.

RESULTS AND DISCUSSION

*Protein Isolation.* The genes for the seven essential proteins encoded by the *phnGHIJKLM* gene cluster were cloned, expressed in *E. coli* and the proteins purified to

homogeneity individually. The genes for PhnG, PhnK, PhnL and PhnM were amplified and individually ligated into a pET30a(+) vector. Of these proteins only PhnG and PhnM were soluble after cell lysis. PhnG was purified using a standard polyhistine-tag purification strategy and was stable in 150 mM NaCl at pH 8.5. PhnM was cloned without a polyhistidine-tag and was largely insoluble at pH values below 8.5. This protein was isolated using gel filtration and anion exchange chromatography at pH 9.0. Since PhnM is a member of the AHS, the growth cultures and purification buffers were supplemented with 1 mM $ZnCl_2$. The identity of PhnM and PhnG was validated by N-terminal amino acid analysis of the purified proteins. PhnK and PhnL were insoluble when expressed from a standard pET30a(+) vector. These genes were subsequently recloned with N-terminal glutathione S-transferase (GST) solubility tags using a pET42a(+) vector. These clones resulted in the expression of GST fused to the N-terminus of the target protein with a linker containing a Factor-Xa cleavage site. The PhnK and PhnL GST-fusion proteins were soluble and purified using a GST-affinity column (GE Healthcare). These two proteins required 1mM dithiothreitol (DTT), 500 mM NaCl and 10% glycerol, pH 8.8, for stability.

A pET28b(+) vector was used for the initial cloning of the genes for PhnH, PhnI and PhnJ. Of these proteins, only PhnH was soluble after cell lysis. This protein was purified as described previously (*104*). Since PhnI and PhnJ were insoluble, they were recloned into a pET42a(+) vector with a GST-tag using the same strategy as that for PhnK and PhnL. The purification of PhnI required 1 mM EDTA, 1 mM DTT, 500 mM NaCl and 10% glycerol at pH 8.5. PhnJ required 1 mM EDTA, 500 mM NaCl and 10%

glycerol at pH 8.8. Of the seven proteins critical for cleavage of phosphorus-carbon bonds, PhnG, PhnH and PhnM were purified without any solubility tags. PhnI, PhnJ, PhnK and PhnL were purified as N-terminal GST-fusion proteins. The GST-fusion proteins precipitated within ~15 minutes after removal of the N-terminal GST-tag by Factor-Xa. All protein purifications contained 100 mM HEPES buffer at the specified pH.

*Catalytic Function of PhnI.* Prior experiments have hinted of a ribose intermediate during the metabolism of phosphonate substrates prior to the conversion to phosphate (*103, 107-108*). Since PhnI showed a distant relationship to enzymes that are functionally annotated as nucleosidases, we incubated this protein (10 μM) with a small and focused library of nucleosides, nucleotides and other ribose bearing compounds such as $NAD^+$, NADP and ADP-ribose at concentrations of ~2 mM for up to 6 hours in the presence of 3 mM $MgCl_2$ at pH 8.5 (**Scheme 6.5**).

The liberation of the free base was determined spectrophotometrically at 240-350 nm in the presence of coupling enzymes (1 μM) that are capable of deaminating adenine (*20*), guanine (*111*) or cytosine (*8*). Xanthine oxidase (50 Units) was added to all inosine containing compounds (*113*). The only active substrates found in these preliminary screening assays were the purine nucleoside di- and tri- phosphates i.e. ATP, ADP, GTP, GDP, ITP and IDP. The best substrates for PhnI were GTP and ATP with kinetic constants for the nucleosidase activity of ~$10^4$ $M^{-1}$ $s^{-1}$ for $k_{cat}/K_m$. The products of this reaction were D-ribose-5-triphosphate (RTP) and the free base (adenine or

guanine when ATP and GTP were utilized). The reaction catalyzed by PhnI with ATP is presented in **Scheme 6.6**.

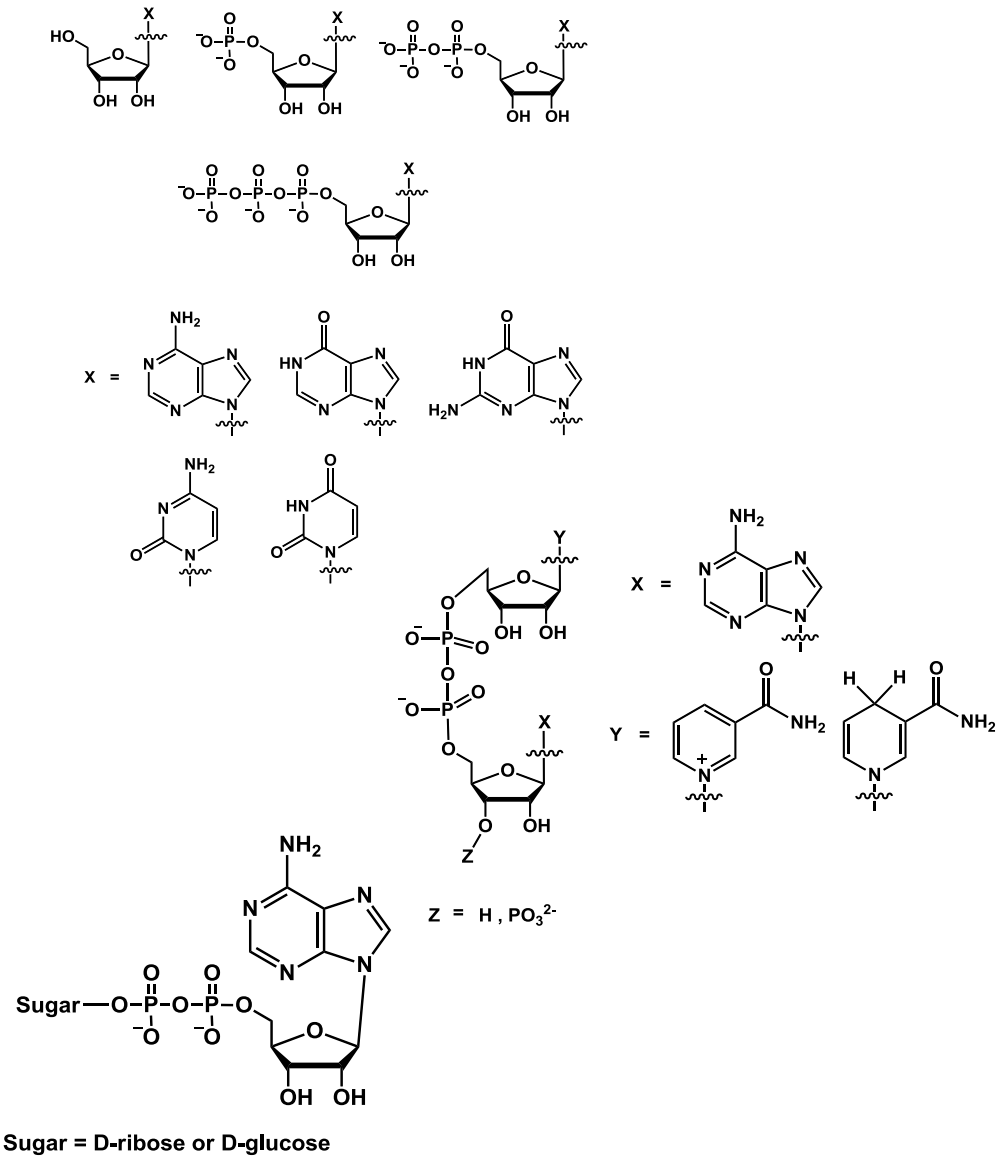


**Scheme 6.5:** Scaffolds of compounds tested against PhnI for nucleosidase activity

The RTP could be purified using a ResourceQ anion exchange column (GE Healthcare). The structure of RTP was initially identified by $^{31}$P-NMR spectroscopy and further confirmed by one- and two-dimensional NMR spectra. Various NMR spectra for RTP are presented in **figures 6.1-6.7**.

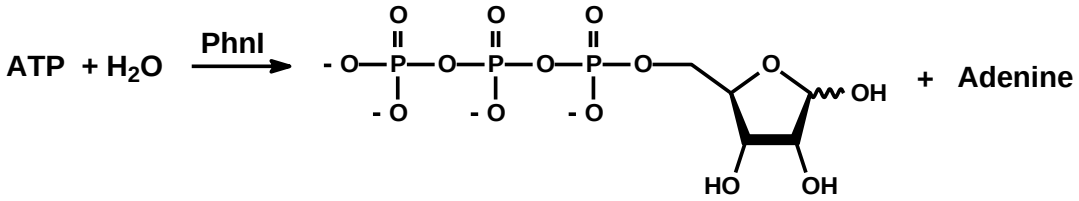


**Scheme 6.6:** Reaction catalyzed by PhnI in the presence of MgATP.

The formation of D-ribose-5-triphosphate from either ATP or GTP did not appear to be a productive pathway for the C-P lyase pathway since the phosphonate substrate was not connected to the ribose moiety. We therefore incubated phosphate and a small library of phosphonate derivatives (5 mM) with MgATP in the presence of PhnI to determine if any of these compounds (rather than water) could displace adenine. Surprisingly, phosphate, pyrophosphate, methylphosphate and sulfate inhibited the displacement of adenine from ATP but no inhibition was observed with methylphosphonate, ethylphosphonate, phosphonoacetic acid or 2-aminoethylphosphonate. The apparent inhibition constant for phosphate at an ATP concentration of 0.1 mM was ~0.30 mM. RTP and adenine were the only products formed in the presence of either phosphate or methylphosphonate. There were no further changes in the reaction products whether we used the GST-tagged PhnI in the presence or absence of Factor Xa (*116*).

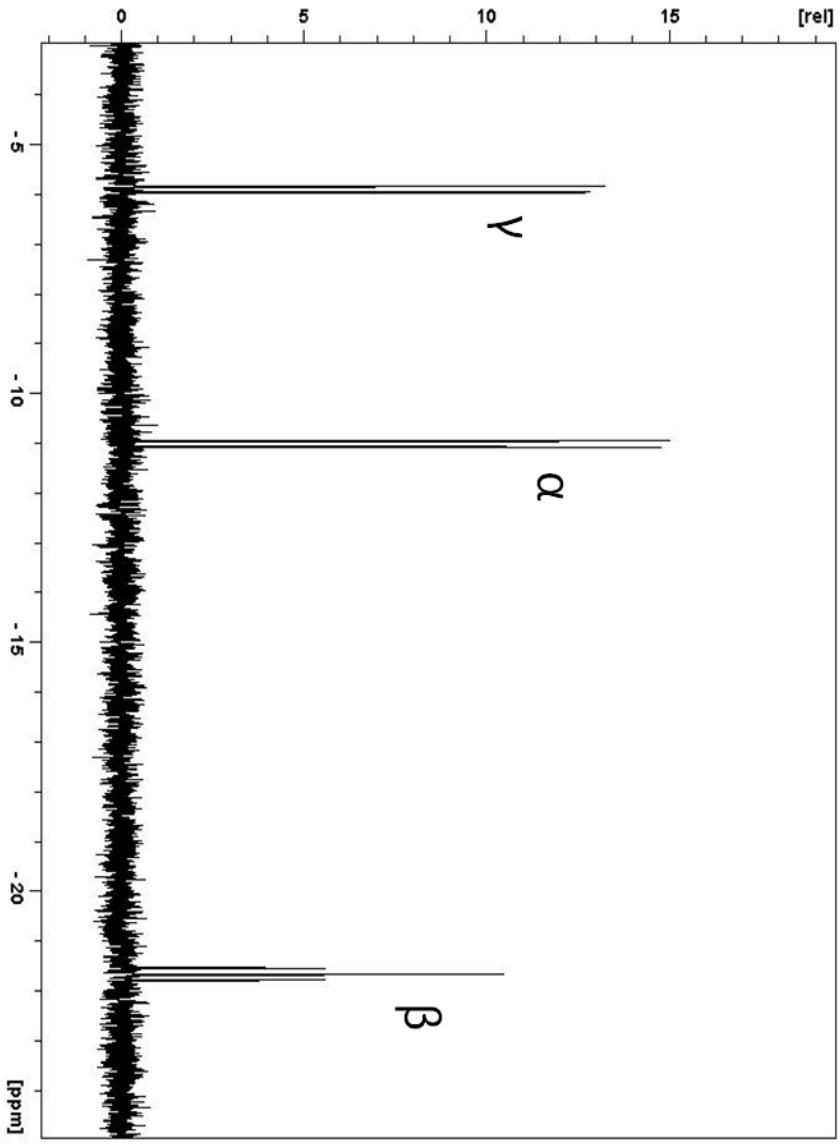


**Figure 6.1:** *$^{31}$P NMR spectrum of D-ribose-5-triphosphate* (RTP). The product of the reaction of PhnI (10 μM) with MgATP (5 mM) in 100 mM HEPES buffer pH 9.0. The spectrum shows the tri-phosphate moiety of RTP.

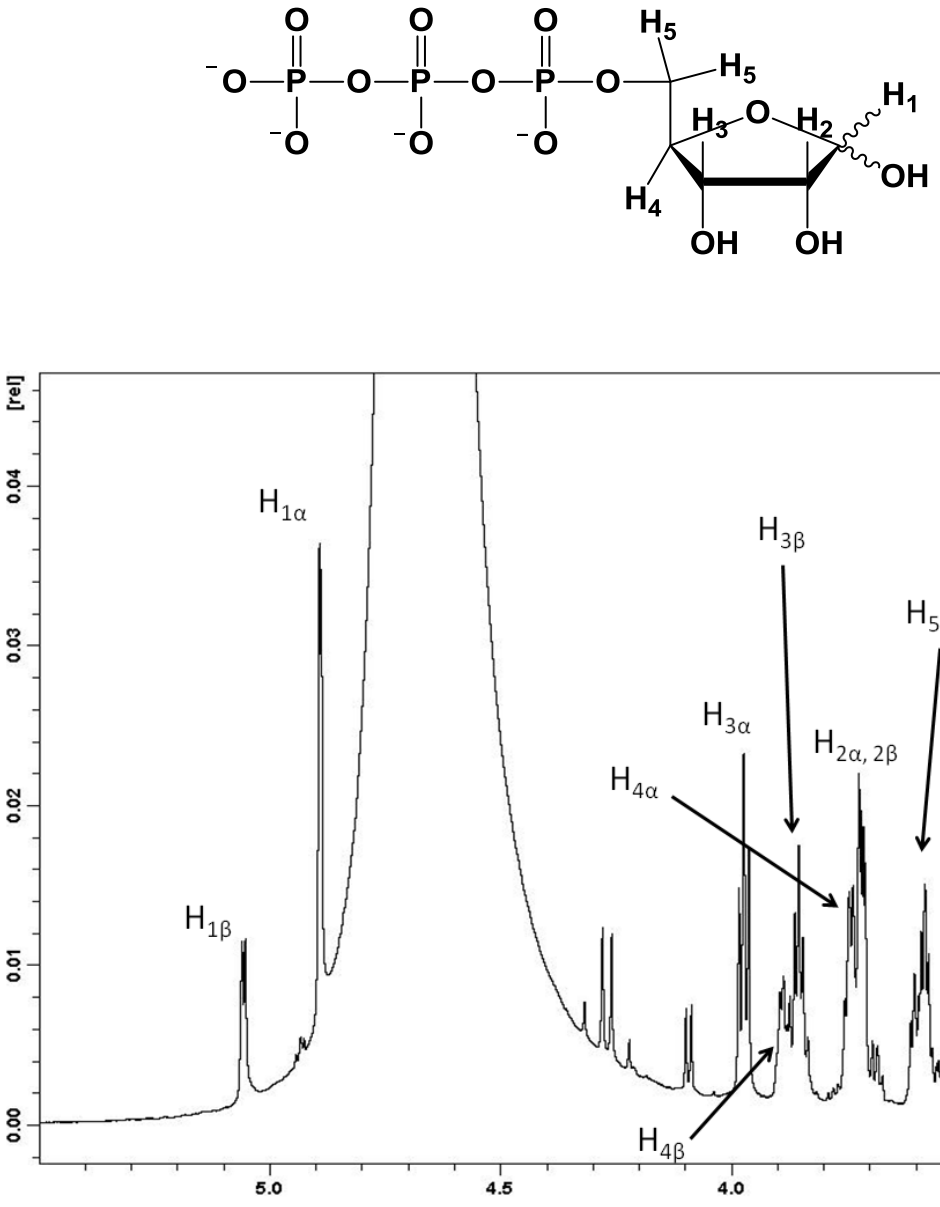


**Figure 6.2**: *$^{1}$H NMR spectra of RTP* (in 100 mM phosphate buffer pH 8.5, 10% $D_2O$). In the $^{1}$H NMR spectra, α and β represent the two anomers of RTP.

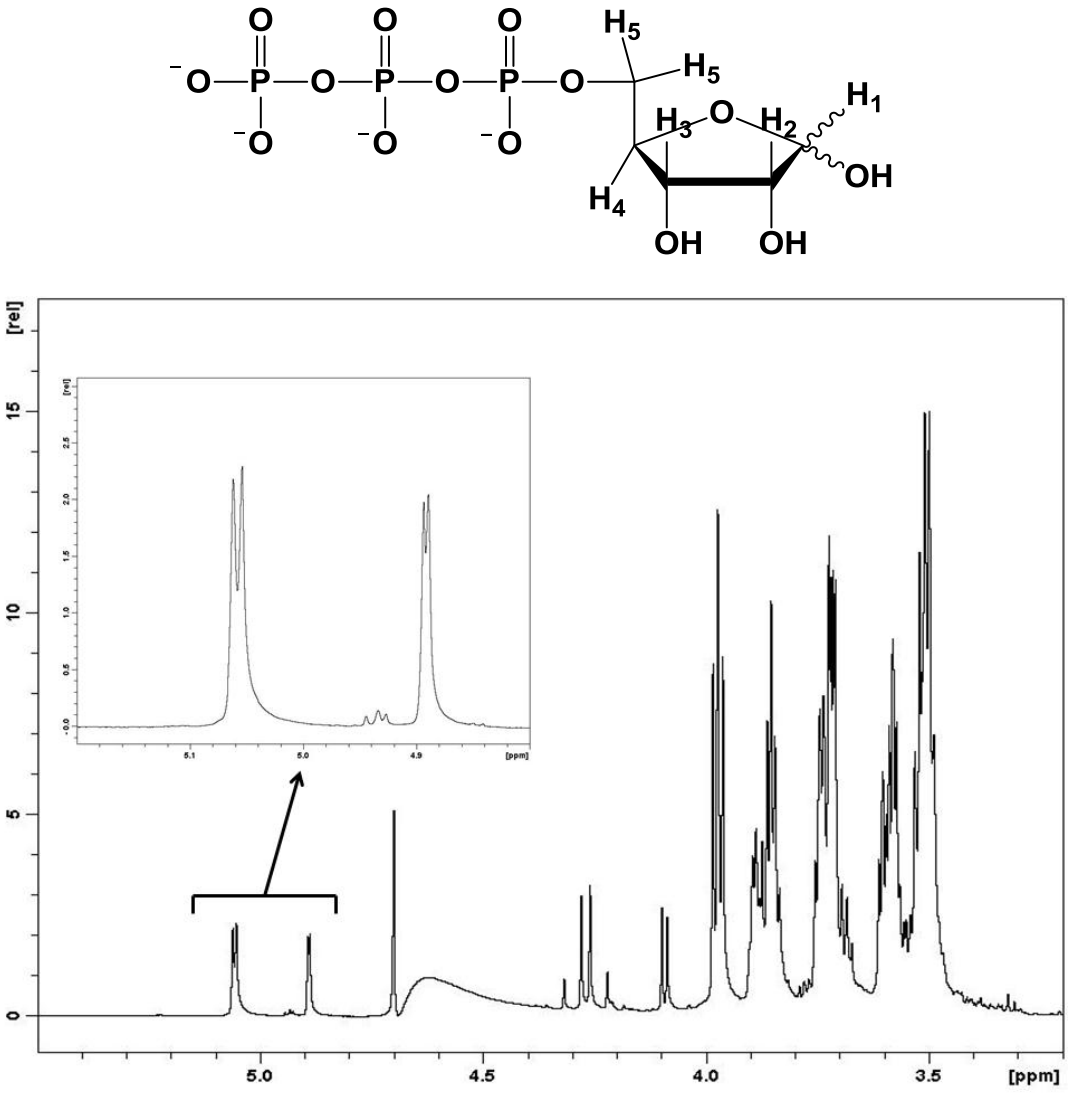


**Figure 6.3:** *$^{1}H$ NMR spectrum of RTP acquired with WATERGATE solvent suppression* (in 100 mM phosphate buffer, pH 8.5, 10% $D_2O$, on a Bruker Avance III 500 MHz NMR). The inset shows the anomeric protons (H1) as doublets (H1-H2 coupling). The coupling constants determined for these were $J_{H1\alpha} = 2.4$ Hz and $J_{H1\beta} = 3.5$ Hz.

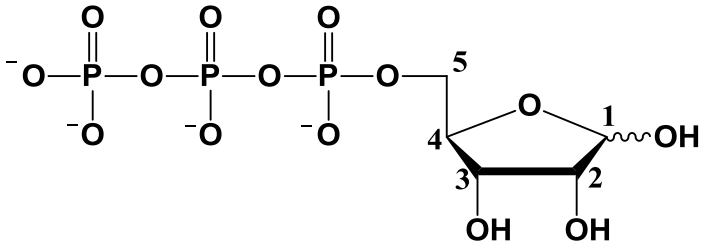


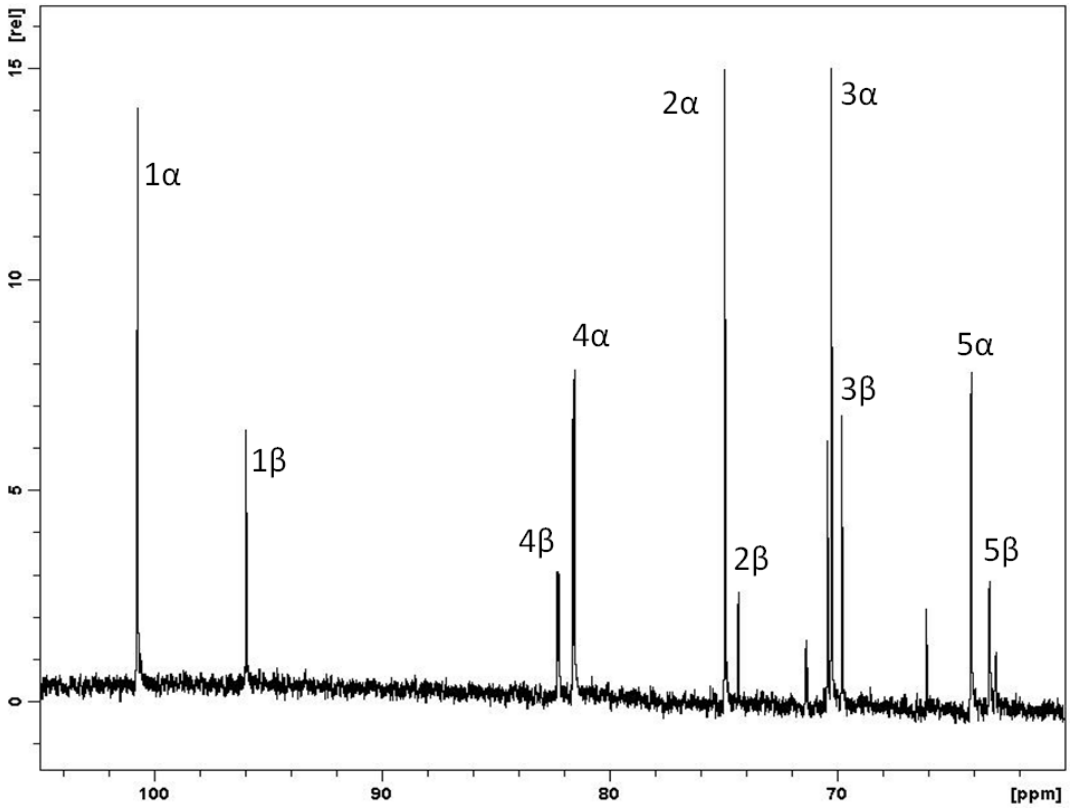


**Figure 6.4**: *$^{13}$C NMR spectrum of RTP* (in 100 mM phosphate buffer, pH 8.5, 10% $D_2O$). The numbers represent the numbering of the ribose carbon atoms. Glycerol was an impurity with the RTP during the purification from the reaction buffer.

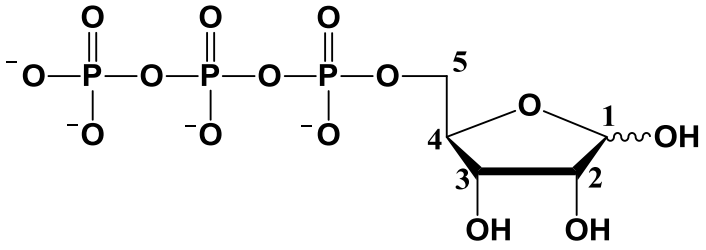

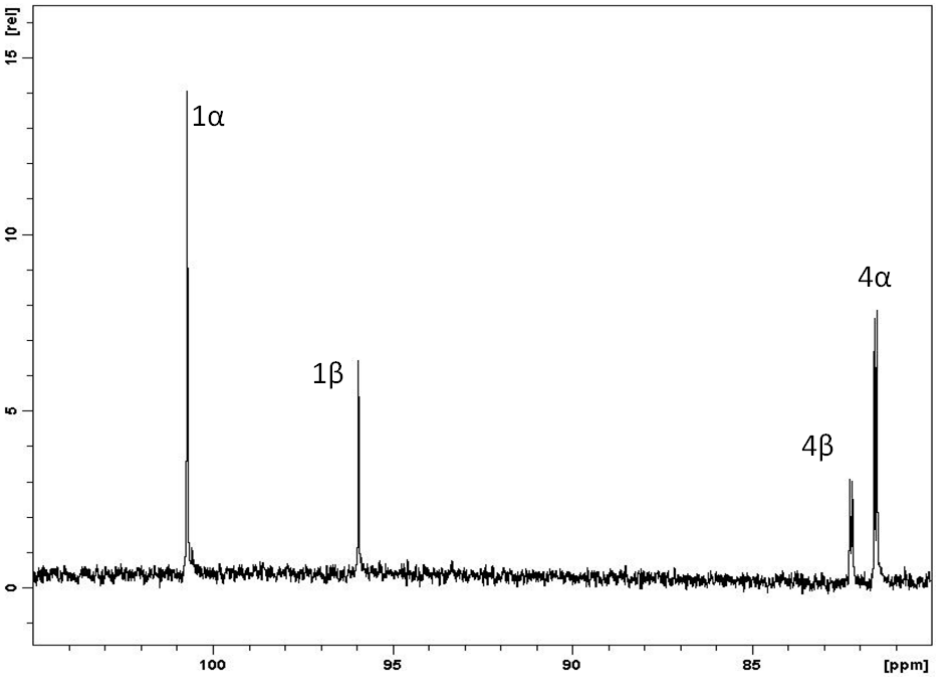


**Figure 6.5**: *$^{13}$C NMR spectrum of RTP showing C-1 and C-4 of the ribose moiety* (in 100 mM phosphate buffer, pH 8.5, 10% $D_2O$). The C-1 is a singlet (due to the lack of phosphorus coupling at C-1), whereas the C-4 is a doublet from the coupling of the phosphorus at C-5.

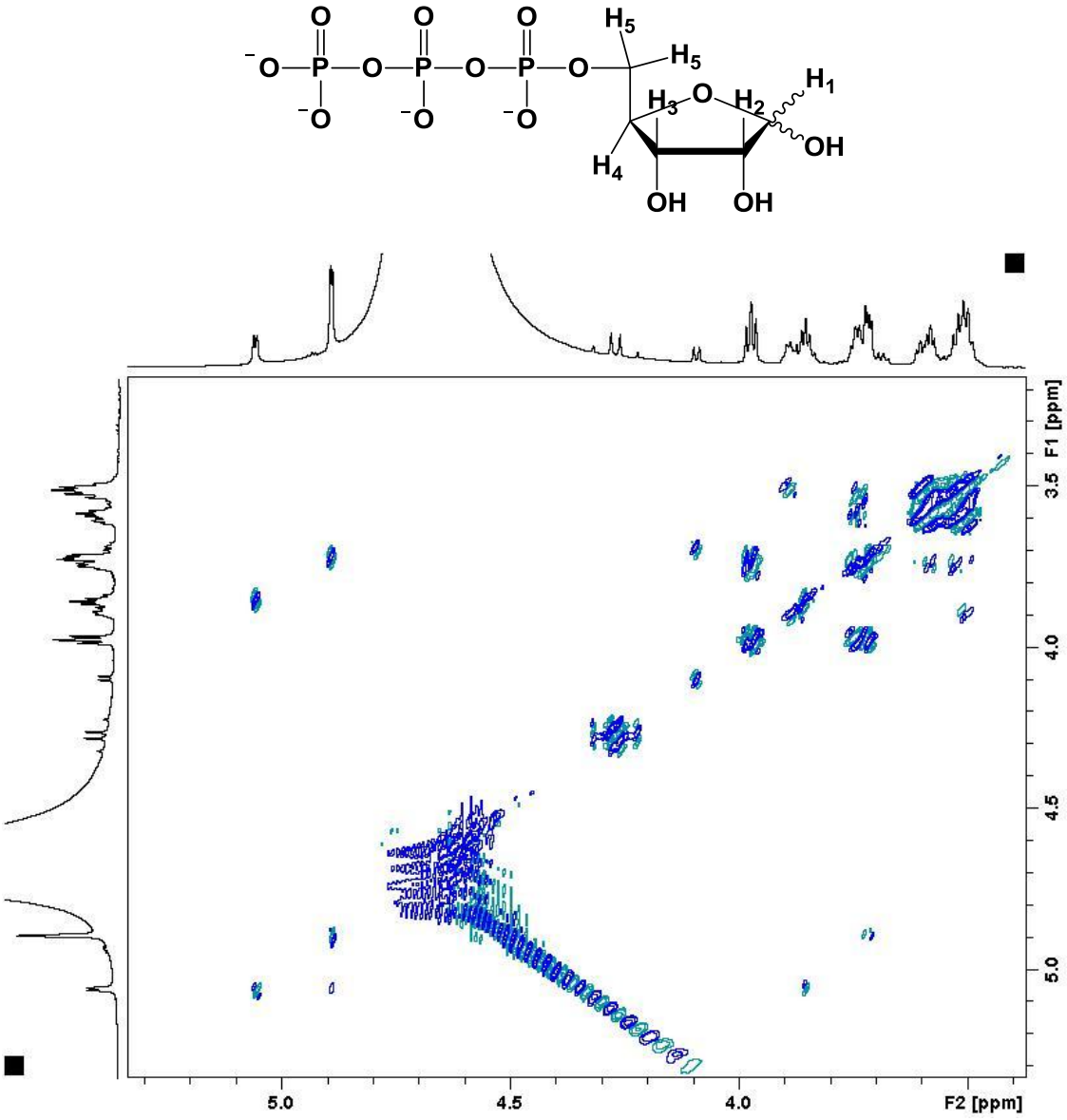


**Figure 6.6**: *COSY ($^{1}$H-$^{1}$H) NMR spectrum of RTP* (in 100 mM phosphate buffer at pH 8.5 on a Bruker Avance III 500 MHz NMR).

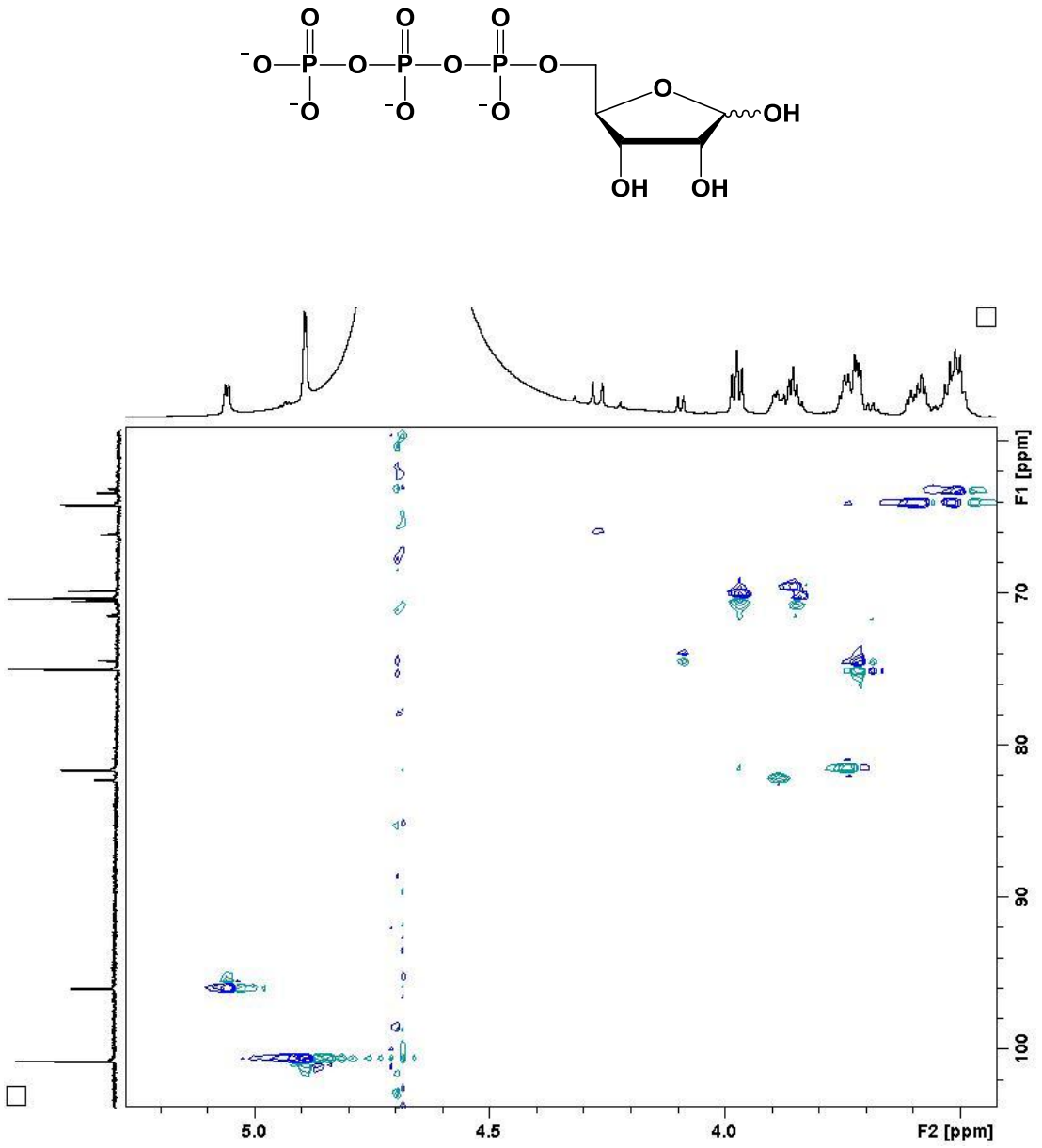


**Figure 6.7**: *HSQC ($^{1}H$-$^{13}C$) NMR spectrum of RTP* (in 100 mM phosphate buffer at pH 8.5 on a Bruker Avance III 500 MHz NMR).

Since it was previously postulated that the C-P lyase reaction involved a multi-protein complex, all of the recombinantly purified proteins were added to the reaction mixture. No new products were detected other than RTP and adenine. Since PhnI, PhnJ, PhnK and PhnL were all GST-fusion proteins, Factor-Xa (50 Units) was added to the reaction mixture for *in situ* cleavage of the GST-tags. With the addition of Factor-Xa, a new compound was observed by $^{31}$P NMR spectroscopy at 17.8 ppm. Anion exchange chromatography was used to purifiy the newly formed compound. One- and two-dimensional NMR spectra were consistent with the formation of α-D-ribose-1-methylphosphonate-5-triphosphate (RPnTP) as shown in **Scheme 6.7**. A small amount of the β-anomer was also detected (approximately 5-10 % of the α-anomer). In this transformation, all of the ATP was consumed but the overall yield of the phosphonylated product was approximately 30-35%; the rest of the ATP was converted to RTP.

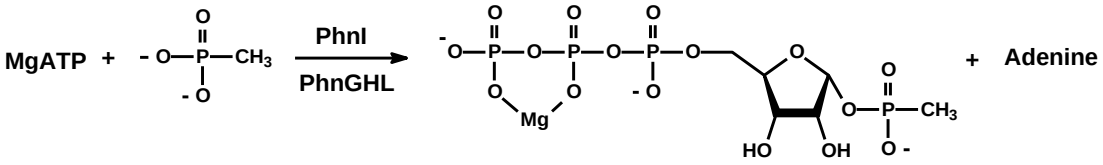


**Scheme 6.7:** Formation of RPnTP by PhnI in the presence of PhnGHL

To determine whether all of the proteins were required for this transformation, each protein was removed individually from the reaction mixture. The minimal set of proteins required for the nucleophilic attack of methylphosphonate on the anomeric carbon of MgATP to form adenine and form RPnTP were PhnI, PhnG, PhnH and PhnL. The kinetic constants for the reaction of methylphosphonate with ATP and GTP in

presence of PhnI, PhnG, PhnH and PhnL were ~$10^5$ $M^{-1}s^{-1}$ for $k_{cat}/K_m$ (**Table 6.1**). No reaction was observed with the fusion proteins and the GST-tags must be removed *in situ* for this activity. The partitioning of ATP to RTP and RPnTP likely results from partially cleaved GST-tagged protein and the precipitation of PhnI, PhnK, and PhnL after cleavage of these tags. The stoichiometry of the four proteins required for complex formation and the individual functions of PhnG, PhnH and PhnL are uncertain. RPnTP was purified from an anion exchange column (ResourceQ 1 mL GE Healthcare) and **figures 6.8-6.15** represent the NMR spectra of the isolated compound.

**Table 6.1:** *Kinetic constants for the nucleosidase reactions catalyzed by PhnI*

| Substrate | $k_{cat}$ ($s^{-1}$) | $K_m$ (μM) | $k_{cat}/K_m$ ($M^{-1}s^{-1}$) |
|---|---|---|---|
| **PhnI only** | | | |
| GDP | 0.20 ± 0.02 | 225 ± 37 | (1.0 ± 0.1) x $10^3$ |
| GTP | 5.3 ± 0.2 | 64 ± 8 | (8.3 ± 0.8) x $10^4$ |
| ADP | 0.065 ± 0.003 | 204 ±18 | (0.32 ± 0.02) x $10^3$ |
| ATP | 1.40 ± 0.04 | 95 ± 12 | (1.3 ± 0.2) x $10^4$ |
| ITP | 0.8 ± 0.1 | 108 ± 12 | (7.4 ± 0.6) x $10^3$ |
| **PhnG + PhnH + PhnI + PhnL + Factor Xa** | | | |
| GTP | 27 ± 2 | 80 ± 10 | (3.4 ± 0.3) x $10^5$ |
| ATP | 20 ± 1 | 56 ± 7 | (3.5 ± 0.3) x $10^5$ |

All assays were performed at 30 $^oC$ at pH 8.5

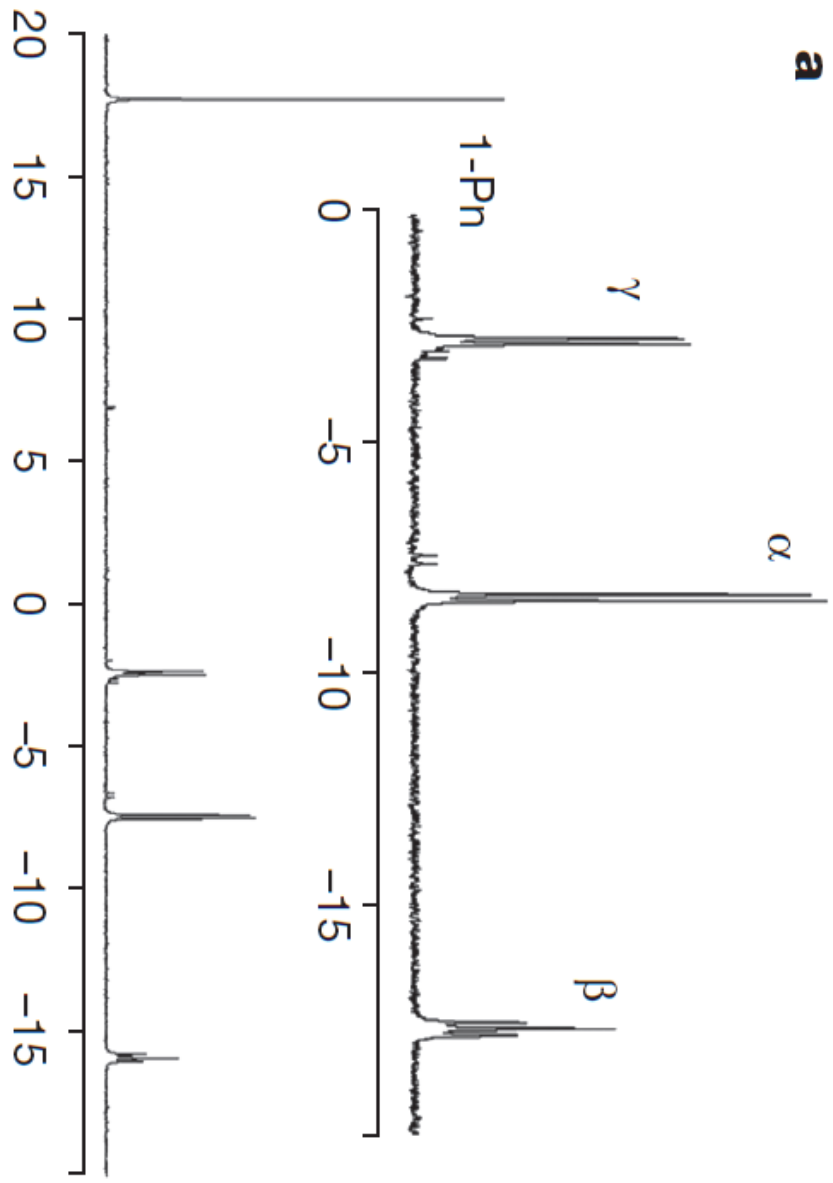


**Figure 6.8**: *$^{31}$P NMR spectra of RPnTP purified using anion exchange chromatography*. The methylphosphoryl group is represented as 1-Pn. Inset, $^{31}$P-$^{31}$P coupling of the triphosphate moiety of the RPnTP product.

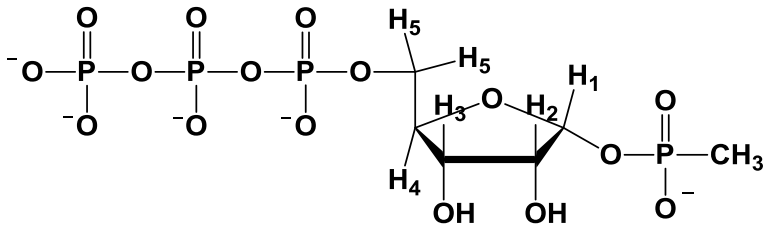


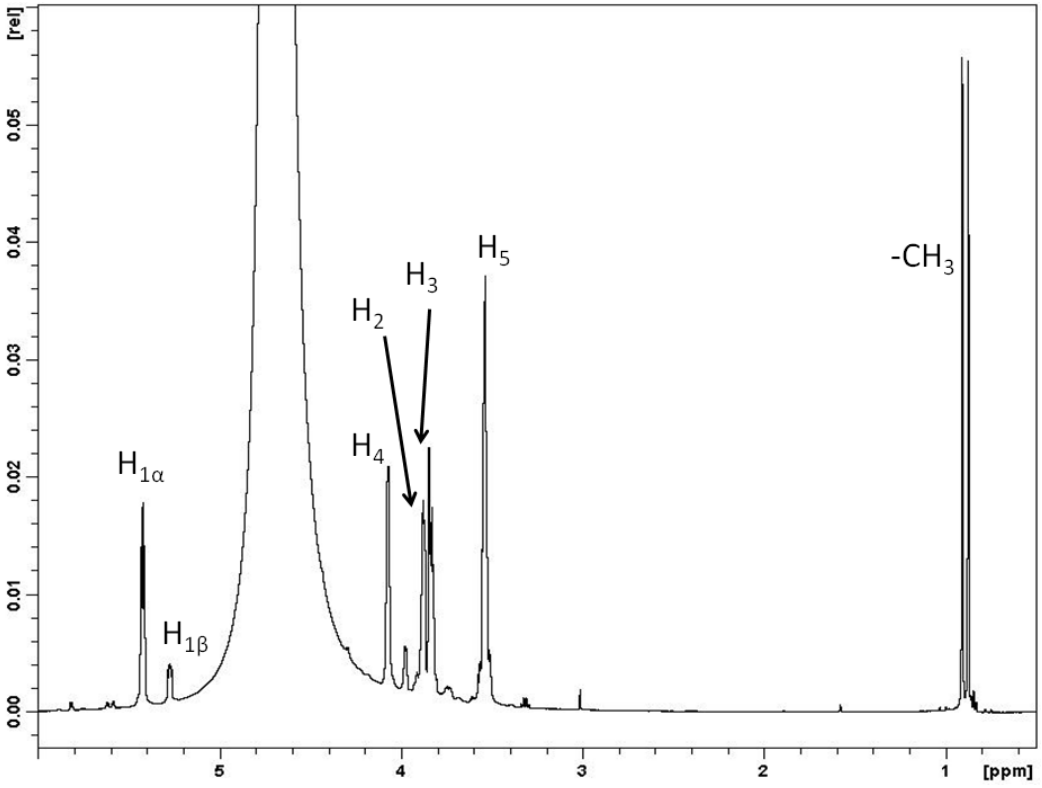


**Figure 6.9**: *$^{1}$H NMR spectrum of α-D-ribose-1-methylphosphonate-5-triphosphate* (RPnTP) (in 100 mM phosphate buffer, pH 8.5 on a Bruker Avance III 500 MHz NMR). A small amount of the β-anomer is also formed in the reaction (10 % of the α-anomer).

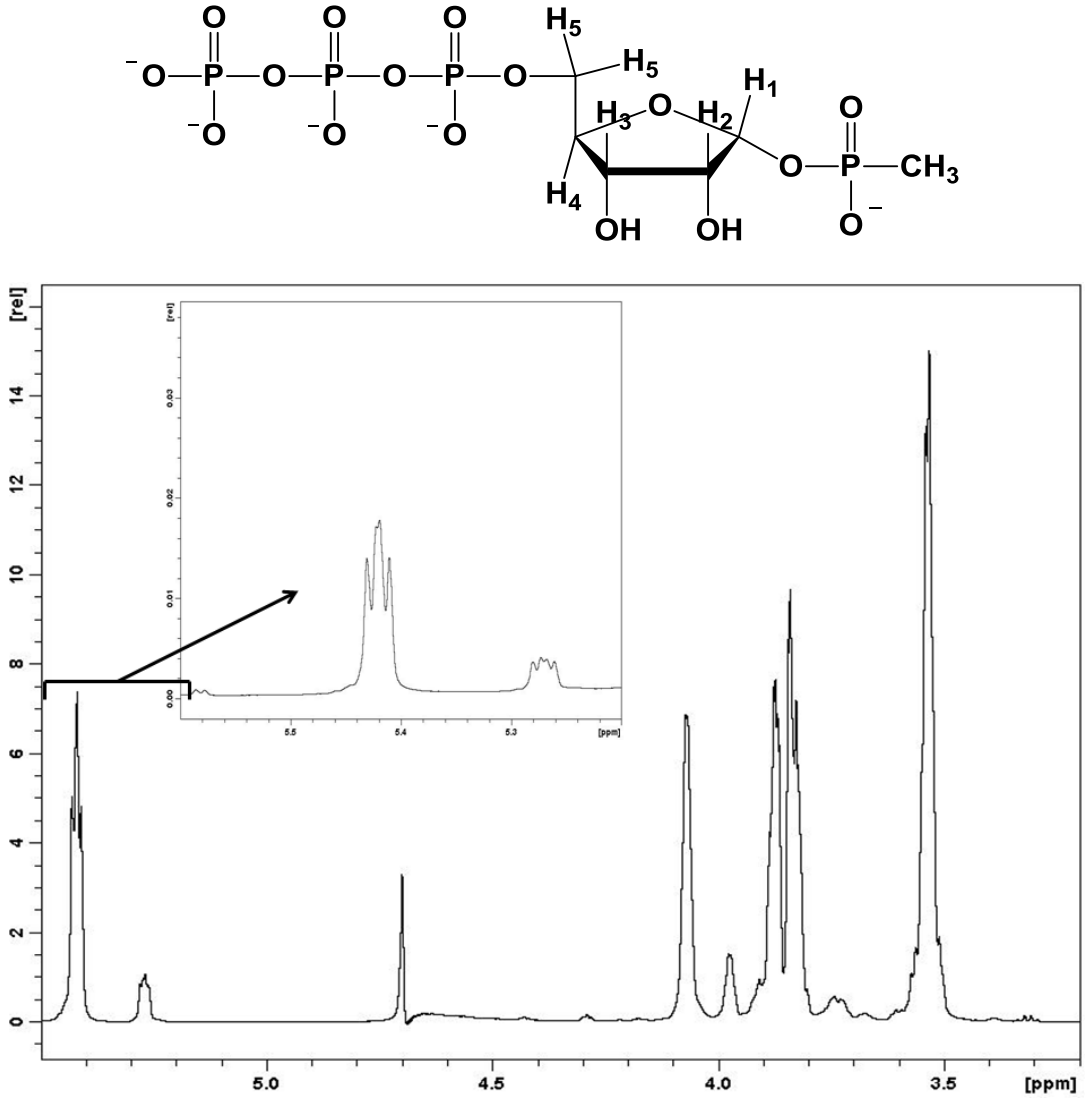


**Figure 6.10**: *$^{1}H$ NMR spectrum of the ribose moiety of RPnTP using WATERGATE solvent suppression* (in 100 mM phosphate buffer, pH 8.5 on a Bruker Avance III 500 MHz NMR). The inset shows the anomeric protons split as a quartet (doublet of doublets) resulting from the phosphorus of the methylphosphonate attached to C-1. The coupling constants for the major product: $H_{1\alpha}$ are $J_{(H1\text{-}H2)} = 4.3$ Hz and $J_{(H1\text{-}P1)} = 6.1$ Hz.

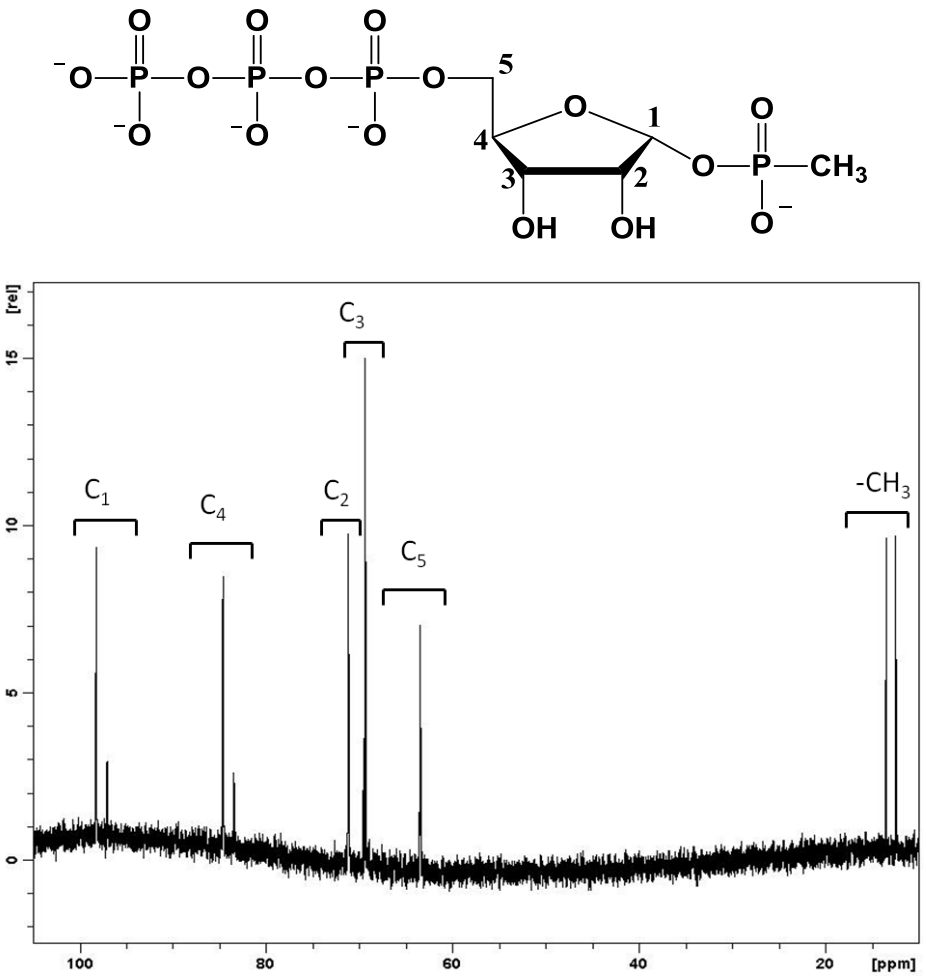


**Figure 6.11**: *$^{13}$C NMR spectrum of RPnTP* (in 100 mM phosphate buffer, pH 8.5 on a Bruker Avance III 500 MHz NMR). The carbon atoms of RPnTP are labeled in the $^{13}$C NMR spectrum. There are two anomers observed in the $^{13}$C NMR spectrum with the α-anomer being the major enzymatic product. The six carbon atoms of the molecule are observed in this spectrum with the methyl group of the 1-methylphosphonate upfield from the ribose carbon atoms and split as doublet from the strong coupling to the phosphorus.

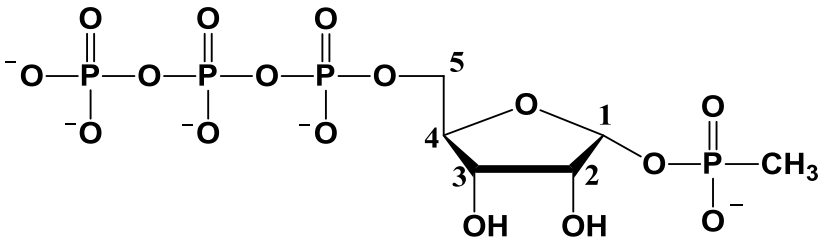


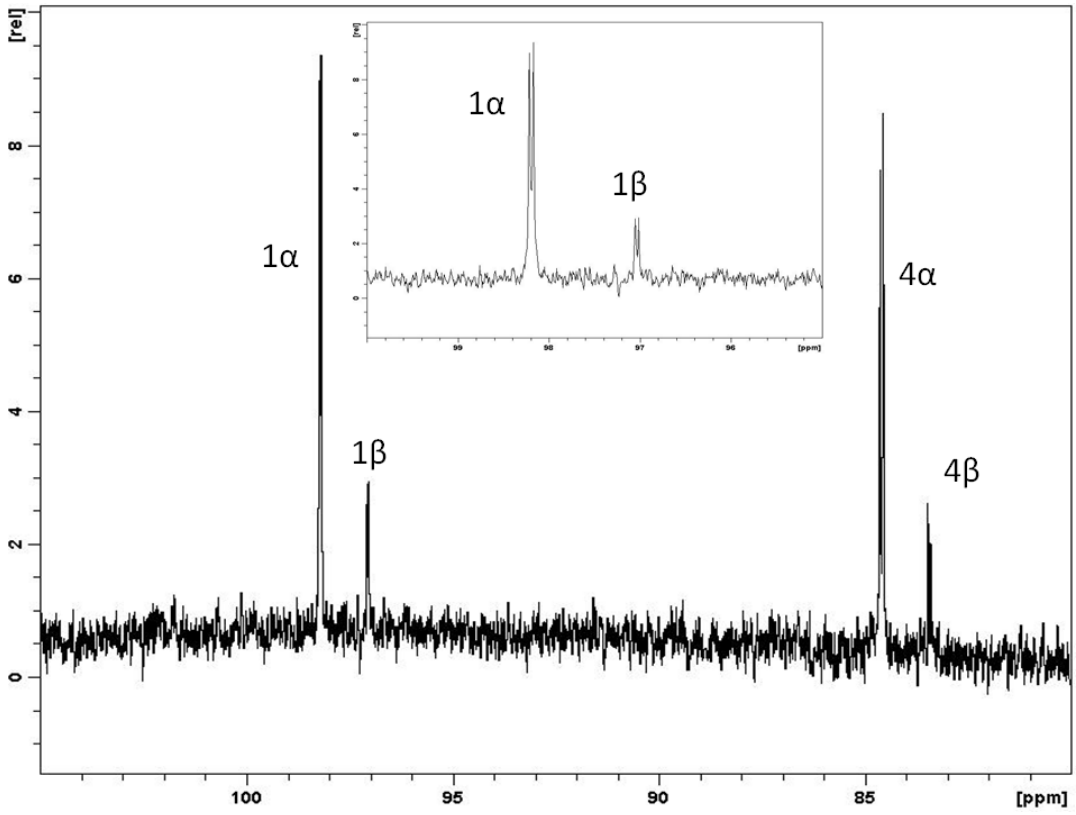


**Figure 6.12**: *$^{13}$C NMR spectrum of RPnTP showing C-1 and C-4 of the ribose moiety* (in 100 mM phosphate buffer at pH 8.5 on a Bruker Avance III 500 MHz NMR). Both C-1 and C-4 are doublets for both anomers. The inset shows the splitting of the C-1 anomers from the 1-methylphosphonate adduct to form RPnTP.

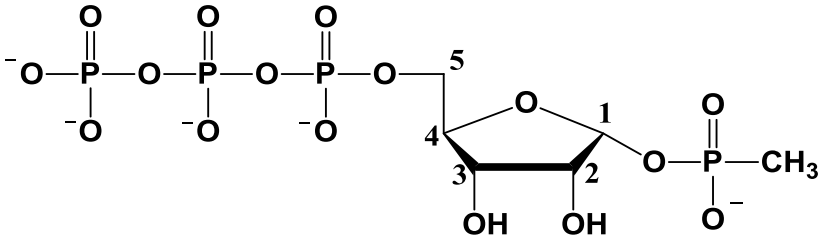


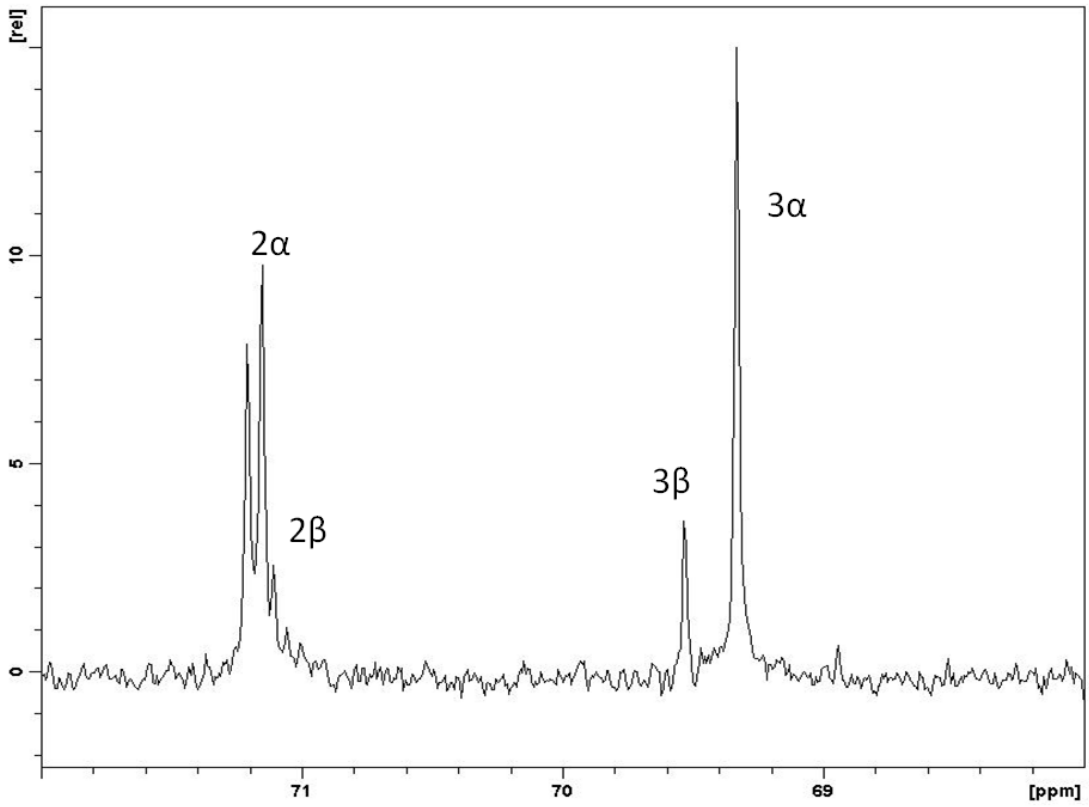


**Figure 6.13**: *$^{13}$C NMR spectrum of RPnTP showing C-2 and C-3 of the ribose moiety* (in 100 mM phosphate buffer pH 8.5 on a Bruker Avance III 500 MHz NMR). The C-2 of the ribose moiety is a doublet and C-3 of the ribose moiety is a singlet.

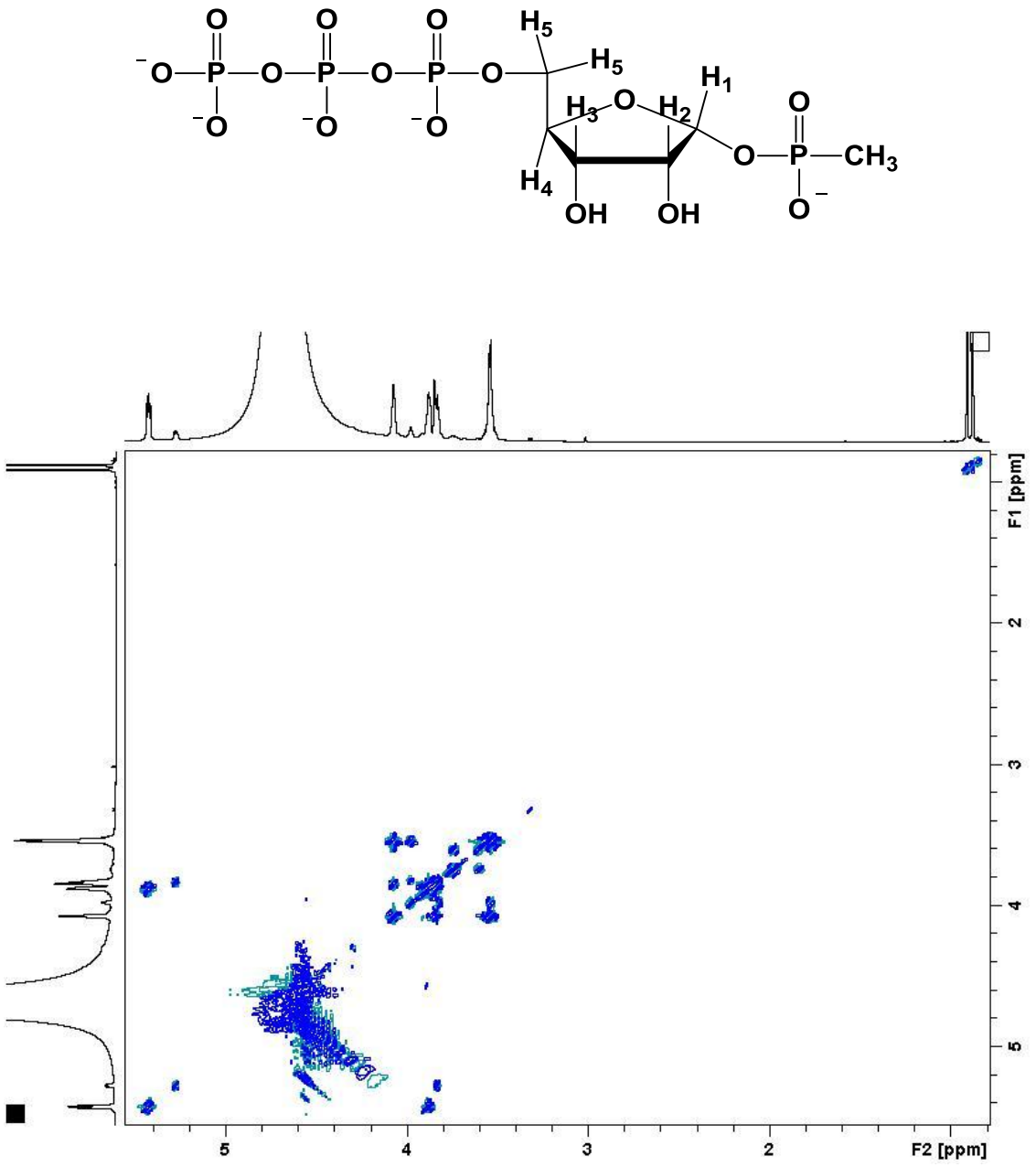


**Figure 6.14**: *COSY ($^{1}H$-$^{1}H$) NMR spectrum of RPnTP* (in 100 mM phosphate buffer at pH 8.5 on a Bruker Avance III 500 MHz NMR).

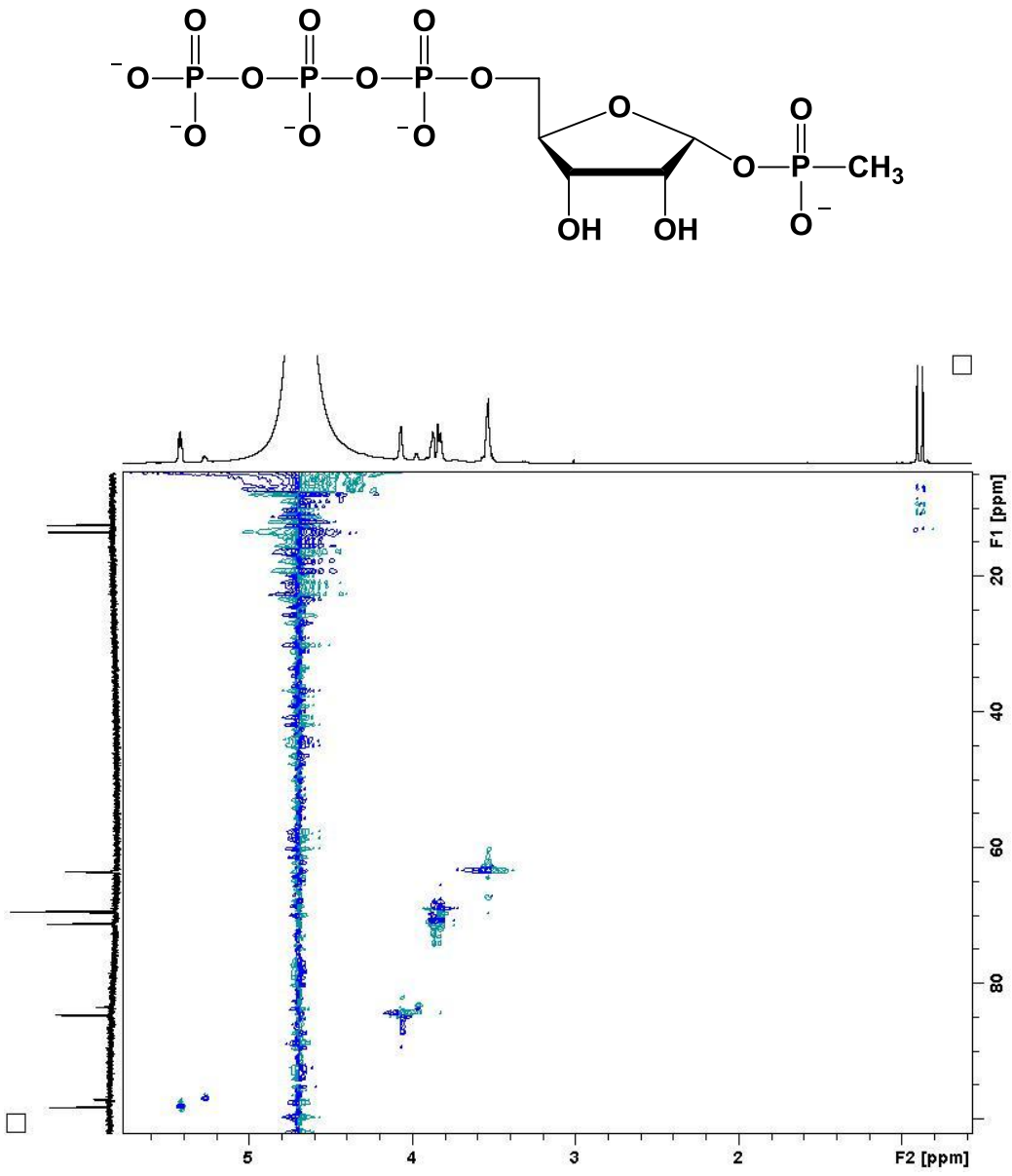


**Figure 6.15**: *HSQC ($^{1}H$-$^{13}C$) NMR spectrum of RPnTP* (in 100 mM phosphate buffer at pH 8.5 on a Bruker Avance III 500 MHz NMR).

*Catalytic Function of PhnM.* PhnM is a member of the amidohydrolase superfamily (*7*). Enzymes within this superfamily use a mono- or binuclear metal center to catalyze hydrolytic reactions at carbon and phosphorus centers. PhnM is grouped within Cluster of Orthologous Group (COG) 3454. This COG consists of approximately 200 proteins of similar sequence from different bacteria. All proteins from the amidohydrolase superfamily have a $(\beta/\alpha)_8$-barrel structural fold. Sequence alignment analysis indicated that all of the enzymes in COG3454 have a highly conserved HxD motif at the end of β-strand 1, a histidine at the end of β-strand 5, a glutamate at the end of β-strand 6 and an aspartate at the end of β-strand 8. These protein sequences lacks a clearly defined ligand from β-strand 4 that could serve to bridge two divalent cations and thus PhnM was predicted to bind a single divalent metal cation in the active site at the α-metal binding site. PhnM was previously predicted to be a hydrophobic membrane bound protein (*32, 33*). Variation of the solution pH demonstrated that PhnM was soluble at pH values greater than 9.0. At this pH PhnM was soluble and could be purified without a solubility or affinity tag. Inductively coupled plasma mass spectrometry (ICP-MS) demonstrated that the purified PhnM contained ~1.2 equivalents of $Zn^{2+}$ per monomer when $Zn^{2+}$ was supplemented in the growth media during protein expression.

Previous studies have suggested that α-D-ribose-1-phosphonate-5-phosphate (PRPn) as a potential intermediate in the conversion of alkylphosphonates to phosphate by *E. coli* (*103, 107*). Hence it was rational to assume that one of the proteins in the *phn* operon would catalyze the hydrolysis of the β- and γ-phosphoryl groups from RPnTP

that was isolated from the action of PhnI, PhnG, PhnH and PhnL. PhnM was the prime candidate to perform this hydrolytic reaction. In addition to a set of highly conserved residues believed to coordinate the active site zinc, PhnM also possess five highly conserved arginine residues on the various loops that connect the eight β-strands and α-helices. These loops are essential in determining substrate specificity. The positively charged arginine residues may participate in the coordination of the tri-polyphosphate moiety of the RPnTP substrate.

When PhnM was incubated with purified RPnTP in the presence of 1 mM $ZnCl_2$ and 5 mM $MgCl_2$, $^{31}$P-NMR identified 2 new reaction products, consistent with α-D-ribose-1-methylphosphonate-5-phosphate (PRPn) and pyrophosphate (*99*). This observation was consistent with the hydrolytic cleavage of α- and β- phosphoryl groups of the triphosphate moiety of RPnTP. This reaction is shown in **Scheme 6.8**.

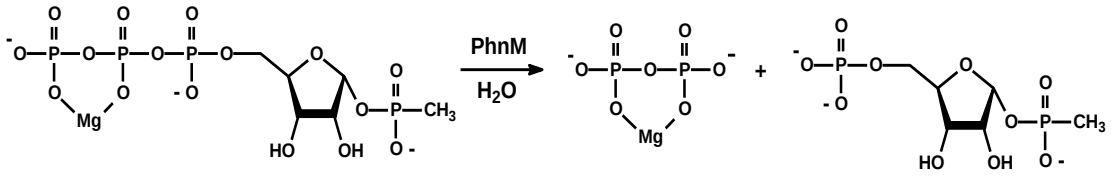


**Scheme 6.8:** Reaction catalyzed by PhnM.

The products of the reaction of PhnM were PRPn and pyrophosphate. The enzyme PhnM was filtered from the reaction and the products were characterized by NMR spectroscopy. **Figures 6.16 - 6.22** represent NMR characterization of the products of the reaction characterized by PhnM.

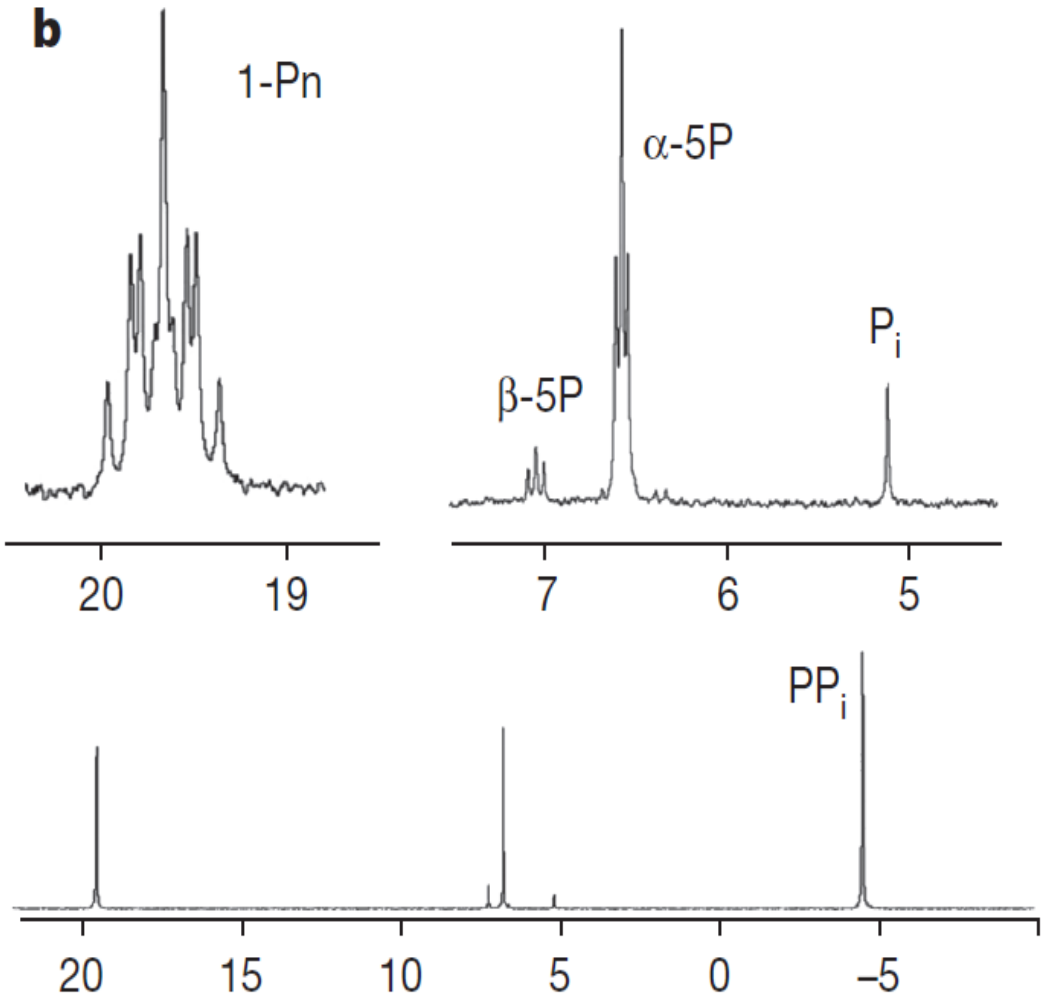


**Figure 6.16:** *The formation of PRPn and pyrophosphate ($PP_i$) from RPnTP by PhnM*. Spectrum collected at pH 8.5. Inset, proton coupled spectrum of PRPn showing multiplet corresponding to 1-Pn and triplet corresponding to 5-phosphate (major α-anomer and minor β-anomer) as well as inorganic phosphate ($P_i$).

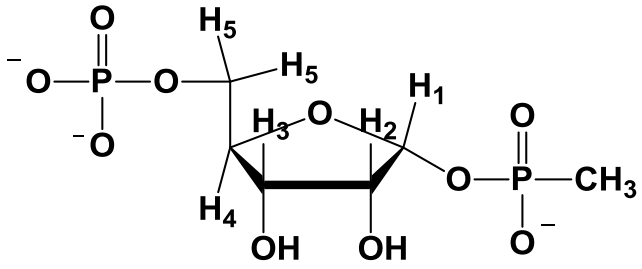


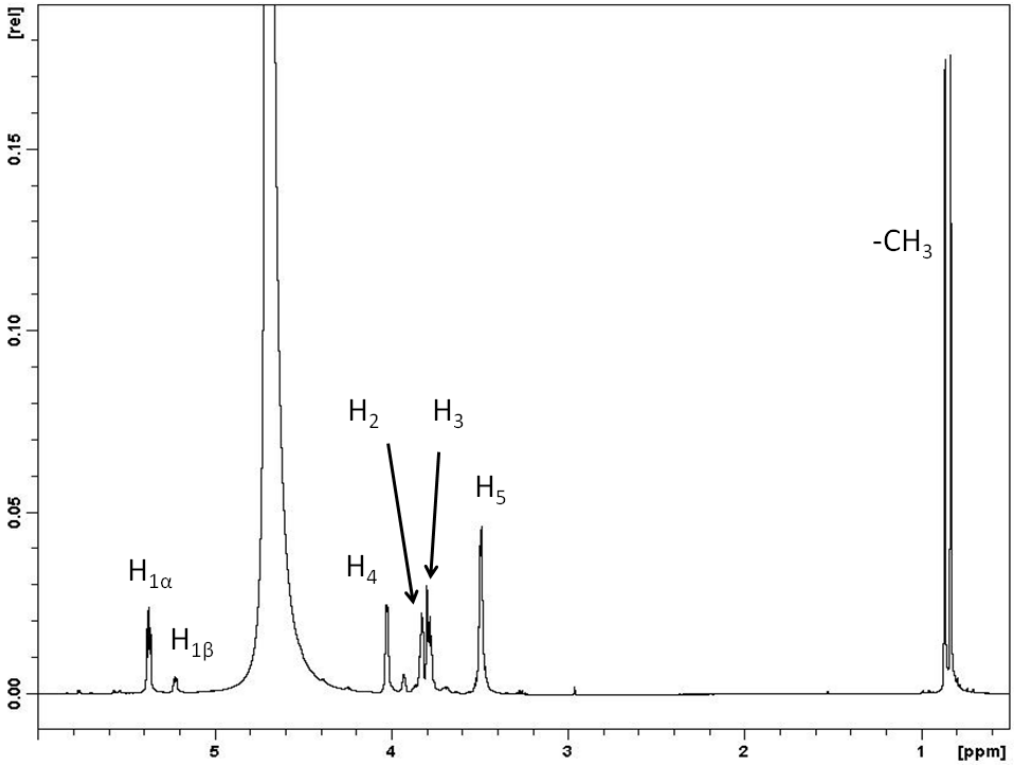


**Figure 6.17**: *$^{1}$H NMR spectrum of α-D-ribose-1-methylphosphonate-5-phosphate* (PRPn) in 100 mM phosphate buffer pH 8.5 on a Bruker Avance III 500 MHz NMR.A small amount of the β-anomer is also formed in the reaction.

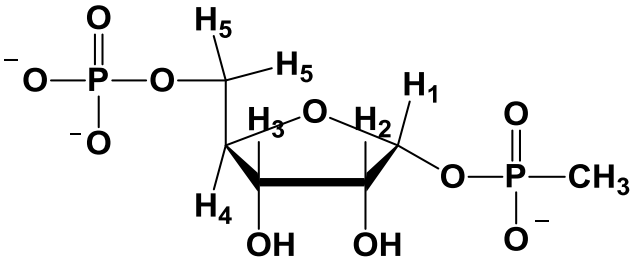


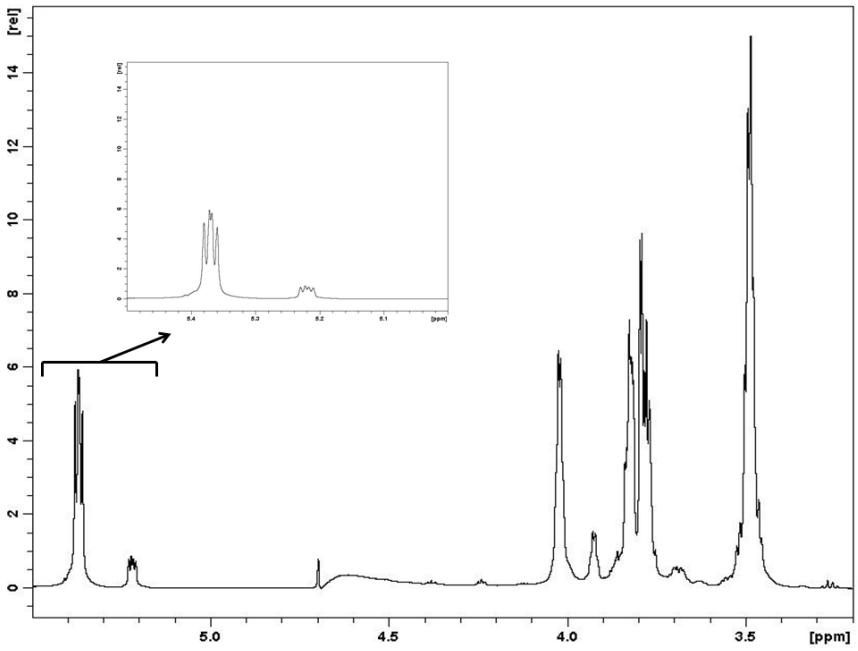


**Figure 6.18**: *$^{1}$H NMR spectrum of the ribose moiety of PRPn using WATERGATE solvent suppression* (in 100 mM phosphate buffer pH 8.5 on a Bruker Avance III 500 MHz NMR). The inset shows the anomeric protons split as a quartet (doublet of doublets) resulting from the phosphorus of the methylphosphonate attached to C-1. The coupling constants for the major product are $H_{1\alpha}$ are $J_{(H1\text{-}H2)}$ = 4.2 Hz and $J_{(H1\text{-}P1)}$ = 6.3 Hz.

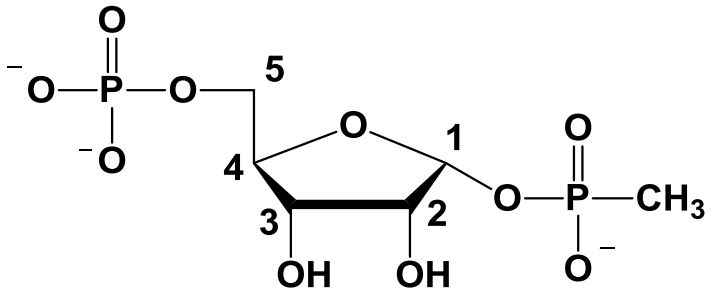


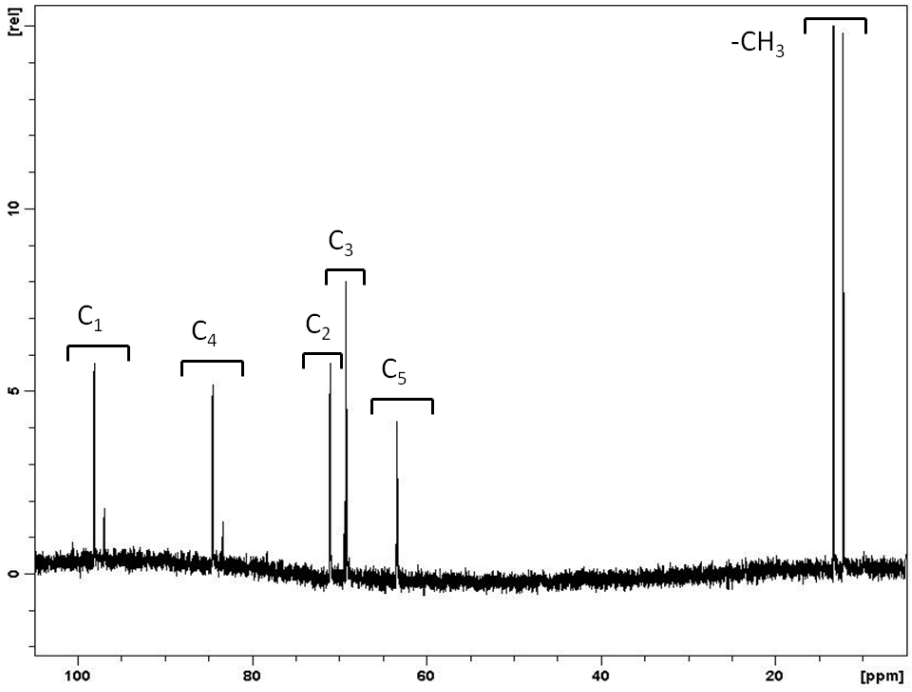


**Figure 6.19**: *$^{13}$C NMR spectrum of PRPn* (in 100 mM phosphate buffer pH 8.5 on a Bruker Avance III 500 MHz NMR). The carbon atoms of the RPnP are identified in the $^{13}$C NMR spectrum. The two anomers are clearly seen in the $^{13}$C NMR spectrum with the α-anomer being the major product of the reaction of PhnM with RPnTP in the presence of $Zn^{2+}$.

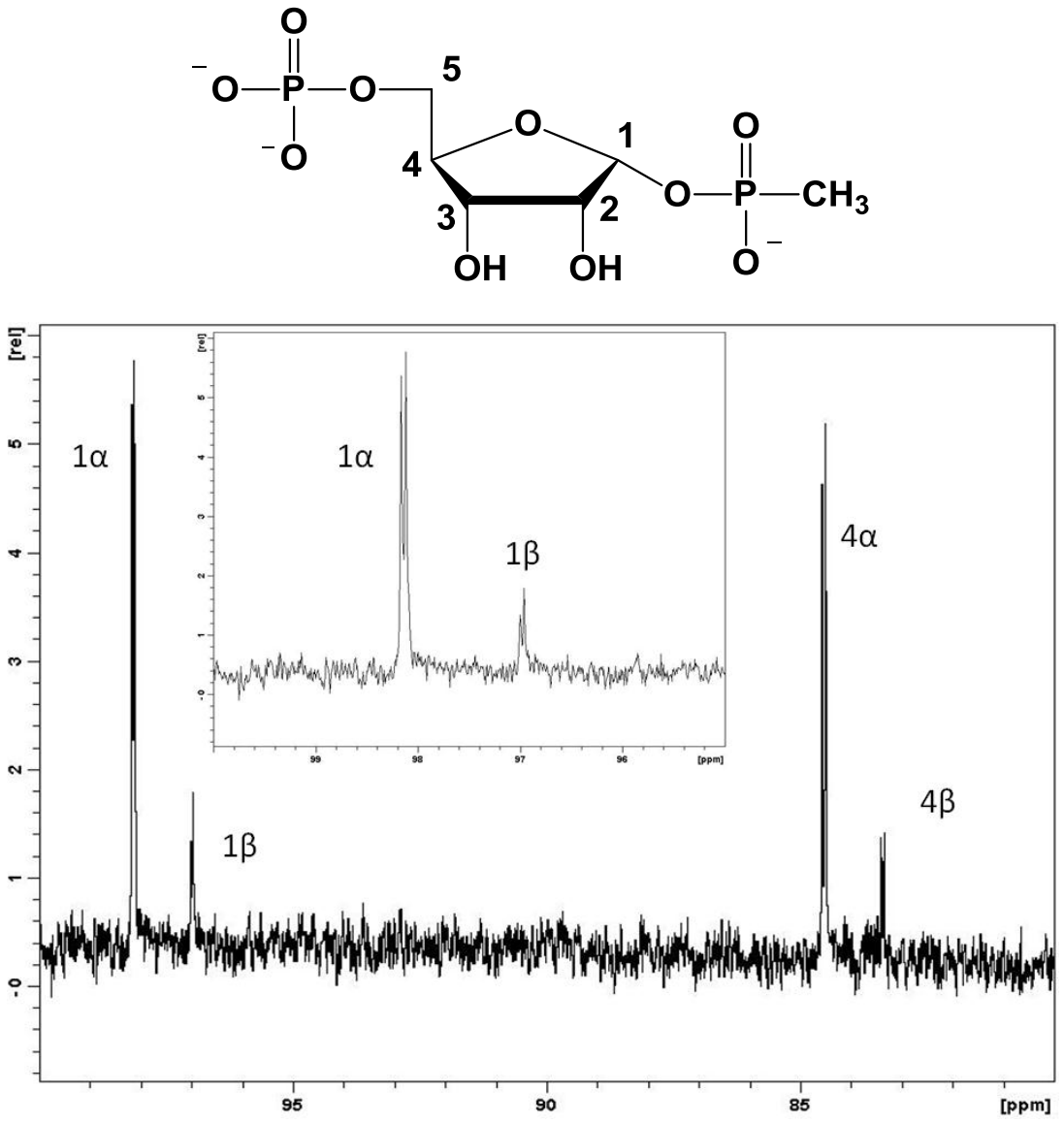


**Figure 6.20**: *$^{13}$C NMR spectrum of PRPn showing C-1 and C-4 of the ribose moiety* (in 100 mM phosphate buffer at pH 8.5 on a Bruker Avance III 500 MHz NMR). The inset shows the splitting of C-1 by the phosphorus of the phosphonate moiety.

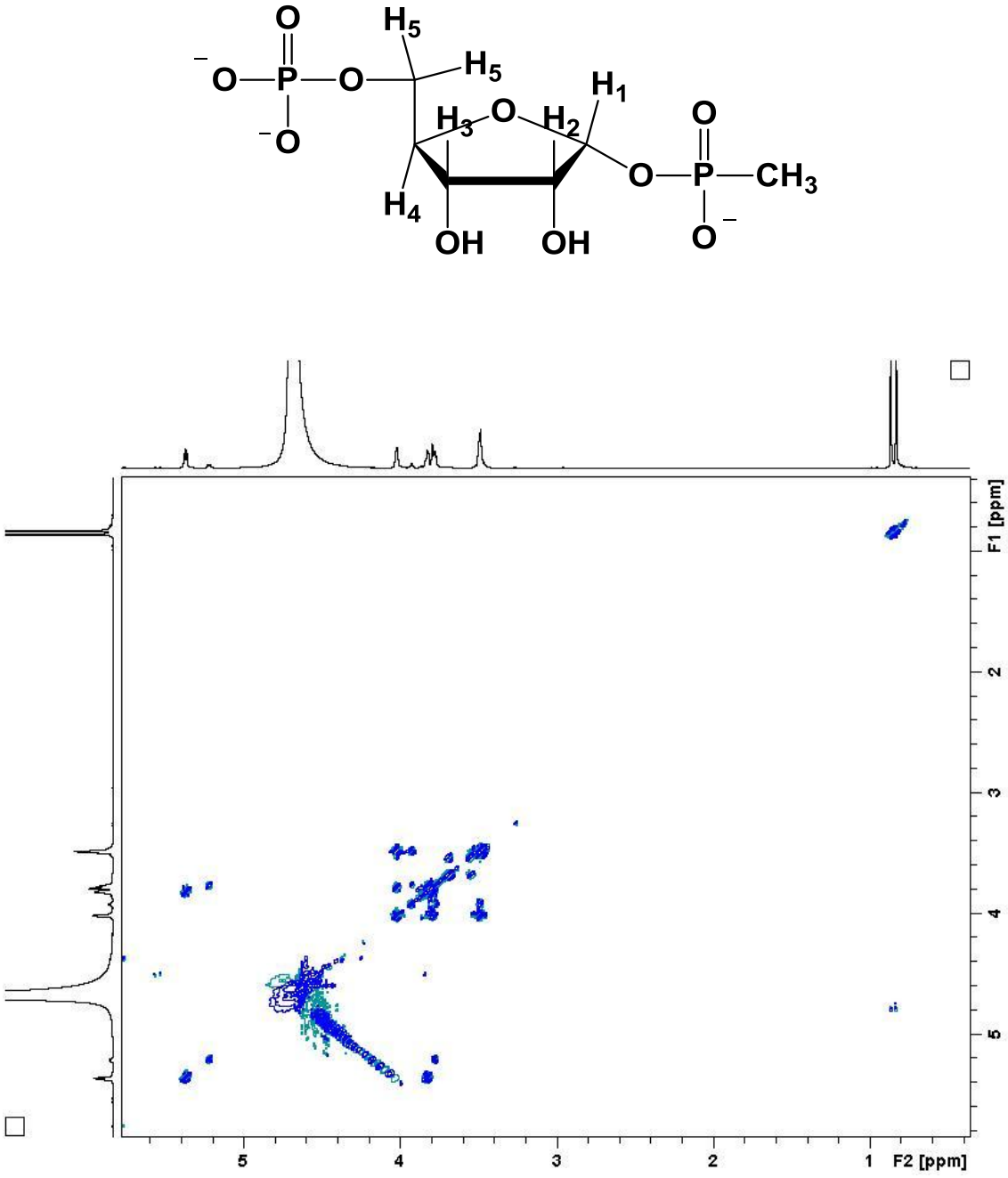


**Figure 6.21**: *COSY ($^{1}H$-$^{1}H$) NMR spectrum of PRPn* (in 100 mM phosphate buffer at pH 8.5 on a Bruker Avance III 500 MHz NMR).

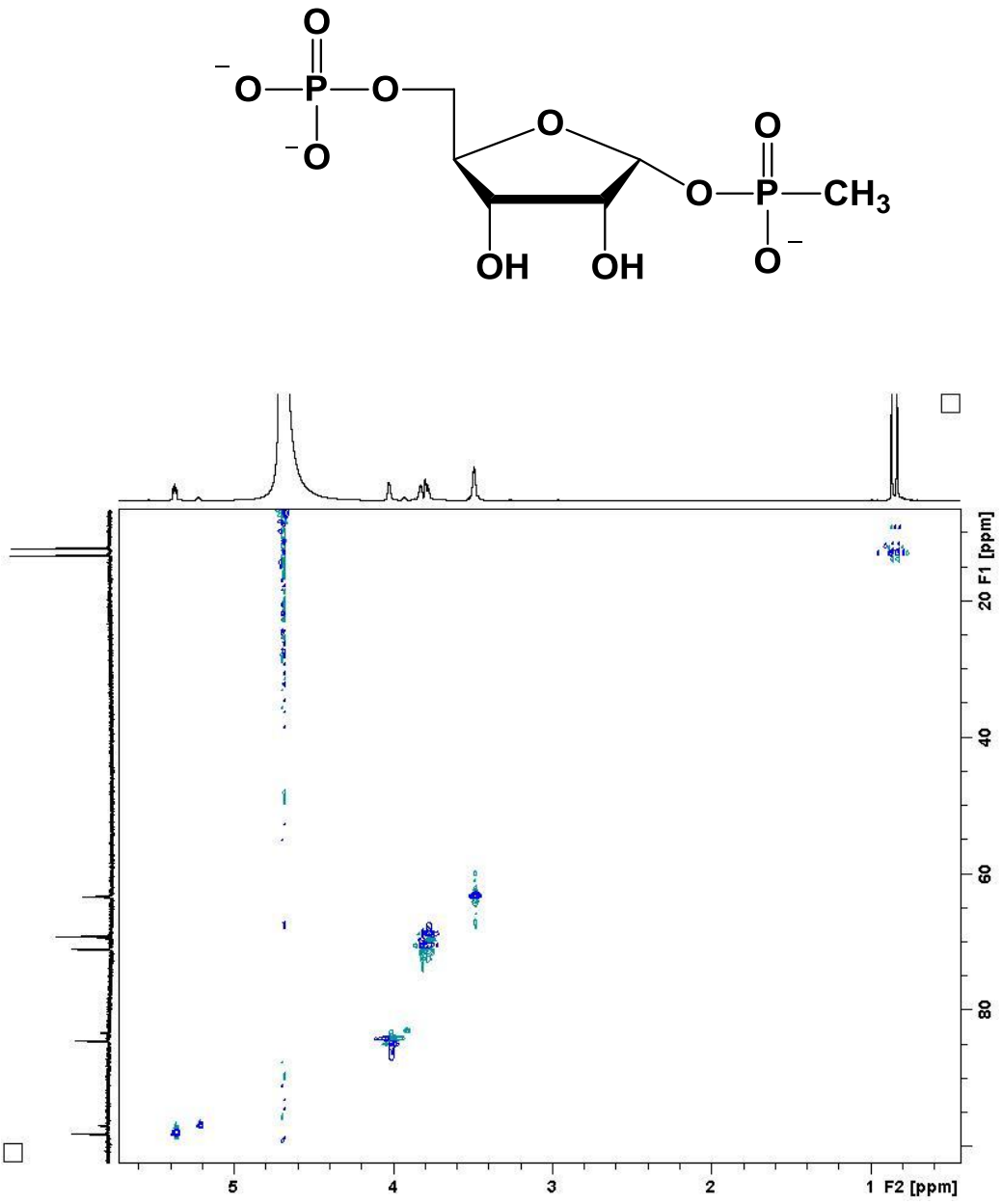


**Figure 6.22***: HSQC ($^{1}H$-$^{13}C$) NMR spectrum of PRPn* (in 100 mM phosphate buffer at pH 8.5 on a Bruker Avance III 500 MHz NMR).

To determine the exact position of the hydrolytic attack, the reaction was performed in a 1:1 mixture of $H_2O$ and $H_2O^{18}$. The $O^{18}$ label was found exclusively in

the PRPn product. This result was indicative of an attack of the activated hydroxide on the α-phosphorus of the triphosphate moiety of the substrate (**figure 6.23)**.

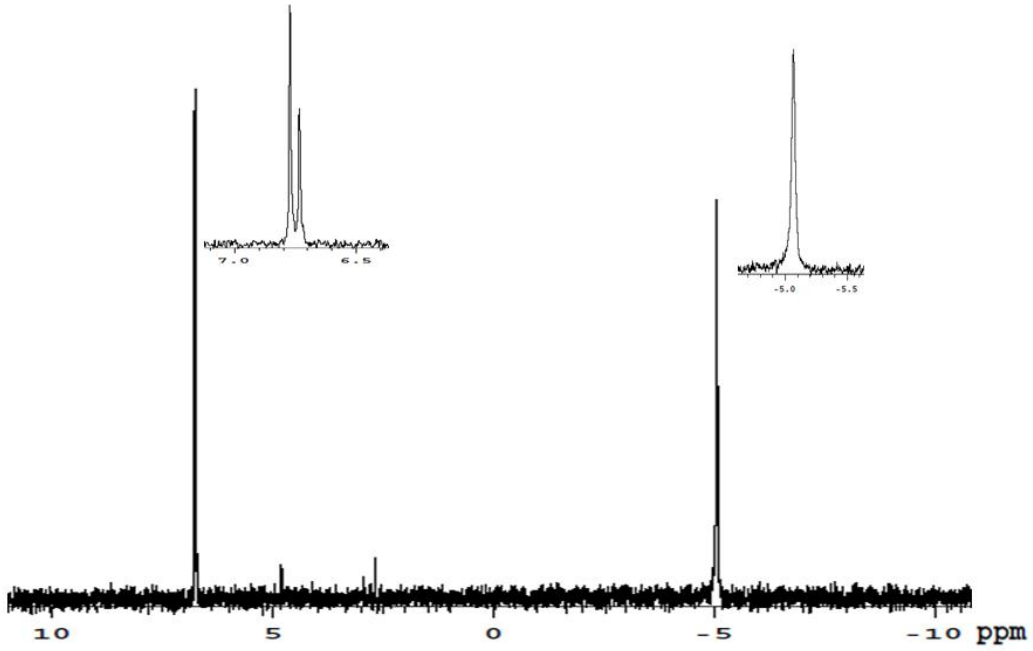


**Figure 6.23**: *$^{31}P$ NMR spectrum of PhnM reaction in $H_2O^{18}$*. PhnM (10 μM) with 1 mM RTP in the presence of 2 mM $Mg^{2+}$ and 1 mM $Zn^{2+}$ in 50 mM HEPES buffer pH 8.5 containing 35 % $H_2O^{18}$. The phosphoryl group of ribose-5-phosphate is at ~ 6.8 ppm and the pyrophosphate is at -5.0 ppm. There are two resonances at ~6.8 ppm due to the partial $O^{18}$-labelling of the phosphate. There is no extra resonance for the pyrophosphate and thus the attack of water on the triphosphate moiety of RTP in on the α–phosphoryl group.

All of the kinetic measurements were performed on this reaction using the Pi Colorlock (Gold) phosphate detection kit from Innova Biosciences according to the manufacturer's instruction at pH 8.5. The pyrophosphate produced in this reaction was

converted to inorganic phosphate by the addition of inorganic pyrophosphatase from Baker's yeast (Sigma). The kinetic constants obtained for the hydrolysis of RPnTP by PhnM were $k_{cat}$ = 6.4 $s^{-1}$, $K_m$ = 56 μM and $k_{cat}/K_m$ = 1.1 x $10^5$ $M^{-1}s^{-1}$. $Zn^{2+}$ and $Mg^{2+}$ supplementation were essential for optimal activity of PhnM. To determine the substrate profile for PhnM, D-ribose-5-triphosphate (RTP) and D-ribose-5-diphosphate (RDP) were tried as substrates. Both RTP and RDP were synthesized by the action of PhnI on ATP and ADP, respectively, and purified using anion exchange chromatography (*99*). Both RTP and RDP were substrates for PhnM. In both cases D-ribose-5-phosphate was one product. The other product was pyrophosphate for RTP and inorganic phosphate for RDP.

The kinetic constants for the hydrolysis of RTP by PhnM were $k_{cat}$ = 6.0 $s^{-1}$, $K_m$ = 98 μM and $k_{cat}/K_m$ = 6.1 x $10^4$ $M^{-1}s^{-1}$. For RDP the kinetic constants were $k_{cat}$ = 0.08 $s^{-1}$, $K_m$ = 200 μM and $k_{cat}/K_m$ = 3.8 x $10^2$ $M^{-1}s^{-1}$ (*99*). Thus, the substrate profiles showed that the RPnTP was the best substrate and that PhnM hydrolyzes the triphosphate moiety to form the PRPn and pyrophosphate. RTP is 100-fold more active than RDP. The kinetic constants did not change for the hydrolysis of RPnTP when PhnG, PhnH, PhnI, PhnK, PhnL and Factor-Xa were added to the assay mixture. Therefore there is no evidence that PhnM forms a complex with these other proteins.

*Catalytic Function of PhnJ.* The deletion of *phnJ* from *E. coli* led to the identification of α-D-ribose-1-methylphosphonate (RPn) in the growth medium and this has led to the prediction that α-D-ribose-1-methylphosphonate-5-phosphate (PRPn) is the ultimate substrate for the actual C-P lyase reaction (*103*). This conjecture was

consistent with our experimental results since this compound was synthesized from ATP and methylphosphonate by the combined actions of PhnI, PhnG, PhnH, PhnL and PhnM. Of the remaining two enzymes in the *phn* operon, the most likely protein to catalyze the actual carbon-phosphorus bond cleavage was PhnJ. PhnJ has four conserved cysteine residues with a spacing of $Cx_2Cx_{21}Cx_5C$ near the C-terminal end of the protein. These four conserved cysteine residues could form a metal-thiolate cluster or more likely, an iron-sulfur cluster. The cleavage of PRPn to PRcP (or PRP) was assumed to require a radical mechanism and such reactions could be catalyzed by radical SAM enzymes.

The radical SAM superfamily was first identified in 2001 by Sofia and co-workers, based on the structural and mechanistic similarities of lysine aminomutase (LAM), biotin synthase (BioB), lipoic acid synthase (LipA) and pyruvate formate lyase activating enzyme (PflA). Each of these enzymes uses a structurally conserved $(\beta/\alpha)_8$-TIM barrel motif to produce a 5'-deoxyadenosyl radical from S-adenosyl-L-methionine (SAM) using a unusual $[Fe_4S_4]$-cluster which is redox active in the reduced $[Fe_4S_4]^{1+}$ and the oxidized $[Fe_4S_4]^{2+}$ oxidation states (*117*). A recent comprehensive review by Frey et al. (*118*), has suggested that more than 2800 proteins belong to this superfamily. A signature feature for the members of this superfamily is a $Cx_3Cx_2C$ motif near the N-terminal end of the protein. These three cysteine residues nucleate the $[Fe_4S_4]$-cluster. This cluster binds SAM to the unique Fe that is not ligated to any three cysteine residues. The 5'-deoxyadenosyl radical generated from the reductive cleavage of SAM, abstracts a hydrogen atom from the substrate or the protein (to generate a protein radical) initiating the reaction. With the successful reconstitutions of ThiC (*119*) ($Cx_2Cx_4C$), HmdA (*120*)

($Cx_5Cx_2C$), and Dph2 (*121*), a more diverse combination of conserved cysteine residues can function for the assembly of the $[Fe_4S_4]$-cluster and perform similar radical reactions. Another comprehensive review by Booker et al. (*122*), lists more examples of members of the radical SAM superfamily lacking the canonical $Cx_3Cx_2C$ motif as well as enzymes possessing multiple iron-sulfur clusters. Elp3, a component of the factor required for transcriptional elongation ($Cx_4Cx_9Cx_2C$) is one such example. Another example is PqqE, which is one of the six proteins required for the biosynthesis of pyrroloquinoline quinone. This protein contains a non-canonical $Cx_2Cx_{27}C$ motif binding a $[Fe_4S_4]$-cluster capable of producing a 5'-deoxyadenosyl radical upon reduction along with another cluster of the canonical $Cx_3Cx_2C$ motif.

Literature precedents have hinted at the formation of some sort of metal-thiolate cluster on PhnJ (*99, 109*), based on the highly invariant $Cx_2Cx_{21}Cx_5C$ motif at the C-terminal of the protein. PhnJ purified aerobically with a GST-tag, had a black color. This was presumably due the non-specific binding of iron sulfide from the degradation of an iron-sulfur cluster upon exposure to air. Metal analysis using ICP-MS showed the presence of ~2.2 equivalents of Fe per monomer of PhnJ when purified aerobically. Thus PhnJ appeared to be capable of binding iron and sulfide. The metals ions bound to the aerobically purified PhnJ were removed with the addition of EDTA to the purification buffers. The apo-PhnJ was made anaerobic by passing argon through the protein solution and then an excess of sodium dithionite was added (5 mM). PhnJ was incubated in the glove box for four hours. Throughout the reconstitution experiments the oxygen concentration was maintained below 4 ppm. Reconstitution of the $[Fe_4S_4]$-

cluster was initiated by slow dropwise addition of a 50-fold enzyme excess of $FeSO_4$. After equilibrating anaerobically for three hours, a 50-fold excess of $Na_2S$ was added and the mixture incubated for an additional three hours. The excess iron and sulfide that formed insoluble iron sulfide (black solid) was removed by centrifugation, followed by ultrafiltration through a 10 kDa membrane. The protein with the reconstituted iron-sulfur cluster had a reddish-brown color. The UV-visible absorption spectrum of PhnJ, reconstituted with iron and sulfide, had a broad absorption band centered at 403 nm that is indicative of a $[Fe_4S_4]$-cluster (*99*). The absorption band disappears upon addition of 1 mM dithionite, suggesting the reduction of the $[Fe_4S_4]^{2+}$ cluster to the $[Fe_{44}S]^{1+}$ species, which is the active form for most radical SAM enzymes (*117-122*) (**figure 6.24)**. The discoloration was also indicative of the redox activity of the proteins within the radical SAM superfamily (*117-122*). Quantitation of the UV-visible spectrum of PhnJ suggested that the chemical reconstitution yield was approximately 40%. Even though there were prior suggestions that PRPn was the ultimate substrate for PhnJ, the putative C-P bond cleaving enzyme from the gene knockout studies carried out by Zechel, Hove-Jensen and co-workers (*103*), there were still two compounds that could have been potential substrates for cleavage by PhnJ of the C-P bond: PRPn and RPnTP. Both of these compounds were incubated with 125 μM PhnJ that was chemically reconstituted with a $[Fe_4S_4]$-cluster, 2 mM SAM and 1 mM dithionite, under anaerobic conditions at pH 6.8.

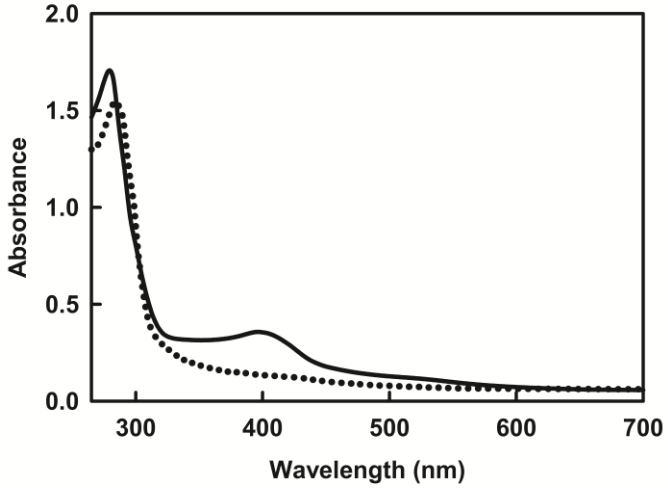


**Figure 6.24:** *UV-visible absorbance spectrum of PhnJ*. PhnJ (31 μM) after anaerobic chemical reconstitution of the Fe-S cluster (solid line). The peak at 280 nm is due to the protein absorbance and the absorbance peak centered around 403 nm represents the $[4Fe\text{-}4S]^{2+}$ cluster. The dotted line represents the absorbance spectrum of PhnJ (27 μM) reconstituted with a $[4Fe\text{-}4S]^{2+}$ cluster after reduction with sodium dithionite to form the $[4Fe\text{-}4S]^{+}$ cluster.

The reactions were analyzed by $^{31}P$ NMR spectroscopy but there was no change in the NMR spectrum for either substrate. Since PhnJ was expressed and purified as an N-terminal GST-fusion protein, the reaction was supplemented with Factor-Xa to cleave the GST-tag. No change in the $^{31}P$ NMR spectrum was observed with RPnTP, but a new resonance appeared at 16.2 ppm using PRPn as a substrate (*99*). The increase in the resonance at 16.2 ppm correlated with a decrease in the phosphonate resonance of PRPn at 16.6 ppm. The new resonance splits into a triplet in the $^{1}H$-coupled $^{31}P$ spectrum (*99*) demonstrating that the product is no longer a methyl phosphonate (**figure 6.25**). The

new resonance was consistent with a cyclic phosphate and the proton coupling constant of 21 Hz indicates that the phosphate moiety of the product was esterified to the protons attached to C1 and C2 of the ribose. This result was consistent with the findings of Zechel, Hove-Jensen and co-workers for the substrate of PhnP (*103*). Thus, PhnJ requires a reduced [$Fe_4S_4$]-cluster and SAM to catalyze the formation of α-D-ribose-1,2-cyclic phosphate-5-phosphate from PRPn. The overall reaction is illustrated in **Scheme 6.9**.

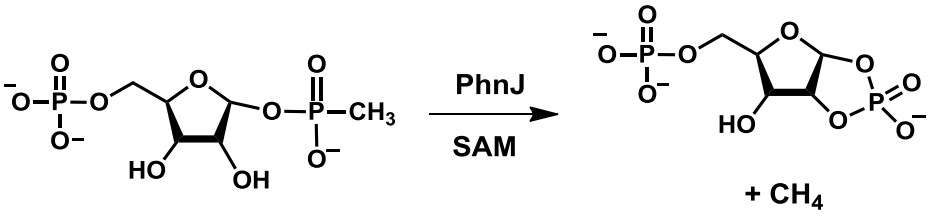


**Scheme 6.9:** Reaction catalyzed by PhnJ in the presence of SAM.

Gas chromatography (GC) and GC-mass spectrometry (MS) were used to confirm the formation of methane. All GC and GC-MS samples were prepared anaerobically. Gas chromatographic analysis of the headspace above the liquid showed a single peak that co-eluted with a methane standard (**Figure 6.26**). The formation of methane was confirmed by coupling the output of the GC to a mass spectrometer and detection of a mass of 16. Thus, the two products formed from the action of PhnJ on PRPn are methane and PRcP. To determine whether there were any byproducts of this reaction, an analysis was conducted to check for the formation of methanol and formaldehyde. Alcohol dehydrogenase was used to test the formation of methanol using $NAD^+$. A calibration curve was established based on the formation of NADH for

varying methanol. The reaction showed no formation of methanol. For the detection of formaldehyde, purpald was used. A standard curve was made and the reaction mixture showed no formation of formaldehyde. The addition of SAM, PhnJ, a reductant (dithionite) and Factor-Xa were required for the formation of PRcP and methane from the $[Fe_4S_4]^{1+}$ reconstituted PhnJ under strictly anaerobic conditions.

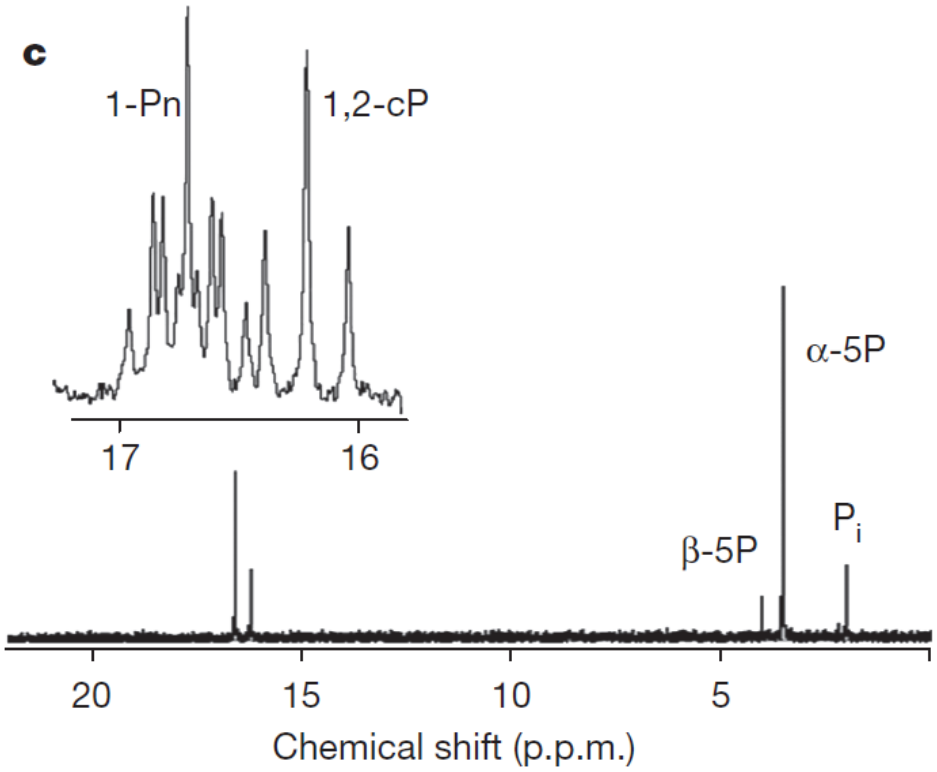


**Figure 6.25:** *The formation of PRcP from PRPn in the presence of PhnJ and SAM* (at pH 6.8). Inset, proton-coupled spectrum showing the formation of a new triplet that corresponds to the 1,2-cyclic moiety of PRcP (1,2,cP). The chemical shifts of the phosphate moiety on the fifth carbon atom of PRcP and PRPn are coincident with one another at 3.4 ppm.

To determine the fate of SAM during the reaction, HPLC and amino acid analysis were employed. Amino acid analysis of the reaction products from SAM in the reaction catalyzed by PhnJ was performed by the Protein Chemistry Laboratory, Texas A&M University. The control reaction showed less than 0.01 μM L-methionine. In the reaction mixture with PhnJ (120 μM), 150 μM of L-methionine was detected. This established that one of the products of SAM was methinonine. The HPLC analysis was used for determining the other reaction products of SAM with PhnJ. All of the reactions were kept anaerobic for 3 hours after which the precipitated enzyme was removed by centrifugation. HPLC analysis showed the formation of 5'-deoxyadenosine (**Figure 6.27)** and amino acid analysis confirmed the formation of methionine.

These products were only formed when PhnJ (with a reconstituted iron-sulfur center), Factor-Xa, SAM, dithionite and PRPn were added to the reaction mixture under strictly anaerobic conditions. The omission any one of the above components resulted in no formation of 5'-deoxyadenosine. The small number of turnovers per enzyme may reflect the poor solubility of PhnJ after proteolytic cleavage of the N-terminal GST-fusion tag. The concentration of PRcP, 5'-deoxyadenosine, methionine, and methane formed in the presence of PhnJ showed that 1-10 turnovers of product were formed per PhnJ.

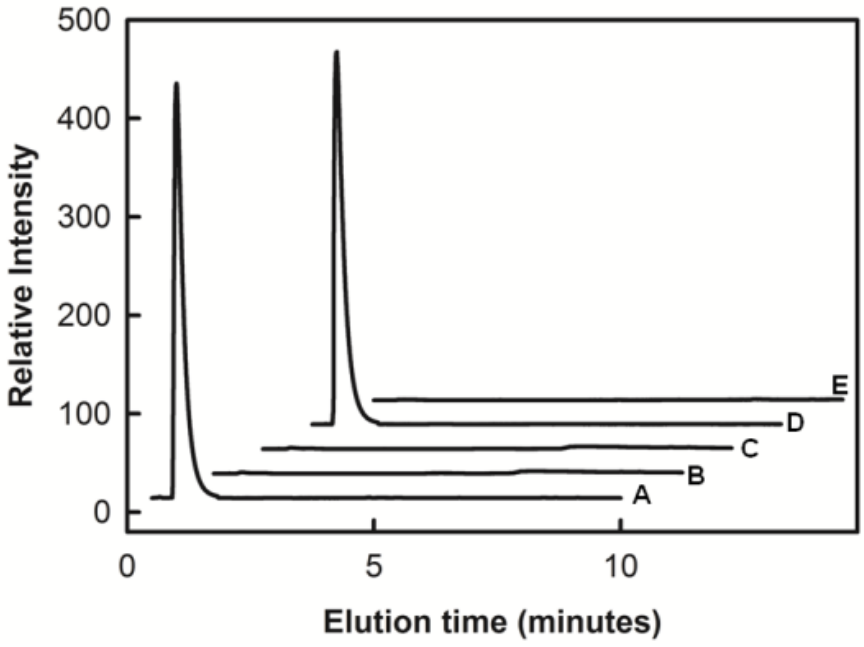


**Figure 6.26**: *Gas chromatographic analysis of PhnJ reaction*. GC analysis for methane formation after incubation of PhnJ (150 μM), SAM (2 mM), dithionite (1 mM), and PRPn (2 mM) in the presence of 50 units Factor-Xa and 1X Factor-Xa buffer in a volume of 2.3 mL with a headspace of ~500 μL. (A) Methane standard (714 ng). (B) Incubation of reaction mixture with deletion of PhnJ. (C) Incubation of reaction mixture with deletion of PRPn. (D) Incubation of entire reaction mixture. (E) Incubation of the reaction mixture with deletion of SAM. (In samples B, C, D and E; 50 μL of the headspace was injected in the GC instrument).

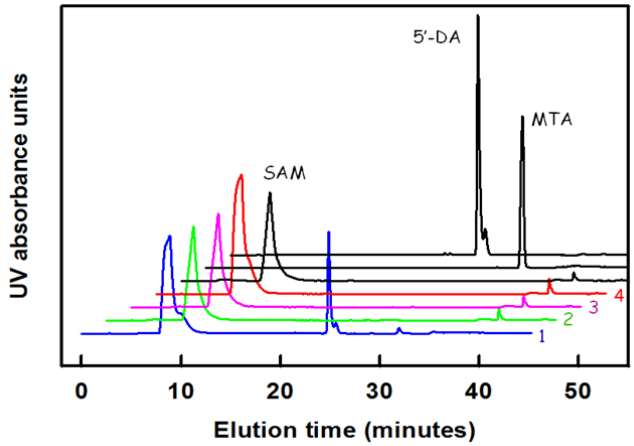


**Figure 6.27**: HPLC trace analysis for products of SAM by PhnJ. Standards for the detection of the reaction products from S-adenosyl-L-methionine (SAM) by PhnJ in presence of dithionite and Factor-Xa. Standards (black traces): 0.5 mM S-adenosyl-L-methionine (SAM) in 150 mM HEPES, 250 mM NaCl, 10 % v/v glycerol, 50 units Factor Xa and 1X Factor Xa reaction buffer at pH 8.5; 0.5 mM 5'-deoxyadenosine (5'-DA) in 150 mM HEPES, 250 mM NaCl, 10 % v/v glycerol, 50 units Factor Xa and 1X Factor Xa reaction buffer at pH 8.5; 0.5 mM 5'-deoxy-5'-methylthioadenosine (MTA) in 150 mM HEPES, 250 mM NaCl, 10 % v/v glycerol, 50 units Factor Xa and 1X Factor Xa reaction buffer at pH 8.5. The reaction products of SAM in the reaction catalyzed by PhnJ with PRPn: (1) Reaction products after mixing 60 µM PhnJ, 0.5 mM SAM, 1 mM dithionite, 2 mM α-D-ribose-1-methylphosphonate-5-phosphate in 150 mM HEPES, 250 mM NaCl, 10 % v/v glycerol, 50 units Factor-Xa and 1X Factor-Xa reaction buffer at pH 8.5. (2) Same as 1 except PhnJ was omitted. (3) Same as 1 except that dithionite was omitted. (4) Same as 1 except Factor-Xa omitted. 5'-deoxyadenosine was identified as the major reaction product from SAM during the reaction with PhnJ.

*Reconstitution of the C-P Lyase Pathway.* PhnJ is a putative radical SAM enzyme and the working model for the cleavage of the C-P bond of the phosphonate moiety is **Scheme 6.10**. The cleavage of the C-P bond is PRPn by PhnJ reconstituted with a [4Fe-4S]+ cluster and SAM is initiated by electron transfer from the Fe-S cluster to reductively cleave SAM and thus transiently generate L-methionine (L-met) and a 5'-deoxyadenosyl radical (Ado-$CH_2^{\bullet}$). This radical may subsequently catalyze the formation of a protein radical (PhnJ-$X^{\bullet}$), presumably a cysteine-based thiyl radical. Thiyl radicals have been previously demonstrated in pyruvate-formate lyase (*123, 124*), methyl coenzyme M reductase (*125*) and ribonucleotide reductase (*126*). The thiyl radical may attack the phosphonate moiety of the substrate to liberate a methyl radical with the formation of a thioester intermediate. Intramolecular attack by the hydroxyl of the second carbon atom of the substrate would generate PRcP and the free thiol group. Methane would be formed through hydrogen atom abstraction from either 5-deoxyadenosine or the putative cysteine residue.

The mechanism for the conversion of alkyl phosphonates to phosphate in *E. coli* was elucidated. PhnI (a novel nucleosidase), in the presence of PhnG, PhnH, and PhnL, catalyzes the formation of RPnTP from MgATP and methylphosphonate. PhnM (an amidohydrolase) catalyzes the hydrolysis of RPnTP to form pyrophosphate and PRPn. PhnJ can be chemically reconstituted with a [$Fe_4S_4$]-cluster with ferrous sulfate, sodium sulfide and sodium dithionite under strictly anaerobic conditions. The reconstituted PhnJ catalyzes the homolytic cleavage of the C-P bond of PRPn to form PRcP and

methane in the presence of SAM. The C-P lyase pathway is summarized in **Scheme 6.11.**

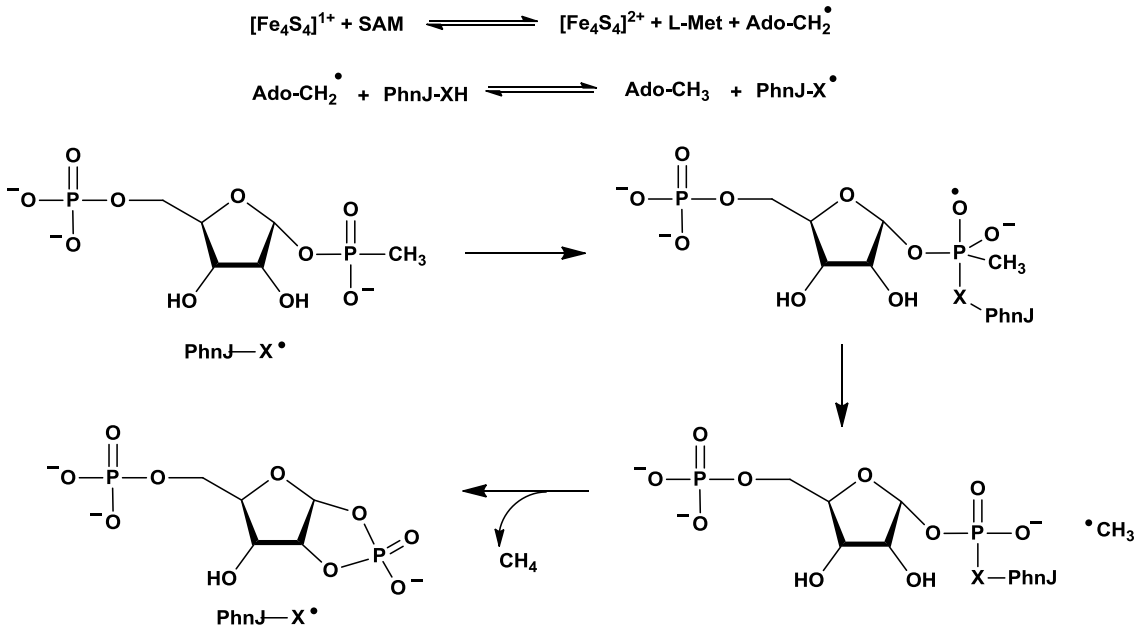


**Scheme 6.10:** Working model for the transformation of PRPn to PRcP

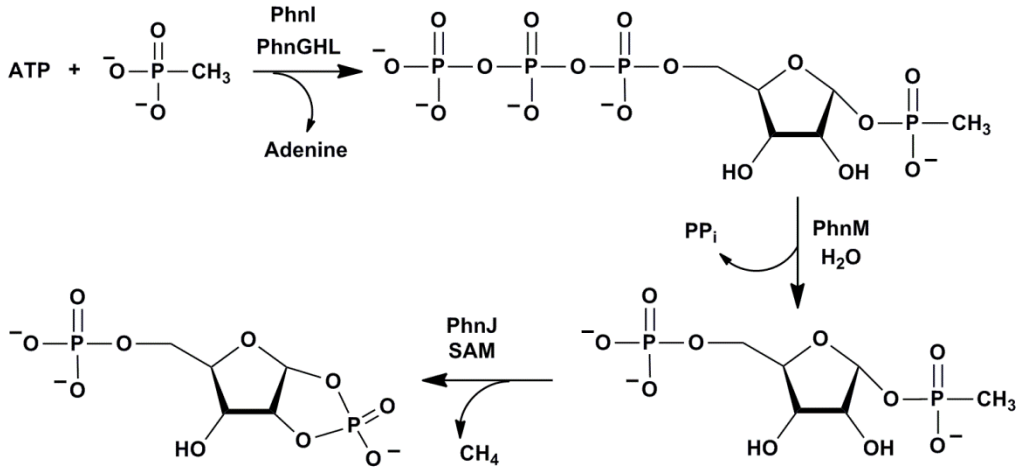


**Scheme 6.11:** Reaction pathway for the conversion of methyl phosphonate to methane and PRcP.

# CHAPTER VII

# SUMMARY AND CONCLUSIONS

Adenine deaminase (ADE) catalyzes the conversion of adenine to hypoxanthine and ammonia. The enzyme isolated from *Escherichia coli* using standard expression conditions was largely inactive towards the deamination of adenine ($k_{cat}$ ~2 $s^{-1}$). When iron was sequestered with a metal chelator (2,2'-dipyridyl) and the growth medium was supplemented with $Mn^{2+}$ prior to induction, the purified enzyme was substantially more active for the deamination of adenine with values of $k_{cat}$ and $k_{cat}/K_m$ of 200 $s^{-1}$ and 5 x $10^5$ $M^{-1}s^{-1}$, respectively. The apo-enzyme was prepared and reconstituted with $Fe^{2+}$, $Zn^{2+}$, or $Mn^{2+}$. In each case, two enzyme-equivalents of metal were necessary for reconstitution of the deaminase activity. This work provides the first example of any member within the deaminase sub-family of the amidohydrolase superfamily (AHS) to utilize a binuclear metal center for the catalysis of a deamination reaction. [$Fe^{II}/Fe^{II}$]-ADE was oxidized to [$Fe^{III}/Fe^{III}$]-ADE with ferricyanide with inactivation of the deaminase activity. Reducing [$Fe^{III}/Fe^{III}$]-ADE with dithionite restored the deaminase activity and thus the di-ferrous form of the enzyme is essential for catalytic activity. No evidence for spin-coupling between metal ions was evident by EPR or Mössbauer spectroscopies. The three-dimensional structure of adenine deaminase from *Agrobacterium tumefaciens* (Atu4426) was determined by X-ray crystallography at 2.2 Å resolution and adenine was modeled into the active site based on homology to other members of the amidohydrolase superfamily. Based on the model of the adenine-ADE

complex and subsequent mutagenesis experiments, the roles for each of the highly conserved residues were proposed. Solvent isotope effects, pH rate profiles and solvent viscosity were utilized to propose a chemical reaction mechanism and the identity of the rate limiting steps.

Adenine deaminase (ADE) from the amidohydrolase superfamily of enzymes catalyzes the conversion of adenine to hypoxanthine and ammonia. The enzyme isolated from *Escherichia coli* using standard expression conditions was largely inactive towards the deamination of adenine ($k_{cat}$ ~2 $s^{-1}$). Molecular weight determinations by mass spectrometry provided evidence that multiple histidine and methionine residues were oxygenated. When iron was sequestered with a metal chelator and the growth medium supplemented with $Mn^{2+}$ prior to induction, the post-translational modifications disappeared. The enzyme expressed and purified under these conditions was substantially more active for the deamination of adenine, with values of $k_{cat}$ and $k_{cat}/K_m$ of 200 $s^{-1}$ and 5 x $10^5$ $M^{-1}s^{-1}$, respectively. Apo-enzyme was prepared and reconstituted with two equivalents of $FeSO_4$; ICP-MS and Mössbauer spectroscopy demonstrated that this protein contained two high-spin ferrous ions per monomer of ADE. In addition to the adenine deaminase activity, [$Fe^{II}/Fe^{II}$]-ADE catalyzed the conversion of $H_2O_2$ to $O_2$ and $H_2O$. The values of $k_{cat}$ and $k_{cat}/K_m$ for the catalase activity are 200 $s^{-1}$ and 2.4 x $10^4$ $M^{-1}s^{-1}$ respectively.

[$Fe^{II}/Fe^{II}$]-ADE underwent more than 100 turnovers with $H_2O_2$ before the enzyme was inactivated due to oxygenation of histidine residues critical for metal binding. A model is proposed for the disproportionation of hydrogen peroxide by [$Fe^{II}/Fe^{II}$]-ADE

that involves the cycling of the binuclear metal center between the di-ferric and di-ferrous oxidation states. Oxygenation of active site residues occurs from the release of hydroxyl radicals. The three-dimensional structure of [$Fe^{II}/Fe^{II}$]-ADE was determined by X-ray diffraction methods. This is the first report of a redox reaction for any member of the amidohydrolase superfamily.

Adenine deaminase (ADE) is a member of the amidohydrolase superfamily (AHS). ADE has shown to catalyze two distinct reactions, the hydrolytic deamination of adenine and the redox disproportionation of hydrogen peroxide for diiron ADE. Kinetic studies for ADE yield similar inverse solvent isotope effects as adenosine deaminase and cytosine deaminase, which are the other kinetically characterized members of the AHS. Proton inventory studies on ADE show two distinct patterns, for $k_{cat}$ and $k_{cat}/K_m$, suggesting involvement of two distinct protons in the kinetic mechanism. A single downfield proton with a chemical shift ($\delta \sim 17.0$ to 18.0 ppm) consistent with those identified for low-barrier hydrogen bonds (LBHBs) was identified using $^1$H-NMR analysis for the Zn/Zn-ADE. LBHBs have been found to be critical in other enzymes and have been extensively studied for serine proteases. Here we use mutagenesis and inhibitor studies coupled to $^1$H-NMR analysis to reveal the nature of the downfield proton and found it was associated with the deaminase activity. The exact assignment of the downfield proton still remains unknown; however this study reports the first instance of any metalloenzyme possessing a LBHB in catalysis. Previous experiments performed on serine proteases in the identification of the LBHB might prove useful in finding the LBHB of ADE.

Two enzymes from the amidohydrolase superfamily (AHS) were discovered to catalyze the deamination of N-6-methyladenine to hypoxanthine and methylamine. The methylation of adenine in bacterial DNA is a common modification for protection of the host DNA against restriction endonucleases. The enzyme from *Bacillus halodurans*, Bh0637, catalyzes the deamination of N-6-methyladenine with a $k_{cat}$ of 185 $s^{-1}$ and a $k_{cat}/K_m$ of 2.5 x $10^6$ $M^{-1}s^{-1}$. Bh0637 catalyzes the deamination of N-6-methyladenine 2 orders of magnitude faster than adenine. A comparative model of Bh0637 was computed using the three dimensional structure of Atu4426 (PDB code: 3nqb) as a structural template and computational docking was used to rationalize the preferential utilization of N-6-methyladenine over adenine. This is the first identification of an N-6-methyladenine deaminase (6-MAD).

The reaction mechanism for the enzymatic conversion of methyl phosphonate to phosphate and methane in *Escherichia coli* has eluded researchers over the last three decades despite significant genetic and *in-vivo* studies. The *phn* operon governs the C-P lyase activity in *E. coli.* The essential genes within the *phn* operon are *phnGHIJKLM*. The proteins encoded by *phnGHM* were over-expressed in *E. coli* and purified to homogeneity using standard protocols. The proteins encoded by *phnIJKL* were soluble only when expressed as N-terminal fusion proteins with glutathione S-transferase (GST). PhnI catalyzes the formation of α-D-ribose-1-methylphosphonate-5-triphosphate (RPnTP) from MgATP and methylphosphonate in the presence of PhnG, PhnH, and PhnL after *in situ* cleavage of the GST-tags. PhnI alone catalyzes the hydrolytic cleavage of MgATP to adenine and D-ribose-5-triphosphate. PhnM catalyzes the

hydrolysis of α-D-ribose-1-methylphosphonate-5-triphosphate to α-D-ribose-1-methylphosphonate-5-phosphate (RPnP) and pyrophosphate with attack of water on the α-phosphoryl group of the triphosphate moiety of RPnTP. PhnJ was reconstituted with an iron-sulfur cluster via the anaerobic addition of $FeSO_4$, $Na_2S$ and $Na_2S_2O_4$ under strictly anaerobic conditions. The $[Fe_4S_4]$-reconstituted PhnJ GST-fusion protein catalyzes the radical cleavage of the phosphorus-carbon bond of α-D-ribose-1-methylphosphonate-5-phosphate to α-D-ribose-1,2-cyclic-phosphate-5-phosphate and methane in the presence of *S*-adenosyl-L-methionine under strictly anaerobic conditions, upon *in situ* cleavage of the GST-tag.

# REFERENCES

1. Gerlt, J. A., Allen, K. N., Almo, S. C., Armstrong, R. N., Babbitt, P. C., Cronan, J. E., Dunaway-Mariano, D., Imker, H. J., Jacobson, M. P., Minor, W., Poulter, C. D., Raushel, F. M., Sali, A., Shoichet, B. K., and Sweedler, J. V. (2011) The enzyme function initiative. *Biochemistry 50*, 9950-9962.

2. Schnoes, A. M., Brown, S. D., Dodevski, I., and Babbitt, P. C. (2009) Annotation error in public databases: Misannotation of molecular function in enzyme superfamilies. *PLoS Comp. Biol. 5*, e1000605.

3. Holm, L., and Sander, C. (1997) An evolutionary treasure: Unification of a broad set of amidohydrolases related to urease, *Proteins: Struct., Funct., Genet. 28*, 72-82.

4. Benning, M. M., Kuo, J. M., Raushel, F. M., and Holden, H. M. (1995) Three dimensional structure of the binuclear center of phosphotriesterase. *Biochemistry 34*, 7973-7978.

5. Wilson, D. K., Quiocho, F. A. (1993) A pre-transition state mimic of an enzyme: X-ray structure of adenosine deaminase with bound 1-deazaadenosine and zinc-activated water. *Biochemistry 32*, 1689-1694.

6. Jabri, E., Carr, M. B., Hausinger, R. P., and Karplus, P. A. (1995) The crystal structure of urease from *Klebsiella aerogenes. Science 268*, 345-347.

7. Seibert, C. M., and Raushel, F. M. (2005) Structural and catalytic diversity within the amidohydrolase superfamily. *Biochemistry 44*, 6383-6391.

8. Hall, R. S., Federov, A. A., Xu, C., Federov, E. V., Almo, S. C., and Raushel, F. M. (2011) Three dimensional structure and catalytic mechanism of cytosine deaminase. *Biochemistry 50*, 5077-5085.

9. Hall, R. S., Brown, S., Federov, A. A., Federov, E. V., Xu, C., Babbitt, P. C., Almo, S. C., and Raushel, F. M. (2007) Structural diversity within the mononuclear and binuclear active sites of N-acetyl-D-glucosamine-6-phosphate deacetylase. *Biochemistry 46*, 7953-7962.

10. Raushel, F. M. (2010) Functional annotation of orphan enzymes within the amidohydrolase superfamily. *Beilstein Institut ESCEC Proceedings 4*, 9-19.

11. Tatusov, R. L., Galperin, M. Y., Natale, D. A., and Koonin, E. V. (2000) The COG database: A tool for genome-scale analysis of protein functions and evolution. *Nucleic Acids Res. 28*, 33-36.

12. Shannon, P., Markiel, A., Ozier, O., Baliga, N. S., Wang, J. T., Ramage, D., Amin, N., Schwikowski, B., Ideker, T. (2003) Cytoscape: A software environment for integrated models of biomolecular interaction networks. *Genome Res. 13*, 2498-2504.

13. Koch, A. L., and Vallee, G. (1959) The properties of adenosine deaminase and adenosine nucleoside phosphorylase in extracts of *Escherichia coli. J. Biol. Chem. 234*, 1213-1218.

14. Leung, H. B., and Schramm, V. L. (1980) Adenylate degradation in *Escherichia coli. J. Biol. Chem. 255*, 10867-10874.

15. Nygaard, P., Duckert, P., and Saxild, H. H. (1996) Role of adenine deaminase in purine salvage and nitrogen metabolism and the characterization of the *ade* gene in *Bacillus subtilis. J. Bact. 178*, 846-853.

16. Matsui, H., Shimoka, M., Kawasaki, H., Takenaka, Y., Kurahashi, O. (2001) Adenine deaminase activity of the *yicP* gene product of *Escherichia coli. Biosci. Biotech. Biochem. 65*, 1112-1118.

17. Petersen, C., Moller, L. B., Valentin-Hansen, P. (2002) The cryptic adenine deaminase gene of *Escherichia coli. J. Biol. Chem. 277*, 31373-31380.

18. Oestreicher, N., Ribard, C., Scazzocchio, C. (2007) The *nadA* gene of *Aspergillus nidulans*, encoding adenine deaminase is subject to a unique regulatory pattern. *Fungal Genet. Biol. 45*, 760-775.

19. Voet, D., Voet, J. G., and Pratt, C. W. (2006) Fundamentals of Biochemistry, 2nd Edition. *Nucleotide Metabol. 22*, 787-816.

20. Kamat, S. S., Bagaria, A., Kumaran, D., Holmes-Hampton, G. P., Fan, H., Sali, A., Sauder, J. M., Burley, S. K., Lindahl, P. A., Swaminathan, S., and Raushel, F. M. (2011) Catalytic mechanism and three dimensional structure of adenine deaminase. *Biochemistry 50*, 1917-1927.

21. Kamat, S. S., Holmes-Hampton, G. P., Bagaria, A., Kumaran, D., Tichy, S. E., Gheyi, T., Zheng, X., Bain, K., Groshong, C., Emtage, S., Sauder, J. M., Burley, S. K., Swaminathan, S., Lindahl, P. A., and Raushel, F. M. (2011) The catalase activity of diiron adenine deaminase. *Protein Sci. 20*, 2080-2094.

22. Marti-Arbona, R., Fresquet, V., Thoden, J. B., Davis, M. L., Holden, H. M., and Raushel, F. M. (2005) Mechanism of the reaction catalyzed by isoaspartyl dipeptidase from *Escherichia coli. Biochemistry 44*, 7115-7124.

23. Kreb, D., Alhapel, A., Pierik, A. J., and Essen, L. O. (2008) The crystal structure of enamidase: A bifunctional enzyme of the nicotinate catabolism. *J. Mol. Biol. 384*, 837-847.

24. Kamat, S. S., Fan, H., Sauder, J. M., Burley, S. K., Shoichet, B. K., Sali, A., and Raushel, F. M. (2011) Enzymatic deamination of the epigenetic base N-6-methyladenine. *J. Am. Chem. Soc. 133*, 2080-2083.

25. Hsieh, Y. J, and Wanner, B. L. (2010) Global regulation by the seven component Pi signaling system. *Curr. Opin. Microbiol. 13*, 198-203.

26. VanBogelen, R. A., Olson, E. R., Wanner, B. L., and Neidhardt, F. C. (1996) Global analysis of proteins synthesized during phosphorus restriction in *Escherichia coli. J. Bact. 178*, 4344-4366.

27. Ternan, N. G., McGrath, J. W., McMullan, G., and Quinn, J. P. (1998) Organophosphates: Occurrence, synthesis and biodegradation by microorganisms. *World J. Microbiol. Biotechnol. 14*, 635-647.

28. Kononova, S. V., and Nesmeyanova, M. A. (2002) Phosphonates and their degradation by microorganisms. *Biochemistry (Moscow) 67*, 184-195.

29. Quinn, J. P., Kulakova, A. N., Cooley, N. A., and McGrath, J. W. (2007) New ways to break an old bond: The bacterial carbon-phosphorus hydrolases and their role in biogeochemical phosphorus cycling. *Environ. Microbiol. 9*, 2392-2400.

30. Villareal-Chiu, J. F., Quinn, J. P., and McGrath, J. W. (2012) The genes and enzymes of phosphonate metabolism by bacteria, and their distribution in the marine environment. *Frontiers in Microbiol. 3*, 19.

31. Zhang, Q., van der Donk, W. A. (2012) Answers to the carbon-phosphorus lyase conundrum. *ChemBioChem 13*, 627-629.

32. Metcalf, W. W., and Wanner, B. L. (1993) Mutational analysis of an *Escherichia coli* fourteen-gene operon for phosphonate degradation, using Tn*phoA'* elements. *J. Bact. 175*, 3430-3442.

33. Metcalf, W. W., and Wanner, B. L. (1993) Evidence for a fourteen-gene *phnC* to *phnP* locus for phosphonate metabolism in *Escherichia coli. Gene 129*, 27-32.

34. Wang, Z., and Quiocho, F. A. (1998) Complexes of adenosine deaminase with two potent inhibitors: X-ray structures in four independent molecules at pH of maximum activity. *Biochemistry 37*, 8314-8324.

35. Wilson, D. K., Rudolph, F. B., and Quincho, F. A. (1991) Atomic structure of adenosine deaminase complexed with transition state analog: Understanding catalysis and immunodeficiency mutations. *Science 252*, 1278-1284.

36. Benning, M. M., Shim, H., Raushel, F. M., and Holden, H. M. (2001) High Resolution structures of different metal substituted forms of phosphotriesterase from *Pseudomonas diminuta. Biochemistry 40*, 2712-2722.

37. Benning, M. M., Hong, S-B., Raushel, F. M., and Holden, H. M. (2000) The binding of substrate analogs to phosphotriesterase. *J. Biol. Chem. 275*, 30556-30560.

38. Thoden, J. B., Marti-Arbona, R., Raushel, F. M., and Holden, H. M., (2003) High-resolution X-ray structure of isoaspartyl dipeptidase from *Escherichia coli. Biochemistry 42*, 4874-4882.

39. Pace, C. N., Vajdos, F., Fee, L., Grimsley, G., and Gray, T. (1995) How to measure and predict the molar absorption coefficient of a protein. *Protein Sci. 4*, 2411-2423.

40. Hall, R. S., Xiang, D. F., Xu, C., and Raushel, F. M. (2007) N-acetyl-D-glucosamine-6-phosphate deacetylase: Substrate activation via a single divalent metal ion. *Biochemistry 46*, 7942-7952.

41. Muszbek, L., Polgar, J., and Fesus, L. (1985) Kinetic determination of blood coagulation factor XIII in plasma. *Clin. Chem. 31*, 35-40.

42. Chenlo, F., Moreira, R., Pereira, G., and Ampudia, A. (2002) Viscosities of aqueous solutions of sucrose and sodium chloride of interest in osmotic dehydration processes. *J. Food Eng. 54,* 347-352.

43. Morrison, J. F. (1969) Kinetics of the reversible inhibition of enzyme-catalysed reactions by tight-binding inhibitors. *Biochim. Biophys. Acta 185*, 269-286.

44. Shim, H., and Raushel, F. M. (2000) Self-assembly of the binuclear metal center of phosphotriesterase. *Biochemistry 39*, 7357-7364.

45. Dewitt, J. G., Bentsen, J. G., Rozenweig, A. C., Hedman, B., Green, J., Pilkington, S., Papaefthymiou, G. C., Dalton, H., Hodgson, K. O., and Lippard, S. J. (1991) X-ray absorption, Mössbauer and EPR studies of the dinuclear iron center in the hydroxylase component of methane monooxygenase. *J. Am. Chem. Soc. 113,* 9219-9235.

46. Thomann, H., Bernardo, M., McCormick, J. M., Pulver, S., Andersson, K. K., Lipscomb, J. D., and Solomon, E. I. (1993) Pulsed EPR studies on the mixed valent [Fe(II)Fe(III)] forms of hemerythrin and methane monooxygenase: Evidence for a hydroxide bridge. *J. Am. Chem. Soc. 115*, 8881-8882.

47. Kurtz, D. M. Jr. (2006) Avoiding high-valent iron intermediates: Superoxide reductase and ruberythrin. *J. Inorg. Biochem. 100*, 679-693.

48. Weiss, P. M., Cook, P. F., Hermes, J. D., and Cleland, W. W. (1987) Evidence from nitrogen-15 and solvent deuterium isotope effects on the chemical mechanism of adenosine deaminase. *Biochemistry 26*, 7378-7384.

49. Cleland, W. W. (1992) Low-barrier hydrogen bonds and low fractionation factor bases in enzymatic reactions. *Biochemistry 31*, 317-319.

50. Merkler, D. J., and Schramm, V. L. (1993) Catalytic mechanism of yeast adenosine 5'-monophosphate deaminase. Zinc content, substrate specificity, pH studies, and solvent isotope effects. *Biochemistry 32*, 5792-5799.

51. Noble, R. W., and Gibson, Q. H. (1970) The reaction of ferrous horseradish peroxidase with hydrogen peroxide. *J. Biol. Chem. 245*, 2409-2413.

52. Hartmann, T., Hartmann, P. P., Wetteland, C., and Lu, N. (2003) Spectroscopic determination of hypochlorous acid, in chloride brine solutions, featuring 5 MeV proton beam line experiments. *Rad. Phys. Chem*. *66*, 335-341.

53. Zielonka, J., Vivar, J. V., and Kalyanaraman, B. (2008) Detection of 2-hydroxyethidium in cellular systems: A unique marker product of superoxide and hydroethidine. *Nature Protocols 3*, 8-21.

54. Murray, L. J., Naik, S. G., Ortillo, D. O., Serres, R. G., Lee, J. K., Huynh, B. H., and Lippard, S. J. (2007) Characterization of the arene-oxidizing intermediate in ToMOH as a diiron(III) species. *J. Am. Chem. Soc. 129*, 14500-14510.

55. Das, K. C., and Misra, H. P. (1992) Lidocaine: A hydroxyl radical scavenger and singlet oxygen quencher. *Mol. Cel. Biochem. 115*, 179-185.

56. Dukan, S., and Toutati, D. (1996) Hypochlorous Acid Stress in *Escherichia coli:* Resistance, DNA damage and comparison with hydrogen peroxide stress. *J. Bact. 178*, 6145-6150.

57. Jacob, H. E. (1970) Redox Potential. *Methods in Microbiol.*, 94-95.

58. Sukumaran, V. S., and Ramalingam, A. (2006) Spectral characteristics and nonlinear studies of crystal violet dye. *Spectrochemica Acta 63*, 673-676.

59. Bertini, I., Gray, H. B., Stiefel, E. I., and Valentine, J. S. (2006) Peroxidase and catalases. *Biol. Inorg. Chem.*, 343-354.

60. Messerchmidt et al. (2001) Heme catalases. *Handbook of Metalloproteins 1*, 486-502.

61. Imlay, J. A. (2008) Cellular defenses against superoxide and hydrogen peroxide. *Annu. Rev. Biochem. 77*, 755-776.

62. Waldo GS, Penner-Hahn JE (1995) Mechanism of manganese catalase peroxide disproportionation: Determination of manganese oxidation states during turnover. *Biochemistry 34*, 1507-1512.

63. Barynin VV, Whittaker MM, Antoyuk SV, Lamzin VS, Harrison PM, Artymiuk PJ, Whittaker JW (2001) Crystal structure of manganese catalase from *Lactobacillus plantarum. Structure 9*, 725-738.

64. Friedle, S., Kodanko, J. J., Morys, A. J., Hayashi, T., Loccoz, P. M., and Lippard, S. J. (2009) Modeling the syn disposition of nitrogen donors in non-heme diiron enzymes. Synthesis, characterization, and hydrogen peroxide reactivity of diiron(III) complexes with syn N-donor ligand $H_2BPG_2DEV$. *J. Am. Chem. Soc. 131*, 14508-14520.

65. Lee, J., and Helmann, J. D. (2006) The perR transcription factor senses $H_2O_2$ by metal catalysed histidine oxidation. *Nature 340*, 363-367.

66. Moye, W. S. R. (2006) Redox sensing and histidine oxidation: no longer perR-fect strangers. *Nature Chem. Biol. 5*, 234-235.

67. Sobota, J. M., and Imlay, J. A. (2011) Iron enzyme ribulose-5-phosphate 3-epimerase in *Escherichia coli* is rapidy damaged by hydrogen peroxide but can be protected by manganese. *PNAS 108*, 5402-5407.

68. Liu, A., and Zhang, H. (2006) Transition metal-catalyzed non-oxidative decarboxylation reactions. *Biochemistry 45*, 10407-10411.

69. Nguyen, T. T., Brown, S., Federov, A. A., Federov, E. V., Babbitt, P. C., Almo, S. C., and Raushel, F. M. (2008) At the periphery of the amidohydrolase superfamily : Bh0493 from *Bacillus halodurans* catalyzes the isomerization of D-galacturonate to D-tagaturonate. *Biochemistry 47*, 1194-1206.

70. Nguyen, T. T., Federov, A. A., Williams, L., Federov, E. V., Li, Y., Xu, C., Almo, S. C., and Raushel, F. M. (2009) The mechanism of the reaction catalyzed by uronate

isomerase illustrates how an isomerase may have evolved from a hydrolase within the amidohydrolase superfamily. *Biochemistry 48*, 8879-8890.

71. Schiott, B., Iversen, B. B., Madsen, G. K. H., Larsen, F. K., and Bruice, T. C. (1998) On the electronic nature of low-barrier hydrogen bonds in enzymatic reactions. *PNAS 95*, 12799-12802.

72. Cleland, W. W., Frey, P. A., and Gerlt, J. A. (1998) The low barrier hydrogen bond in enzymatic catalysis. *J. Biol. Chem. 273*, 25529-25532.

73. Cleland, W. W., and Kreevoy, M. M. (1994) Low-barrier hydrogen bonds and enzymic catalysis. *Science 264*, 1887-1890.

74. Ash, E. L., Sudmeier, J. L., Fabo, E. C. D., and Bachovchin, W. W. (1997) A low-barrier hydrogen bond in the catalytic triad of serine proteases? Theory versus experiment. *Science 278*, 1128-1132.

75. Robillard, G., and Shulman, R. G. (1972) High resolution nuclear magnetic resonance study of the histidine-aspartate hydrogen bond in chymotrypsin and chymotrypsinogen. *J. Mol. Biol. 71*, 507-511.

76. Markley, J. L. (1978) Hydrogen bonds in serine proteases and their complexes with protein proteinase inhibitors. Proton nuclear magnetic resonance studies. *Biochemistry 17*, 4648-4656.

77. Frey, P. A. (2002) Characterization of a low barrier hydrogen bond in the active site of chymotrypsin. *J. Mol. Struct. 615*, 153-161.

78. Frey, P. A. (2004) Strong hydrogen bonding in chymotrypsin and other serine proteases. *J. Phys. Org. Chem. 17*, 511-520.

79. Frey, P. A. (2001) Strong hydrogen bonding in molecules and enzymatic complexes. *Magn. Reson. Chem. 39*, S190-S198.

80. Lin, J., Westler, W. M., Cleland, W. W., Markley, J. L., and Frey, P. A. (1998) Fractionation factors and activation energies for exchange of the low barrier hydrogen bonding proton in peptidyl trifluoromethyl ketone complexes of chymotrypsin. *PNAS 95*, 14664-14668.

81. Frey, P. A., Whitt, S. A., and Tobin, J. B. (1994) A low-barrier hydrogen bond in the catalytic triad of serine proteases. *Science 264*, 1927-1930.

82. Bachovchin, W. W. (1985) Confirmation of the assignment of the low-field proton resonance of serine proteases by using specifically nitrogen-15 labeled enzyme. *PNAS 82*, 7948-7951.

83. Poi, M. J., Tomaszewski, J. W., Yuan, C., Dunlap, C. A., Andersen, N. H., Gelb, M. H., and Tsai, M. D. (2003) A low-barrier hydrogen bond between histidine of secreted phospholipase A2 and a transition state analog inhibitor. *J. Mol. Biol. 329*, 997-1009.

84. Hur, O., Leja, C., and Dunn, M. F. (1996) Evidence of a low-barrier hydrogen bond in the tryptophan synthase catalytic mechanism. *Biochemistry 35*, 7378-7386.

85. Yamaguchi, S., Kamikubo, H., Kurihara, K., Kuroki, R., Niimura, N., Shimizu, N., Yamazaki, Y., and Kataoka, M. (2009) Low-barrier hydrogen bond in photoactive yellow protein. *PNAS 106*, 440-444.

86. Venkatasubban, K. S., and Schowen, R. L. (1984) The proton inventory technique. *CRC Crit. Rev. Biochem. 17*, 1-44.

87. Sideraki, V., Mohamedali, K. A., Wilson, D. K., Chang, Z., Kellems, R. E., Quiocho, F. A., and Rudolph, F. B. (1996) Probing the functional role of two conserved aspartates in mouse adenosine deaminase. *Biochemistry 35*, 7862-7872.

88. Wion, D., and Casadesus, J. (2006) $N^6$-methyl-adenine : An epigenetic signal for DNA-protein interactions. *Nature Rev. Microbiol. 4,* 183-192.

89. Ratel, D., Ravanat, J. L., Berger, F., and Wion, D. (2006) N6-methyladenine : The other methylated base of DNA. *Bioessays 28*, 309-315.

90. Remy, C. N. (1961) Metabolism of 6-methylaminopurine: Synthesis and demethylation by *Escherichia coli. J. Biol. Chem. 236,* 2999-3005.

91. Duggan, D. E., Weigert, M. G., Grieb, W. E., and titus, E. O. (1963) The metabolism of 6-methylaminopurine in *Salmonella typhimurium. Biochim. Biophys. Acta 68,* 519-525.

92. Duggan, D. E. (1963) The metabolism of 6-methylaminopurine in cell-free systems. *Biochim. Biophys. Acta 68,* 319-321.

93. Buchbinder, B., Stephenson, R. C., Dresser, M. J., Pitera, J. W., Scanlan, T. S., and Fletterick, R. J. (1998) Biochemical characterization and crystallographic structure of an *Escherichia coli* protein from the phosphotriesterase gene family. *Biochemistry 37*, 5096-5106.

94. Quiggle, K., Wejrowski, M. L., and Chladek, S. (1978) Design of new photoaffinity labels for ribosomal peptidyltransferase. *Biochemistry 17,* 94-101.

95. Cercignani, G. (1987) The pH dependence of spectral parameters for Kalckar's adenosine deaminase assay. *Anal. Biochem. 166,* 418-423.

96. Atkinson, H. J., Morris, J. H., Ferrin, T. E., and Babbitt, P. C. (2009) Using sequence similarity networks for visualization of relationships across diverse protein superfamilies. *PLoS ONE 4*, e4345.

97. Trewick, S. C., Henshaw, T. F., Hausinger, R. P., Lindahl, T., and Sedgwick, B. (2002) Oxidative demethylation by *Escherichia coli* AlkB directly reverts DNA base damage. *Nature 419,* 174-178.

98. Hashiguchi, K., Zhang, Q. M., Sugiyama, H., Ikeda, S., and Yonei, S. (2002) Characterization of 2-hydroxyadenine DNA glycosylase activity of *Escherichia coli* MutY protein. *Int. J. Rad. Biol. 78,* 585-592.

99. Kamat, S. S., Williams, H. J., and Raushel, F. M. (2011) Intermediates in the transformation of phosphonates to phosphate by bacteria. *Nature 480 (7378)*, 570-573.

100. White, A. K., and Metcalf, W. W. (2007) Microbial metabolism of reduced phosphorus compounds. *Annu. Rev. Microbiol. 61*, 379-400.

101. Hove-Jensen, B., Rosenkrantz, T. J., Haldimann, A., and Wanner, B. L. (2003) *Escherichia coli phnN*, encoding ribose 1,5-bisphosphokinase activity (phosphoribosyl diphosphate forming): Dual role in phosphonate degradation and NAD biosynthesis pathways. *J. Bact. 185*, 2793-2801.

102. Errey, J. C., and Blanchard, J. S. (2006) Functional annotation and kinetic characterization of PhnO from *Salmonella enterica, Biochemistry 45*, 3033-3039.

103. Hove-Jensen, B., McSorley, F. R., and Zechel, D. L. (2011) Physiological role of *phnP*-specified phosphoribosyl cyclic phosphodiesterase in catabolism of

organophosphoric acids by the carbon-phosphorus lyase pathway. *J. Am. Chem. Soc. 133*, 3617-3624.

104. Adams, M.A., Luo, Y., Hove-Jensen, B., He, S.M., van Staalduinen, L.M., Zechel, D.L., and Jia, Z. (2008) Crystal structure of PhnH: An essential component of the carbon-phosphorus lyase in *Escherichia coli*. *J. Bact. 190*, 1072-1083.

105. Jochimsen, B., Lolle, S., McSorley, F.R., Nabi, M., Stougaard, J., Zechel, D.L., and Hove-Jensen, B. (2011) Five phosphonate operon gene products as components of a multi-subunit complex of the carbon-phosphorus lyase pathway. *PNAS 108*, 11393-11398.

106. Ahn, Y., Ye, Q., Cho, H., Walsh, C. T., and Floss, H. G. (1992) Stereochemistry of carbon-phosphorus cleavage in ethylphosphonate catalyzed by C-P lyase from *Escherichia coli. J. Am. Chem. Soc. 114*, 7953-7954.

107. Avila, L. Z., Draths, K. M., and Frost, J. W. (1991) Metabolites associated with organophosphonate C-P bond cleavage: Chemical synthesis and microbial degradation of [$^{32}$P]-ethylphosphonic acid. *Bioorg. Med. Chem. Lett. 1*, 51-54.

108. Frost, J. W., Loo, S., Cordeiro, M. L., and Li, D. (1987) Radical-based dephosphorylation and organophosphonate biodegradation. *J. Am. Chem. Soc. 109*, 2166-2171.

109. Parker, G. F., Higgins, T. P., Hawkes, T., and Robson, R. L. (1999) *Rhizobium* (*Sinorhizobium*) *meliloti phn* genes: characterization and identification of their protein products. *J. Bact. 181*, 389-395.

110. Hartley, L. E., Kaakoush, N. O., Ford, J. L., Korolik, V., and Mendz, G. L. (2009) Characterization of *Campylobacter jejuni* genes potentially involved in phosphonate degradation. *Gut Path. 1*, 13.

111. Maynes, J. T., Yuan, R. G., and Snyder, F. F. (2000) Identification, expression and characterization of *Escherichia coli* guanine deaminase. *J. Bact. 182*, 4658-4660.

112. Cavalieri, L. F., Bendich, A., Tinker, J. F., and Brown, G. B. (1948) Unltraviolet absorption spectra of purines, pyrimidines and triazolopyrimidines. *J. Am. Chem. Soc. 70*, 3875-3880.

113. Krenitsky, T. A., Neil, S. M., Elion, G. B., and Hitchings, G. H. (1972) A comparison of the specificities of xanthine oxidase and aldehyde oxidase. *Arch. Biochem. Biophy. 150*, 585-599.

114. Quesenberry, M. S., and Lee, Y. C. (1995) A rapid formaldehyde assay using purpald reagent: Application under periodation conditions. *Anal. Biochem. 234*, 50-55.

115. Avigad, G. (1983) A simple spectrophotometric determination of formaldehyde and other aldehydes: Application to periodate-oxidized glycol systems. *Anal. Biochem. 134*, 499-504.

116. La. Vallie, E. R., McCoy, J. M., Smith, D. B., and Riggs, P. (1994) Enzymatic and chemical cleavage of fusion proteins. *Curr. Protocols Mol. Biol.* Unit 16.4B.

117. Sofia, H. J., Chen, G., Hetzler, B. G., Reyes-Spindola, J. F., and Miller, N. E. (2001) Radical SAM, a novel protein superfamily linking unsolved steps in familiar biosynthetic pathways with radical mechanisms: Functional characterization using new analysis and information visualization methods. *Nucleic Acids Res. 29*, 1097-1106.

118. Frey, P. A., Hegeman, A. D., and Ruzicka, F. J. (2008) The radical SAM superfamily. *Crit. Rev. Biochem. Mol. Biol. 43*, 63-88.

119. Chatterjee, A., Li, Y., Zhang, Y., Grove, T. L., Lee, M., Krebs, C., Booker, S. J., Begley, T. P., and Ealick, S. E. (2008). Reconstitution of ThiC in thiamine pyrimidine biosynthesis expands the radical SAM superfamily. *Nature Chem. Biol. 4*, 758-765.

120. McGlynn, S. E., Boyd, E. S., Shepard, E. M., Lange, R. K., Gerlach, R., Broderick, J. B., and Peters, J. W. (2010). Identification and characterization of a novel member of the radical AdoMet enzyme superfamily and implications for the biosynthesis of the Hmd hydrogenase active site cofactor. *J. Bact. 192*, 595-598.

121. Zhang, Y., Zhu, X., Torelli, A. T., Lee, M., Koralewski, R. M., Wang, E., Freed, J., Krebs, C., Ealick, S. E., and Lin, H. (2010) Diphthamide biosynthesis requires an organic radical generated by iron-sulphur enzyme. *Nature 465*, 891-896.

122. Booker, S. J., and Grove, T. L. (2010) Mechanistic and functional versatility of radical SAM enzymes. *F1000 Biol. Rep.* 2:52.

123. Parast, C. V., Wong, K. K., Lewisch, S. A., and Kozarich, J. W. (1995) Hydrogen exchange of the glycyl radical of pyruvate formate lyase is catalyzed by cysteine 419. *Biochemistry 34*, 2393-2399.

124. Buis, J. M., and Broderick, J. B. (2005) Pyruvate formate lyase activating enzyme: Elucidation of a novel glycyl radical formation. *Arch. Biochem. Biophys. 433*, 288-296.

125. Thauer, R. K., and Shima, S. (2008) Methane as fuel for anaerobic microorganisms. *Ann. NY Acad. Sci. 1125*, 158-170.

126. Stubbe, J., and Van der Donk, W. A. (1995) Ribonucleotide reductases: Radical enzymes with suicidal tendencies. *Chem. Biol. 2*, 793-801.

# VITA

Name: Siddhesh Shashikant Kamat

Address: Department of Chemistry,

Texas A&M University,

PO Box 30012

College Station, TX 77842-3012

Email address: skamat@chem.tamu.edu

Education: B. Tech, Pharmaceuticals and Fine Chemicals, University of Mumbai, 2007

Ph.D, Chemistry, Texas A&M University, 2012